Investigating mechanisms that ensure partitioning of peroxisomes during cell growth and division

Tarad Abdulaziz Abalkhail

This thesis is submitted to the University of Sheffield for the degree of Doctor of Philosophy

Faculty of Science
School of Bioscience
May 2023

Abstract

Eukaryotic cells contain various organelles, enclosed structures that execute specialized functions, crucial for maintaining cell metabolism under diverse growth conditions. The careful regulation of organelle dynamics and maintenance is central to cell growth and division, and disruptions can lead to a multitude of illnesses in humans. The budding yeast, *Saccharomyces cerevisiae*, is a model organism that has significantly contributed to our understanding of these processes, leading to the discovery of numerous factors and mechanisms vital for organelle function, many of which are evolutionarily conserved.

Eukaryotic cells have developed certain strategies to control the position, quantity and size of their organelles. These mechanisms involve molecular anchors that are vital for the multiplication of organelles, their spatial arrangement, and the creation of inter-organellar contact points. In *S. cerevisiae*, as in many other cell types, the distribution and dynamics of organelles are indeed critically important. This balance between organelle anchoring and motility does indeed play a key role in determining where organelles are located within the cell and how they are distributed when the cell divides. The distribution of peroxisomes, for example, is controlled through two main mechanisms: anchoring to the cortex in the mother cell and transport towards the bud that is dependent on Myosin. This process is made possible by the Inp1-Pex3 tethering complex which facilitates this transport. Like other organelles, peroxisomes in yeast engage in interactions with various cellular structures. These include the plasma membrane, mitochondria, endoplasmic reticulum, lipid bodies and vacuole.

This thesis provides novel insights into the interactions between Inp1, a component of the tethering complex, and the actin cytoskeleton. We found that the initial 100 amino acids of Inp1 (its N-terminal) provide enough capability for binding to actin, revealing a novel connection essential for peroxisome organization. This mechanism is distinct from the Inp2-Myo2-mediated process, indicating the existence of multiple strategies for the organization of peroxisomes and their association with the actin cytoskeleton.

Our research also demonstrates that the middle domain of Inp1 interacts with the conserved actin-binding protein Srv2 through its C-terminus. Srv2 demonstrates a strong inclination towards ADP-G-actin and facilitates the recycling of actin monomers, a vital process for the quick turnover of the actin network. Moreover, we discovered an interaction between Srv2 and Vps1, a key protein in peroxisome fission. Based on these findings, we propose a new model for the fission of peroxisomes during asymmetric cell division, where Srv2 functions as a central negative regulator, with its C-terminal playing a critical role in peroxisome regulation.

Acknowledgments

First and foremost, I want to express my deepest gratitude to Prof Kathryn Ayscough and Dr Ewald Hettema. They have been more than just my supervisors during my Doctorate journey; they have been my guiding lights, my sounding boards, and my cheerleaders. Without their constant support, motivation, and mentorship, this achievement would not have been attainable, and I would not have evolved into the researcher I am presently. I consider myself lucky to have had the chance to collaborate with such extraordinary people, whose zeal and devotion have been genuinely motivational. My deepest gratitude to all of you.

I feel extraordinarily privileged to have been part of collaborations with many distinguished members from the Hettema Lab, spanning both former and current colleagues. Their support, encouragement, and companionship have been instrumental in my PhD experience. I must give individual recognition to Dr. Donald Watts for his unwavering patience and fellowship, as well as for the expansive knowledge he's shared with me, shaping who I am today. I am also thankful to Dr Georgia Hulmes, Dr Sondos Alhajouj and Dr Selve Turkolmez who were wonderful lab colleagues. Lastly, gratitude to the current E28 members, Abdulaziz, Ibrahim, Yousof, Quentin, Afroza and Nourah.

I want to convey my deep appreciation to Dr. Ellen Allwood for her substantial contribution to the actin assays, which greatly enhanced this work. I would also like to express my appreciation to all the participants of the Ayscough lab for their warmth and welcoming nature that made my time in the lab a truly enriching experience.

I am deeply grateful to King Saud University for its unwavering financial support, which has enabled me to fully dedicate myself to my research and academic pursuits. Their generosity has not only allowed me to pursue my passion for knowledge and innovation, but has also helped me develop the skills and expertise necessary to achieve my career goals.

Special thanks to my wife Latifah for her unwavering support, patience, and affection in all aspects of my life, but most notably during my PhD journey. In numerous ways, her selfless contributions over the past four years have made this accomplishment possible, for which my thankfulness is endless.

I would like to express my deepest gratitude to my family for their unwavering support and encouragement throughout my PhD journey. Without their love, understanding, and constant motivation, I could not have reached this point in my academic career.

Finally, I would like to thank my relatives, friends, and other mentors who have supported me throughout my PhD journey. Your encouragement and guidance have been instrumental in shaping my academic and personal growth.

Table of Contents

Abbreviations

ACBD	Acyl-CoA-binding domain
cER	Cortical endoplasmic reticulum
CHO	Chinese hamster ovary
Drps	Dynamin related proteins
ECL	Enhanced Chemiluminescence
EPCON	ER-peroxisome contact site
ERMES	Endoplasmic reticulum-mitochondrial encounter structure
ESCRT	The endosomal sorting complexe required for transport
GET	Guided entry of Tail-anchored pathway
Gpd1	Glyercol-3-phosphate dehydrogenase 1
GST	Glutathione S-transferase
IPTG	Isopropyl-β-D-1- thiogalactopyranoside
IRD	Infantile Refsum disease
Inp1	Inheritance of peroxisomes 1
LiAc	Lithium acetate
LTP	Lipid transport protein
MBP	Maltose binding protein
MCS	Membrane contact site
Mdh3	The malate dehydrogenase isozyme 3
MECA	Mitochondrial endoplasmic reticulum cortical anchor
MHD	Middle homology domain
mPTS	Membrane peroxisome targeting signal
MTOC	Microtubule-organizing centre
OD	Optical density
ORF	Open reading frame
PBD	Peroxisome biogenesis disorder
PBS	Phosphate buffer saline
PC	Phosphatidylcholine
PCR	The polymerase chain reaction
PE	Phosphatidylethanolamine
PED	Peroxisomal enzyme deficiencies

PEG	Polyethylene glycol
pER	Peroxisomal endoplasmic reticulum
PEX	Peroxin
PI	Phosphoinositide
PI(4)P	Phosphatidylinositol 4-phosphate
PI(4,5)P2	Phosphatidylinositol 4,5-bisphosphate
PM	Plasma membrane
PMP	Peroxisomal membrane protein
PM-PER	Plasma membrane-peroxisome
PMSF	Phenylmethylsulfonyl fluoride
pPV	Pre-peroxisomal vesicle
PS	Phosphatidylserine
PTS	Peroxisome targeting signal
SDS-PAGE	Sodium dodecyl sulphate polyacrylamide gel electrophoresis
TCA	Trichloroacetic acid
UV	Ultraviolet
VAP	Vesicle-associated membrane protein–associated protein
VLCFA	Very long chain fatty acid
YM1	Yeast minimal medium 1
YM2	Yeast minimal medium 2
ZS	Zellweger syndrome
ZSD	Zellweger spectrum disorder

List of Figures

Chapter –1

Chapter –2

Chapter –3

Chapter –4

Chapter –5

Chapter –6

List of Tables

Chapter 1 – Introduction

1.1 Peroxisomes

Peroxisomes are small organelles that are bounded by a single membrane and can be identified in almost all eukaryotic cells. The discovery of these organelles dates back to 1954 when Rhodin identified cytoplasmic components within the cells of mouse kidneys, labeling them as 'microbodies' due to their morphological characteristics (Rhodin, 1954). Later, these microscopic entities were isolated and defined biochemically by de Duve and his team using equilibrium density gradients. The presence of enzymes within these 'microbodies' that trigger reactions leading to the generation and then decomposition of hydrogen peroxide was identified, leading to the coining of the phrase 'peroxisome' (DeDuve and Baudhuin, 1966; Baudhuin et al., 1965).

Peroxisomes are notably adaptable organelles and their contents, morphology, quantity, and size are able to rapidly vary according to extracellular and intracellular conditions. They contain many enzymes needed for a number of metabolic activities and play crucial functions in a wide range of biochemical processes. Organism-specific variations exist in peroxisomal reactions. For instance, in the case of *Photinus pyralis*, a widely found firefly species in North America, the luciferase, which is a light-producing enzyme responsible for its bioluminescent glow, is specifically localized within peroxisomes (Keller et al., 1987). On the other hand, certain processes occurring within peroxisomes, including the β-oxidation cycle for fatty acid breakdown, are remarkably preserved among nearly all eukaryotes (Lazarow and Fujiki, 1985).

In many fungi and plants, fatty acid β-oxidation is solely dependent on peroxisomes, while in more complex eukaryotes, the process of beta oxidation additionally happens within the mitochondria. Prior to the 1980s, the prevailing belief was that the sole essential role of peroxisomes in mammals was fatty acid β-oxidation once the cell's mitochondria reached their maximum oxidative capability (Poirier et al., 2006). Nonetheless, this hypothesis was contradicted by evidence showing that tissues from individuals suffering from peroxisomal disorders exhibit accumulations of very long chain fatty acids (VLCFA) (consisting of 22 carbons or more), while certain medium-chain fatty acids may remain unaffected (Wanders and Waterham, 2006). Despite the presence of functional mitochondria, VLCFA fail to undergo beta-oxidation in the absence of active peroxisomes (Brown et al., 1982). Currently, it is understood that more complex eukaryotes display unique selectivity for substrates in the breakdown process of fatty acid within mitochondria and peroxisomes (Wanders and Waterham, 2006).

1.2 Peroxisomal disorders

Peroxisomes are essential for maintaining the metabolism and subsequently ensuring the continuity of life in the organism. Abnormalities in their activities result from mutations in over 30 genes associated with peroxisome biogenesis and function (Wanders, 2018). These mutations lead to peroxisome biogenesis disorders (PBDs), a cluster of autosomal recessive conditions, which are the most severe among peroxisome-related diseases.

The creation of peroxisomes and efficient import of peroxisomal proteins depend on the coordinated function of a group of 16 PEX genes encoding PEX proteins, also known as peroxins. Any alterations in these PEX genes cause complete or partial obstruction in peroxisome biogenesis, disrupting several metabolic pathways and resulting in metabolic abnormalities in affected individuals (Braverman et al., 2013).
Among PBDs, there are Severe Zellweger Spectrum Disorders (ZSDs), which encompass varying phenotypes like Zellweger syndrome (ZS), Heimler syndrome, Neonatal adrenoleukodystrophy (NALD), and Infantile Refsum disease (IRD) (Klouwer et al., 2015; Poll-The et al., 1987). These conditions were initially identified based on clinical symptoms but later recognized as different manifestations within the same clinical range due to biochemical characterization.
Another group of disorders related to peroxisome formation is peroxisomal enzyme deficiencies (PEDs) (Fidaleo, 2010). PEDs can result from deficiencies in a single enzyme, leading to clinically severe diseases comparable to PBDs. These disorders impact various metabolic pathways, including peroxisomal α and β-oxidation processes, as well as ether-phospholipid synthesis. They are further categorized into specific smaller groups (Wanders and Waterham, 2006).
Heimler syndrome, a rare genetic disorder caused by mutations in peroxisome-biogenesis genes Pex1 and Pex6, is characterized by symptoms such as sensorineural hearing loss, imperfect tooth enamel development (amelogenesis imperfecta), abnormal nails, and, in some cases, retinal pigmentation issues (Ratbi et al., 2015; Varela et al., 2020).
Another special group of PBDs results from mutations in Pex7, the PTS2 receptor, or the PTS2 containing protein alkyl dihydroxyacetone phosphate synthase (alkyl-DHAP-synthase), leading to rhizomelic chondrodysplasia punctata (RCDP) due to a lack of ether lipid synthesis (Motley et al., 1997). Clinical symptoms of RCDP include extremely short stature, abnormal facial appearance, severe growth and mental retardation, and inherited contractures (Heikoop et al., 1990; Hoefler et al., 1988; Motley et al., 1997).
The third group of PBDs comprises peroxisomal fission defects, linked to genetic defects in peroxisome division genes such as Dlp1, Mff, Gdap1, and Pex11β (Ebberink et al., 2012; Huber et al., 2013; Shamseldin et al., 2012; Waterham et al., 2007). These defects were identified relatively recently, and their recognition was delayed due to limited biochemical abnormalities associated with peroxisomes in patient-derived cells (Waterham et al., 2016).
The final type of defect in peroxisomal function is referred to as single peroxisomal enzyme deficiencies (PEDs) (Fidaleo, 2010; Klouwer et al., 2015; Steinberg et al., 2006; Subramani, 1993). This category includes impairments in peroxisomal matrix enzymes and peroxisomal membrane proteins responsible for metabolite transport. Disorders within this group involve various metabolic pathways, such as peroxisomal fatty acid β-oxidation, peroxisomal fatty acid α oxidation, peroxisomal glyoxylate metabolism, peroxisomal ether phospholipid biosynthesis, and peroxisomal bile acid synthesis, as well as peroxisomal H2O2 metabolism (Waterham et al., 2016).

1.3 Peroxisome biogenesis

The investigation into the biogenesis of peroxisome originated from the observation that *Saccharomyces cerevisiae* exhibits peroxisome proliferation when cultured on oleic acid media (Veenhuis et al., 1987). Subsequent investigations have unveiled the vital role of

peroxisomes in the growth of this yeast when oleic acid is the exclusive carbon source. This finding served as the foundation for a negative selection test in which peroxisome biogenesis mutants lacking peroxisomal structures were discovered because they are unable to grow on media containing oleic acid (Erdmann et al., 1989). The scope of this study was expanded to include additional yeast species, including *Pichia pastoris* (Gould et al., 1992; Liu et al., 1992). Additionally, research has been performed in Chinese hamster ovary (CHO) cells, a mammalian cell line that is widely used in biotechnology. Peroxisomes are important for plasmalogen biosynthesis in CHO cells, which are a class of phospholipids found in the cell membrane. This requirement for peroxisomes in plasmalogen biosynthesis provides an additional means of negative selection for identifying mutations involved in peroxisome formation (Morand et al., 1990; Tsukamoto et al., 1990), these furthered our understanding of the process in a mammalian context.

In addition to the use of negative selection assays to identify key genes, mutants within peroxisome biogenesis were also recognised through positive selection screenings. This assay worked on the expression of a bleomycin-resistant chimeric protein and the luciferase enzyme in *S. cerevisiae*. This experimental design was based on the idea that the absence of phleomycin resistance in cells would indicate the successful transport of the protein into peroxisomes. Conversely, in modified cells where peroxisomes are absent, the fusion protein responsible for the resistance of phleomycin will remain in the cytoplasm. As a result, peroxisome biogenesis mutants can be selectively identified based on their resistance to phleomycin, as reported by Elgersma et al. in 1993.

The genes discovered during this time were first given names and characteristics based on their roles or the order in which they were discovered. Distel et al. summarised the system by which they are currently recognised, and the proteins were named peroxins, which are encoded by *PEX* genes, as described by Distel et al. in 1996. *PEX* genes have been additionally identified through the utilization of DNA microarray methods for studying yeast genes induced by oleic acid, as well as through proteomic methodologies. 36 peroxins are discovered up to the present time. In the table below, the identified *PEX* genes in *S. cerevisiae* are presented, along with the specific roles of each gene.

Table 1. 1 - Peroxins and their functions in *Saccharomyces cerevisiae* (adapted from Smith and Aitchison, 2013).

Peroxin	Functional classifications	References
Matrix protein targeting		
Pex5	The shuttling receptor for PTS1	(Klein et al., 2001)
Pex7	The shuttling receptor for PTS2	(Marzioch et al., 1996)
Pex18, Pex21	PTS2 cargo coreceptor	(Purdue et al., 1998)
Pex9	The shuttling receptor for PTS1	(Effelsberg et al., 2016)

Peroxisomal matrix proteins		
Pex4	Export receptor engagement mediated by ubiquitin-conjugating enzyme	(Distel et al., 1996)
Pex1, Pex6	Receptor recycling, AAA-type ATPase	(Erdmann et al., 1991)
Pex8	Facilitating the relationship between export machinery and the docking complex for importer assembly	(Rehling et al., 2000)
Pex22	serves as an anchor for Pex4 and is involved in receptor export	(Koller et al., 1999)
Pex10,Pex2,Pex12	Components of the RF (RING finger) complex involved in receptor ubiquitylation	(Warren et al., 1998)
Pex13, Pex14, Pex17	Receptor docking complex	(Girzalsky et al., 1999)
Pex15	Pex1 and Pex6 membrane receptor	(Elgersma et al., 1997)
Peroxisomal membrane proteins (PMPs) direct targeting		
Pex3	Pex19 docking, PMPs insertion	(Höhfeld et al., 1991)
Pex19	Soluble cytosolic chaperone and import receptor for class I peroxisomal membrane proteins	(Götte et al., 1998)
Peroxisomal membrane formation from the endoplasmic reticulum		
Pex3, Pex19	necessary for peroxisome *de novo* biosynthesis	(Tam et al., 2005)
Pex25	Necessary for peroxisome *de novo* biosynthesis	(Huber et al., 2012)
Pex30	Regulates peroxisome *de novo* pathway	(David et al., 2013)
Fission		
Pex11	Involvement in membrane elongation and recruitment of fission machinery	(Opaliński et al., 2011)
Pex25	Membrane remodelling and elongation	(Rottensteiner et al., 2003)
Pex34 and Pex27	Positive fission regulators	(Rottensteiner et al., 2003; Tower et al., 2011)

Peroxisome biogenesis regulation		
Pex32, Pex31, Pex29, and Pex28	A complex comprising proteins containing the reticulon homology domain establishes peroxisomes–endoplasmic reticulum contact sites	(Vizeacoumar et al., 2004)
Pex35	Regulates peroxisome abundance and Interacts with Arf1	(Yofe et al., 2017)

Peroxisomal matrix proteins are a group of proteins synthesized by free ribosomes in the cytosol, and they undergo post-translational transport across the peroxisomal membrane to be localized within the peroxisomes (Lazarow and Fujiki,1985). Within the peptide sequences of the majority of matrix proteins, either of the two peroxisomal targeting signal sequences (PTS), namely PTS1 or PTS2, is present. While some proteins carry only a single (PTS1 or PTS2), there are rare proteins that have both signals. The predominant PTS1 sequence is characterized by a consensus motif of [A/C/S-H/K/R-L] located at the C-terminal ends of the proteins (Gould et al., 1989). In contrast, the less frequent PTS2 sequence is located near the N-terminal region of proteins with [K/R-I/L/V-X5-H/L-Q/A] consensus sequences (Swinkels et al., 1992; Petriv et al., 2004).

PTS1-containing matrix proteins interact with the cytosolic receptor Pex5, while PTS2-containing matrix proteins associate with the cytosolic receptor Pex7. In *S. cerevisiae*, the recognition of PTS2 proteins is facilitated by Pex7 protein, which necessitates the presence of co-receptors Pex18 and Pex21 (the *Pichia pastoris* Pex20p) (Titorenko et al., 1998). In the process of protein import into mammalian peroxisomes, two distinct isoforms of the Pex5 receptor, called PEX5S and PEX5L, perform different roles (Fujiki et al., 2022; Ebberink et al., 2009; Dodt et al., 2001). PEX5L serves as a coreceptor for PTS2 proteins and also interacts with the protein Pex7, acting as a transition site between the PTS1 and PTS2 pathways. On the other hand, PEX5S likely does a separate role within peroxisome-related mechanisms (Ebberink et al., 2009; Dodt et al., 2001; Braverman et al., 1998).
The latest model for protein import into peroxisomes suggests a stepwise process. First, the receptor binds PTS1 matrix proteins in the cytosol via its C-terminal TPR domain. Then, the cargo-bound receptor is recruited to peroxisomes through N-terminal pentapeptide motifs. Once at the peroxisomal membrane, PEX5, along with the cargo, translocates into the peroxisomal lumen. The high-affinity interaction between the pentapeptide motifs and the lumenal domain of PEX14 prevents the diffusion of PEX5 and bound cargo back into the cytosol (Skowyra and Rapoport).
To initiate recycling, the receptor's unstructured N terminus emerges into the cytosol, inserting into the Ub ligase complex. This interaction requires an amphipathic helix (AH2) within the N-terminal region of PEX5. The receptor is then monoubiquitinated at a conserved cysteine and fully pulled out of the lumen into the cytosol by the PEX1/PEX6 ATPase. Another conserved amphipathic helix (AH1) near the receptor's N terminus is crucial for these steps (Skowyra and Rapoport). The pulling action of the ATPase causes the C-terminal TPR domain to unfold, releasing the cargo inside the lumen. Subsequently, the TPR domain refolds in the

cytosol, and the ubiquitin (Ub) is removed by deubiquitinating enzymes, resetting the receptor for a new import cycle.
The proposed model also accounts for the import of PTS2 cargo. The ternary complex, comprising PEX5, cargo, and the adapter PEX7, docks at peroxisomes and translocates across the membrane using the receptor's pentapeptide motifs. After export of PEX5 through the Ub ligase, both the cargo and PEX7 are left behind in the peroxisomal lumen. The mechanism by which PEX7 returns to the cytosol is currently unclear due to the absence of unstructured regions that could interact with the ligase (Skowyra and Rapoport) (Fig. 1.1).

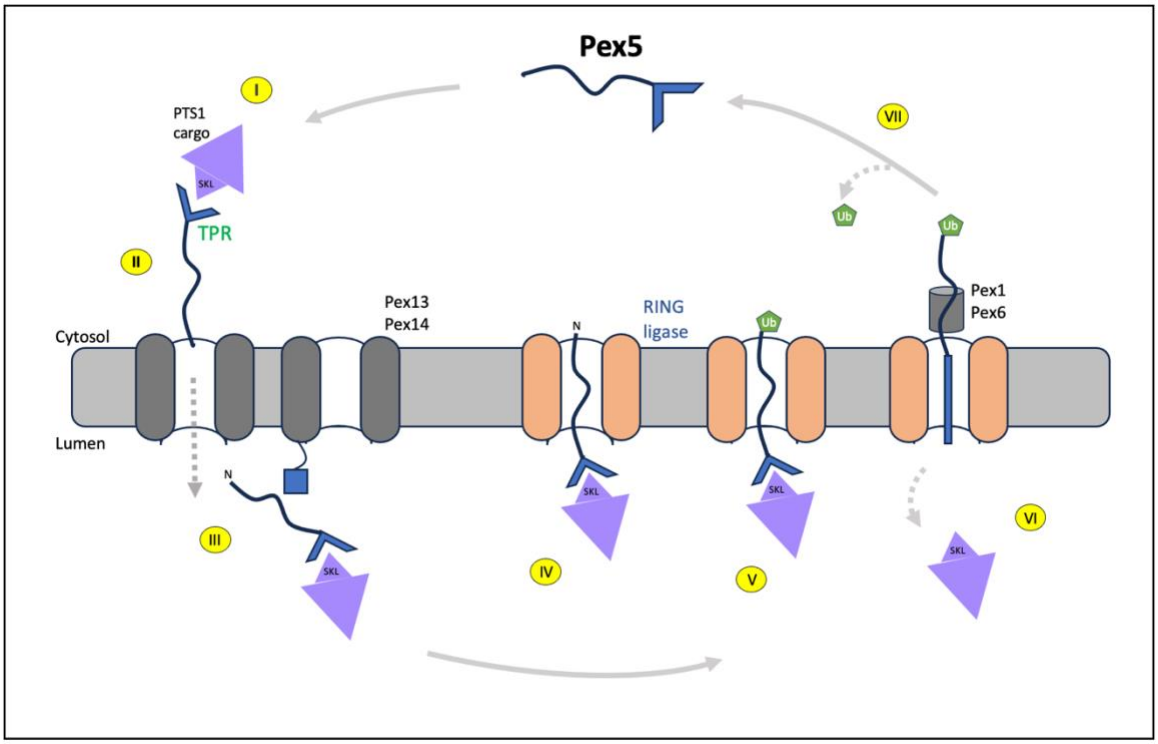

Figure 1. 1: A model illustrating the series of actions of PEX5 shuttling. The import process encompasses seven main steps: (I) In the cytosol, PTS1 cargo binds to the TPR domain of PEX5. (II) The cargo-bound PEX5 is then directed to the docking complex in the peroxisomal membrane, which consists of PEX13 and PEX14. This recruitment occurs through WxxxF/Y pentapeptide motifs (pink), with only the first 5 motifs shown. (III) PEX5, along with the cargo, translocates into the peroxisomal lumen. The high-affinity interaction between the pentapeptide motifs and the lumenal domain of PEX14 (crimson square) prevents diffusion back into the cytosol. (IV) Export of PEX5 is initiated by binding to the ligase complex through an amphipathic helix (blue). Subsequently, the unstructured N terminus inserts into the ligase pore and emerges in the cytosol. (V) The conserved cysteine in PEX5 undergoes monoubiquitination. (VI) PEX5 is then pulled out of the lumen through the ligase pore by the PEX1/PEX6 AAA ATPase. This extraction process involves the unfolding of the TPR domain and the subsequent release of the bound cargo. (VII) After extraction, the TPR domain refolds in the cytosol, and ubiquitin is removed by deubiquitinating enzymes, effectively resetting PEX5 for a subsequent import cycle. Adapted from (Skowyra and Rapoport, 2022).

Peroxisomal membrane proteins (PMPs) utilize distinct pathways for entering the peroxisomal membrane compared to peroxisomal matrix proteins (Santoset al., 1988). The involvement of Pex19 and Pex3 is crucial for peroxisomal membrane biogenesis. Loss of either *PEX3* or *PEX19* leads to the absence of characteristic peroxisomal membrane structures, causing mislocalization of the majority of PMPs to be cytosolic or to be in other membranes such as the mitochondrial outer membrane or the endoplasmic reticulum (Gotte et al., 1998; Matsuzono et al., 1999; Muntau et al., 2000; Hettema et al., 2000; Shimozawa et al., 2000). In the complex eukaryotes, Pex16 has been identified as a key player in peroxisomal membrane biogenesis (South and Gould, 1999; Honsho et al., 1998). However, the presence and conservation of Pex16's function and structure vary among organisms, and it is absent in certain yeast species, including *S. cerevisiae* (Farré et al., 2017).
PEX19 is primarily located in the cytosol, with a small part existing on the peroxisomal membrane, and it plays a critical role in the biogenesis of peroxisomes (Matsuzono et al., 1999; Gotte et al., 1998; Sacksteder et al., 2000). It acts as a cytosolic chaperone responsible for guiding peroxisomal membrane proteins (PMPs) and an import receptor by interacting with multiple PMP targeting signals referred to as mPTSs (Jones et al., 2004). These mPTSs typically consist of a cluster of basic and hydrophobic amino acids along with a transmembrane domain (Honsho and Fujiki, 2001; Dyer et al., 1996). When Pex19 interacts with Pex3 on the peroxisomal membrane, it stabilizes the PMP bound to Pex19 and facilitates its release into the peroxisomal membrane bilayer (Fig. 1.2) (Fang et al., 2004; Muntau et al., 2003; Matsuzono et al., 2006). Most PMPs are classified as Class I PMPs since they are inserted directly and post-translationally into peroxisomal membranes via Pex19.

Independent of Pex19, it is believed that Class II PMPs target the peroxisomal membrane through the ER. Pex3 is one of the few known Class II PMPs that has been well characterised. Pex3 follows a distinct import pathway compared to other PMPs, as its import into peroxisomes does not require binding of its mPTS by Pex19 (Jones et al., 2004). This could be as a result of its crucial function in the production of peroxisomes.

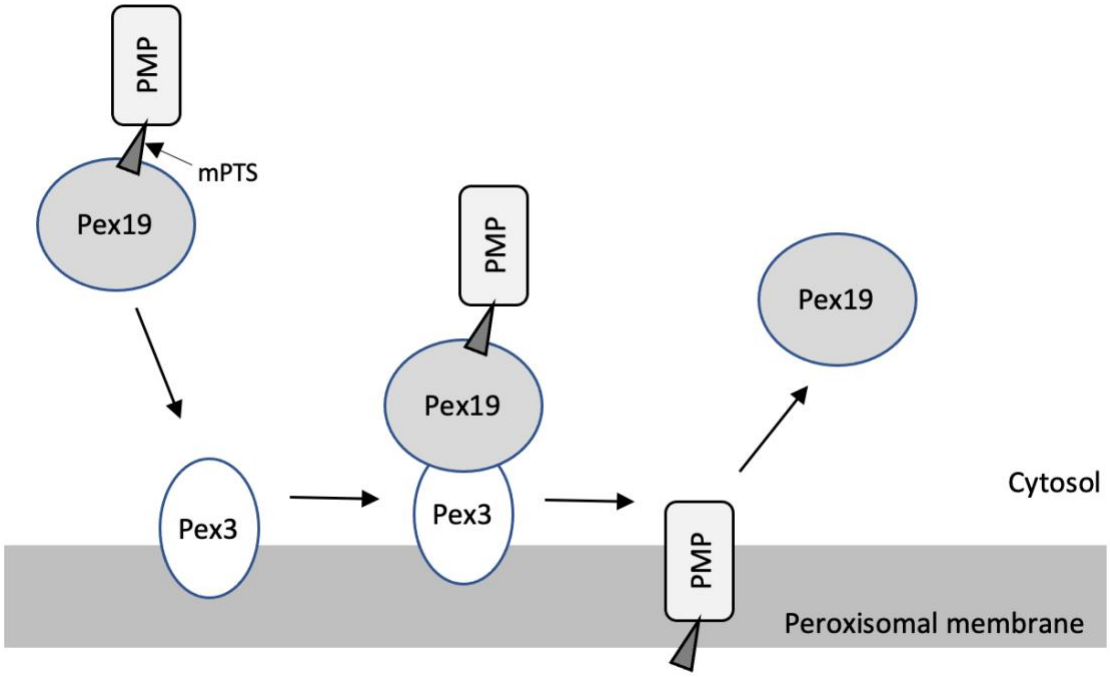

Figure 1. 2: The process model for how peroxisomal membrane proteins are imported into peroxisomes. In the cytosol, PMP docks with the chaperone of Pex19 protein through mPTS. Pex19 chaperones the PMP until docking with Pex3 at the peroxisomal membrane. Finally, Pex19 is returned to the cytosol after the PMP is inserted into the peroxisomal membrane.

Modeling peroxisome growth and fission

The understanding of peroxisome growth and fission is rooted in the notion that peroxisomes originate from preexisting peroxisomes, through a process involving growth of peroxisomes using lipids derived from the ER, and the integration of cytosolic peroxisomal membrane proteins (PMPs) in the membrane of peroxisomes, and subsequent division process that generate new peroxisomes (Fig. 1.3) (Carmichael and Schrader, 2022; Motley and Hettema, 2007; Lazarow and Fujiki, 1985). Upon synthesis in the cytosol, PMPs have the ability to undergo the process of translocation to reach peroxisomes via a post-translational chaperoning process facilitated by Pex19. Within the peroxisomal membrane, Pex19 establishes interactions with Pex3 through its high-affinity N-terminus binding site, facilitating the incorporation of Class 1 PMPs into the peroxisomal lipid bilayer membrane (Matsuzono et al., 2006; Fang et al., 2004; Schmidt et al., 2010). The Pex19-Pex3 complex results in the development of distinct structural and functional units. In this context, Pex3's mPTS is unique compared to other PMPs' mPTS binding locations, allowing to form complexes of Pex3, Pex19, and peroxisomal membrane proteins (PMPs) (Shibataet al., 2004). Additionally, the specific binding region of Pex19 within human Pex3 has been found (Muntau et al., 2003;Fang et al., 2004).

The functional role of the Pex11 protein family in peroxisome proliferation has been extensively studied and characterized. In humans, three PEX11 homologs, which are PEX11alpha, beta, and gamma, are present, while in the majority of fungi, the PEX11 members includes Pex11, Pex25, and Pex27, with Pex27 and Pex25 being paralogs (Kiel et al., 2006). To produce a new peroxisome, peroxisome multiplication happens through three essential steps which are elongation, constriction and fission. Pex11 family proteins, particularly Pex11 perform an elongation step. Pex11 in *S. cerevisiae* and the α, β, and γ isoforms of Pex11 in mammals induce peroxisome tubulation through the elongation step (Carmichael and Schrader, 2022; Kiel et al., 2006). Additionally, when Pex25 is overexpressed, it affects the normal peroxisome shape, resulting in the elongation of peroxisomes (Huber et al., 2012). Elongation of the peroxisome is subsequently followed by constriction. Pex11 (or Pex11β in mammals) interacts with Fis1, a tail anchored protein, leading to the recruitment of Caf4/Mdv1 in yeast (the mitochondrial fission factor Mff1 in mammals) by Fis1 protein (Gandre and Bliek, 2008; Motley et al., 2008). The dynamin 1 GTPase protein (Dnm1 in yeast, or Dlp1 in mammals) is positioned at the constriction region, where the hydrolysis of GTP activates peroxisome fission (Kuraviet al., 2006; Liand Gould, 2003). It has been discovered that Pex11p in mammals serves an additional function as a GTPase activating protein (GAP) for Dynamin-related 1 (Dnm1p). This finding highlights Pex11p's crucial role in the final step of peroxisomal fission, specifically in mediating dynamin-like protein (DLP)-mediated membrane scission. The study demonstrates that yeast Pex11p is essential for Dnm1p's function in vivo, and it physically interacts with Dnm1p, with inhibiting this interaction leading to compromised peroxisomal fission. Furthermore, Pex11p functions as a GAP for Dnm1p in vitro, and similar observations were made for mammalian Pex11β and the corresponding DLP Drp1, indicating the conservation of DLP activation by Pex11p (Williams et al., 2015). In yeast, there is another Drp which is involved in the process of peroxisome fission. During normal growth conditions, Vps1 acts as a significant key protein in peroxisome fission and contributes more to this process compared to Dnm1. Notably, Vps1 functions autonomously from Fis1 (Ekal et al., 2023; Motley et al., 2008; Hoefpner et al., 2001). In the Hettema lab, it has been

shown that Vps1 interacts with Pex27 and Pex27 is crucial and required for Vps1 function in peroxisome fission (Ekal et al., 2023) (Fig. 1.4).

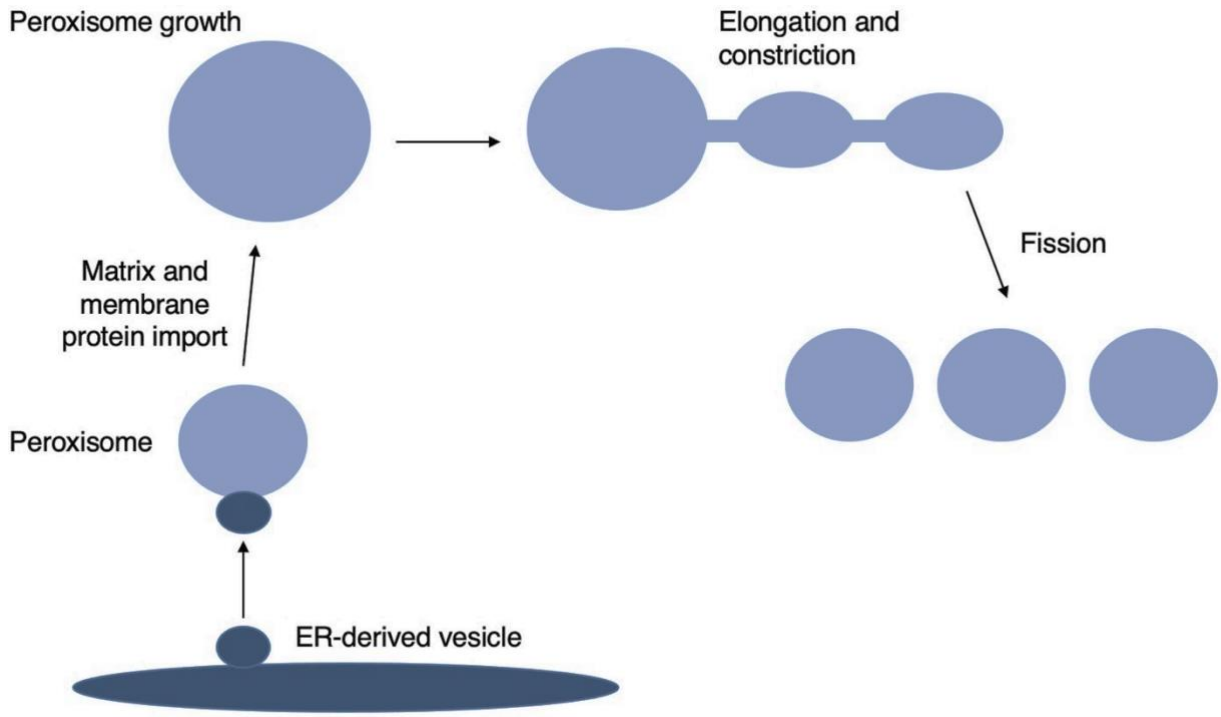

Figure 1. 3: A proposed model of peroxisome growth and fission. Peroxisomes acquire lipids and a specific subset of peroxisomal membrane proteins from the endoplasmic reticulum through vesicular transport and subsequent fusion. They also acquire peroxisomal matrix and membrane proteins newly synthesized in the cytoplasm. These mechanisms facilitate the growth of peroxisomes. When a peroxisome reaches an appropriate size, it enters a series of scission stages, including elongation, constriction, and ultimately fission.

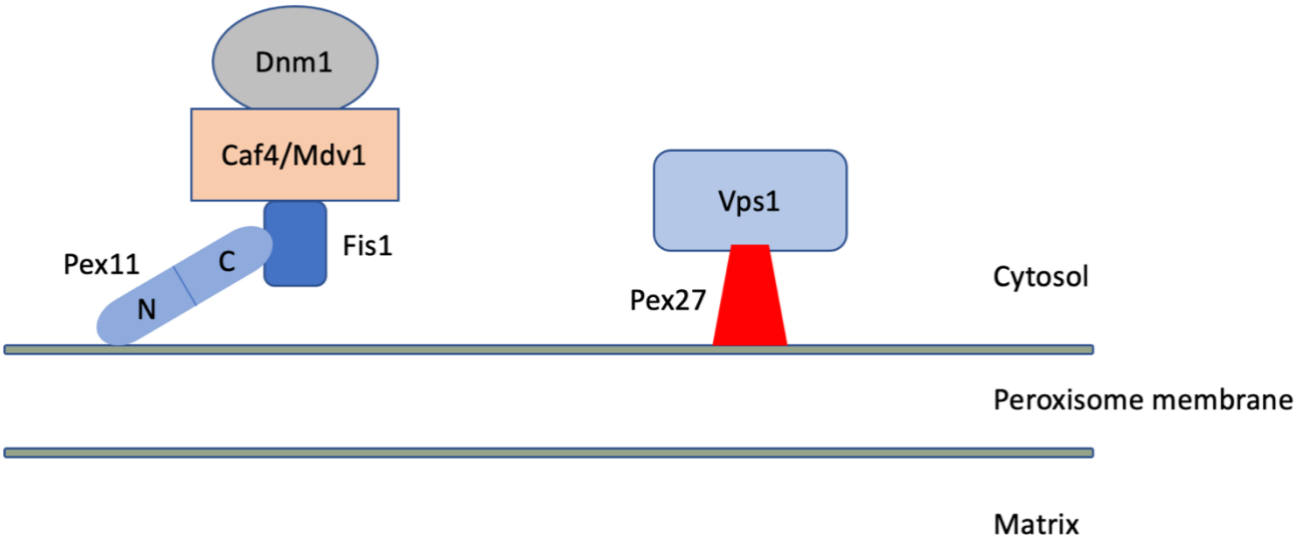

Figure 1. 4: The proposed model for peroxisome scission in *S. cerevisiae* involves the proteins Dnm1 and Vps1. This schematic diagram highlights the key players involved in their respective fission pathways. Dnm1 recruitment requires Fis1 and Mdv1/Caf4. Pex11 is believed to play a role in membrane remodeling and regulation of Dnm1 GTPase activity. Additionally, Pex27 contributes to Vps1-dependent fission.

The *de novo* model of peroxisome biogenesis

The significance of the Pex3-Pex19 binding was demonstrated when cells lacking functional Pex19 or Pex3 were found to be devoid of peroxisomes (Hettema et al., 2000). In the absence of peroxisomes in peroxisome inheritance mutants or peroxisome biogenesis mutants, re-expression of the absent gene can allow forming of peroxisomes when preexisting peroxisomal structures are not present (Hohfeldet al., 1991). This finding resulted in the emergence of the *de novo* peroxisome synthesis model. The process of *de novo* formation involves the generation of new peroxisomes from specific domains within the endoplasmic reticulum (ER), relying on the presence of Pex19 (Fig. 1.5) (Hoepfneret al., 2005).

When peroxisomal structures are absent, Pex3 begins to accumulate at specific domains within the endoplasmic reticulum (ER), forming what is known as the pre-peroxisomal ER (Motley and Hettema, 2007;Kragt et al., 2005; Hoepfneret al., 2005; Tam etal., 2005). In yeast, numerous PMPs, including Pex3, undergo co-translational insertion into the ER with the assistance of the Sec61 translocon complex, while peroxisomal tail-anchored (TA) proteins undergo post-translational insertion and require the involvement of the guiding tail-anchored membrane (GET) proteins as well as Pex19 protein (Thoms et al., 2012; Schuldiner et al., 2008; Mayerhofer et al., 2016). In mammalian cells, the insertion of PMPs may occur directly (Costello et al., 2017).

Pex19 has a critical function in releasing pre-peroxisomal vesicles from the ER, while the precise process guiding the release of Pex3 by Pex19 remain unclear. Currently, no additional essential molecular machinery affected in this process has been determined (Lam et al., 2011; Van Der Zand et al., 2010). The proteins of endosomal sorting complexes required for transport (ESCRT)-III specifically Snf7 and Vps20, are believed to play a part in the scission of pre-peroxisomal vesicles (Mastet al., 2018). These pre-peroxisomal vesicles subsequently undergo fusion to induce a pre-peroxisome qualified for importing matrix proteins. Over time, this pre-peroxisome matures to form a fully active peroxisome (VanDer et al., 2012).

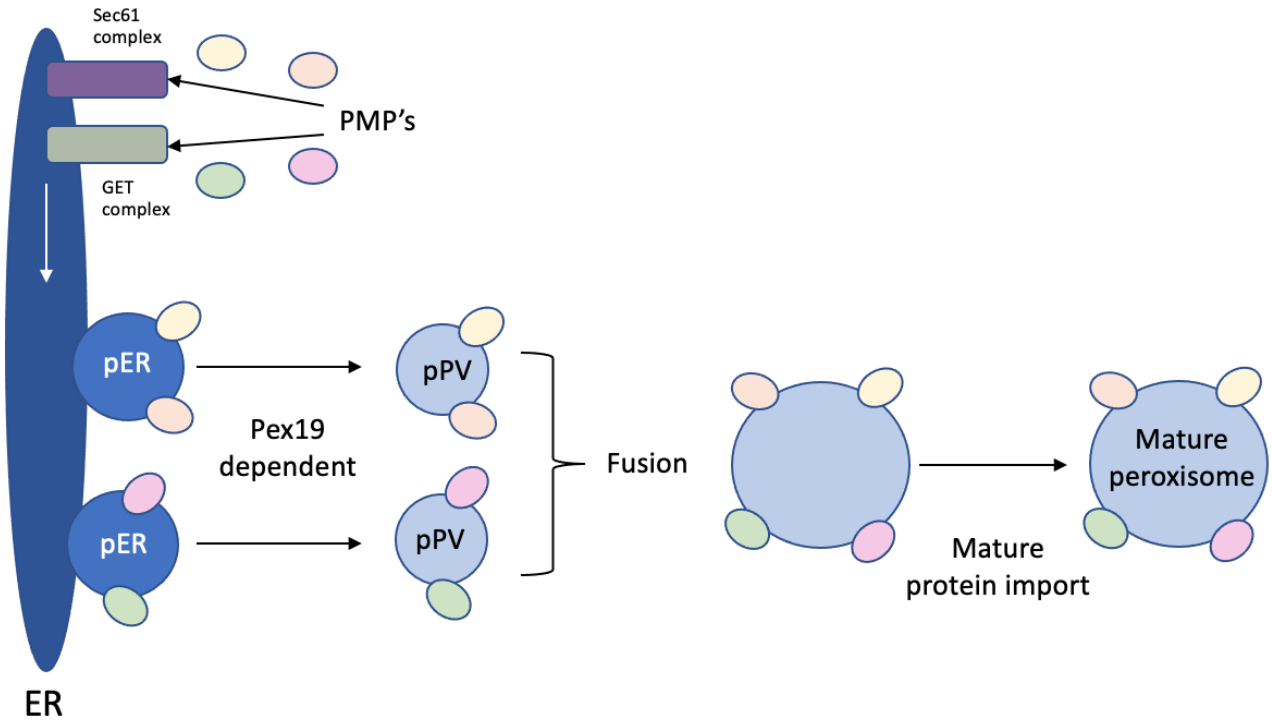

Figure 1. 5: The model of the *de novo* pathway of peroxisome biogenesis. PMPs undergo co-translational insertion into the endoplasmic reticulum (ER) through the complex of Sec61 and post-translational insertion through the complex GET. These PMPs are specifically targeted to ER subdomains known as peroxisomal ER (pER). Subsequently, the formation of pre-peroxisomal vesicles (pPVs) takes place, with Pex19 playing a crucial role in their Pex19-dependent budding from the ER. These pPVs exist in two separate classes: one containing Pex2, Pex3, and Pex11, and the other consisting of Pex3, Pex10, Pex12, Pex13, Pex14, and Pex17. Following their formation, these pPVs undergo fusion, resulting in the formation of a pre-peroxisome. Importantly, pre-peroxisomes have the ability to import matrix proteins and finally grown into functional peroxisomes.

Peroxisomes in mammals

The process of peroxisome inheritance in mammals is less well understood than it is in yeast. Although Inp1 and Inp2 are essential for peroxisome retention and transfer in yeast, mammalian cells do not contain direct homologs of these proteins. Mammalian cells do, however, contain a few proteins that have an effect on peroxisome distribution and inheritance.
Peroxisome trafficking in mammalian cells is principally controlled by the microtubule network and related motor proteins. The two primary motor proteins involved in peroxisome trafficking are dynein and kinesin (Covill-Cooke et al., 2020). Microtubules' minus ends, which are often found close to the microtubule-organizing centre (MTOC), are where dynein travels. It is in charge of peroxisomes moving backwards towards the MTOC. Through interacting with dynein and its cofactor dynactin, the membrane protein Pex14, which has a vital part in peroxisomal import (Bharti et al., 2011; Baker et al., 2016), enables the retrograde transport of peroxisomes across microtubules (Bharti et al., 2011). On the other hand, Kinesin travels along microtubules in the direction of the plus end, which is often found at the edge of the cell. Kinesin anchors to the peroxisomal membrane utilising various adaptors, such as Pex1 (Dietrich et al., 2013), to enable the anterograde movement of peroxisomes towards the cell periphery (Covill-Cooke et al., 2020) (Fig. 1.6).

Miro1, a mitochondrial Rho GTPase, plays a critical function in the movement of peroxisomes within mammalian cells. Researchers have identified three distinct splicing variants of Miro1: Miro1-var2, Miro1-var3, and Miro1-var4, each containing specific amino acid sequence insertions. Among these variants, Miro1-var4 and Miro1-var2 are specifically targeted to peroxisomes through a dependency on insertion 1, which is recognized by the cytosolic receptor Pex19p. Introducing Miro1-var4 exogenously results in the accumulation of peroxisomes at the cell periphery and enhances their long-range movement along microtubules. Conversely, the depletion of all Miro1 variants hinders the long-distance peroxisome movement, a defect that can be reversed by reintroducing peroxisomal Miro1 variants. Overall, these research findings establish the role of Miro1 variants as adapter proteins, facilitating interactions between peroxisomes and microtubule-dependent transport complexes, thereby playing a vital role in intracellular peroxisome translocation in mammalian cells (Castro et al., 2017; Okumoto et al., 2018).

The ER is now connected to several different organelles by many tethering components, but limited information is available regarding the processes that link it to peroxisomes. Since the biosynthetic processes of sterols, ether-phospholipids, and unsaturated fatty acids depend on peroxisome-ER interaction, defects in these processes can result in serious illnesses. The interaction between the endoplasmic reticulum (ER) membrane proteins vesicle-associated membrane protein-associated protein (VAPA or VAPB) and the peroxisomal proteins acyl-CoA binding domain protein (ACBD4 or ACBD5) facilitates the binding of peroxisomes to the ER. This binding is essential for oscillatory peroxisomal movement. The peroxisomal protein ACBD4 isoform 2 is tail-anchored and interacts with the endoplasmic reticulum (ER) protein VAPB, facilitating the establishment of contact between these two organelles. Based on the findings, ACBD4, similar to ACBD5 and E-Syts, can function as a molecular anchor, directly connecting the endoplasmic reticulum (ER) and peroxisomes. This discovery identifies ACBD4 as the third protein in mammalian cells that contributes to ER-peroxisome contact, in addition

to the previously known ACBD5 and E-Syts (Costello et al., 2017). Moreover, the absence of VAP-A/B or ACBD4/5, which are essential proteins for establishing ER peroxisome contact sites in mammalian cells, results in elevated peroxisomal motility. This is likely due to the release of these organelles from their tethering, enabling them to move more freely (Costello et al., 2017). A recent study has uncovered a molecular mechanism that regulates peroxisome-endoplasmic reticulum contacts in mammals. The research demonstrates that peroxisome-ER associations are controlled through the phosphorylation of the ACBD5-VAPB tether. The study identifies phosphorylation points within both the flanking sequences and the central core of the FFAT motif, which differentially modulate interactions with VAPB and, consequently, peroxisome-ER contact sites. The FFAT motif (two phenylalanines in an acidic tract) is a conserved amino acid sequence motif that plays a critical role in mediating the interaction between proteins residing in the endoplasmic reticulum (ER) and certain organelles, such as peroxisomes. Furthermore, the study reveals that glycogen synthase kinase-3-beta (GSK3β) has a function in regulating their interaction (Kors et al., 2022).

Like fission in yeast, peroxisome fission in mammals is subdivided into three processes, including elongation followed by constriction and then scission (Schrader et al., 2012; Schrader and Fahimi 2006). Several human proteins associated with these processes have been discovered in recent years. This includes the PEX11 proteins, which contribute to elongation and constriction stages, as well as the DRP1/DLP1, Mff, FIS1, and GDAP1 proteins, which essentially affect the process of peroxisome fission. Interestingly, these proteins including DLP1/Drp1,Mff,Fis1,and GDAP1 participate in the fission processes of peroxisomes as well as mitochondria (Schrader et al., 2012; Schrader et al., 2015). PEX11 and its related proteins can be found in every organism containing peroxisomes and seem to be involved in peroxisome elongation and the deformation of peroxisome membrane (Opaliński et al., 2011a; Opaliński et al., 2011b). PEX11 in humans has three homologous isoforms known as—PEX11α, PEX11β, and PEX11γ—which exhibit significant sequence similarity but seem to do unique roles in the division pathway of peroxisomes. For instance, when PEX11α and PEX11β are overexpressed, peroxisome abundance is affected resulting in a high number of peroxisomes, while PEX11γ overexpression does not affect peroxisome abundance. Furthermore, Pex11β is suggested to be involved in the growth and scission pathways, participating in the elongation and constriction stages of peroxisome fission and in the absence of MFF, PEX11β can stimulate peroxisome division through a DRP1- and FIS1-dependent mechanism (Carmichael et al., 2022; Li et al., 2002). In contrast, PEX11γ seems to play a role in the *de novo* peroxisome formation pathway, potentially facilitating the peroxisomal matrix proteins to be imported into the pre peroxisomal vesicles originating from the ER (Waterham et al., 2016) (Fig. 1.7).

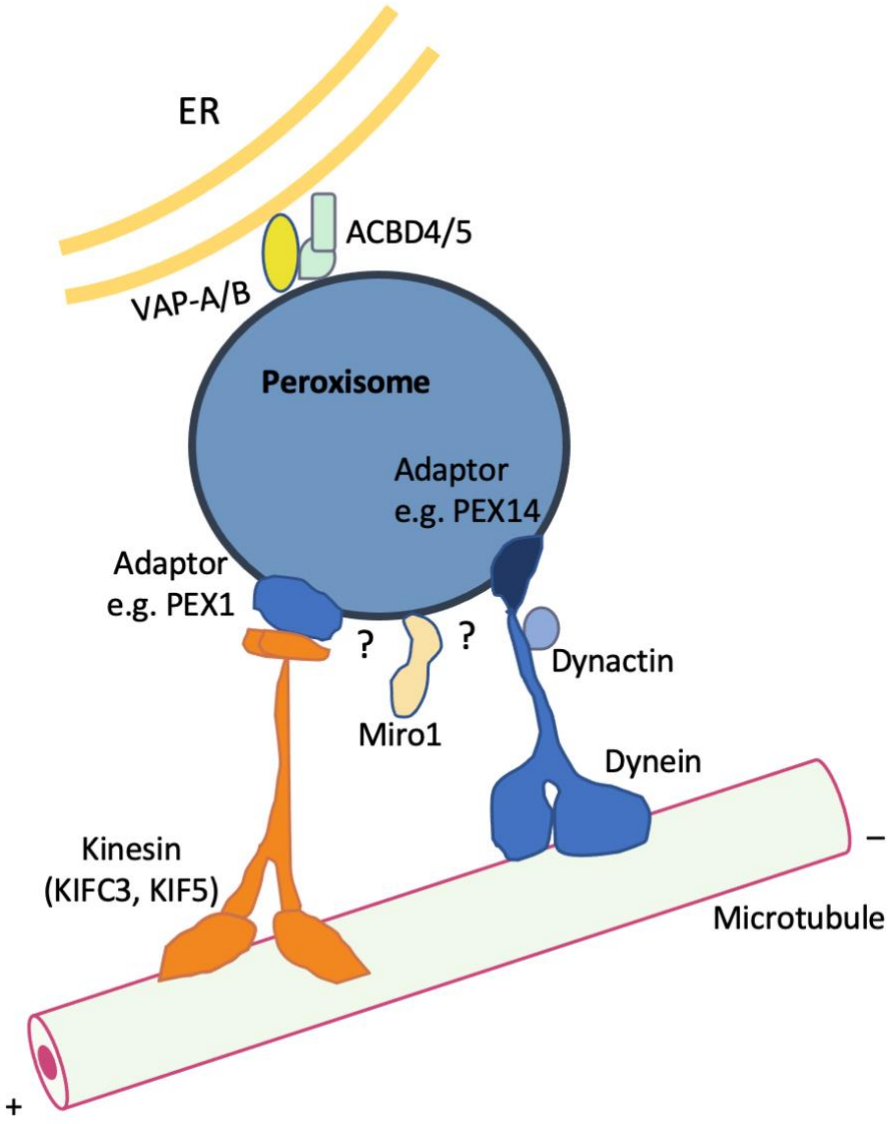

Figure 1. 6: Molecular mechanisms of peroxisomal trafficking and interactions with the ER. The machinery responsible for peroxisomal trafficking involves long-range movement across microtubules, enabled by motor proteins like dynein and kinesin (KIFC3, KIF5). PEX14 enables the peroxisomes' backward motion across microtubules through interactions with the dynein–dynactin motor complex. KIFC3 and KIF5 kinesins aid in peroxisomal transport over long distances in the direction of the microtubules' positive end by interacting with the peroxisome membrane through various receptors, (KIFC3 and its receptor PEX1). Miro1 may have a regulatory role in peroxisomal trafficking through its interactions with one of the transport motors, dynein or kinesin. The motility of peroxisomes relies on their attachment to the ER through the binding of VAPA/B to ACBD4/5 (Adapted from Covill-Cooke et al., 2020).

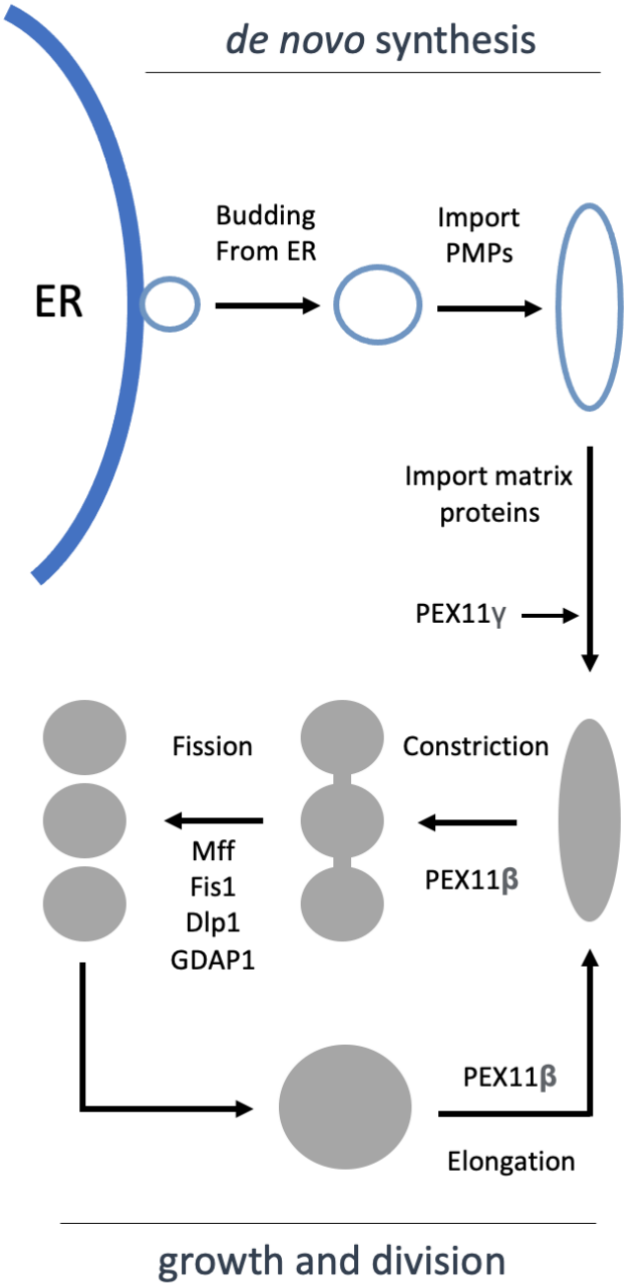

Figure 1. 7: A proposed model for growth and fission of peroxisomes. Peroxisomes originate through the growth and fission of preexisting ones or by emerging *de novo* derived from specific regions of the ER. These peroxisomes then mature into metabolically active organelles by sequentially importing peroxisomal membrane proteins (PMPs) and matrix proteins. The division of peroxisome entails separate consecutive stages: elongation followed by constriction, and then scission (Adapted from Waterham et al., 2016).

1.4 Peroxisome Maintenance and the Function of Pex3

In *S. cerevisiae*, the morphology and quantity of peroxisomes are controlled by four key processes: fission, *de novo* formation, pexophagy, and inheritance (Fig. 1.8). While there are some claims suggesting that peroxisome *de novo* formation happens in all cells (VanDer Zand et al., 2012; Kimet al., 2006), most studies in yeast suggest that peroxisome multiplication primarily relies on growth and fission, with *de novo* pathway occurring when a cell lacks pre-existing peroxisomes (Knoblach et al., 2013; Motley and Hettema, 2007; Motley et al., 2015).

Pex3 is an extensively conserved peroxisomal membrane protein that exerts its influence on several genetically distinct peroxisomal functions via its bindings with diverse proteins. It functions as a central protein, coordinating various processes including membrane protein import, retention biogenesis and pexophagy (Fig. 1.9). The involvement of Pex3 in peroxisome biogenesis and the import of membrane proteins has been discussed in detail in Section 1.3.

Pexophagy is a selective autophagic breakdown of peroxisomes. It is critical for peroxisome turnover under nitrogen starvation conditions (Hutchins et al., 1999; Klionsky, 1997). Pexophagy necessitates the binding between Atg36 and Pex3 in *S. cerevisiae* (Atg30 in *Pichia pastoris*). Atg36 is the peroxisomal receptor for autophagy that interacts with autophagy machinery components Atg11 and Atg8. Atg36 (or its orthologue Atg30 in Pichia pastoris) functions as a specific pexophagy adaptor. It plays a crucial role in linking peroxisomes to the autophagic machinery by interacting with Atg8 and Atg11 (Motley et al., 2012; Burnett et al., 2015). The binding of Atg11 and Atg36 relies on the Atg36 phosphorylation by Hrr25. However, the precise processes regulating the interaction of Pex3–Atg36 are currently unknown (Tanaka et al., 2014).

Pex3 also acts as a critical key in the retention of peroxisomes during cell division and is involved in the peroxisome position at the cells' cortex, a topic which will be further discussed in more detail in Section 1.5.

In addition to the contribution of Pex3 in peroxisome retention, Pex3 was found to be involved in the inheritance of peroxisomes. In *Yarrowia lipolytica*, which is a unique yeast because it carries both Pex3 and its paralogue called Pex3B. Pex3 and Pex3B interact with the classV MyosinV. In this way they function as peroxisome specific myosin receptors that assist in the peroxisome movement to the daughter cells through the asymmetric division. Furthermore, the *Y. lipolytica* Pex3 and Pex3B have the ability to interact with ScMyo2 (a class V myosin in *S. cerevisiae*), indicating that Pex3 and Pex3B may function as a counterpart of *S. cerevisiae* Inp2. Notably, the homologue of the S. cerevisiae Myo2p receptor, Inp2p, is not readily identifiable in *Y. lipolytica* (Chang et al., 2009).

A recent study demonstrated that Pex3 in *Hansenula polymorpha* plays a role in forming contact sites between vacuoles and peroxisomes, particularly during the rapid growth of peroxisomes. Specifically, when the organism was grown on methanol, Pex3 was observed to accumulate at sites where peroxisomes make contact with the vacuole. Interestingly, the overexpression of Pex3 led to forming of contact sites between vacuoles and peroxisomes even in states where such sites are not typically present (Wu et al., 2019). The exact mechanism of how Pex3 binds to the membrane of vacuoles is currently unknown.

Nonetheless, this finding highlights a further function of Pex3 in the formation of organelle contact sites, which will be further described in Section 1.6.

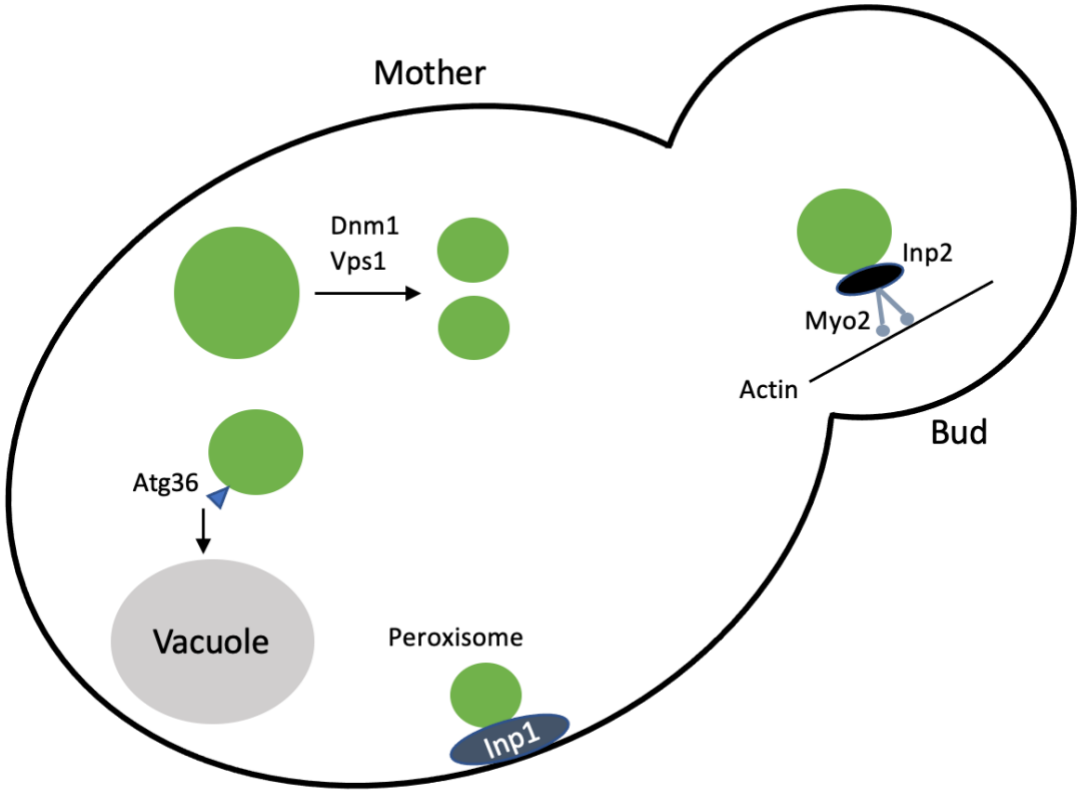

Figure 1. 8: Regulation of Peroxisome Dynamics in *S. cerevisiae*. Peroxisomes are regulated through various processes, including fission, segregation, and pexophagy. These mechanisms ensure the proper maintenance and turnover of peroxisomes within the cell. Fission: The proteins Vps1 and Dnm1 contribute to the fission of peroxisome, leading to an increase in peroxisome quantity. Pexophagy: The activation of Atg36 triggers pexophagy, a selective degradation process in which peroxisomes are directed to the vacuole for breakdown. Peroxisome retention and inheritance: During the asymmetric growth and division of the cell, two proteins, Inp1 and Inp2, play important roles. Inp1 is involved in tethering peroxisomes to the mother cell periphery, ensuring the retention of peroxisome. Inp2 recruits the Class V Myosin Myo2, facilitating the transfer of peroxisomes across actin filaments to the growing bud, enabling their inheritance.

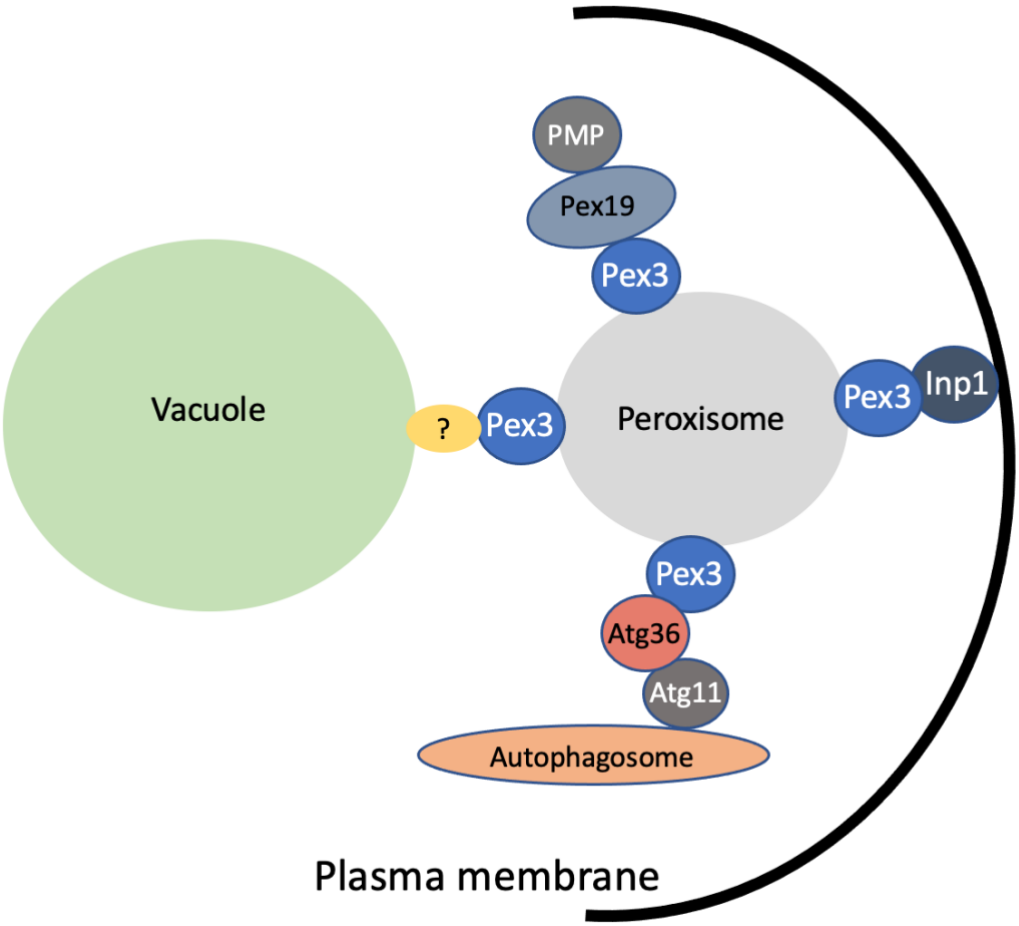

Figure 1. 9: Pex3 plays multiple functions in the biology of peroxisomes. The schematic diagram depicted Pex3 roles. These include its involvement in peroxisome membrane import facilitated by Pex19, the retention of peroxisomes mediated by Inp1, pexophagy regulated by Atg36, as well as the formation of vacuole-peroxisome contact sites through factors that are currently unidentified. (Adapted from Wu et al., 2019).

1.5 The inheritance of organelles

One of the fundamental characteristics of eukaryotes is the presence of membrane bound organelles within their cells. While these lipid-encased structures include multiple chemical microenvironments, they have grown to coexist and continue to fulfill a variety of particular activities. Cellular processes depend on the entire complement of organelles. The presence of genetic material-containing organelles, such as the nucleus and mitochondria, is crucial for cellular survival. The generation of these organelles is not possible *de novo*, thus necessitating their inheritance from pre-existing organelles. Conversely, some organelles can emerge *de novo* like peroxisomes and vacuoles, but compared to the replication and partition of pre-existing organelles, this is not energetically favourable. As a result, cells employ diverse molecular processes to strictly control the partition of organelles between two daughter cells throughout the process of cell division (Nunnari and Walter, 1996; Knoblach and Rachubinski, 2015; Warren and Wickner, 1996).

In the budding yeast *S. cerevisiae*, asexual reproduction is characterized by the asymmetric growth and division of the cell. The simultaneous activities of transporting organelles from the mother to the developing bud and retaining them there during cell growth contribute to the predetermined equity of organelle content that is inherited during cell growth. As a result, *S. cerevisiae* has emerged as a key example organism for understanding the fundamental molecular processes that manage organelle segregation.

The classV myosin proteins Myo2 and Myo4 are part of the machinery that transports organelles. The hydrolysis of ATP powers these myosin motors. The C-terminal cargo-binding domains (CBDs) of Myo2 and Myo4 have the capability to bind to receptors present on the organelles, and they use their N-terminal domains to transport organelles along actin cables (Sellers and Veigel, 2006; Knoblach and Rachubinski, 2015). Myo2 is a vital protein in the development of cells, whereas Myo4 does not exhibit the same level of significance. Most organelles, including nuclei, mitochondria, peroxisomes, Golgi bodies, vacuoles, lipid bodies and secretory vesicles, are delivered via Myo2. A subset of mRNAs and cortical ER (cER) are transported by Myo4 (Knoblach and Rachubinski, 2015).

Actin in yeast

Actin, a highly conserved protein across species, plays a fundamental role in cellular biology. In *S. cerevisiae*, actin is a linchpin of cellular processes, orchestrating a wide array of functions, including cell division, cytoskeleton organization, intracellular transport, and polarized growth. The dynamic properties of actin, particularly its ability to polymerize and depolymerize rapidly, underpin its versatility in responding to diverse cellular demands.

Understanding the intricacies of actin function in *S. cerevisiae* has been a longstanding pursuit in cell biology. Central to this endeavor is the utilization of mutant libraries, a valuable resource that allows researchers to probe the functional consequences of specific genetic alterations. In this context, Wertman et al. (1992) made seminal contributions by embarking on the systematic construction and characterization of a synoptic set of site-directed mutations distributed throughout the single actin gene of *S. cerevisiae*.

Wertman et al. (1992) meticulously designed their study by targeting charged residues within the actin protein's primary sequence, particularly those forming clusters of two or more charged residues. These charged residues, crucial for the protein's electrostatic interactions, were systematically replaced with alanine. The resultant mutations were then thoroughly examined in yeast.

Their findings were compelling. Out of the 36 constructed mutations, 34 were successfully recovered in yeast as heterozygous diploids, forming a rich repository of actin variants with distinct properties. The ensuing analysis revealed a diverse array of mutant phenotypes, including 11 recessive lethal mutations, 16 conditional-lethal mutations (encompassing temperature-sensitive and salt-sensitive phenotypes), and 7 mutations with no discernible impact on actin function (Fig. 3.10). Notably, Wertman and colleagues suggested that the two mutations that could not be recovered in yeast might harbor dominant defective phenotypes, highlighting the importance of their future investigation. This will be discussed in detail in Section 3.6, including the mutants used in this study.

1.5.1 Peroxisome inheritance

Proper inheritance of peroxisomes is achieved through a delicate balance between Myosin-dependent transport to the developing bud and cortical anchoring in the parent cell. This balance is crucial for the correct distribution and positioning of peroxisomes during cell growth and division.
The proteins Inp1 and Inp2 play direct functions in the inheritance of peroxisomes (Fig 1.8). The Pex3–Inp1 interaction is of particular importance in retaining a specific population of peroxisomes during the process of asymmetric cell division. It also contributes to the accurate positioning of peroxisomes within the parental cell (Munck et al., 2009; Fagarasanu et al., 2005; Knoblach et al., 2013).

The Inheritance of peroxisomes 1 (Inp1) is a peroxisomal peripheral membrane protein. The initial indication that it was involved in peroxisome retention came from the fact that cells lacking Inp1 exhibit an abnormal peroxisome distribution, with practically all of them located in the bud cell. On the other hand, when Inp1 is overexpressed, almost all peroxisomes are confined to the parent cell (Fagarasanuet al., 2005). Inp1 is recruited to peroxisomes through a direct interaction with Pex3. This interaction has been observed to occur independently of peroxisome biogenesis, as mutants of Pex3 retaining functionality in peroxisome biogenesis still show defects in peroxisome inheritance (Munck et al., 2009). However, recent studies from the Rachubinski research group have raised questions about the clarity of this concept. It is now proposed that the tethering between the endoplasmic reticulum and peroxisomes likely involves additional factors at the cortical level. The group is suggested that Inp1 may serve as a tether not only among peroxisomes but also between peroxisomes and other organelles. Furthermore, it is speculated that interactions between peroxisomes and the ER might work without assistance of Inp1 (Knoblach and Rachubinski, 2019).

A recent study by the Hettema lab has identified Inp1 to be the first recognized tether that links the plasma membrane with peroxisomes. As a contact site tether protein, Inp1 satisfies the predetermined requirements. A plasma membrane peroxisome tether (PM-PER) can be formed by Inp1 because it is structurally and functionally capable of interacting with both the

peroxisomal membrane and the plasma membrane and can be found in the appropriate subcellular site. Additionally, it has been demonstrated that Inp1 contributes to the retention of peroxisomes through its N-terminal region, which interacts with phosphatidylinositol 4,5-bisphosphate (PI(4,5)P2), and its C-terminal domain, which facilitates binding to Pex3. This establishes a physical linkage between the plasma and peroxisomal membranes (Fig. 1.8) (Hulmes et al., 2020).

The transportation of peroxisomes from the mother cell to the growing bud is promoted by the presence of Inp2. Inp2 is a key component of the peroxisomal membrane, being an integral protein that opposes Inp1 in function (Fagarasanu et al., 2006). It acts as a dedicated receptor on peroxisomes for the Myo2 (a classV myosin). Myo2 is an actin motor protein that interacts with Inp2 through its C-terminus, facilitating the specific transport of peroxisomes to the developing bud through actin cables (Fig. 1.8) (Sellers and Veigel, 2006; Hoepfner et al., 2001; Knoblach and Rachubinski, 2015; Fagarasanu et al., 2006). The loss of *inp2* results in a delayed peroxisome inheritance, leading to buds that lack peroxisomes resulting in peroxisome-free buds. However, when Inp2 is overexpressed, it leads to a lacking of peroxisomes in parent cells, where all peroxisomes are transferred into the bud (Fagarasanu et al., 2006). The peroxisome population remains in the parent cell through tethering to the cortex of the parent cell. Furthermore, once peroxisomes are transported to the growing bud cortex, they are anchored to it in a process dependent on Pex3 and Inp1 proteins, preventing them from returning to the parent cell (Fagarasanuet al., 2005). In addition, it has been reported that Pex19 promotes the peroxisome transport from the mother cell to the developing bud by interacting with Inp2. Moreover, in *H. polymorpha*, the interaction between Inp2 and Myo2 requires the presence of Pex19, which is indeed essential (Saraya et al., 2010; Otzen et al., 2012).

It has been possible to discriminate between the locations of the peroxisomal proteins Inp2 and Inp1 throughout cell growth and fission in the double mutant strain *Δvps1Δdnm1*. The scission of peroxisome in these cells is absent, resulting in tubular or 'sausage shaped' peroxisome. Inp1 is located at the elongated end of the maternal peroxisome, while Inp2 is located at the peroxisome tip within the budding region (Knoblach et al., 2013). Further deletion of either *INP1* or *INP2* alters the peroxisomes' position and shape (Motley and Hettema, 2007). It has been suggested that the peroxisome inheritance and fission are connected according to the previously mentioned model (Knoblach et al., 2013) (Fig. 1.10).

During asymmetric cell division, the efficient movement of peroxisomes towards the developing bud and their cortical tethering are crucial for ensuring proper maintenance of the peroxisomal population. Inp1 and Inp2 play crucial roles in the positioning and timing of peroxisome distribution, as they are involved in maintaining appropriate peroxisome segregation across the mother-daughter axis. They perform antagonistic functions that contribute to the precise localization of peroxisomes throughout the process of cell division (Fagarasanu et al., 2006; Fagarasanu et al., 2005).

1.5.2 Mitochondrial inheritance

During every cell division, multiple pathways are used to ensure mitochondria partition. Similar to other organelles, mitochondria are actively transported to the growing bud throughout asymmetric cell growth in *S. cerevisiae* along the actin cables (Simon et al., 1997). Directed mitochondrial movement also requires the association of Arp2 with mitochondria. The actin related protein Arp2 is an essential part of the Arp2/3 complex, known to act as a nucleation site for the actin filament formation (Fehrenbacher et al., 2004; Boldogh et al., 2001). Both Mmr1 and Ypt11 interact with Myo2 and are redundant in the transport function. Mmr1 is a protein that is located on the peripheral membrane, and Ypt11 is a Ras-related GTPase. In *Δmmr1Δypt11* cells, mitochondrial inheritance is fully eliminated which results in cell death (Itoh et al., 2004; Chernyakov et al., 2013; Itoh et al., 2002). For mitochondrial retention through anchoring in the mother cell, there are three known mechanisms these are Num1 protein, Mfb1 protein and the ERMES complex which are all crucial components of the anchors. The PH domain (pleckstrin homology) of Num1 is critically involved in anchoring mitochondria at the cell cortex. This tethering process is facilitated by the Num1–Mdm36 interaction (Knoblach and Rachubinski, 2015; Ping et al., 2016). The ERMES complex is formed of four core mitochondrial components (Mmm1, Mdm10, Mdm12, and Mdm34). Mitochondria is connected to the cortical ER through the ERMES (Knoblach and Rachubinski, 2015). Moreover, Mfb1 is essential for preserving optimal mitochondrial functionality specifically at the tip of the mother cell (Pernice et al., 2016).

1.5.3 Inheritance of the vacuole and other cellular organelles

Vacuoles of yeast correspond to lysosomes in higher eukaryotes and have diverse functions, including playing a role in the cell cycle, degradation, and nutrient storage (Jin and Weisman, 2015). During the G1 phase, vacuoles undergo a process of segregation, forming distinct structures that are subsequently transported from the tip to the developing bud through the action of Myo2 motors. The movement of vacuoles relies on the interaction between Myo2 and Vac17, the receptor protein that binds Myo2 to the vacuole (Peng and Weisman, 2008; Legesse-Miller et al., 2006). When the vacuole reaches the bud tip, the protein Vac17 undergoes degradation, leading to the release of vacuoles into the bud cell by the Myo2 protein (Tang et al., 2003; Yau et al., 2017). Additionally, Vac8 is vital for the maintenance and proper functioning of vacuoles. It forms an interaction complex with both Vac17 and Myo2, known as the vacuole carrier complex (Tang et al., 2003; Yau et al., 2017). The loss of *VAC8* leads to the blocking of vacuole inheritance (Wang et al., 1998). The cell cycle stops in the G1 phase in cells with an inherited deficiency until a vacuole forms *de novo* in the bud. *De novo* vacuole formation requires Pep12 and Vps45 proteins (Jin and Weisman, 2015).

Myo2 is also involved in the transportation of secretory vesicles to the site where the bud is growing (Johnston et al., 1991). Interactions with proteins such as Ypt31, Ypt32, Sec4, and Sec15 regulate the polarized movement of these vesicles (Lipatova et al., 2008; Jin et al., 2011).
Ypt11 contributes to mitochondrial and late Golgi element inheritance (Arai et al., 2008; Itoh et al., 2002; Chernyakov et al., 2013). The binding of Ypt11 and the Golgi protein Ret2 is essential for the accurate division of the Golgi apparatus (Arai et al., 2008).

The transportation of lipid droplets to the developing bud, similar to other organelles, relies heavily on Myo2 (Knoblach and Rachubinski, 2015). Nonetheless, the specific Myo2 receptors present on these lipid droplets remain unidentified.
Myo4 is essential for delivering the cortical ER and mRNAs to the developing bud (Estrada et al., 2003; Bobola et al., 1996). She3 functions as an adapter for Myo4 in both cases, making She3 critical to the transport of cortical ER and mRNA. In addition to She3 role, She2 is also needed for the transfer of mRNAs. She2 interacts with certain mRNAs, which makes the She3-Myo4 complex more likely to recognise them (Estrada et al., 2003; Bohl et al., 2000; Long et al., 2000; Takizawa and Vale, 2000).

The process of mitosis in budding yeast involves the equal division of duplicate nuclear chromosomes between the mother cell and its daughter. The Spindle Pole Body (SPB), which is replicated before the onset of nuclear inheritance, serves as a centre for organising microtubules (Adams and Kilmartin, 2000; Yamamoto et al., 1990). The duplicating SPBs play a crucial role in aligning the mitotic spindle across the axis of cell polarity. Moreover, the proper alignment of the spindle and subsequent nuclear inheritance require both Dyn1, a microtubule-based motor protein, and Kar9, a Myo2 receptor (Hwang et al., 2003; Eshel et al., 1993; Miller and Rose, 1998; Li et al., 1993). In contrast to other organelles, actin and the microtubule cytoskeleton are needed for nuclear inheritance. Kar9 connects astral microtubules and actin filaments, whereas Dyn1 requires association with microtubules to work. The interaction between Myo2 and Kar9 guides the microtubules from the cell center to the cell cortex, across the actin filaments. Kar9 localization along microtubules requires the microtubule-binding protein Bim1 (Miller et al., 2000; Beach et al., 2000; Miller and Rose, 1998).
The spindle position (SPOC) and the spindle assembly (SAC) checkpoints monitor the chromosomal segregation process to ensure accuracy (Caydasi and Pereira, 2012). The SAC is activated when the microtubules are unable to establish a bipolar attachment to the kinetochores during metaphase stage before cells enter the anaphase stage (Musacchio and Salmon, 2007). Conversely, during the anaphase stage, the SPOC prevents cells from undergoing mitotic exit if the alignment of the spindle deviates from being parallel to the cellular polarity axis (Caydasi et al., 2010).

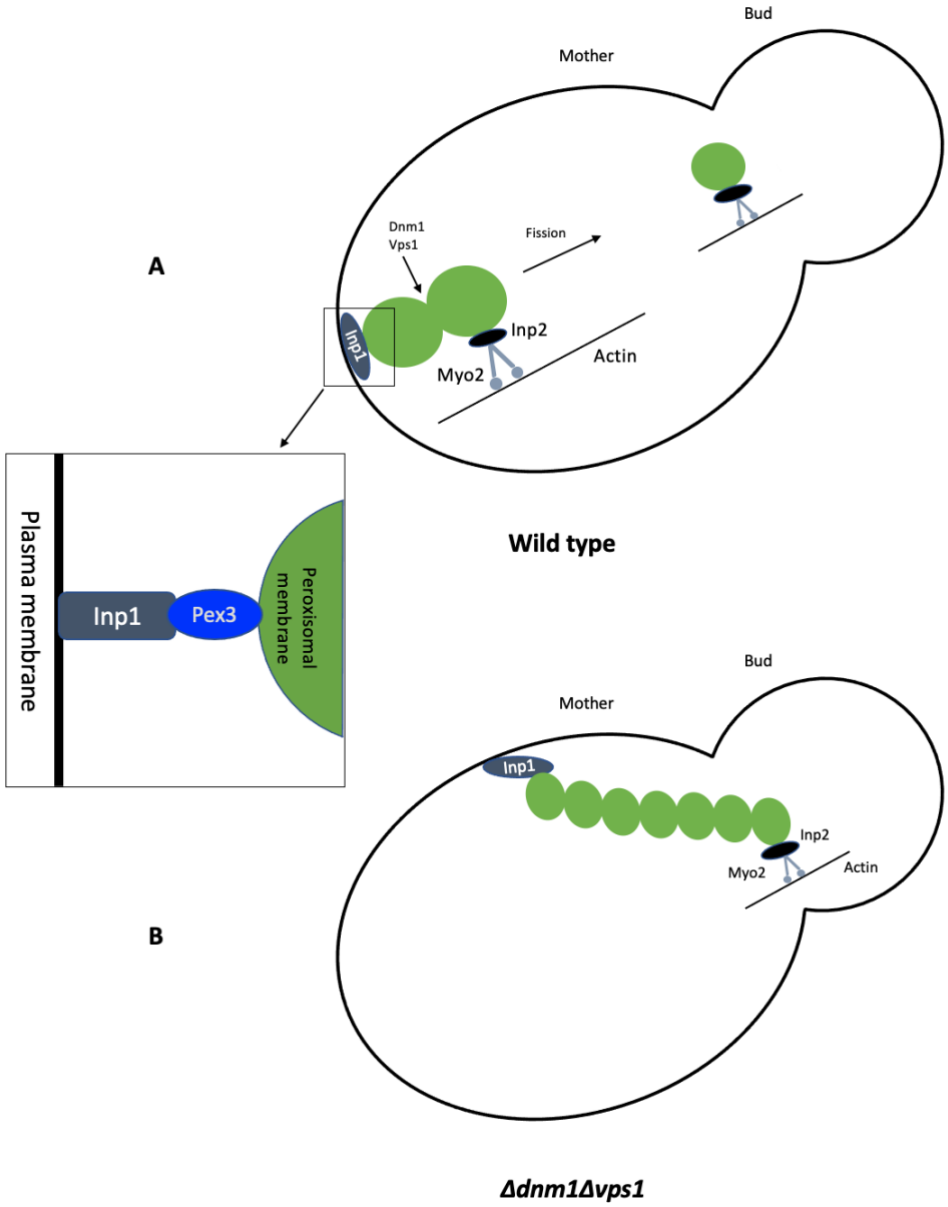

Figure 1. 9: The current model of the retention and inheritance of peroxisomes. A) In wild-type cells, the peroxisome transportation to the growing bud relies on Inp2, the Myo2 receptor. The C-terminal domain of Myo2 interacts with Inp2, facilitating the transport of peroxisomes to the bud via actin cables, while the retention of peroxisomes occurs via Inp1which acts as a linkage between the plasma and peroxisomal membranes. Inp1 binds to the plasma membrane via its N-terminal region and Pex3 via its C-terminal region. B) In *Δdnm1Δvps1* cells, fission is inhibited leading to both transport and retention machineries competing for the same peroxisome. As a result, the peroxisome becomes anchored at the bud neck and undergoes division during cytokinesis.

1.6 Organelle contact sites

Eukaryotic cells are distinguished by their compartmentalization into distinct organelles bound by membrane, which results in a diverse array of micro–environments and enhances the effectiveness of subcellular processes. However, this organizational framework also indicates the presence of actual physical barriers that can hinder the movement of molecules within the cell. Studies using electron microscopy in the middle of the 20th century discovered that organelles were commonly located in close proximity to one another with distinct specific points of contact (Copeland and Dalton, 1959; Bernhard and Rouiller, 1956; Gray, 1963). These studies provided initial evidence suggesting that organelles can establish direct communication with each other. Nevertheless, the prevailing belief at that time was that the main mechanisms for inter-organellar exchange of cellular components were active transport, diffusion, and trafficking of vesicles in the cytosol. Yet, it is now more evident that organelles do not exist in isolation. Instead, frequent physical interactions among organelles occur, facilitated through membrane contact sites (MCS), which promote cross-membrane communication and enhance organelle functionality. Contact sites between membranes can be described as localized regions where the lipid bilayers of two distinct intracellular compartments are bound together through lipid or protein interactions, consequently impacting the functionality of either or both organelles (Prinz, 2014 and 2020; Shai et al., 2018). As per current knowledge, each organelle maintains a minimum of one operational MCS with another organelle, and most of them even possess multiple (Shai et al., 2018; Valm et al., 2017).

Membrane contact sites exhibit a diverse array of characteristics. The distance separating the organelles can either remain constant or fluctuate, and in instances of variability, the span between two organelles can be notably vast. For example, the gap between the endoplasmic reticulum and the plasma membrane at membrane contact sites in *S. cerevisiae* can extend anywhere from 16 to 60 nanometers (West et al., 2011). In their study, West et al. (2011) investigated membrane contact sites between the ER and the PM in Saccharomyces cerevisiae using advanced imaging techniques. They observed a unique domain of the ER, called pmaER, closely apposed to the PM. Distance measurements showed variations between 16 to 60 nanometers, confirming the variability in these contact sites. The stability of these contact sites also differs greatly; some persist throughout the cell's entire lifespan, while others are markedly ephemeral, enduring less than a second (Lewis et al., 2016). Certain organelles simultaneously share several physically and functionally different membrane contact sites. For example, it has been observed that distinct interaction sites between the PM and the ER coexist, enabling functionally diverse processes like store-operated calcium entry (SOCE) and cholesterol exchange (Besprozvannaya et al., 2018).

There are some instances of multi-way organelle contact sites, demonstrating that membrane contact sites can involve interactions among more than two distinct organelles. As an illustration, the ER is found at the points of contact between mitochondria and PM as an element of the multisubunit complex known as mitochondrial ER cortical anchor (MECA) (Lackner et al., 2013). Moreover, it has been suggested that in *S. cerevisiae*, the ER protein Mdm1 binds to both the vacuole and lipid droplets to form a three way junction among these organelles (Hariri et al., 2019). Intraorganellar membrane contact sites are an additional kind

of MCS. Atlastin, a membrane-anchored GTPase, has been discovered to function as a tether protein in the ER, forming connections within the ER (Wang et al., 2016).

The functions of membrane contact sites are known to be diverse, encompassing a range of processes such as metabolic non-vesicular movement, including the exchange of lipids, as well as cell communication and signaling pathways. Intracellular lipid movement is promoted by lipid transfer proteins (LTPs), which promote non-vesicular lipid exchange. LTPs are typically found in high abundance within membrane contact sites and interact with MCS associated proteins. Lipid exchange at membrane contact sites helps shift the lipid composition of certain organelles or membranes. It also has a role in the regulation of lipid-centric signalling pathways, which includes phosphoinositide (PI) signaling at the interface between the endoplasmic reticulum and plasma membrane (Murley et al., 2015; Osman et al., 2011). These contact sites can function as communication centers in the presence of any environmental triggers like nutrition or stress. The ER is responsible for the production of phosphatidylinositol. However, the kinases responsible for converting it into phosphoinositide (such as PI4P or PI(4,5)P2) are also found in other organelles, including the Golgi and the plasma membrane (Walch-Solimena and Novick, 1999; Agranoff et al., 1958; Audhya and Emr, 2002). As a result, the establishment of membrane contact sites between other organelles and the ER allows for the production or depletion of different amounts of PI, depending on the needs of the cell (Kim et al., 2011). Ultimately, these phosphoinositides play diverse roles in cellular processes, including endocytosis, cell signaling, vesicular transport and modulation of ion channel activity (Dickson and Hille, 2019; Balla et al., 2009).

MCS play a vital role in facilitating the active exchange of metabolites, including calcium ions, between various organelles (Hirve et al., 2018). This process amplifies reaction speeds and minimizes metabolite leakage into the extracellular space surrounding the cell. A prominent model is store-operated calcium entry (SOCE), wherein extracellular calcium ions are directed straight into the endoplasmic reticulum (ER) lumen via the plasma membrane at ER-PM contact sites in response to diminished calcium levels within the ER (Hirve et al., 2018). Additionally, the accumulation of ER calcium channels at ER and mitochondria contact sites leads to elevated calcium concentrations at these points, boosting the effectiveness of metabolite interchange between these two organelles (Csordás et al., 2010; Rizzuto et al., 1993).

1.7 Positioning and tethering of organelles

1.7.1 Mitochondrial tethering

In *S. cerevisiae*, MCSs have emerged as crucial regulators for the retention and inheritance of organelles, including mitochondria, peroxisomes, and lipid droplets. At least three known MCSs play a role in the proper positioning of mitochondria at the cell periphery during asymmetric cell division. The mitochondrial endoplasmic reticulum cortex anchor (MECA), multisubunit tethering complexes, is responsible for cortical mitochondrial anchoring (Lackner et al., 2013). The main constituent of the MECA complex is Num1, a protein linked to the cell cortex, which interacts with both the mitochondrial outer membrane and the plasma membrane through unique lipid binding regions (Ping et al., 2016; Lackner et al.,

2013). Despite reports that MECA serves as a tether connecting more than two membranes, the specific molecular processes governing its connection with the ER are not yet fully understood. Further evidence implicating the plasma membrane to mitochondrial tethering comes from Mfb1-mediated site-specific mitochondrial anchoring at the mother cell tip (Pernice et al., 2016). Within the growing bud, the mitochondrial outer membrane protein Mmr1, which acts as a Myo2 receptor, facilitates endoplasmic reticulum mitochondria membrane contact sites to anchor the mitochondria at the tip of the budding cell (Swayne et al., 2011). The diverse contact sites among mitochondria, ER, and PM guarantee that active organelles can be preserved within the parent cells and passed down to the buds.

1.7.2 Peroxisome contact sites

Peroxisome – ER MCS

In mammals, the endoplasmic reticulum is known to harbour the highest number of peroxisome contact sites, facilitating contact with nearly all peroxisomes (Valmet al., 2017). As mentioned previously, the tethers that link peroxisomes and the ER in mammals are VAMP, comprising two distinct subtypes of VAPA and VAPB which engage with the FFAT motif present in ACBD4/5 (Costello et al., 2017a; Loewen and Levine, 2003; Costello et al., 2017b; Hua et al., 2017). The disturbance of the ER tethers significantly impacts cholesterol maintenance, plasmalogen synthesis, and beta-oxidation. This indicates the important role of peroxisome-ER contact in lipid transportation (Yagita et al., 2017; Hua et al., 2017).

Numerous instances of contact sites between peroxisome and ER membranes have been recognised in yeast. One of these MCSs is responsible for peroxisome retention and is dependent on the presence of Inp1–Pex3 interaction, as discussed in Section 1.5.1. In *S. cerevisiae*, the connection between peroxisomes and the ER is facilitated by the family of Pex23 proteins, including Pex29 and Pex30. These proteins establish a complex with Yop1 and Rtn1, members of the reticulon family that play a role in ER structure, resulting in the formation of contact sites between peroxisome and the ER, commonly referred to as EPCON (Joshi et al., 2018). During growth on glucose, the specific domains on the ER that host Pex30 and Pex29 proteins actively link to peroxisomes, and this association becomes stable when growing on oleate. It has been proposed that the EPCON, ER-Peroxisome Contact site, is involved in the peroxisome *de novo* formation (Mast et al., 2016; David et al., 2013; Wang et al., 2018; Joshi et al., 2016; Joshi et al., 2018). Analogous findings have been reported in *H. polymorpha*, where the family of Pex23 proteins Pex24 and Pex32 were shown to act as tethers facilitating ER-peroxisome contact sites. The deletion of *PEX24* and *PEX32* has been found to interrupt the peroxisome-ER interactions, thereby disrupting peroxisome biogenesis and the standard typical peroxisomes distribution between parent and daughter cells (Wu et al., 2020).

Table 1. 2 - Comparison of Pex23 family proteins in *S. cerevisiae* and *H. polymorph* (Kiel et al., 2006; Wu et al., 2020).

S. cerevisiae	Known functions	References	*H. polymorph*	Known functions	References
Pex28	A complex comprising proteins containing the reticulon	(Vizeacoumar et al., 2004)	Pex23	Proteins localize to the ER and establish	(Wu et al., 2020)
Pex29			Pex24		
Pex31			Pex32		

	homology domain establishes peroxisomes-RE contact sites			peroxisome–ER contact sites	
Pex32			-		
Pex30	Regulates peroxisome *de novo* pathway	(David et al., 2013)	-		

Peroxisome - Mitochondria MCS

Peroxisomes and mitochondria collaborate closely together in the process of Fatty acid β-oxidation. They also participate in proteins that are necessary for their respective division machinery. Thus, this interaction emphasises the requirement for a close physical connection between the two organelles (Schrader et al., 2012). Locations in close contact between mitochondria and peroxisomes have been discovered in mammalian cells and *S. cerevisiae*, with the presence of multiple tethering complexes hypothesized in *S. cerevisiae* (Fan et al., 2016; Shai et al., 2018).

Distinct tether complexes are proposed to exist for Pex34, a peroxisomal membrane protein, and Fzo1, a mitochondrial outer membrane protein. These complexes are more prevalent in mitochondria–peroxisome MCS, and an increase in their expression leads to an augmented number of contact points between these two organelles. The identities of the specific proteins that interact with them, however, are yet unknown. Associations between mitochondria and peroxisomes enable effective transfer of metabolites to improve metabolic processes. Pex34 is believed to facilitate the transfer of fatty acid beta-oxidation intermediates between mitochondria and peroxisomes (Shai et al., 2018). Furthermore, it has been proposed that the membrane contact sites (MCS) between mitochondria and peroxisomes in mammalian cells enable the interorganellar exchange of metabolites involved in steroid metabolic pathway (Fan et al., 2016). Pex11 binds directly to Mdm34 indicating a possible tether between mitochondria and peroxisomes. Mdm34 is a member of the ERMES complex, endoplasmic reticulum -mitochondrial encounter structure (Usajet al., 2015). Moreover, Pex11 is known to interact with Fis1, an essential protein for the fission of both mitochondrial and peroxisomal. This suggests that the complex of MCS, Pex11, and Mdm34 may have a function in the scission of peroxisome (Joshi et al., 2012; Koch et al., 2010).

Peroxisome – Vacuole and Lipid droplets MCS

Through the use of split-GFP technology in *S. cerevisiae*, researchers have discovered the presence of MCSs between peroxisomes and vacuoles (Kakimoto et al., 2018; Shai et al., 2018). In the yeast *Hansenula polymorpha*, these MCS are further defined, and Pex3 is suggested to act as a significant protein in the creation of contact sites between vacuoles and peroxisomes (Wu et al., 2019).

For lipid droplets, it has been demonstrated that yeast growth on oleate increases peroxisome proliferation and raises the quantity and stability of contact sites between peroxisomes and lipid droplets (Binns et al., 2006). It is believed that the major purpose of communication between these two organelles is to transfer lipids. Lipid droplets form close

contacts with peroxisomes not only in fungi but also in plants and mammals (Chen et al., 2020; Esnay et al., 2020).

1.8 Aims

The Hettema lab originally revealed the molecular binding between Pex3 and Inp1 (Munck et al., 2009), and the existing model of peroxisome retention mediated by the Pex3–Inp1 complex was established in 2013 (Knoblach et al., 2013). A recent study by Rachubinski (2019) has cast doubt on the widely accepted model of ER-peroxisome tethering. The study's results suggest the existence of regulatory cues influencing ER-peroxisome tethers, and they propose the presence of membrane contact sites between peroxisomes and other organelles besides the ER. Interaction analysis with Inp1p mutants revealed that Pex3p and Inp1p are not the sole components of the ER-peroxisome tether. Deletion of these Inp1p interactors, whose steady-state localization lies outside of ER-peroxisome tethers, had an impact on peroxisome dynamics. These findings imply the involvement of additional factors beyond Pex3p and Inp1p in this process, challenging the current understanding and necessitating further research to uncover the intricate interactions governing peroxisome dynamics. Rachubinski's proposal suggests that Inp1 might serve as a key linker between peroxisomes and other organelles within the cell. In 2020, the Hettema lab introduced a novel model for the retention of peroxisomes during asymmetric cell division. They delivered evidence demonstrating that Inp1 functions as a tethering protein at MCS between the plasma membrane and peroxisomes (Hulmes et al., 2020), instead of the ER-peroxisome contacts proposed by Rachubinski group.

Similar results to Inp1 function *in S. cerevisiae* have been shown in *H. polymorpha*. In this study, it has been found that the N-terminal region of the Inp1 protein is vital for its binding with the plasma membrane, and the C-terminus is crucial for its binding to peroxisomes. Interestingly, they suggested that cortical Inp1 localization requires an intact actin cytoskeleton, as cells treated with latrunculin A (Lat-A), a depolymerizing agent for actin filaments, lose cortical Inp1 patches, particularly around the bud neck. Additionally, they showed that the middle region of Inp1 is necessary for its tethering function of peroxisomes to the plasma membrane (Krikken et al., 2020).

The initial aim of this study was to molecularly characterise the Inp1 protein. However, the data published about the Inp1 function in *S. cerevisiae* and *H. polymorpha* led to a more focused investigation to explore the Inp1 function as an actin-binding protein (Chapter 3). A second aim was to examine the precise role of Inp1's middle domain in its functionality, as the role of this part of the protein was still relatively unclear. Data obtained then led to further inquiry into the role of Srv2, which was found to interact with Inp1 on peroxisomes and to function as a factor controlling the peroxisome fission (Chapter 4).
A distinct avenue of research was undertaken prior to and during the COVID-19 pandemic. This aimed to establish an efficient genome modification approach to work with *D. hansenii*. This final chapter will discuss the use of the CRISPR system and a novel gene deletion method using PCR-mediated homologous recombination with short 50bp flanking regions.

Chapter 2 – Material and Methods

2.1 Chemicals and enzymes

The majority of chemicals, materials and primers used in this study were provided by MERCK. Buffers and restriction enzymes were provided by NEB (New England Biolabs). DNA polymerases, dNTPs and PCR buffers, were provided by Bioline UK. Gel extraction kits and miniprep kits were delivered by Qiagen.
D-Glucose was supplied by Fisher Scientific UK. Growth media components were provided by ForMedium and Difco Laboratories.
Protein work buffers were supplied by Geneflow. Equipment used for protein and DNA work was provided by BioRad.

2.2 Strains and plasmids

2.2.1 Strains

Table 2. 1 – The yeast strains used in this study. Gene modifications or deletions were performed following the protocol described in (Longtine et al., 1998).

Strain	Genotype	Source
BY4741 WT	MAT**a** his3-1 leu2-0 met15-0 ura3-0	Euroscarf
BY4742 WT	MAT**α** his3-1 leu2-0 lys2-0 ura3-0	Euroscarf
inp1Δ	BY4741 his3-1 leu2-0 met15-0 ura3-0 inp1::KanMX4	Euroscarf
srv2Δ	BY4741 his3-1 leu2-0 met15-0 ura3-0 inp1::KanMX4	Euroscarf
srv2Δ	BY4741 srv2::HIS3MX6	This study
pex27Δ	BY4742 pex27::kanMX4	Euroscarf
dnm1Δ	BY4742 dnm1Δ::kanMX4	Euroscarf
pex27Δdnm1Δ	BY4742 dnm1Δ::kanMX4 pex27Δ::hygro	Lab stock
pex27Δsrv2Δ	BY4742 pex27::kanMX4 srv2::HIS3MX6	This study
Δdnm1Δpex27Δsrv2	BY4742 dnm1Δ::kanMX4 pex27Δ::hygro srv2::HIS3MX6	This study
srv2Δdnm1Δ	BY4742 dnm1Δ::kanMX4 srv2::HIS3MX6	This study

Pex25Δ	BY4742 pex25::kanMX4	Euroscarf
Srv2/pex25Δ	BY4742 pex25::kanMX4 srv2::HIS3MX6	This study
Srv2-GFP	BY4741 *Srv2::Srv2-TAP-HIS3MX6*	(Ghaemmaghami et al., 2003)
Mvp1-GFP	SEY6210 Mvp1::Mvp1-GFP-HISMX6	(Robinson et al., 1999)
Pnc1-GFP	BY4741 Pnc1::Pnc1-GFP-HIS3MX6	(Ghaemmaghami et al., 2003)
Srv2-TAP	BY4741 Srv2::Srv2-TAP-HIS3MX6	(Ghaemmaghami et al., 2003)
pJ69-4A	MATa trp1-901, leu2-3,112, ura3-52, his3Δ200, gal4Δ, gal80Δ, LYS2::GAL1UAS-GAL1TATA-HIS3, GAL2UAS -GAL2 TATA -ADE2, met2::GAL7-LacZ)	(James et al., 1996)
pJ69-4α	MAT trp1-901, leu2-3,112, ura3-52, his3Δ200, gal4Δ, gal80Δ, LYS2::GAL1UAS-GAL1TATA-HIS3, GAL2UAS -GAL2 TATA -ADE2, met2::GAL7-LacZ	(James et al., 1996)

Table 2. 2 – The *E. coli* strains used in this study. The strain, genotype, usage and source of each E. coli strain are displayed.

Strain	**Genotype**	**Usage**	**Source**
DH5α	supE44 ΔlacU169 (Φ80 lacZ ΔM15) hsdR17 recA1 endA1gyrA96 thi-1 relA1	Plasmids amplification and plasmid DNA recovery from *S. cerevisiae* following *in vivo* homologous recombination	(Hanahan, 1983)
BL21 DE3	hsdS gal (λcIts857 ind1 Sam7 nin5 lacUV5-T7 gene1)	Expression of MBP fusion proteins	(Studier and Moffatt, 1986)

2.2.2 Plasmids

The table below (Table 2.3) shows the plasmids employed in this study, which were generated either through classical cloning and subsequent transformation into *E. coli* or through homologous recombination in *S. cerevisiae*. The plasmids Ycplac111 and Ycplac33 (Gietz and Sugino, 1988) were employed for expressing the plasmids in yeast cells, and the original vectors pET30a and pET42a (Rosenberg et al., 1987) were used for *E. coli* expression.

Table 2. 3 – Plasmids used in this study.

Plasmid name	Insert	Vector	Source
pAUL3	mNG-PTS1	YCplac33	Lab stock
pAUL4	mNG-PTS1	YCplac111	Lab stock
pAUL28	mRuby2-PTS1	YCplac111	Lab stock
pAUL52	MDH1-mRuby	YCplac33	Lab stock
pTA09	N terminus of Srv2	YCplac111	This study
pTA10	C terminus of Srv2	YCplac111	This study
pTA17	Srv2-GFP-Pex15	pJL001	This study
pTA18	Srv2-GFP	pEH126	This study
pAS5	GFP-Inp1	YCplac33	Lab stock
pEH12	*GFP-PTS1*	YCplac33	Lab stock
pGAD-C1	empty activation domain plasmid, LEU, CEN	pGAD	(James et al., 1996)
pGBD-C1	empty binding domain plasmid, TRP, CEN	pGBD	(James et al., 1996)
pTA19	Inp1 1-280	pGAD	This study
pTA20	Inp1 FL	pGAD	This study
pDA67	pGBD-ACT1 TRP1, CEN	pGBD	(Amberg et al., 1995)
pDA67	pGBD-ACT1-104 TRP1, CEN	pGBD	(Amberg et al., 1995)
pDA67	pGBD-ACT1-116 TRP1, CEN	pGBD	(Amberg et al., 1995)
pDA67	pGBD-ACT1-119 TRP1, CEN	pGBD	(Amberg et al., 1995)
pDA67	pGBD-ACT1-120 TRP1, CEN	pGBD	(Amberg et al., 1995)
pDA67	pGBD-ACT1-123 TRP1, CEN	pGBD	(Amberg et al., 1995)

pMAL-c5x	MBP	pMAL-c5x	Lab stock
pGH081	MBP-Inp1 1-100	pMAL-c5x	Lab stock
pGH129	MBP-Inp1 1-280	pMAL-c5x	Lab stock
pGH75	pInp1-Inp1 FL-ProtA	pLE106	Lab stock
pTA01a	gRNA targeting ADE2 gene	pCT-tRNA	This study
pTA01b	gRNA targeting GUT2 gene	pCT-tRNA	This study
pTA01c	*Candida famata* CfARS16	pCT-tRNA	This study

2.3 Growth media

The cell growth media were prepared by dissolving all the ingredients in Millipore water and autoclaved at 121˚C. Amino acid stocks or antibiotics were included in the media at their final concentrations when these were required. The growth media reagents are listed in Table below.

Table 2. 4 – Growth media.

Culture Media	Description
2TY	1% yeast extract, 1.6% Bacto-tryptone, 0.5% NaCl. Ampicillin was added to autoclaved media at final concentrations of 75g/ml when required. (2% (w/v) agar was added to liquid growth media for solid media).
YPD	2% D-Glucose, 2% Bacto-peptone, 1% yeast extract. (2% (w/v) agar was added to liquid growth media for solid media).
Yeast minimal medium 1 (YM1)	0.5% ammonium sulphate, 0.17% yeast nitrogen base (without amino acids and ammonium sulphate), 2% D-Glucose, raffinose or galactose. Adjusted to pH 6.5. (2% (w/v) agar was added to liquid growth media for solid media).
Yeast minimal medium 2 (YM2)	0.5% ammonium sulphate, 0.17% yeast nitrogen base (without amino acids and ammonium sulphate), 2% D-Glucose, raffinose or galactose, 1% casamino acids. Adjusted to pH 6.5. (2% (w/v) agar was added to liquid growth media for solid media).
Amino acid stocks	The following amino acids were added to YM1 and YM2 medium as needed; 100x stocks (0.2% histidine, 0.3% leucine, 0.3% lysine, 0.2% methionine, 0.2% tryptophan, 0.2% uracil)

2.4 *S. cerevisiae* protocols

2.4.1 Yeast growth and maintenance

YPD, YM1 or YM2 media were used to grow all yeast strains at 30˚C. For liquid media, samples were placed on an oscillating shaker at 200 rpm. For auxotrophic strains, amino acids and uracil were supplemented as needed. To induce gene expression from the GAL1/10 promoter, cells were cultured in a selective medium containing 2% raffinose overnight. Subsequently, cells were shifted to a medium containing 2% YM2 galactose. To ensure long-term storage, cells were cultured overnight, and glycerol stocks with a concentration of 15% v/v were prepared. These stocks were then stored at -80°C in cryogenic vials (Nunc). The yeast two hybrid screens: strains that carry activation domain constructs and binding domain constructs were crossed by mating and diploid strains were then selected on selective media.

2.4.2 One step transformation

Plasmids were transformed in yeast strains using the 'One Step' protocol discussed in (Chen et al., 1992). Yeast cells were introduced into 3 ml of YPD liquid media and incubated at 30°C overnight with agitation at 200 rpm. On the following day, 200 µl of the culture was subjected to centrifugation at 12,000 rpm for 1 minute in an Eppendorf tube. The supernatant was removed the cell pellet was mixed with 5 µl (5 µg) of single-stranded DNA (ssDNA) from Salmon sperm, approximately 100 ng of plasmid DNA (-400 ng), and 50 µl of one-step buffer by vortexing. Subsequently, the sample was incubated for 2-3 hours at room temperature with intermittent vortexing. Afterward, the sample was heat shocked at 42˚C in a water bath for 30 minutes, and the resulting suspension was plated onto selective solid media. The plates were then incubated at 30˚C for 2-3 days.
One Step buffer: 0.2M LiAc pH 5.0, 40% (w/v) PEG 4000 (polyethylene glycol), 0.1M DTT.

2.4.3 High-efficiency transformation

Yeast high efficiency transformations were carried out following the Lithium Acetate protocol (Gietz and Woods, 2006) to create gene deletion and plasmids using the reagents listed below.
The yeast strains were grown overnight in 5 ml YPD liquid media at 30˚C with shaking at 200 rpm. The next day morning, cells from overnight culture was added to 5 ml media to start with an OD of 0.1 after measuring the optical density (O.D.600) in a Jenway spectrophotometer at 600 nm wavelength, and cells were grown at 30˚C with shaking at 200 rpm until they reached log phase (~0.5-0.6OD). The cells (5 ml per transformation) were then centrifuged at room temperature for 5 minutes at 3000 rpm and the supernatant was removed. The pellet was washed with 1 ml of freshly prepared 1X TE/LiAc solution, centrifuged as before then washed again in 1 ml 1xTE/LiAc solution. The supernatant was totally removed, and the cells was resuspended in 50 µl 1xTE/LiAc in an Eppendorf tube.
5 µl (50 µg) ssDNA, 5 µl digested vector (0.3-0.6 µg), 5 µl PCR product, and 300 µl 40% PEG 4000 were added to the suspension pellet. The sample was left for 30 minutes at room temperature, then incubated for another 30 minutes at 30˚C then heat shocked for 15 minutes in a 42˚C water bath. Then, the cells were centrifuged at 8000 rpm for 30 seconds, the supernatant was removed, and the pellet was resuspended in 50µl of 1xTE buffer.

Subsequently, the suspension was plated on selective solid media and incubated at 30˚C for 2-3 days.
1X TE/LiAc: 1ml 10x TE (0.1M Tris-HCl and 0.01M EDTA) (pH 7.4), 1ml 1M Lithium Acetate solution (pH 7.5) and 8ml dH20
40% Polyethylene Glycol solution PEG w/v: 3.2ml 50% (w/v) PEG 4000 dissolved in Millipore water, 0.4 ml 10x TE (0.1M Tris-HCl and 0.01M EDTA) (pH 7.4) and 0.4 ml 1M Lithium Acetate (pH 7.5).
1X TE: 1 ml 10xTE (0.1 M Tris-HCl and 0.01M EDTA) (pH 7.4) and 9 ml dH20.

2.4.4 *D. hansenii* transformation

D. hansenii cells were inoculated into a 50ml YM medium and incubated at 25°C overnight with shaking at 200 rpm. Next morning, a 50 YM medium at OD_{600}=0.0125 was re-inoculated and grown until the OD_{600} reached 2.6. Then, 10ml (per transformation) of the culture was harvested by centrifugation for 5 min at 3,300 rpmThe cells were suspended in 1ml of 50mM sodium phosphate buffer pH 7.5 with 25mM dithiothreitol (DTT) and incubated at 30°C for 15 minutes. Subsequently, the mixture was centrifuged. The cells were resuspended in 8ml of sterile cold water and centrifuged as mentioned earlier. The supernatant was removed, and the cell pellets were then resuspended in 200µl of sterile ice-cold 1M sorbitol and centrifuged. The supernatant was once again discarded, and the cells were resuspended in the remaining liquid to achieve a dense suspension. Finally, 1µl of plasmid was added to the suspension. The mixture was transferred into an electroporation cuvette and electroporated at 2.3 kV and placed back on ice. The mixture was then resuspended with 1ml YM medium containing 0.1M sorbitol and transferred into 2ml Eppendorf tube. Samples were then incubated at 30°C with shaking at 120 rpm for 4 hours. After the incubation, the cells were centrifuged again, and the supernatant was discarded. The cells were then resuspended in the remaining liquid, approximately 100µl. A total of 50µl of the cell suspension was spread onto YM plates supplemented with either 1.5µg/mL or 5µg/mL nourseothricin or YM-Adenine. The plates were incubated at 25°C for 3-4 days. Following that, a single colony from the *ade2Δ* plate was streaked onto YM plates containing 5µg/mL nourseothricin, while colonies from the *gut2Δ* plates were streaked on YM2-glycerol agar medium.

2.4.5 Isolation of genomic DNA

Overnight cultures of yeast strains were grown in 5 ml of liquid media, and 3 ml of the culture was collected in a 2 ml screw cap tube. The cells were spun by centrifugation for 1 minute at 12,000 rpm, and the supernatant was discarded. 200µl of TENTS solution, 200µl of glass beads, and 200µl of phenol/chloroform were added to the pellet. The cells were lysed using a bead beater at full speed for 45 seconds, followed by centrifugation for 30 seconds at 12,000 rpm. 200µl of TENTS solution was added to the mixture and vortexed. After centrifugation at 12,000 rpm for 5 minutes, 350µl from the supernatant was taken to a new Eppendorf tube, followed by the addition of 200µl of phenol/chloroform. The sample was vortexed and centrifuged as previously described. Next, 300µl of the supernatant was transferred to another Eppendorf tube. To precipitate the nucleic acids, 750µl of 100% ethanol and 30µl of 3M Sodium acetate were added. After vortexing, the sample was kept on ice for 15 minutes and then centrifuged at 12,000 rpm for 15 minutes. The supernatant was discarded, and the pellet was washed with 400µl of 70% ethanol, followed by centrifugation at 12,000 rpm for 5 minutes. The supernatant was removed, and the pellet was resuspended in 200µl of 1X TE +

2µl of RNase (100µl RNase/TE (10µg/ml)) and incubated at room temperature for 10 minutes. Subsequently, 20µl of 3M Sodium acetate and 500µl of 100% ethanol were added, and the sample was vortexed and left on ice for an additional 15 minutes. The sample was centrifuged again, and the pellet was washed with 70% ethanol and dried at 56˚C. Finally, the pellet was resuspended in a final volume of 50µl of 1xTE.
TENTS: 20mM Tris-HCl pH 8.0, 1mM EDTA, 100mM NaCl, 2%(v/v) Triton X-100, 1%(w/v) SDS.
1X TE: 10mM Tris-Cl pH8.0, 1mM EDTA.

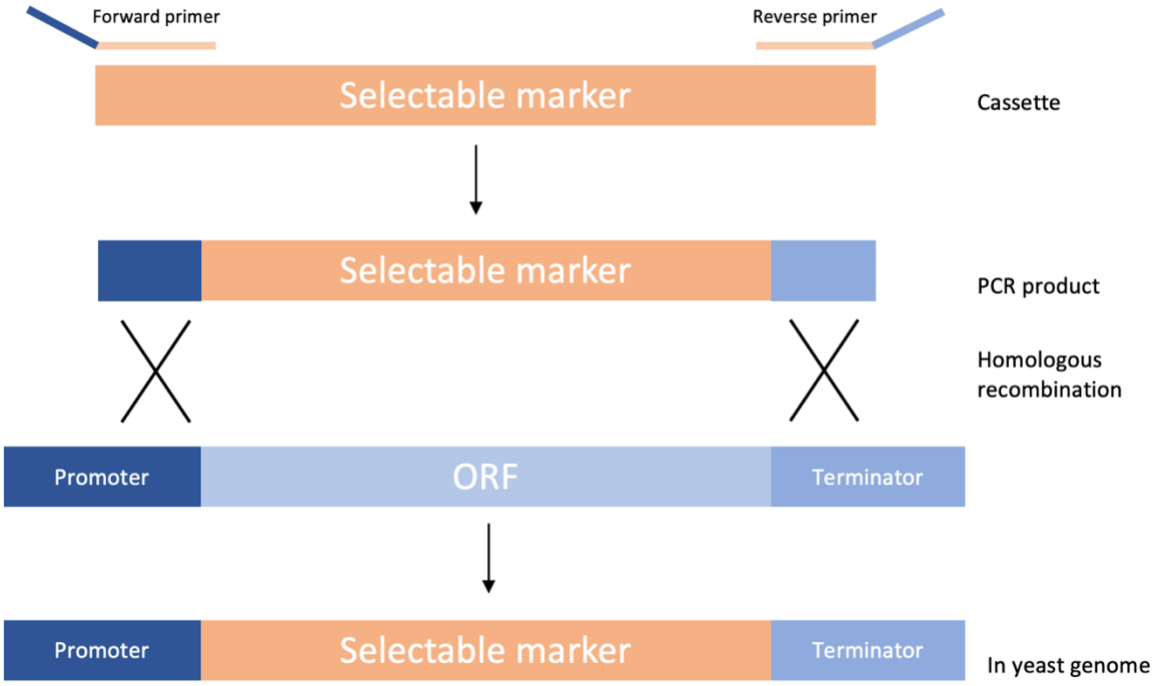

Figure 2. 1: Gene deletion strategies in yeast. The PCR products were introduced into yeast strains using a high-efficiency transformation protocol, resulting in the generation of the desired modified strains.

2.4.6 Gene deletion

Deletion cassettes carrying selection markers were amplified using PCR. The forward primers were designed to include 50 nucleotides identical to the upstream region of the open reading frame (ORF) for gene deletion, while the reverse primers contained 50 nucleotides corresponding to the downstream region of the stop codon (Fig 2.1). The PCR products were subsequently introduced into yeast strains using a high-efficiency transformation method (Section 2.4.3) and plated on appropriate selective media. The correctness of the clones was confirmed by PCR analysis.

2.4.7 Fluorescence microscopy

Yeast cells were studied using an Axiovert 200M microscope (manufactured by Carl Zeiss, Inc.) fitted with an Exfo Xcite 120 excitation light source and band-pass filters (supplied by Carl Zeiss, Inc., and Chroma). The microscope used a Plan-Fluar 100x/1.45 NA or Plan-Apochromat 63x 1.4 NA objective lens (also from Carl Zeiss, Inc.) and was coupled with a digital camera (Orca ER; provided by Hamamatsu Phototonics). Image capture was facilitated by Volocity software (developed by PerkinElmer).
Typically, fluorescence images were collected as 0.5µm z-stacks, which were then amalgamated into a single plane using Openlab (PerkinElmer), and further processed in Adobe Photoshop. Where noted, single focal planes are displayed. Brightfield images were manipulated to depict the cell perimeter in blue.

2.4.8 Phalloidin Staining of Filamentous actin

For visualizing filamentous actin, a solution of 0.134 ml of 37% formaldehyde was added to 1 ml of actively growing yeast culture (OD600nm 0.3) and incubated for 1 hour at room temperature. The samples were then subjected to centrifugation and washed twice with 1 ml of PBS containing 1 mg/ml BSA and 0.1% Tx-100. Subsequently, the cells were suspended in 50 µl of the same buffer, and 5 µl of Rhodamine phalloidin was added. The mixture was incubated at room temperature in the dark for 30 minutes. Following incubation, the cells were washed twice with PBS containing 1 mg/ml BSA and resuspended in 200 µl of the same buffer. Finally, the cells were allowed to settle before visualization using fluorescence microscopy.

2.5 *E. coli* protocols

2.5.1 Growth and maintenance

3 ml of 2TY liquid medium containing 75 µg/ml ampicillin was inoculated with *E. coli* and incubated at 37˚C overnight on an oscillating shaker at 200 rpm. Alternatively, *E. coli* was spread onto 2TY solid agar plates contains 75 µg/ml ampicillin and incubated overnight at 37˚C.

2.5.2 Production of chemically competent *E. coli* DH5α cells

A single colony of *E. coli* DH5α was inoculated into 5 ml of 2TY medium and incubated overnight at 37˚C on an oscillating shaker at 200 rpm. Next day, a secondary culture was prepared by diluting the overnight culture to achieve an initial OD600 of 0.1 in 200 ml of 2TY medium in a 1-liter flask. The culture was then incubated at 37˚C on an oscillating shaker at 200 rpm until reaching an OD600 of 0.5. The culture was transferred to ice and kept for 15 minutes.
Next, the culture was centrifuged for 10 minutes at 4˚C and 3000 rpm (Sigma4-16K). The supernatant was removed, and the cell pellets were resuspended in 75 ml of ice-cold RF1 solution and kept for 20 minutes on ice. The suspension was centrifuged as before, and the supernatant was removed. The cell pellets were then resuspended in 16 ml of ice-cold RF2

solution. The cell suspension was aliquoted into pre-cooled Eppendorf tubes (100 µl each), flash-frozen in liquid nitrogen, and stored at -80˚C.
RF1 solution: 100mM rubidium chloride, 50mM manganese chloride, 10mM calcium chloride, 30mM potassium acetate, 15% w/v glycerol, pH 5.8.
RF2 solution: 10mM MOPS, 10mM rubidium chloride, 75mM calcium chloride, 15% w/v glycerol, pH 6.8.

2.5.3 Production of electrocompetent cells

A starting culture of *E. coli* DH5α was prepared by inoculating a single colony into 5 ml of 2TY medium. The culture was grown overnight on an oscillating shaker at 200 rpm and 37˚C. The following day, a secondary culture was prepared by inoculating 100 ml of 2TY medium with cells from an overnight culture to achieve an initial OD600 of 0.1. The culture was then incubated on ice for 15 minutes. The culture was centrifuged at 3,000 rpm for 15min at 4˚C. After discarding the supernatant, the pellets were resuspended in 50 ml of ice-cold 10% (v/v) glycerol. The cells were centrifuged again as described earlier and then resuspended in 25 ml of ice-cold 10% (v/v) glycerol. Finally, the cells were centrifuged for the third time. The cells were then resuspended in 5ml ice-cold 10%(v/v) glycerol and centrifuged as above. The supernatant was removed, and the pellet was resuspended in 0.75ml 10%(v/v) ice-cold glycerol. 40µl of the cell suspension was aliquoted in pre-cooled Eppendorf tubes then flash-frozen in liquid nitrogen and stored at -80˚C.

2.5.4 Transformation of chemically competent cells

Per transformation, 30 µl of chemically competent *E. coli* DH5α or BL21 DE3 cells were thawed on ice. To the cells in an Eppendorf tube, either 10 µl of ligation mixture or 1 µl of plasmid DNA was added, followed by a 20-minute incubation on ice. The cells were then subjected to heat shock in a 42˚C water bath for 2 minutes (or 10 seconds for BL21 DE3) and subsequently placed on ice for 5 minutes. Next, 900 µl of 2TY medium was added to the sample, which was then incubated for 45 minutes at 37˚C. The sample was centrifuged at 8000 rpm for 1 minute, and approximately 850 µl of supernatant was discarded. The remaining volume was gently resuspended and plated onto 2TY agar media containing 75 µg/ml ampicillin, followed by overnight incubation at 37˚C.

2.5.5 Transformation of electrocompetent cells

Per transformation, 40 µl of electrocompetent cells were thawed on ice. To the electrocompetent cells, 10 µl of 10x diluted gDNA (1 µl genomic DNA + 9 µl water) was added, and the mixture was transferred to a chilled 2 mm electroporation cuvette (Fisher). The cuvette was then loaded into the Bio-Rad MicroPulser, and a single pulse was applied using the EC2 setting (V= 2.5 kV). Immediately after electroporation, 800 µl of 2TY medium was added to the cells, and the mixture was transferred to a clean Eppendorf tube. The sample was incubated for 45 minutes at 37˚C. Following the incubation, the sample was centrifuged at 5000 rpm for 1 minute, and the supernatant was carefully removed. The cell pellet was then plated onto 2TY + 75µg/ml ampicillin agar media and incubated overnight at 37˚C.

2.6 DNA procedures

2.6.1 PCR

PCR was utilized to amplify a DNA specific region using VELOCITY™ or MyTaq™ DNA polymerases. A total volume of 25µl was made up in each tube. The reaction mixtures are shown in Table 2.5.

Table 2. 5 – PCR reaction mixture compositions.

MyTaq™ DNA polymerase	**VELOCITY™ DNA polymerase**
5µl 5x MyTaq™ reaction buffer	5µl 5x Hi-Fi buffer
2.5µl forward and reverse primer (5µM)	2.5µl forward and reverse primer (5µM)
-	2.5µl 2.5mM dNTP's (0.15mM)
1µl 1/50 diluted plasmid DNA (5- 10ng) or 1µl gDNA	1µl 1/50 diluted plasmid DNA (5- 10ng) or 1µl gDNA
0.5µl MYTAQ™ DNA polymerase (1.25 unit)	0.25µl VELOCITY™ polymerase (1.25 unit)
13.5µl dH20	13.75µl dH20

Table 2. 6 – PCR conditions. Depending on the AT/GC content of the individual primers used the annealing temperature was calculated [4(G + C) + 2(A + T) - 5˚C]. Steps 2-4 were repeated for 30 cycles in each PCR reaction.

	MyTaq™ DNA polymerase	**VELOCITY™ DNA polymerase**
1- Initial denaturing	95˚C 1-3 min	98˚C 1 min
2- Denaturing	95˚C 30 Sec	98˚C 30 Sec
3- Annealing	50-65˚C 30 Sec	50-65˚C 30 Sec
4- Elongation	72˚C 1 min/kb	72˚C 15 Sec/kb
5- Final extension	72˚C 10 min	72˚C 10 min

Table 2. 7 – Primers used in this study. Sequences are 5' to 3'. F = Forward and R = Reverse.

Name code	**Sequence 5'-3'**	**Description**
VIP 4185 F	CCAGACCGCCAATAATGCGGCGT	Target *ADE2* gene
VIP 4186 R	AACACGCCGCATTATTGGCGGTC	Target *ADE2* gene
VIP 4187 F	CCACCTTGCGTACTACCGGAACC	Target *GUT2* gene
VIP 4188 R	AACGGTTCCGGTAGTACGCAAGG	Target *GUT2* gene

VIP 4294 F	GCCATCGACAACAAGTGG	Primer 25bp upstream to *ADE2* Ca9 cut
VIP 4295 R	GGTAGCGACTGGAATACC	Primer 25bp downstream to *ADE2* Ca9 cut
VIP 4284 F	CAAGGCTGAAGTCTCTC	Primer 150bp upstream to *ADE2* Ca9 cut
VIP 4283 R	CAAGTGAGCAGCACCAC	Primer 150bp downstream to *ADE2* Ca9 cut
VIP 4264 F	GAGGGACTCGAGAAAGCAGC	Primer 500bp upstream to *ADE2* Ca9 cut
VIP 4265 R	GACTGAGGCATTTGGAG	Primer 500bp downstream to *ADE2* Ca9 cut
VIP 4281 F	GACGAGAGTTGGCATTGGAG	Primer 1500bp upstream to *ADE2* Ca9 cut
VIP 4286 R	GTGGTGGCCAATTAGGTCG	Primer 1500bp downstream to *ADE2* Ca9 cut
VIP 4266 F	CTGGAGTTCTGGCGTATTCG	Primer 500bp upstream to *GUT2* Ca9 cut
VIP 4267 R	GATTACCGGTGTCCTCGCTG	Primer 500bp downstream to *GUT2* Ca9 cut
VIP 4342 F	CTTCATTACACGAAATCGAAATGCACGAT TTATTCATATATAGAGAGACGGAATGATCCAGAGGC	*ADE2* knockout primer using HygR with 50bp flank
VIP 4343 R	TCTATCTAATACTAGAAATAAGTATAAAGC AAACTCTATAACAACCGAATCCCAATCTATCTTCTGAGG	*ADE2* knockout primer using HygR with 50bp flank
VIP 4520 F	AAACTTTTCGTAATTGAGTAGGCCAAGTTGCAACCGTGT GAAATCGAATCCGTACGCTGCAGGTCGAC	*SRV2* knockout primer
VIP 4521 R	AAATGTGATTTATTTCTTTTAACTAAATACATTAATGCTCCT CGCAATAGCATAGGCCACTAGTGGATCTG	*SRV2* knockout primer
VIP 4882 F	GCCAGTGAATTCGAGCTCGGTACCGCTAA TACAAACAGGC	Amplifying SRV2 ORF
VIP 4883 R	GCCAAGCTTGCATGCCTGCAGTCGTCGTG TATTGTTGC	Amplifying SRV2 ORF
VIP 4884 R	GCCAAGCTTGCATGCCTGCAGATTCTTCG TTGATTGTGCCATCG	Amplifying N-terminus of SRV2

VIP 4886 F	CCGTGTGAAATCGAATCATGGCACAATCAACGAAG	Amplifying C-terminus of SRV2
VIP 4530 F	GGACGTTGAAGCCACATCC	Primer 500bp upstream to SRV2 ORF
VIP 5025 F	GTAAAACGACGGCCAGTGAATTCGCTAATACTCAAAAC AGGC	Amplifying Srv2-GFP-Pex15 fusion
VIP 5040 R	GTTCTTCTCCTTTACTCATTGCACCCGCCC CTGCTCCGAGCTCACCAGCATGTTCGAAAAC	Amplifying Srv2-GFP-Pex15 fusion
VIP 4885 R	ATTCTTCGTTGATTGTGCCATGATTCGATTTCACACGG	Amplifying Srv2p-GFP-Pex15 fusion
VIP 5100 F	ACTGGGATCCATGGTTTTATCAAGGGGAG	Amplifying Inp1
VIP 5102 R	CAGTGTCGACGCAGTTTGAATTTATCGCTC	Amplifying Inp1 1-280
VIP 5103 R	CAGTGTCGACTCAAAGGTCGCCAAGAC	Amplifying Inp1 FL
VIP 727 R	CCCATTAACATCACCATC	Primer 50bp from star codon of GFP
VIP 142	CTGCAGCGAGGAGCCGTAAT	Check Knockout of *SRV2*

2.6.2 Restriction digest

Each restriction digest mixture was performed in a 25 µl reaction volume for each sample, comprising 2.5 µl of 10x NEB CutSmart™ Buffer, 1 µl of each required restriction enzyme, 1 µg of plasmid DNA, and the volume was adjusted to 25 µl with dH2O. The mixtures were prepared on ice and then incubated at 37˚C overnight.

2.6.3 Agarose gel electrophoresis

The DNA samples were subjected to agarose gel electrophoresis for analysis. To prepare the gel, 0.7% (w/v) agarose powder was dissolved in 1x TAE buffer solution (40 mM Tris, 20 mM acetic acid, 1 mM EDTA, pH 8), and Ethidium bromide was added to achieve a final concentration of 0.5 µg/ml. The DNA samples were mixed with 6x loading buffer (0.25% bromophenol blue, 0.25% xylene cyanol FF, 30% (v/v) glycerol) to obtain a 1x final concentration. In order to estimate the size of DNA fragments, a Bioline Hyper ladder was included in the analysis alongside the DNA samples. The agarose gel was run at a constant voltage of 96V in 1x TBE buffer solution for a duration of 36 minutes. Finally, the samples were analyzed by observing them with an ultraviolet (UV) transilluminator imaging system known as GeneSys.

2.6.4 Gel extraction

Following the agarose gel electrophoresis procedure outlined in Section 2.6.3 and visualizing the DNA samples on a UV transilluminator, the desired DNA bands were carefully removed from the gel. Subsequently, the extraction of the gel bands was conducted utilizing the QIAquick gel extraction kit (Qiagen), following the instructions provided by the manufacturer.

2.6.5 Ligation

Typically, a molar ratio of 3:1 between the insert and vector was employed for each ligation reaction, with a final volume of 20 µl. 50ng digested vector, a relevant amount of the insert fragment, 2 µl 10x ligase buffer and 0.5 µl T4 DNA ligase (NEB) were added to the mixture and made up to 20 µl with dH2O. The reaction was then incubated for overnight and transformed into chemically competent E. coli cells next day.

2.6.6 Miniprep

Overnight cultures of *E. coli* cells were cultivated in 3 ml of 2TY ampicillin medium. The following day, plasmids were extracted from the overnight cultures using the QIAprep miniprep kit, following the instructions provided by the manufacturer. Subsequently, the concentration of the plasmids was determined using a Nanodrop device.

2.6.7 Homologous Recombination

In *S. cerevisiae*, homologous recombination was employed for gene cloning to incorporate tags or open reading frames into a vector (refer to Fig. 2.2). Fragments of interest, such as promoters, ORFs, and tags, were initially amplified through PCR. The design of the primers ensured that the resulting product had flanking regions of at least 20 nucleotides, which were identical to the insertion sites within the vector. The vector was then digested using specific restriction enzymes. Subsequently, the linearized vector and PCR products were introduced into yeast cells through high-efficiency transformation (Section 2.4.3). Through the process of homologous recombination, gap repair took place, leading to the circularization of the vector, incorporating the PCR product. To identify cells containing the recombinant plasmids, selective yeast medium was used for their growth.

2.6.8 Sequencing

Source Bioscience was used to sequenced plasmids using the Sanger sequencing service. The data received from Source Bioscience was analysed using SnapGene program and the online multiple sequence alignment tool ClustalW.

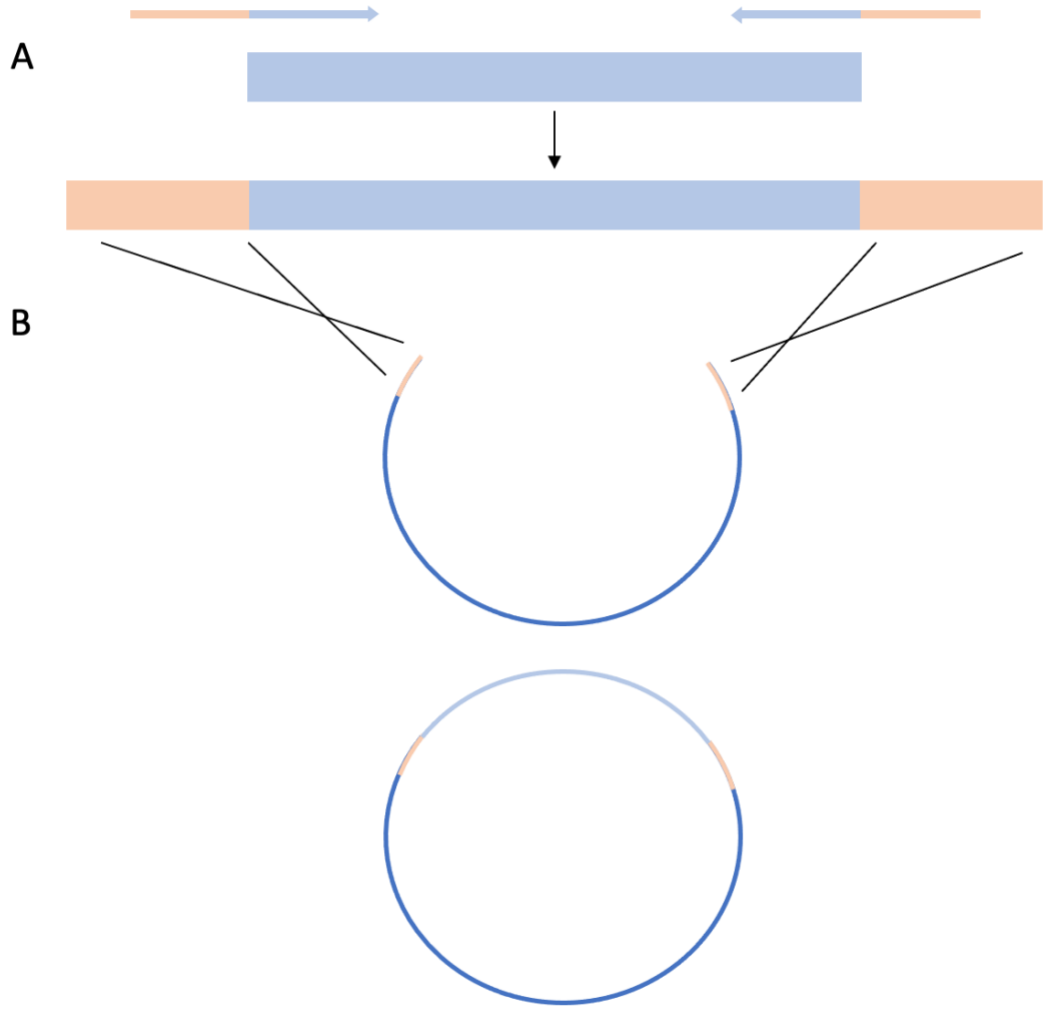

Figure 2. 2: Homologous recombination method for plasmid construction used in *S. cerevisiae.* A) Primers (indicated by blue and orange arrows) were designed to generate a PCR product containing the desired DNA insert (in blue) with approximately 18 nucleotides of homologous flanking sequences to regions within the vector (in orange). B) The digested vector and the PCR product were introduced into S. cerevisiae through transformation. As a result of homologous recombination, a recombinant vector was formed, incorporating the desired insert.

2.7 Protein procedures

2.7.1 SDS-PAGE

SDS PAGE (Sodium dodecyl sulphate polyacrylamide gel electrophoresis) was run following the protocol described by (Sambrook and Russell, 2006). 10% gels were used as shown in Table 2.7. The samples were supplemented with a 1X final concentration of protein loading dye (4X) and subsequently loaded onto the gel. The gels were then subjected to electrophoresis at a voltage of 100-130V until the dye migrated to the bottom of the gel.
Protein running buffer (1X): 3.3g Tris Base, 14.13g Glycine, 1% (w/v) SDS, dH20 up to 1L.
Protein loading dye (4X): 250mM Tris pH 6.8, 9.2% (w/v) SDS, 40% (w/v) Glycerol, 0.2% (w/v) Bromophenol brilliant blue, 100mM DTT.

Table 2. 8 – SDS-PAGE gel reagents.

Reagents	**Resolving gel (10%)**	**Stacking gel (4%)**
Protogel (Acrylamide, Bisacrylamide mix) 30% stock	3.3 ml	650 µl
Resolving buffer 4X stock	2.6 ml	-
Stacking buffer 4X stock	-	1.25 ml
APS 10% (w/v) stock	100 µl	50 µl
TEMED 1000X stock	10 µl	5 µl
dH20	4.1 ml	3.02 ml
Total volume	10 ml	5 ml

2.7.2 Protein induction

E. coli cultures were inoculated in 4ml 2TY/Ampicillin and then incubated overnight at 37˚C. Next day, 2TY/Ampicillin cultures were reinoculated from 0.1 OD_{600} to reach 0.8. Then 1mM of IPTG was added to cells for 3 hours at 37˚C with shaking. This was followed by centrifugation at 800 rpm for 15 min at 4˚C. The supernatant was discarded, and pellets were stored at –80˚C till required.

2.7.3 Protein purification from *E. coli*

Bacterial cells were resuspended in 1ml ice cold 1xPBS + 1mM PMSF, then cells were sonicated 1x 30sec, 2x 15sec at 40% amplitude and samples were kept on ice. 1mM PMSF was then added to suspension followed by centrifugation at max speed for 10 min at 4˚C. Supernatants were added to prewashed Amylose (NEB) beads (washed twice with 1xPBS) and then incubated at 4°C with end over end mixing for 1 hour. Beads were then washed twice with 1xPBS. For in vitro binding, beads were directly used.
For actin assays, MBP-tagged proteins were eluted using maltose elution buffer. Standard curves were then performed to determine the protein concentration. A dilution series of actin, of known concentration (Section 2.8.1), and the same volume of MBP-Inp1 were run in SDS-PAGE. After running and destaining the gel, Image Lab (from Bio-Rad) was used to

calculate the concentration for each band based on the specified protein standard. Nanodrop Spectrophotometer-Protein A280 was used in addition to stander curves.
Elution buffer: 20 mM Tris-HCl, 400 mM NaCl, 2 mM EDTA, 20 mM maltose, pH 7.4

2.7.4 TCA protein extraction

The yeast cultures were incubated overnight to allow for growth, after which 25 OD600 units of cells were harvested for 1 minute at 12,000 rpm. The resulting pellets were then resuspended in 500µl TCA buffer after the supernatant was discarded. Samples were incubated on ice for 10 min followed by the addition of 71µl of 40% (w/v) TCA (Trichloroacetic acid in Milli-Q water) after which it was left again on ice for 10 min. The samples were then centrifuged at 13,000 rpm for 5 minutes at 4˚C and the precipitated protein pellets were kept. To neutralize the proteins, 10µl of 1M Tris- HCl pH 9.4 was then added followed by 90µl of 1X the sample buffer. After boiling at 95˚C for 10 minutes, samples were loaded onto SDS-PAGE gels (1-2 OD600 equivalent).
TCA buffer: 0.2M NaOH, 0.2% β-Mercaptoethanol.

2.7.5 Protein extraction

The yeast cultures were incubated overnight to allow for growth at 30°C and 200rpm shaking in selective media. The following day, another culture was started with OD_{600} 0.1 into fresh media and incubated for 6h at 30°C and 200rpm shaking. Arround 500 OD_{600} units of cells were harvested by centrifugation at 3000rpm for 5min. The cell pellets were then resuspended in the 400µl of cold F-buffer (G-buffer + 10% 10x KME) or lysis buffer plus 1mM protease inhibitor cocktail and PMSF. 200µl of glass beads were then added to the suspension. The mixture was lysed in a bead beater for 1min and placed on ice immediately. This was followed by centrifugation at 13000 rpm at 4°C for 1min. The supernatants were transferred to clean Eppendorf tubes then centrifuged at 13000 rpm at 4°C for 10min and the supernatant was kept on ice.
G-buffer: 2mM Tris pH8, 0.2mM $CaCl_2$, 1mM NaN_3, 0.2mM ATP, 0.5mM DTT.
Lysis buffer: 20mM Tris/HCl, 110 mM KCl, 5mM MgCl and 1mM DTT.

2.7.6 Protein binding assays

In vitro binding assay

Proteins that were extracted (as described above) were added to MBP-Inp1 coated beads that were prewashed with F-buffer or lysis buffer. The mixture was incubated at 4°C with end over end mixing for 2 hours. Beads were washed 3x with the same buffer used with centrifugation at 200 rpm between each wash. SDS-PAGE was carried out and binding was analysed by Coomassie staining and western blot.

In vivo binding assay (GFP protein pull down)

For co-immunoprecipitation experiments, 50-60 OD_{600} units of logarithmically growing cells were spun down and resuspended in 400µl lysis buffer. Next, 200µl of clean glass beads were added to the mixture. The samples were subjected to lysis using a glass bead beater, performing multiple rounds of 45 seconds at maximum speed. Following lysis, the samples were centrifuged at 4˚C for 10 minutes at maximum rpm. 250µl of clear lysate was added to

25µl per-washed GFP-Trap beads (washed twice with 10 volume lysis buffer), and some of clear lysate was kept as control. The mixture was then incubated at 4˚C for 2h on rotating wheel, and then washed three times with lysis buffer (no protease inhibitors). Bound proteins were eluted with protein loading dye and boiled at 90°C for 10min, and then analysed by western blot.
Lysis buffer: 150mM KCl, 20mM Tris-HCl pH 8.0, 5mM $MgCl_2$, protease inhibitor.

2.7.7 Western blot

The samples were separated through SDS-PAGE and were subsequently transferred onto a nitrocellulose membrane using a Biorad Mini Trans-Blot Electrophoretic transfer cell. This transfer took place at 200mA for 2 hours in a transfer buffer composed of 25mM Tris pH 8.3, 150mM Glycine, and 40% (v/v) methanol. The successful transfer of the protein was confirmed using Ponceau S solution (0.1% (w/v) Ponceau S in 9ml TBS-Tween 20 (containing 50 mM Tris-HCl with a pH of 7.5, 150 mM NaCl, and 0.1% (v/v) Tween 20)).
The blots were then blocked overnight in a buffer containing 5% fat-free milk in TBS-Tween. The membranes were exposed to primary and secondary antibodies for an hour at room temperature in a milk buffer, with the process being followed by three rounds of washing between the incubations using TBS-T (minus the milk).
The antibodies were used at the following dilutions: anti-actin (1:500) from Invitrogen, anti-PAP (1:5000) from Sigma-Aldrich, and anti-GFP (1:3000) from Roche. Anti-mouse polyclonal (1:10000) from Invitrogen, and anti-Pgk1 (1:7000) from Invitrogen were utilized as secondary antibodies.
The proteins were identified using Enhanced Chemi-Luminescence (ECL) substrates and the images were captured using a Syngene GBox imaging system along with the Genesys software.

2.8 Actin assays

2.8.1 Making actin

Rabbit skeletal muscle acetone powder was made by the Ayscough lab according to (Perry, 1955) protocol, and kept as 5g aliquot stocks at -80°C till required. The 5g rabbit skeletal muscle acetone powder was placed in 25ml beaker (inside a larger beaker filled with ice) and 100ml fresh cold G-buffer was added. The mixture was stirred slowly and consistently for 30 mins. The mixture was then poured out into 50ml falcon tube and spun at 20000g for 35 mins at 4°C. The supernatant was filtered through 2 pinches of glass wool packed into a funnel and filtered twice through 0.45µm filter then a 0.2µm filter. Then KCl (to final concentration of 0.8M) and $MgCl_2$ (to final concentration of 0.2 mM) were added to the liquid and left stirred for 30 min at room temperature then stirred for another 30 min at 4°C. The sample was ultracentifuged for 2h at 35000 rpm at 4°C. Supernatant was discard and the F-actin pellets were extracted and put into 15ml glass Teflon homogeniser contain 5ml G-buffer. The actin solution was resuspended 10 times and another 5ml G-buffer was added and resuspended again. The solution was filled into dialysis tubing (washed with a litre of dH_2O and G-buffer) and tied its both ends with clamps and floats. The tubing was left to dialyse in 1L fresh g-buffer for at least 2h and the buffer was changed and left for overnight. For the next 2 days, the actin dialysis buffer was changed three times (every 4h). Next day, the buffer was changed

again 3 times before collecting the sample by cutting tubing and pouring actin into 50ml tube on ice. Sample then centrifuged at 3500 rpm for 2h at 4°C. About ¾ of the fraction was transferred to a clean 50ml tube. The sample was loaded onto the fraction collector column and left flowing for overnight. Finally, the peak fractions were collected concentration using Bradford reagent and then the actin concentration was calculated using the following: A_{290nm} X dilution/0.0264= µM actin. Monomeric actins were stored at 4°C for up to a month.
G-buffer: 2mM Tris pH8, 0.2mM $CaCl_2$, 1mM NaN_3, 0.2mM ATP, 0.5mM DTT

2.8.2 Making pyrene actin

After collecting pre-peak actin fractions from section 2.8.1 actin is diluted to 1 mg/ml with G-buffer then dialysed against G-buffer with no DTT for 3hh with 4 changes of buffer. The actin then polymerized by adding 100mM KCl and 2mM $MgCl_2$ with slowly stirring at room temperature for 2 mins. Then pyrene (10mg/ml) is added to actin at 10:1 molar ratio pyrene: actin (10 mg pyrene/ 100 mg actin) and stirring for overnight at 4°C in the dark. Next day, pyrene actin is dialyzed with G-buffer containing 0.5 mM DTT in small diameter tubing with several buffer changes till actin is in solution. Pyrene actin is centrifuged at low speed 500 rpm for 5 min to remove any excess pyrene precipitation. Pyrene actin was then polymerized again as above followed by centrifugation at 40000 rpm for 1h at 4°C. The pellet was resuspended in G-buffer with DTT to approximately 5 mg/ml and homogenized with loose fitting dounce plunger. This followed by dialysed at 4°C with same buffer with several changes (over several days). Then the solution is centrifuged at 25000 rpm for 2h at 4°C. The top 2/3 of supernatant was transferred to a new tube and loaded into fraction collector column (G-150) on foil wrapped with G-buffer containing DTT. Finally, 4ml fractions were collected and actin concentration was determined and stored at 4°C till required.

2.8.3 Alexa488 fluor G and F actin binding assays

Alexa488 fluor actin was obtained at a stock concentration of 18.3 mg/ml (Molecular Probes). A working stock was created by adding 1µl of stock to 99µl G-Buffer (2mM Tris-HCl pH8, 0.2mM CaCl2, 0.2mM ATP and 0.5mM DTT) to give a 10µM working stock. This was centrifuged at 90,000 rpm (Beckman Coulter TLA 100 rotor) for 15 minutes to remove any pre-existing F-actin or aggregates. This was kept at 4˚C till required.
The actin reaction mix (4.5µl of 22µM actin, 1µl Alexa 488, 21.5 µl G-buffer and 3µl of 9µM BSA for G-actin binding OR 4.5µl of 22µM actin, 1µl Alexa 488, 21.5 µl G-buffer +10% of 10x KME and 3µl of 9µM BSA for F-actin binding) was added to MBP-Inp1 beads as described above (section 2.7.3) that were washed with G-buffer or F-buffer (G-buffer + 10% 10x KME). The mixture was incubated for 2 hours at room temperature. Beads were then spun down at 200 rpm for 1 min, followed by washing twice in G-buffer or F-buffer (for f-actin). Beads were analysed by fluorescence microscopy under GFP setting, followed by immunoblot analysis with an anti-actin antibody.
10x KME: 0.1M Tris pH 8.0, 0.5mM KCl, 10mM MgCl2, 10mM EGTA.

2.8.4 Fluorimetry assay

Actin made in Section 2.8.2 and pyrene actin made in Section 2.8.2 were used for the actin mix as following (5uM G-actin, 0.5uM pyrene actin, G-Buffer) in total volume of 300µl then the mixture was vortexed briefly to ensure thorough mixing and added to one well of the 96

well plate. The fluorimeter was run for 3 mins to check that the trace is steady. Then protein of interest was added to the next well of the 96 well plate plus G-buffer to check the actin polymerisation or plus F-actin to check the actin depolymerisation as shown in Table 2.9. Then the protein of interest mixture was added to actin mixture before the assay was started for up to 5h.
G-buffer: 2mM Tris pH8, 0.2mM $CaCl_2$, 1mM NaN_3, 0.2mM ATP, 0.5mM DTT.
10x KME: 0.1M Tris pH 8.0, 0.5mM KCl, 10mM MgCl2, 10mM EGTA.
F-buffer: 40ul 10xKME + 30ul G-buffer.

Table 2. 9 – Fluorimetry assay mixture.

	Actin mix	**Inp1 protein**	**MBP**	**G or F buffers**
Actin only	300µl	-	-	70 µl
Actin and Inp1	300µl	46µl	-	24 µl
Actin and MBP	300µl	-	27.7 µl	42.2 µl

2.8.5 Actin co-sedimentation assays

Protein of interest (Inp1) was pre-spun 15 min at 90k rpm to remove any pelletable material. Then 5µM of actin that made in Section 2.8.1 was mixed with an equimolar amount of protein of interest in the presence of G-buffer plus 1x KME as shown in Table 2.8. The mixture was left at room temperature for 2h for actin to be polymerised. After incubation, the samples were spun at 90k rpm for 15 min at 4˚C in TLA-100 Rotor. Then supernatant and pellet were separated, and the original volume of G-buffer was added to the pellet and resuspended. Then protein loading dye was added to the samples before separating them on gel using SDS-PAGE.

Table 2. 10 – Co-sedimentation reaction mixture.

	5µM final protein of interest	**5µM final actin**	**G-buffer**	**10x KME**
Protein of interest only	10µl	-	80µl	10µl
Protein of interest and actin	10µl	10 µl	70 µl	10 µl
Actin only	-	10 µl	80 µl	10 µl

2.8.6 Lat-A treatment of cells in culture

Cells at logarithmic growth phase were subjected to the addition of Lat-A, which was prepared from a 10 µM DMSO stock solution, resulting in a final concentration ranging from 25 µM to 200 µM. In experiments involving cell recovery from Lat-A treatment, cells were washed three times after a specified duration of Lat-A treatment before being transferred to fresh media.

2.8.7 Yeast two hybrid

Strains carrying *ACT1* and some actin mutants as binding-domain constructs, and a strain carrying PFY1 protein as an activation-domain construct were obtained from Prof. Kathryn

Ayscough's lab. Inp1 full-length and Inp1 1-280 were constructed as activation-domain constructs. The PJ69-4A strain was transformed with activation-domain plasmids, while the PJ69-4α was transformed with binding-domain plasmids. Strains carrying binding-domain constructs and activation-domain constructs were mated and grown on YPD media. Diploids were selected on *LEU- TRP-* selective media plates. Cells were then streaked on *LEU-TRP-ADE-HIS* plates and on the same plates plus 3mM and 4mM of 3AT (3-aminotriazole).

2.9 Statistical Analysis

The data obtained in all experiments were from three independent experiments and analysed using GraphPad (Prism) in two stages. For peroxisome phenotypes and mitochondria phenotypes, statistical analysis was performed with a two-way ANOVA test and Tukey's multiple comparison post-test. For peroxisome numbers, the data were analysed by using one sample t and Wilcoxon test. Statistical significance was determined by unpaired student t test and significance level was set to 0.05. ** indicates $P \leq 0.01$, ***$p \leq 0.001$, ****$p \leq 0.0001$. Error bars represent SEM.

Chapter 3 – Investigating interactions of Inp1

3.1 Introduction

Recently, it has become clearer that cell organelles establish physical interaction with one another at membrane contact sites (MCS). MCS can be described as cellular regions where opposing organelle membranes are closely linked in proximity by the interaction of proteins or lipids, affecting the activity of either one or both organelles (Shai et al., 2018; Prinz, 2014; Prinz et al., 2020). Research into membrane contact sites is advancing quickly, and it has now been demonstrated that each organelle establishes a minimum of one functional membrane contact site with another organelle. In fact, it is now recognised that the majority of organelles have multiple MCSs, and these perform a wide array of functions including organelle inheritance and fission, organisation of the cell and exchange of cellular materials (Valm et al., 2017; Shai et al., 2018). In addition, proteins that bind and control contact sites have been discovered as a result of the characterization of MCSs. Despite the identification of various contact sites, there are still a number of tethering factors for MCS that are still not fully understood, including the contact site between the plasma membrane and peroxisomes (Shai et al., 2016).

Similar to what has been hypothesised for other organelles, it has been found that peroxisomes in yeast engage in interactions with various cellular structures, such as mitochondria, the vacuole, lipid bodies, the plasma membrane, and the endoplasmic reticulum (ER) (Knoblach & Rachubinski, 2019, Eisenberg-Bord et al., 2016; Wu et al., 2019). Although certain peroxisomal interaction sites with other organelles have been found, others remain uncharacterized (Shai et al., 2018). In *S. cerevisiae*, a precise equilibrium between the conflicting processes of myosin-dependent transport towards the bud and cortical anchoring in the mother cell is necessary for faithful peroxisome segregation between the parent cell and the developing bud. These strategies depend on the inheritance proteins Inp1 and Inp2 that have antagonistic functions and maintain an appropriate division of peroxisomes between the mother cell and developing daughter (Fagarasanu et al., 2005; Hoepfner et al., 2001; Fagarasanu et al., 2010). Pex3 interacts directly with the peripheral peroxisomal membrane protein Inp1 to play a crucial function in peroxisome retention (Munck et al., 2009). The tethering complex formed by Inp1 and Pex3 is crucial for maintaining peroxisomes and positioning them along the cortex of the parent cell during cell division (Fagarasanu et al., 2005; Knoblach et al., 2013; Munck et al., 2009).

Inp1 plays a critical role in retention of peroxisomes, as it interacts with the peroxisomal membrane protein Pex3 through a highly conserved leucine-rich motif in its C-terminus (Munck et al., 2009; Hutchinson, 2016). Initially, it was proposed that Inp1 acts as a hinge-like protein, facilitating the interaction of Pex3, which is concurrently attached to both peroxisomes and the cortical ER (Knoblach et al., 2013). However, more recent research has questioned this model, suggesting that additional components may be involved in tethering peroxisomes to the cell cortex, and it appears that Inp1 may also play a role in tethering peroxisomes to other organelles (Knoblach and Rachubinski, 2019).

The Hettema lab identified Inp1 as the first recognised plasma membrane peroxisome (PM-PER) tether by confirming that Inp1 complies with the requirements set out for a contact site tether protein. As a PM-PER tether, it has been shown that Inp1 is structurally and functionally capable of interacting with both the peroxisomal membrane and the plasma membrane when it is present at the appropriate subcellular location. The conducted experiments reveal Inp1's role as a crucial component of the plasma membrane (PM)-peroxisome (PER) tether. Specifically, the first 100 amino acids of Inp1 were found to localize to the plasma membrane and interact with PI(4,5)P2 liposomes, establishing a minimal tether. This minimal tether is essential for peroxisome retention at the cell periphery, and when connected to the peroxisomal membrane, it alone is sufficient to achieve this function.
Furthermore, the researchers constructed an artificial tether using the plasma membrane-binding PH domain of Num1, which, when linked to peroxisomes, effectively restored peroxisome retention in *inp1Δ* cells. Additionally, when both Inp1 and the Inp1 minimal tether were expressed in cER mutants, they exhibited localization at the cell periphery, spatially distinct from the endoplasmic reticulum (ER), and were positioned near peroxisomal foci close to the plasma membrane.
Based on these findings, the proposed model suggests that the PM-PER tether serves a critical function in ensuring peroxisome retention at the cell cortex (Hulmes et al., 2020). However, the specific function of Inp1's middle domain has yet to be determined (Fig. 3.1).

Interestingly, extremely similar results to the Inp1 function in *S. cerevisiae* have been shown in *H. polymorpha* (Krikken et al., 2020). It was demonstrated that Inp1 is divided into 3 functional domains, an N-terminal domain, a middle homology domain (MHD) and a C-terminal domain. The N-terminal domain has been demonstrated to be critical for the connection with the plasma membrane, while the C-terminal region is essential for binding to peroxisomes. In the case of overexpression of N-Inp1-GFP in *Δpex3* H. polymorpha cells, a cytosolic fluorescence pattern was observed due to the absence of Pex3. However, the truncated domain showed a slight accumulation at the cell cortex, with larger quantities of signal being initially detected at the tips of the buds and subsequently at the necks of the buds (Krikken et al., 2020). These findings can be attributed to the non-uniform distribution of PI(4,5)P2 along the plasma membrane in budding yeast, where it tends to be concentrated in regions of polarized growth and the neck of the bud (Garrenton et al., 2010). It was also demonstrated that the middle domain of Inp1 is needed for the N-terminal tethering function of Inp1 (Krikken et al., 2020). Although the central domains of HpInp1 and ScInp1 do exhibit regions of homology, the specific function of the ScInp1 middle homology domain has not been reported.

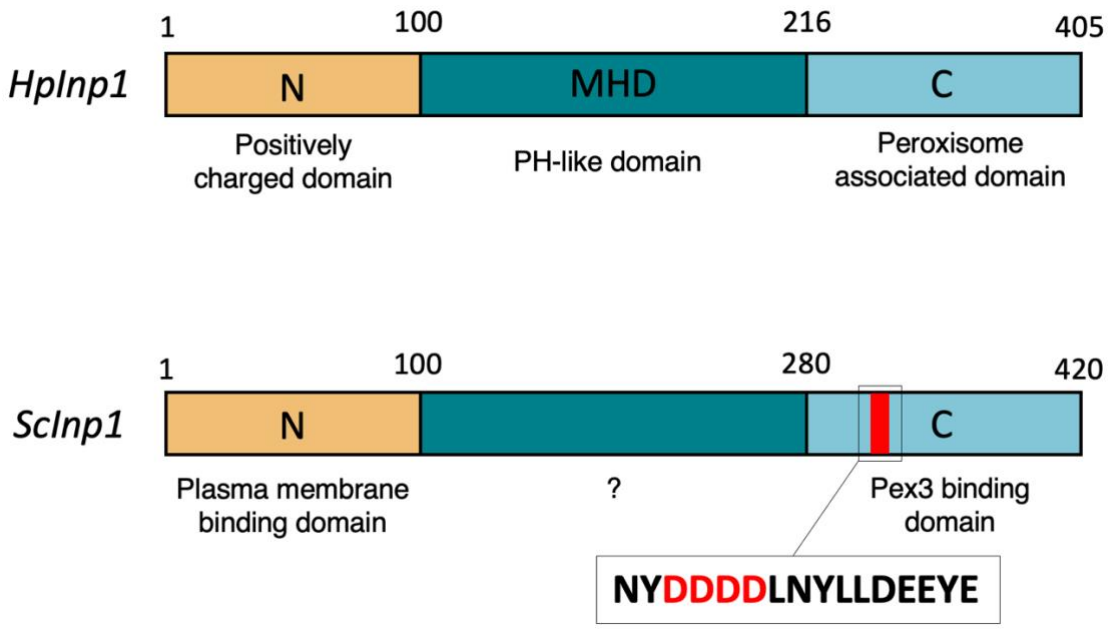

Figure 3. 1: Comparative Schematic Illustrations of Inp1 Domain Structures in *H. polymorpha* and *S. cerevisiae.* The schematic diagrams depict the putative structures of Inp1 in two distinct species, *H. polymorpha* (HpInp1) and *S. cerevisiae* (ScInp1). For HpInp1, the illustration highlights three domains: the N-terminus, featuring conserved positively charged residues; the MHD/predicted PH-like domain; and the C-terminus, which is essential for Inp1's interaction with peroxisomes. In contrast, the ScInp1 schematic presents three domains: the N-terminus (1-100) responsible for plasma membrane binding; the middle domain (100-280) with an unclear function; and the C-terminus (281-420), Pex3 binding domain. Residues highlighted in red emphasize the bioinformatic analysis of negatively charged residues located before the Pex3 binding domain

An interesting finding by Krikken and colleagues was that the cortical localization of Inp1 is influenced by the condition of the actin cytoskeleton. This was observed when the actin cytoskeleton was disrupted by subjecting the cells to the actin inhibitor latrunculin-A, resulting in the depletion of cortical Inp1 patches, particularly in proximity to the bud neck. In this study, the formation and localization of Inp1 patches were checked using Inp1-GFP. Upon latrunculin-A treatment of the cells, the Inp1-GFP signal became cytosolic, leading to the disappearance of cortical Inp1-GFP patches close to the bud's neck. The untreated cells or the ethanol-treated controls still showed cortical patches of Inp1 (Krikken et al., 2020). This result indicated that actin cytoskeleton disassembly is linked to the dissociation of Inp1 from the plasma membrane.

Thus separate studies in two distinct yeast species have reached the consistent finding that the N-terminal region of Inp1 serves as a domain for association with the plasma membrane, while the C-terminal region of Inp1 is responsible for establishing a connection or association with peroxisomes.

It is known that the actin cytoskeleton is crucial for the movement and inheritance of peroxisomes in yeast and so it would generally be assumed that the link between peroxisomes and actin would be via the Inp2-myo2-actin linkage that has been characterised. It was

therefore surprising when Krikken and colleagues reported that Inp1 loses its localization when the actin cytoskeleton is disrupted (Krikken et al., 2020). The presence of a PI(4,5)P2 binding motif in Inp1 suggests the possibility of an indirect interaction between Inp1 and actin, as several actin-binding proteins are known to bind this lipid (Saarikangas et al., 2010). Furthermore, additional evidence supporting an indirect association between Inp1 and actin comes from data obtained from the Saccharomyces Genome Database. A large-scale study reports that the actin assembly factor Las17 genetically interacts with Inp1 (Constanzo et al., 2016). These observations raise an interesting possibility that Inp1 could potentially interact with actin.
Considering these findings, it is conceivable that the observed loss of Inp1 localization upon the addition of Latrunculin-A, which disrupts actin dynamics, might be a secondary impact of actin disassociation. The disruption of the actin cytoskeleton could affect the interactions between Inp1 and actin-binding proteins, leading to the altered localization of Inp1.
The potential interaction between Inp1 and actin warrants further investigation, and the observed changes in Inp1 localization upon actin disruption provide valuable insights into the intricate connections between peroxisomes and the actin cytoskeleton.
The data presented in this chapter reports an investigation of whether Inp1 can interact with actin and therefore whether Inp1 can be characterised as actin-binding protein.

In addition, this study aims to investigate proteins that interact with Inp1's middle domain to gain deeper insights into the functional relevance of this specific region. The middle domain of Inp1 in *H. polymorpha* was found to be required for the N terminal as PM-PER tether (Krikken et al., 2020). However, in *S. cerevisiae*, it has been found that the N-terminal of Inp1 is sufficient for the interaction with the PM. Consequently, can the middle domain of Inp1 in *S. cerevisiae* act as a linker between the N and C domains, or does it possess unique properties or binding partners that play a crucial role in regulating its overall function?
Understanding the functional significance of the middle domain could shed light on novel interactions or regulatory mechanisms that impact Inp1's involvement in peroxisome dynamics and tethering processes. By exploring potential interactions with other proteins, we hope to unravel the intricate network of molecular interactions that contribute to the multifaceted functions of Inp1 in peroxisome biology.
Through this investigation, we aspire to expand our comprehension of Inp1's complex structure-function relationships and uncover the underlying mechanisms that govern peroxisome dynamics and organization in the cell.

3.2 Inp1 binds F-actin not G-actin

Actin, a protein found abundantly across eukaryotes, exhibits high conservation and is involved in vital cellular functions. It plays a fundamental role in multiple processes such as cell organization, shaping, movement, and membrane transport. Actin monomers, known as G-actin, polymerize into polarized filaments called F-actin, which are dynamically regulated by various actin-binding proteins (Winder and Ayscough, 2005). These proteins enable the assembly and disassembly of actin at specific cellular locations in response to internal and external signals, ensuring precise control over actin dynamics. Although the actin cytoskeleton, which is a network of actin filaments, consists of a stiff structure, it is also a dynamic structure that is permanently remodelling (Srivastava & Barber, 2008; Dominguez &

Holmes, 2011). A number of proteins have the ability to bind to the actin cytoskeleton. Studying the binding of proteins to F-actin is essential for gaining insights into the dynamic processes involving actin cytoskeleton remodeling and understanding the functional roles of actin-binding proteins in cellular processes (Dominguez & Holmes, 2011).

The investigation of whether Inp1 can interact with actin begins by identifying the type of actin to which it binds – either G-actin or F-actin.

To test this, G-actin or F-actin was added (as described in section 2.8.3) to amylose beads coated either with Inp1 fragments (1-100 and 1-280) or with Las17, an actin assembly factor and activator of the Arp2/3 protein complex that nucleates branched actin filaments and is known to bind under both conditions. The beads were incubated for 2 hr before being analyzed by fluorescence microscopy (as described in section 2.4.7).

AS shown in Figure 3.1, the control protein Las17 is able to recruit fluorescent actin to the surface of the bead so that beads can be clearly visualized against the dark background. However, in negative controls with the fusion protein MBP alone, there is no recruitment on the beads, and the beads could not be distinguished above the background. Inp1 fragments (1) Inp1 1-100 and (2) Inp1 1-280, that were in F buffer were able to recruit the fluorescent actin and thus beads were visible. In contrast when the same fragments of Inp1 were incubated in G buffer there was no recruitment on the beads and consequently the beads could not be seen (Fig. 3.2). From these results, we can conclude that both fragments of Inp1 can bind to F-actin and not G-actin.

Following visualization of beads, the samples were subjected to centrifugation to separate proteins bound or unbound to beads and used in immunoblotting to detect actin on these samples. The immunoblotting results (Fig. 3.3) show actin bound only when Inp1 fragments were in F buffer, with no actin present in samples that were in G buffer. These results were compared to the positive control Las17. The results confirm the previous findings from fluorescent microscopy indicating that Inp1 can bind directly to F-actin.

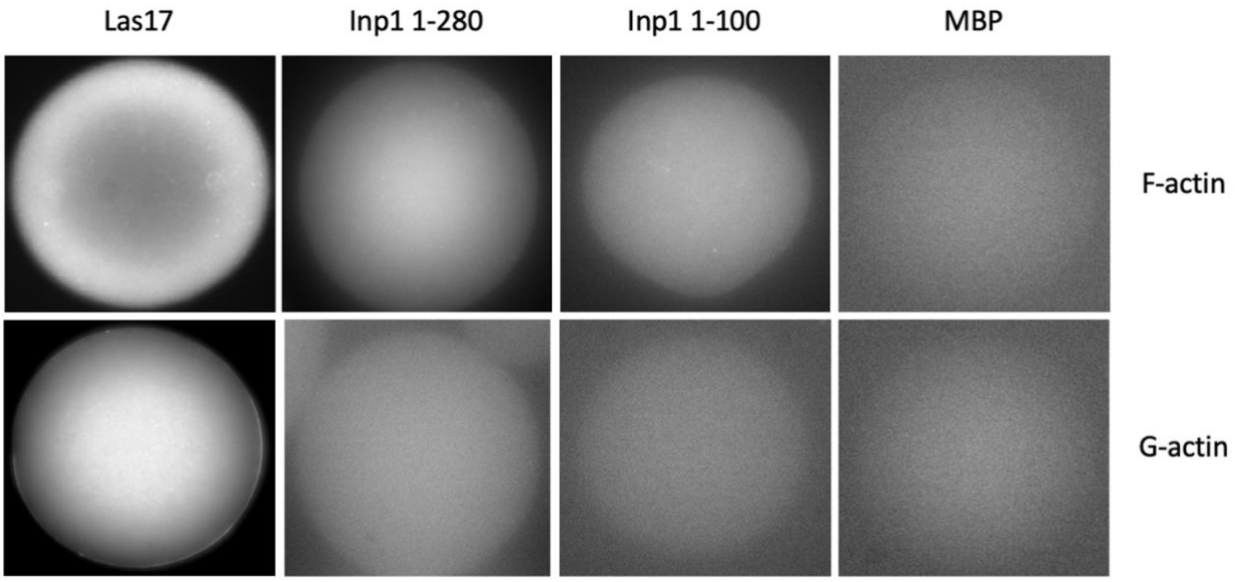

Figure 3. 2: Inp1 interactions with F-actin. MBP, MBP-Inp1 1-100, MBP-Inp1 1-280, and GST-Las17, were expressed and immobilized on amylose beads. These beads were then incubated with F-actin and G-actin in F buffer and G buffer, respectively. Alexa 488 actin was added to all samples for actin visualization. A total of 30 beads were analyzed for each sample.

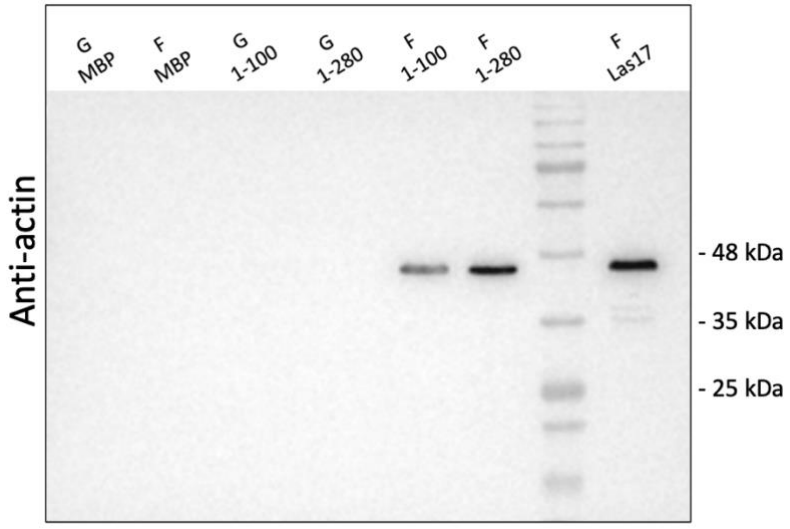

Figure 3. 3: Inp1 binds F-actin. Beads from each sample were run in western blot after the binding assay. MBP, Inp1 1-100 and Inp1 1-280 were either in G buffer (G) or in F buffer (F). Las17 protein was used as a positive control.

3.3 *In vitro*, Inp1 fragments bind F-actin

The MBP-Inp1 truncated fragments, (shown above, section 3.2) that were in F buffer can recruit the fluorescent actin on beads, which indicates that Inp1 can bind F-actin. Another assay was performed to further demonstrate whether purified Inp1 interacts with purified filamentous actin (F-actin).

The actin co-sedimentation, or pelleting, assay is an *in vitro* assay usually used to analyse the binding of protein domains or specific proteins with F-actin, and measure the affinity of the interaction (like the dissociation equilibrium constant). The assay consists of a preliminary incubation of the protein of interest (or domain) with F-actin, followed by ultracentrifugation to harvest F-actin together with any other protein co-sedimented with it. The pellet can then be analysed to determine the extent of protein binding to F-actin. These assays can be designed accordingly to determine actin-binding affinities and in competition assays (Srivastava and Barber, 2008).

The actin co-sedimentation assay is described in detail in Section 2.8.5. In brief, an equimolar amount of each fragments of Inp1 (as indicated in table 2.9) were mixed with 5 µM of actin (as described in section 2.8.1). The mixtures were incubated at room temperature for 2h to allow actin to be polymerised and for binding to take place before ultracentrifugation 90k rpm for 15 min at 4˚C. Subsequently, supernatants and pellets were separately analysed via SDS-PAGE and proteins in the gels were subsequently stained using Coomassie blue.

In this assay, controls were used which were the maltose binding protein (MBP), Inp1 1-100 and Inp11-280, incubated in the absence of actin to determine whether there was any protein pelleting without binding. In the absence of actin, these proteins were detected in the supernatant while no proteins were present in the pellets. Furthermore, MBP in the presence of actin was used as a negative control to determine whether the fusion partner of the fragments could confer actin binding itself. In this case MBP was present in the supernatant while actin alone was found in pellets. A sample containing actin without any additional protein was used as a positive control to determine the polymerizability of the actin preparation used. As expected in this case, most of the actin was in the pellet. In the presence of actin and the MBP-Inp1 fragments (1-100 and 1-280) both fragments were found to be present in the pellet and not the supernatant. It is notable that a higher percentage of the Inp1-fused protein 1-100 than of the MBP-Inp1 1-280 bound to the actin (black arrows shown in Fig. 3.4). These results demonstrate a direct interaction between Inp1 and actin, and increase the validity of our hypothesis, which states that the protein may be an actin binding protein (Fig. 3.4A).

These samples were then tested by immunoblotting using anti-actin to detect the actin in all supernatants and pellets. It is important to note that MBP and actin have similar molecular mass. Hence, it is important to perform an immunoblotting analysis to establish whether the bands in pellet fraction are actin or MBP. The western blot results show the presence of actin in all samples (Fig. 3.4B). This result emphasizes the co-sedimentation result by demonstrating that Inp1 interacts with F-actin *in vitro.*

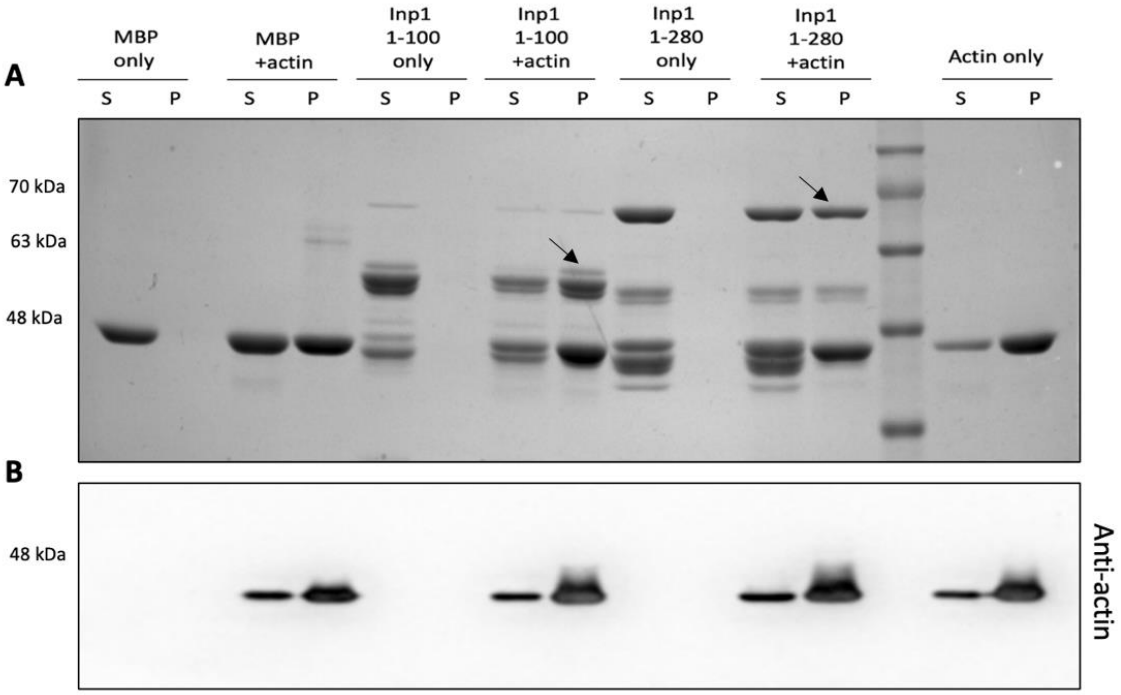

Figure 3. 4: Inp1 short and long fragments co-sedimenting with F-actin. A) Co-sedimentation assay was run at 90k rpm 4˚C after incubating Inp1 fragments with actin for 2h at room temperature. Supernatants and pellets were separated before being analysed by SDS-PAGE followed by Coomassie blue staining. Arrows indicate co-sedimented Inp1 fragments. B) Samples were analysed by immunoblotting by anti-actin antibodies at a ratio of 1:500 (S: supernatant and P: pellet). The graph shows supernatant and pellet values for actin, MBP-Inp1 1-100 and MBP-Inp1 1-280 samples. Bands were normalised against their inputs. Normalised inputs were set to 1 A. U. where A. U. is arbitrary units.

3.4 Does Inp1 affect the actin dynamics and polymerisation?

Since Inp1 interacts with F-actin, it was intriguing to investigate whether this binding affects actin dynamics. Actin polymerization is a reversible process in which monomers associate with and disassociate from actin filament ends though addition primarily occurs at one end "the barbed end" and disassembles from the other end "pointed end". This gives rise to characteristic polymerization stages with a nucleation, an elongation and a steady state phase (Dominguez & Holmes, 2011).

Actin fluorimetry assays were used to test the effect of Inp1 on actin. The assays can be used to determine the polymerization and depolymerization of actin. This happens by measuring the fluorescence of pyrene conjugated with actin (Doolittle et al., 2013). Pyrene is a fluorophore, and when bound to G-actin it emits only a very low level of fluorescent light. When this pyrene G-actin is incorporated into an actin filament, the fluorescence light emitted increases approximately 10-fold because of changes in the environment around the fluorophore. Using this approach, it is possible to assess the impact of factors that affect the nucleation, polymerization, steady state or depolymerization of filaments.
The assay was used to test whether addition of Inp1 protein leads to changes in stages of actin polymerization.

In the assay, 5 µM G-actin and 0.5 µM pyrene actin produced as described in section 2.8.2 were mixed in F-Buffer before adding ~4.9 µM MBP-Inp1 or MBP contained in F buffer as described in section 2.8.4. A sample was also set up containing no additional protein but with just an equivalent volume of maltose buffer to that in the Inp1 protein fragment samples.

The fluorometer results (Fig. 3.5) show that the control actin plus F buffer showed a low level of increase over the time period indicating some polymerization was taking place. This is driven by the increased level of salt (50 mM KCl) which is known to induce actin polymerization. All other samples showed an increased rate and level of polymerization. However, the addition of maltose buffer alone gave a similar level of increase to those samples that contained the Inp1 fragments indicating that the Inp1 fragments do not affect the rate of actin polymerization and that the increased polymerization was due to the high level of salt in maltose buffer (400mM NaCl).

As mentioned above, Inp1 short and long fragments bind actin *in vitro*, but they do not affect actin polymerisation dynamics. However, it remains unclear whether such binding can occur also *in vivo*.

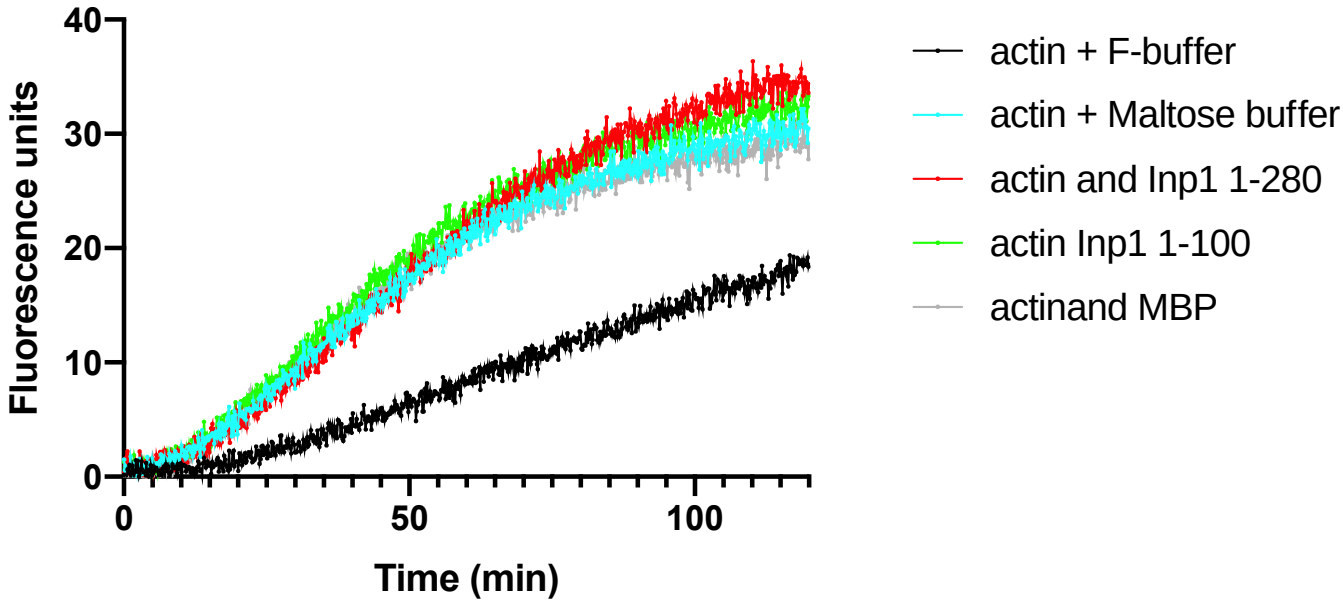

Figure 3. 5: Actin polymerisations. MBP protein, MBP-Inp1 fragments (1-100 and 1-280), maltose buffer and actin samples were mixed with 5uM G-actin and 0.5uM pyrene actin and F buffer in total volume of 300 µl before running them on fluorometer for 5h. B) Samples were in maltose elution buffer, except for the control which was actin plus F buffer (F buffer contains 50 mM KCl).

3.5 Disruption of actin affects peroxisome distribution

Inp1 is known to play a crucial role in retention of peroxisomes. In two different yeast species, *S. cerevisiae* and *H. polymorpha*, Inp1 functions as plasma membrane tether through its N-terminal, and its C-terminal acts as peroxisomal binding domain (Hulmes et al., 2020; Krikken et al., 2020). In *H. polymorpha*, an intact actin cytoskeleton is required for Inp1's cortical localization. Cortical Inp1 patches are lost as a result of actin disruption by latrunculin-A (latA) (Krikken et al., 2020).

Given the localization of Inp1 depends on actin cytoskeleton, it was intriguing to check the peroxisome distribution in the presence of latrunculin-A in *S. cerevisiae*.

In this experiment, WT cells expressing the peroxisomal marker *mRuby-PTS1* and Inp1-GFP, and *Δinp1* cells expressing the peroxisomal marker mRuby-PTS1 and Inp1-GFP were treated with latrunculin-A (LatA). LatA was used in a final concentration of 200 µm before cells being imaged. *Δinp1* cells expressing the peroxisomal marker mRuby-PTS1 and Abp1-GFP were used as control. Abp1p is a protein that binds actin directly and associates with cortical actin patches (Drubin et al., 1988).

In the presence of LatA, the fluorescence of Abp1-GFP patches disappeared confirming the effect of LatA on filaments of actin (Fig. 3.6). Peroxisomes in *Δinp1* cells were in the bud as result of *INP1* deletion.

In WT and *Δinp1* cells expressing GFP-Inp1 and mRuby-PTS1, following addition of LatA, peroxisomes were seen to change their localization and started to cluster at the bud neck (Fig. 3.6). Quantitative analysis showed that in the presence of LatA, more than 80% of cells have clustering peroxisomes (Fig. 3.7). From the results, we can conclude that the distribution of Inp1 and peroxisomes is affected by the disruption of actin.

Interestingly, the same phenotype has been reported in an *inp1* mutant. The Rachubinski group performed random mutagenesis experiments on Inp1 to study the ER-peroxisome tether. One of these mutants was *inp1 T26M* which affects the peroxisome distribution. The phenotype of this mutation consists of peroxisome clustering at the bud neck and affects the peroxisome transfer to the bud (Knoblach & Rachubinski, 2018). In the Hettema lab, the *inp1 T26M* mutation was generated and tagged with GFP by a lab member. The mutation was then tested in this study, and the phenotype mentioned above was verified. *Δinp1* cells were transformed with Inp1-GFP full length and *inp1-GFP T26M* separately. Control cells expressing the full length of Inp1 have a normal peroxisome distribution (Fig. 3.8A). As shown in Fig.3.8B, unlike the wild type, the majority of cells expressing *inp1 T26M* mutation have clustering peroxisomes at the bud neck.

The peroxisome clustering phenotype when actin is disrupted is strikingly similar to the one in the mutant of *inp1 T26M,* which raises the question of whether there might be a link between the residue T26 and actin. Consequently, the T26 mutant was generated in the MBP fusion Inp1 1-100 and a co-sedimentation assay was performed to investigate whether the mutant *T26M* affects the interaction between Inp1 and actin. The experiment was run as described above (section 3.3) using yeast strains expressing *inp1 T26M*. In this assay, actin-free samples MBP, MBP-Inp1 1-100 and *MBP-inp1 1-100 T26M* were used as negative controls. In the absence of actin, these proteins were shown in the supernatant while no proteins were in the pellets. In addition, MBP plus actin was used as a negative control where MBP was present in the supernatant while actin was found in pellets. A sample containing actin with no additional protein was used as a positive control. Most of the actin was in the pellet. However, in the presence of actin and after actin polymerization, both MBP-Inp1 fragments (1-100 and *1-100 T26M*) were found to be present in the pellet but not in the supernatant (Fig. 3.9). This result demonstrates that the clustering peroxisomes caused by mutant T26M did not occur because of a direct impact on actin binding, and that Inp1 still binds actin.

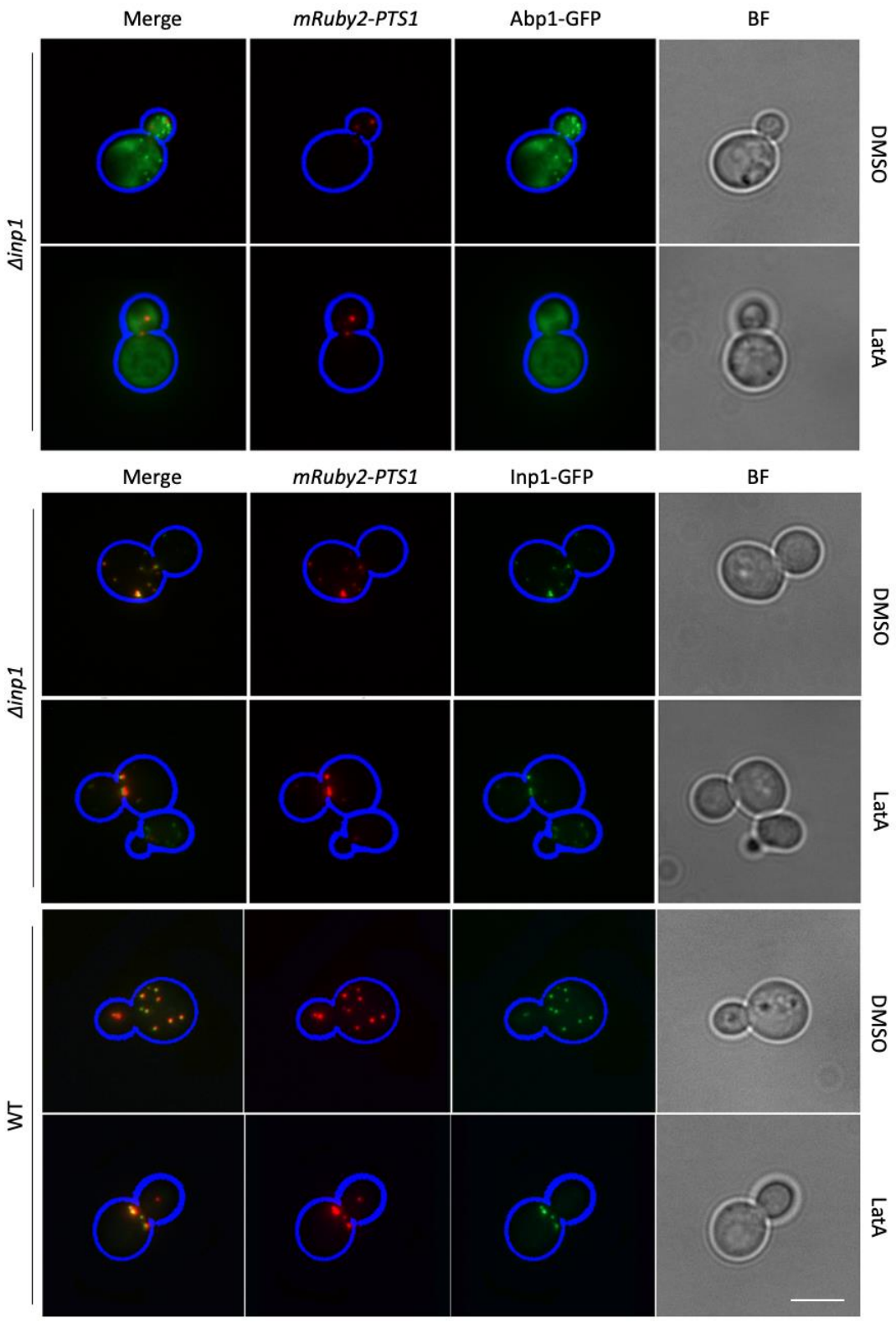

Figure 3. 6: Peroxisomes clustered in the presence of LatA. *inp1Δ* strain expressing Inp1 FL and WT strain were treated with LatA from 10mM DMSO stock in a final concentration of 200 µM for 15 min before being imaged. The same volume of DMSO was used as control. *inp1Δ* strain expressing Abp1-GFP was used to confirm if actin filaments are affected when LatA is added. Bars, 5µm.

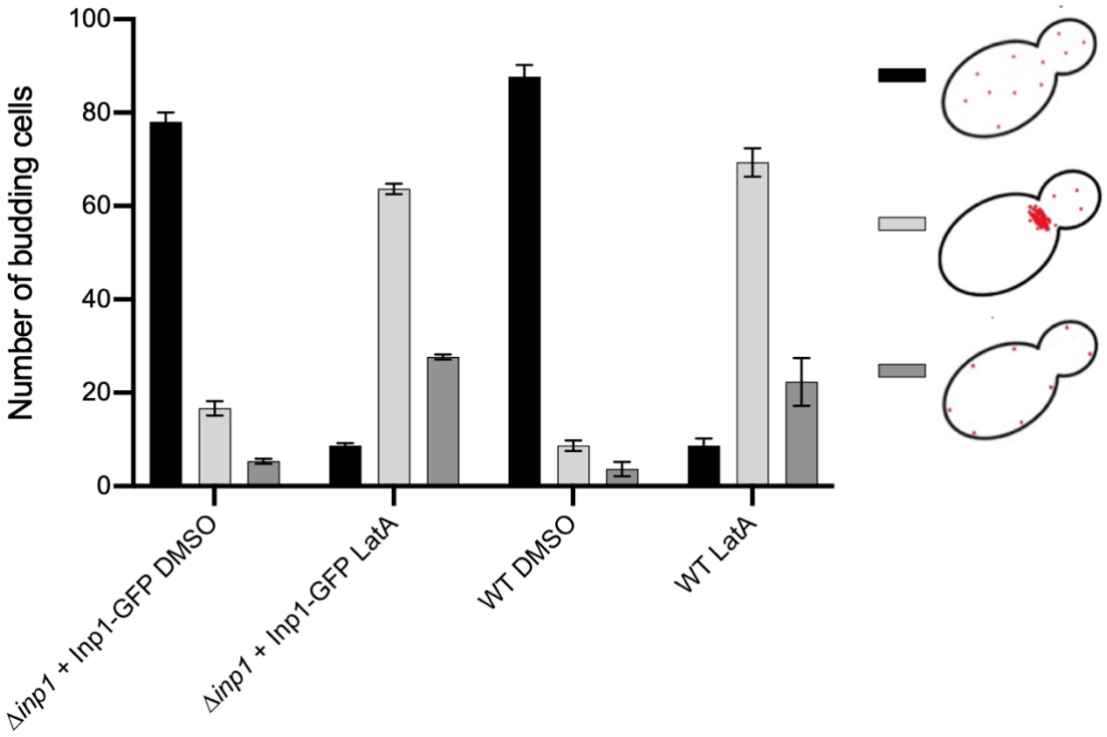

Figure 3. 7: Quantification of the peroxisome bud neck clustering phenotype. Δinp1 cells expressing the full length of Inp1 and WT cells were treated with LatA. A total of 100 cells from each strain were analyzed in three separate experiments. The error bars describe the mean with SEM.

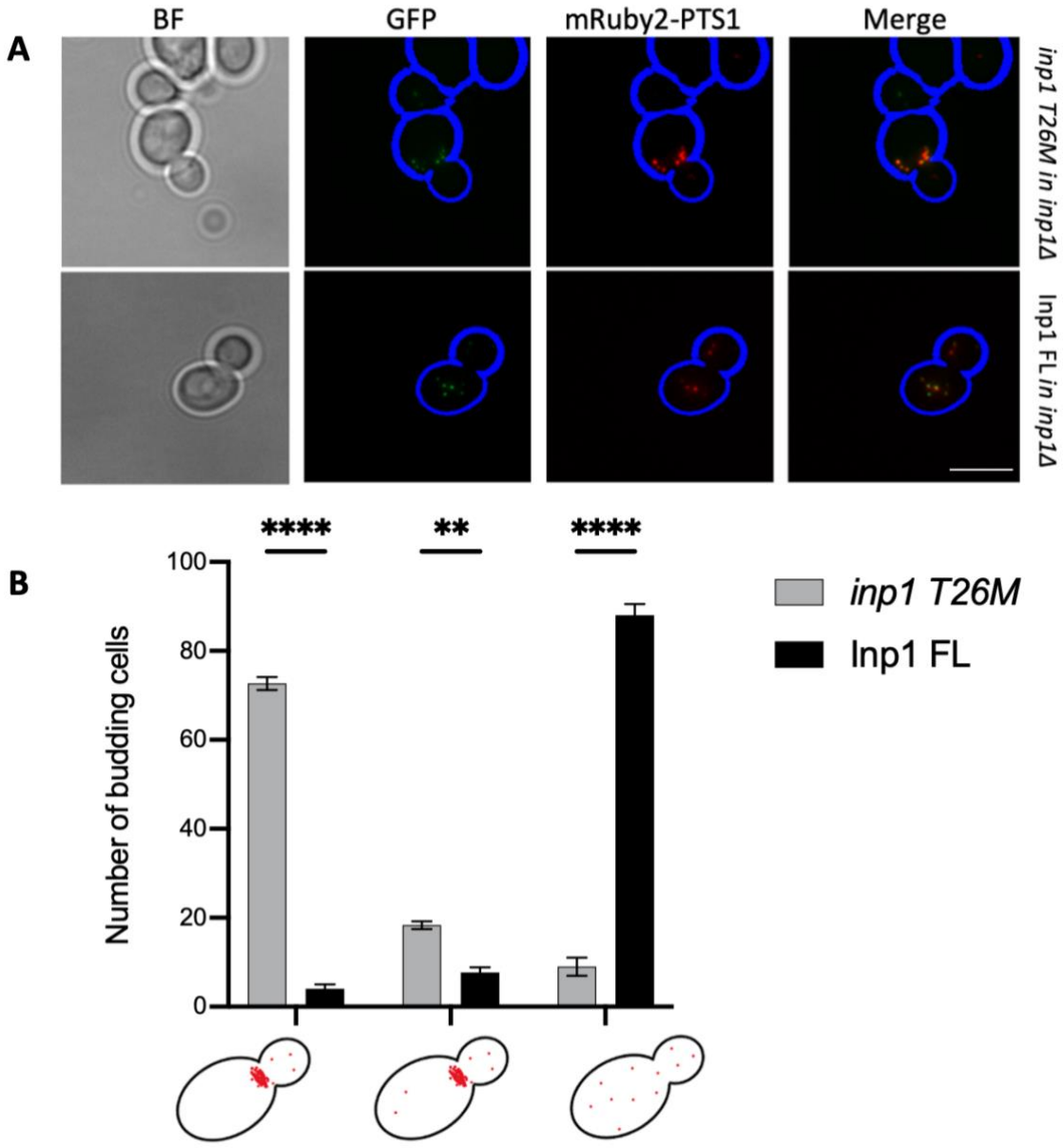

Figure 3. 8: *inp1 T26M* mutation showed clustering peroxisome at the bud neck. A) *inp1 T26M*-GFP and Inp1 FL-GFP plasmids and the peroxisomal marker *mRuby2-PTS1* were transformed into *inp1Δ* strain. Cells grown to log phase before imaging. Bars, 5 µm. B) Quantification of the peroxisome bud neck clustering phenotype marked upon *inp1 T26M-GFP* expression or Inp1 FL-GFP in *inp1Δ*. A total of 100 cells from each strain were analyzed in three separate experiments. The error bars describe the mean with SEM. Statistical significance was determined by unpaired student t test: **P ≤ 0.01,****P ≤ 0.0001.

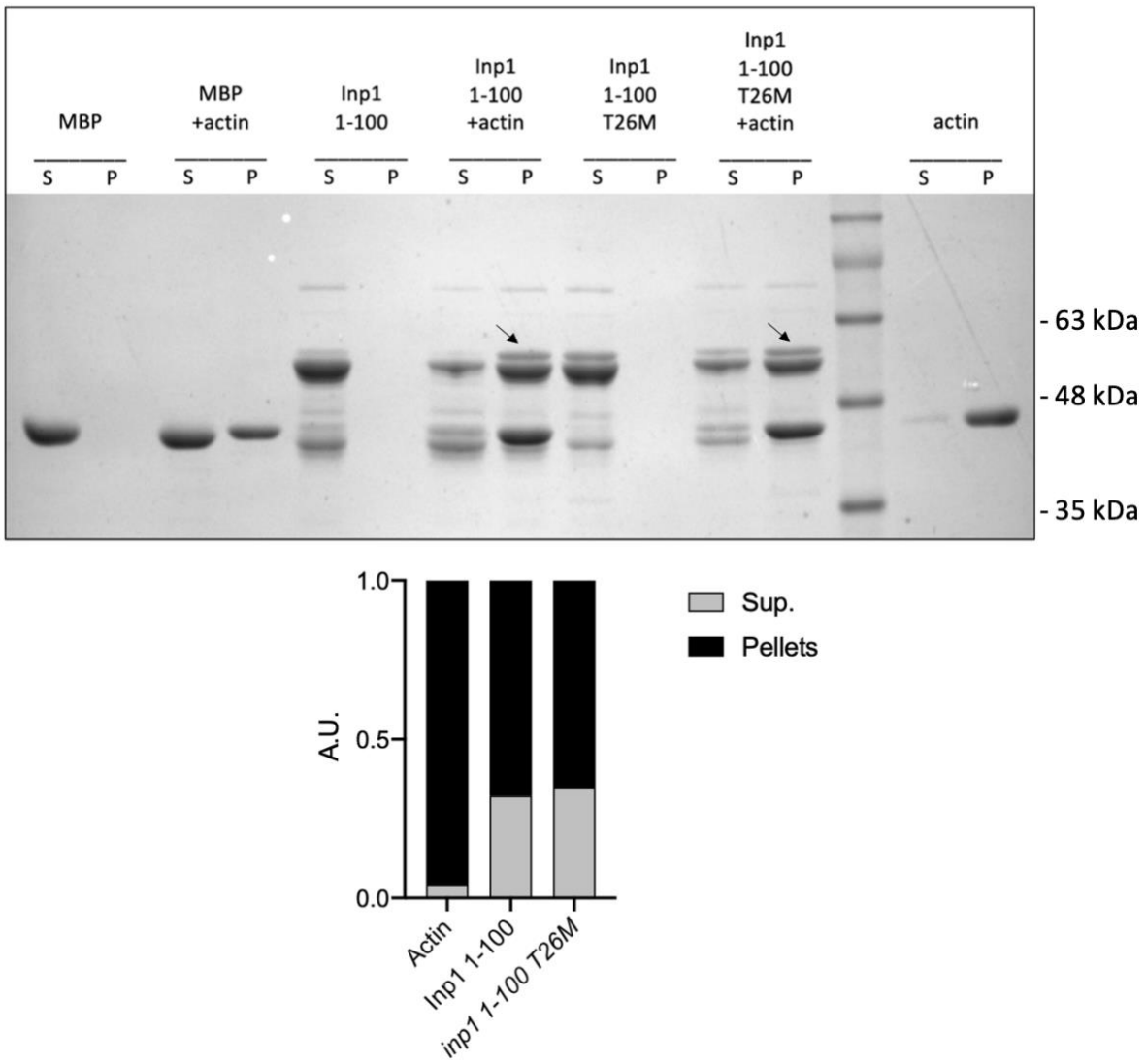

Figure 3. 9: The mutant *inp1 T26M* does not affect the interaction between Inp1 and actin. Co-sedimentation assay was run at 90k rpm 4˚C after incubating Inp1 fragments (1-100 and *1-100 T26M*) with actin for 2h at room temperature. After separating supernatants and pellets, proteins were analysed by SDS-PAGE followed by Coomassie blue staining. Arrows mark the presence of co-sedimented Inp1 fragments. The graph represents supernatant and pellet values for actin, MBP-Inp1 1-100 and *MBP-inp1 1-100 T26M* samples. Bands were normalised against their inputs. Normalised inputs were set to 1 A. U. where A. U. is arbitrary units.

3.6 Mutations of *ACT1* affect the distribution of peroxisomes

Previous studies have mutated the actin gene extensively and this facilitated our understanding of the structure-function relationship of actin. The yeast actin gene *ACT1* was subjected to the first alanine scanning mutagenesis (Wertman et al, 1992). Clusters of 2 or more charged residues in *ACT1* were replaced with alanine (Fig. 3.10) (Wertman et al., (1992). This group of mutants has been shown to be a very effective set of reagents for investigating the structure-function relationships in the actin cytoskeleton. The effect of these mutations varied between lethal, temperature sensitive and wild-type (Wertman et al., 1992).

Learning more about the critical parts on actin that might be involved in peroxisome interaction and function was our next goal. Because the disruption of actin by LatA affects the distribution of peroxisomes, we were curious to analyse peroxisomes in *ACT1* mutant cells and investigate whether some of these mutants have an effect on peroxisomes. Consequently, some of these mutations were collected from the Ayscough lab (listed in table 3.1). Yeast strains expressing mutated actin proteins as the sole form of actin in the cell were grown to log phase before being analysed by fluorescence microscopy. Some of these cells were sick and could not be imaged due to slow growth. Most of the mutations that have been imaged show a normal peroxisome distribution when compared with the wild type. However, two of these mutations, *act1-104* and *act1-116*, displayed an interesting peroxisomal phenotype. Although these mutations had no observable phenotype on yeast growth at different temperatures or on salt containing media (Wertman et al., 1992), they affected the distribution of peroxisomes. Analysis of fluorescent images showed that expression of the *act-104* and *act1-116* mutants cause the clustering of peroxisomes at the bud neck (Fig. 3.11).

Table 3. 1- Yeast actin mutations

Allele	Amino acid replacement	Phenotype
Act1	None	Wild type
act1-101	D363A, E364A	Heat sensitive
act1-102	K359A, E361A	Wild type
act1-104	K315A, E316A	Wild type
act1-105	E311A, R312A	Cold and heat sensitive
act1-113	R210A, D211A	Heat sensitive
act1-116	D187A, K191A	Wild type
act1-119	R116A, E117A, K118A	Heat sensitive
act1-120	E99A, E100A	Heat sensitive
act1-123	R68A, E72A	Wild type
act1-124	D56A, E57A	Heat sensitive
act1-125	K50A, D5 1	Cold and heat sensitive
act1-129	R177A, D179A	Heat sensitive
act1-133	D24A, D25A	Cold and heat sensitive
act1-136	D2A	Cold and heat sensitive

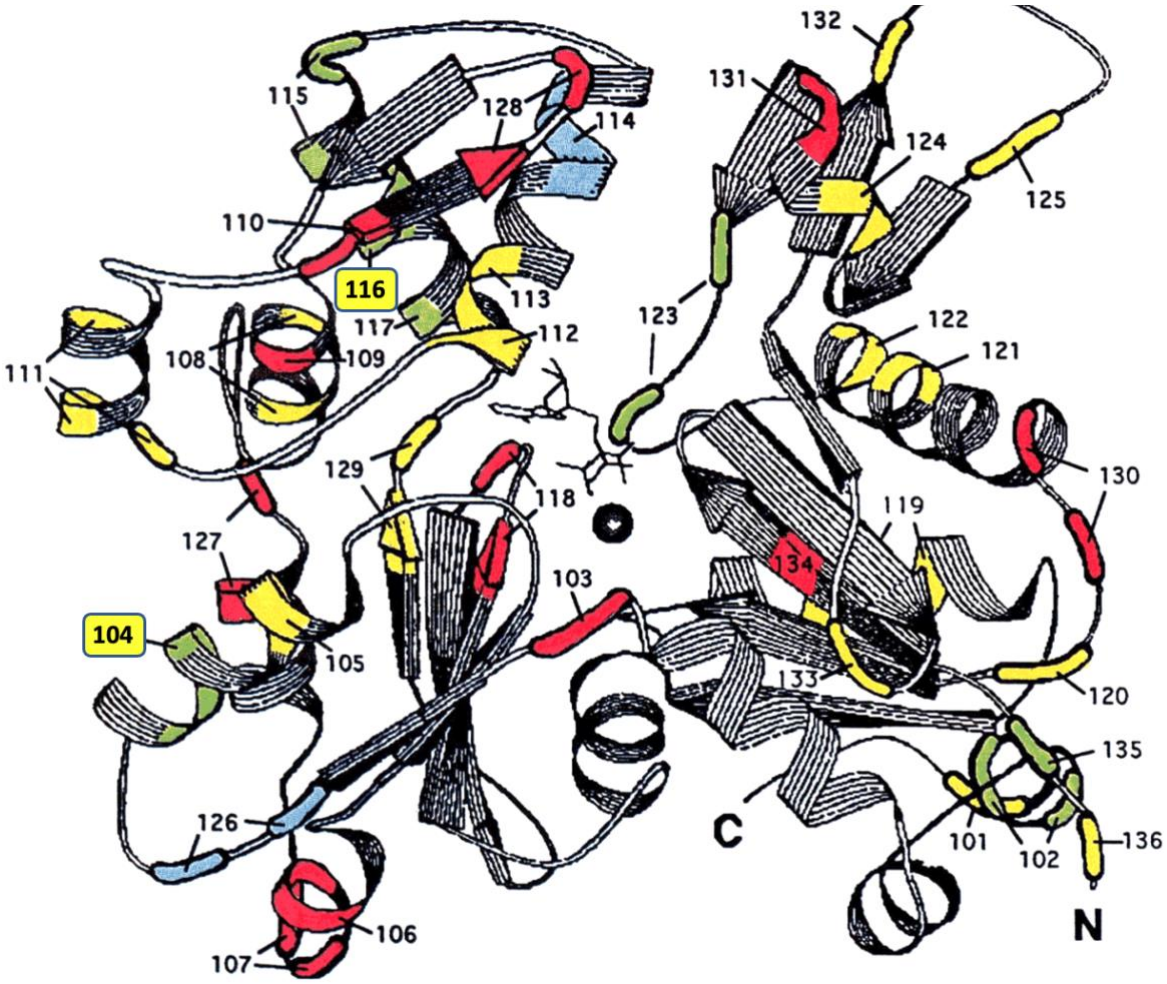

Figure 3. 10: Ribbon diagram of the actin monomer (Wertman et al., 1992). The diagram shows the sites of the backbone residues for the charged group replacements. Residues are color-coded according to the haploid mutant phenotype: green, no phenotype observed; yellow, temperature sensitive; red, lethal; blue, putative dominant lethal. Allele designations are represented by numbers. The adenine nucleotide is depicted as a basic stick model in the noticeable cleft, and the divalent metal ion is represented as a large tilled circle. (Wertman et al., 1992).

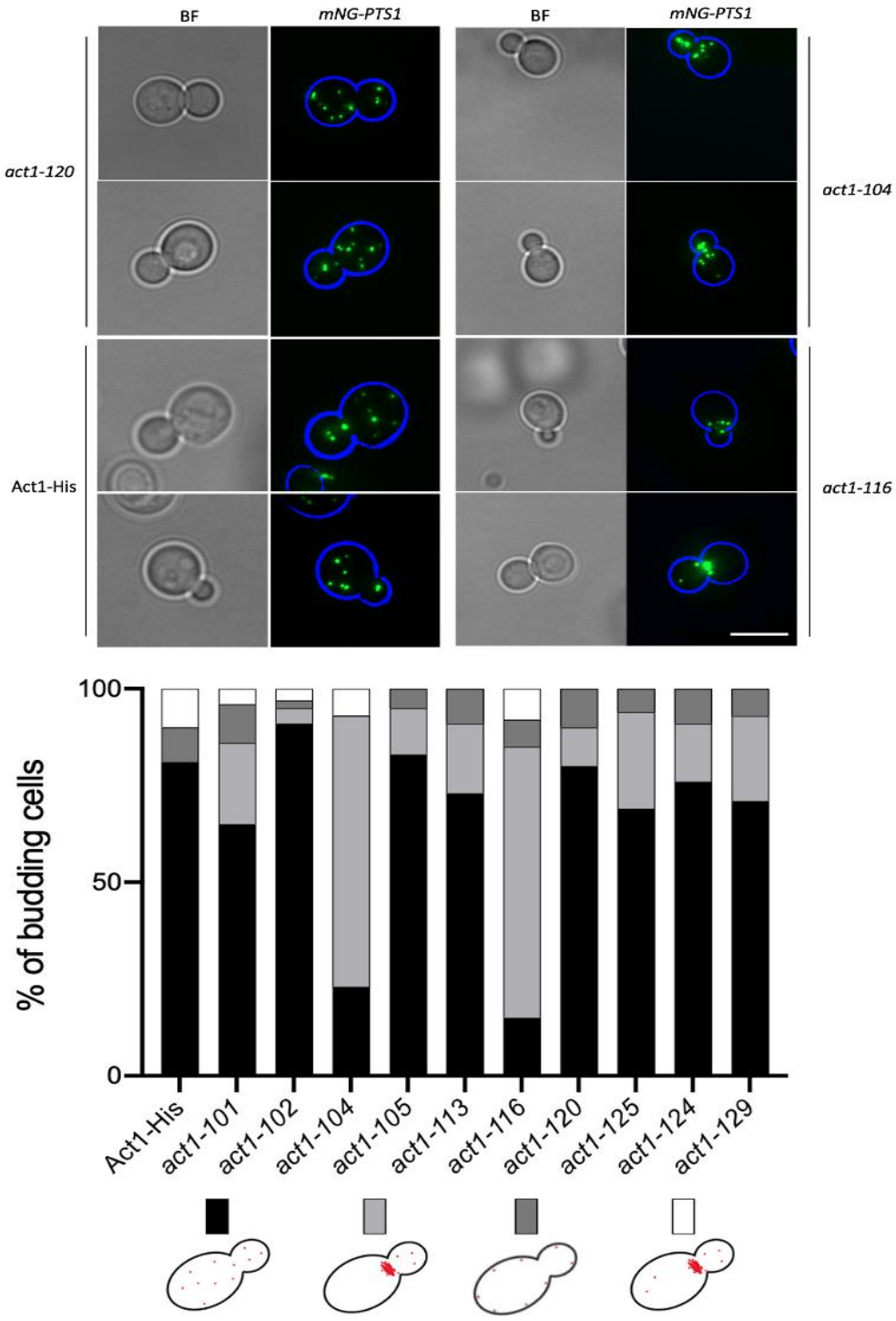

Figure 3. 11: *act1-104* and *act1-116* strains showed clustering of peroxisome in the bud-neck region. Cells expressing mutant actins were grown to the log phase and imaged in the presence of the peroxisomal marker *mNG-PTS1*. Figures show the peroxisomal phenotype in *act1-104* and *act1-116* compared to wild type, and mutant actin that shows a normal distribution of peroxisomes. Bars, 5µM. The graph represents the quantification of yeast strains expressing actin mutants and the peroxisomal marker *mNG-PTS1* and their effect on peroxisomes. More than 200 cells were analysed for each strain.

3.6.1 Actin filaments in *act1-104* and *act1-116* mutants

Although it was apparent that these mutants affected peroxisomes in yeast, their effect on actin dynamics was not clear, yet important to understand. It was shown above (Section 3.5) that the distribution of peroxisomes is affected when actin is completely disrupted. It was therefore beneficial to examine actin filaments in the presence of actin mutants. In order to demonstrate the effect of these actin mutants, actin filaments were checked in strains expressing *act1-104* or *act1-116* mutant genes and the peroxisomal marker *mNG-PTS1* by using rhodamine phalloidin staining. Rhodamine phalloidin was used as described (Section 2.8.6) to stain actin filaments. Cells were then analysed by a fluorescence microscope.

The control which is cells expressing the wild type *ACT1* shows normal actin cables as well as normal peroxisome distribution. In the presence of mutant actins *act1-104* and *act1-116*, actin cables presented as normal as wild type, while peroxisomes clustered at the bud neck (Fig. 3.12). Although these mutants affect the normal location of peroxisomes, these results demonstrate that they have no effect on actin organisation.

3.6.2 Vacuoles in *act1-104* and *act1-116* mutants

The actin mutants *act1-104* and *act1-116* have been shown to influence peroxisome distribution (Section 3.5), but staining the actin filaments in cells expressing these mutant actins demonstrates that these two mutants have no impact on the organisation of actin (see 3.6.1). This led to investigating whether these mutations have an effect on other organelles in addition to peroxisomes. Vacuole is a suitable organelle to test because any effects will be clearly observed because it is known that vacuoles are dramatically impacted by the perturbation of actin. The effect can result in abnormal structure, an increase in number, and shape changes such as fragmented vacuoles (Eitzen et al., 2002).

We then checked whether actin mutants can impinge on vacuole size, shape or inheritance. In this experiment, cells expressing the *act1-104* and *act1-116* mutants in addition to the peroxisomal marker *mNG-PTS1* were stained by lipophilic dye FM4-64 (Invitrogen). To stain the vacuolar membrane, cells were grown to log phase before harvesting. The pellets were then resuspended in 200µl YPD containing lipophilic dye FM4-64 (Invitrogen) (Vida and Emr, 1995) in a final concentration of 1 ng/µl. Cells were incubated at 30˚C for 1h and then washed three times with YM1 media. Cells were then added to 4ml fresh YM1 media and incubated at 30˚C for 4h before being imaged.

In the control sample, which is cells expressing the wild type *ACT1*, vacuoles look normal in shape and number, and they were inherited into the bud. In the presence of actin mutants, the inheritance, shape and number of vacuoles were normal, and no phenotypes were observed compared to the wild type (Fig. 3.13). The results indicate that the effect of these mutations might be specific to peroxisomes.

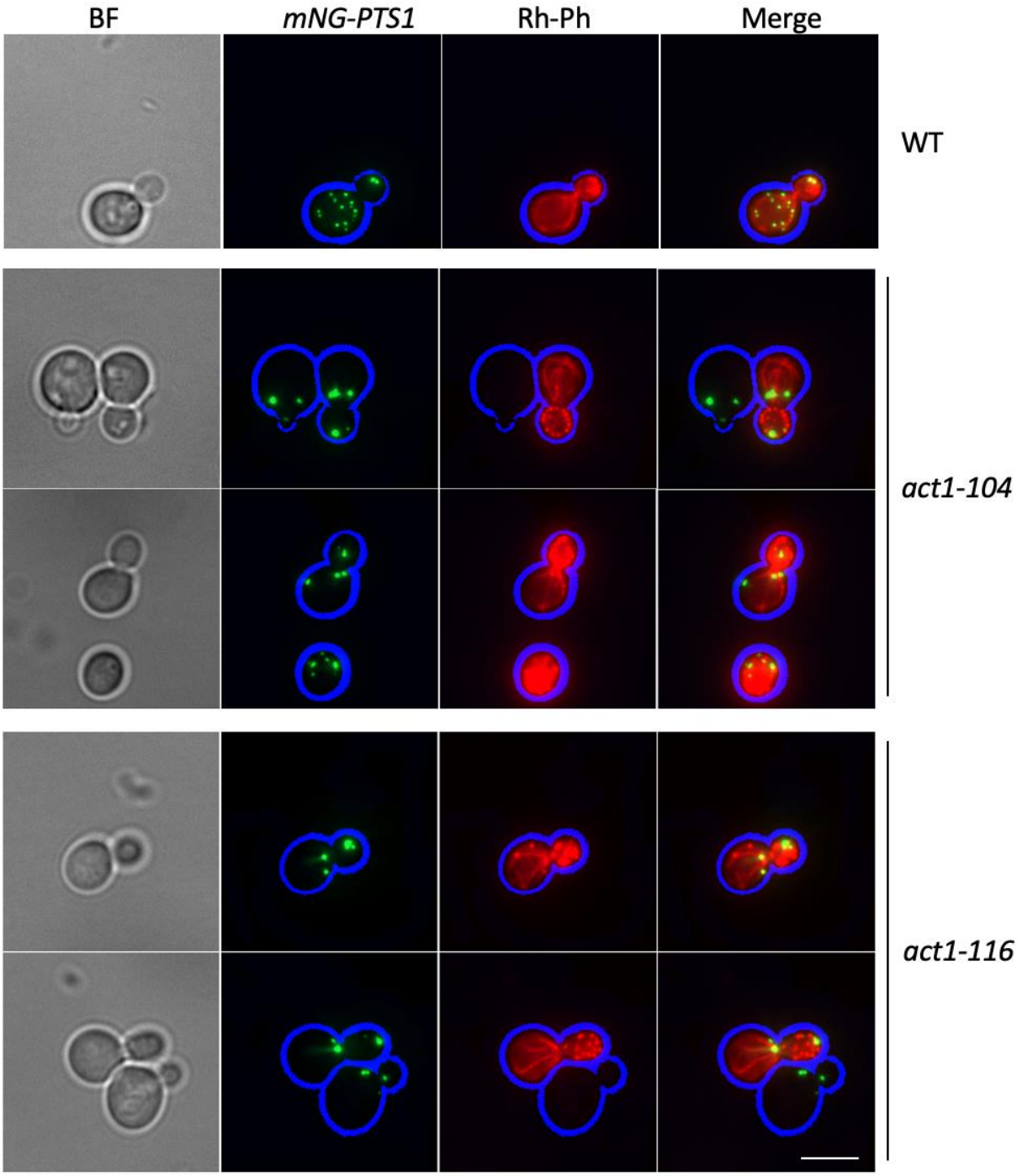

Figure 3. 12: Actin mutants *act1-104* and *act11-116* have no impact on actin dynamics. *act1-104*, *act1-116* and wild type copy cells were grown and stained with rhodamine phalloidin stain and imaged. Bars, 5µm.

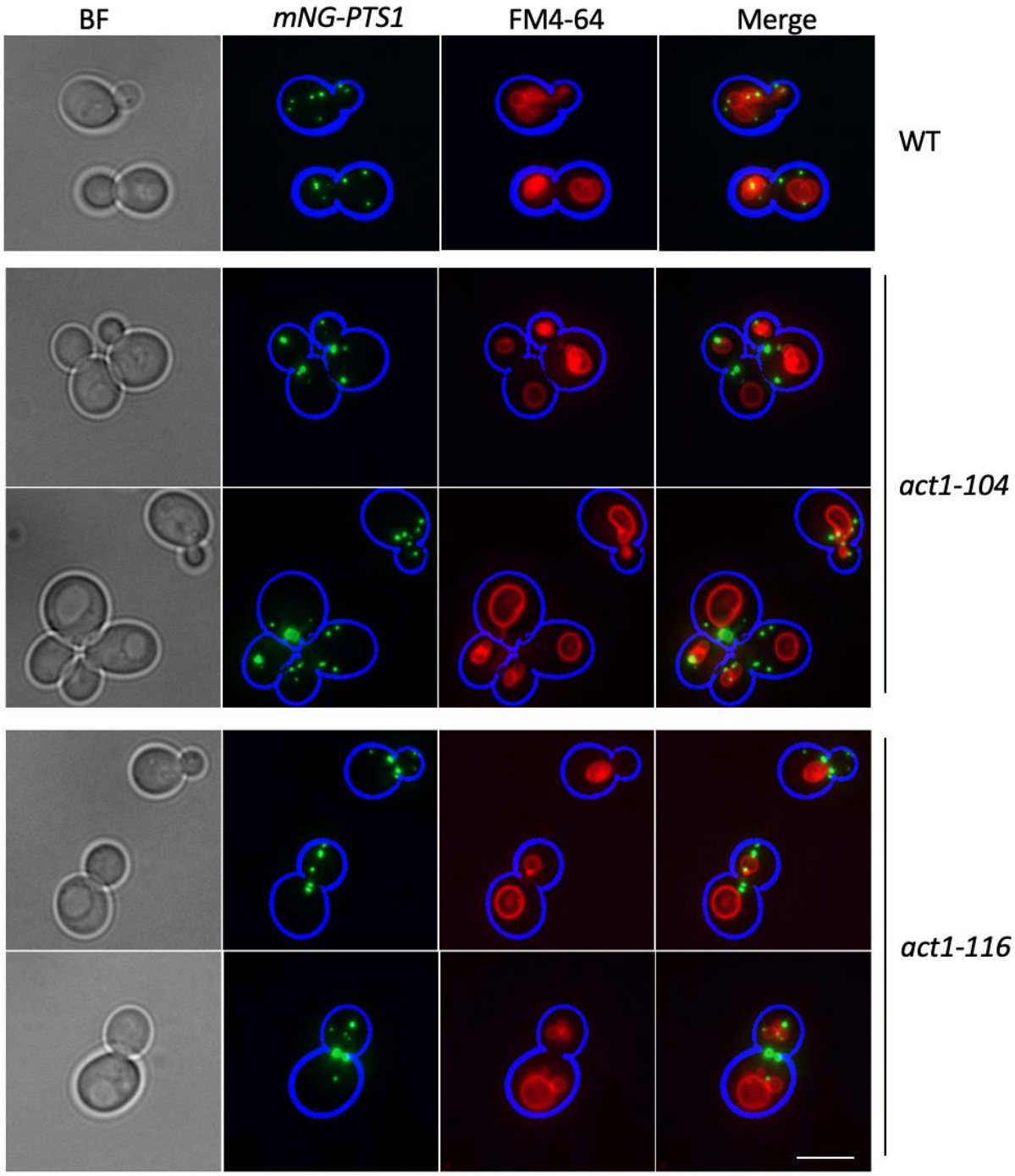

Figure 3. 13: Vacuoles are not influenced in the presence of actin mutants *act1-104* and *act11-116*. Cells carrying the actin mutants *104* and *116* were grown to log phase and stained with the vacuole dye FM4-64 followed by imaging by a fluorescent microscope. Bars, 5µm.

3.7 Inp1 interacts with actin in yeast two-hybrid approach

In previous studies, the yeast two-hybrid approach has proven effective in identifying new proteins that interact with actin (Amberg et al., 1995) and to map actin binding interactions (Ayscough et al, 1997). Using the same actin construct as those above-mentioned studies, we tested whether a full-length Inp1 construct or a construct comprising its first 280 amino acids was able to interact with actin or a number of actin mutants (described in section 2.8.8). In this assay, a profilin (Pfy) fusion was used as a control, as it is known to bind Actin (Drees et al., 2001). Empty pGAD and pGBD plasmids were used as negative controls. Four fusions proteins – wild type Act1 and 3 mutant actins *104,119, 120* were constructed in the pGBD-C1 vector to contain the Gal4 DNA-binding domain. pGAD-C1 vector was constructed separately to contain Pfy, the full-length Inp1 and its first 280 amino acids, which were fused to the transcriptional activation domain.

Negative controls did not interact with any of the samples. Profilin (Pfy) showed interactions with Act1 and mutant actin *act1-120*. However, there were no interactions shown with *104* and *119* actin mutants.
Interestingly, no interaction was detected between the full-length Inp1 and actin or actin mutant samples. However, the first 280 amino acids of Inp1 did show an interaction with the wild type copy of Act1 and a weak interaction with mutant actin *act1-120*. Similar to Pfy, there were no interactions between the mutant actins *104* and *119* and Inp1 1-280 (Fig. 3.14).

These results indicate several things. First, the data supports other data that shows Inp1 1-280 interacts with actin. This experiment gives the first data that this interaction can occur in cells. However, the full-length Inp1 does not interact with actin suggesting parts of Inp1 have the capacity to block or inhibit binding. For example, the negatively charged cluster preceding the Pex3 binding domain could prevent the interaction.
The interaction with *act1-120* suggests that this mutant actin still has the capacity to bind Inp1-280 but that ability is lost in the *act1-104* and *act1-119* mutants. It is notable that cells expressing *act1-119* are very sick and so no-binding might be due to the actin being generally not very well folded. *Act1-104* mutants on the other hand are able to grow well in the absence of wild type actin and their actin is well organised. This allows a tentative suggestion that the mutations in *act1-104* might highlight a binding site for Inp1.

In conclusion, the Y2H approach demonstrates the interaction between actin and the first 280 amino acids of Inp1, and the non-interaction of the full-length Inp1. The Y2H approach leads to possible indication of a binding site in the Act1 protein.

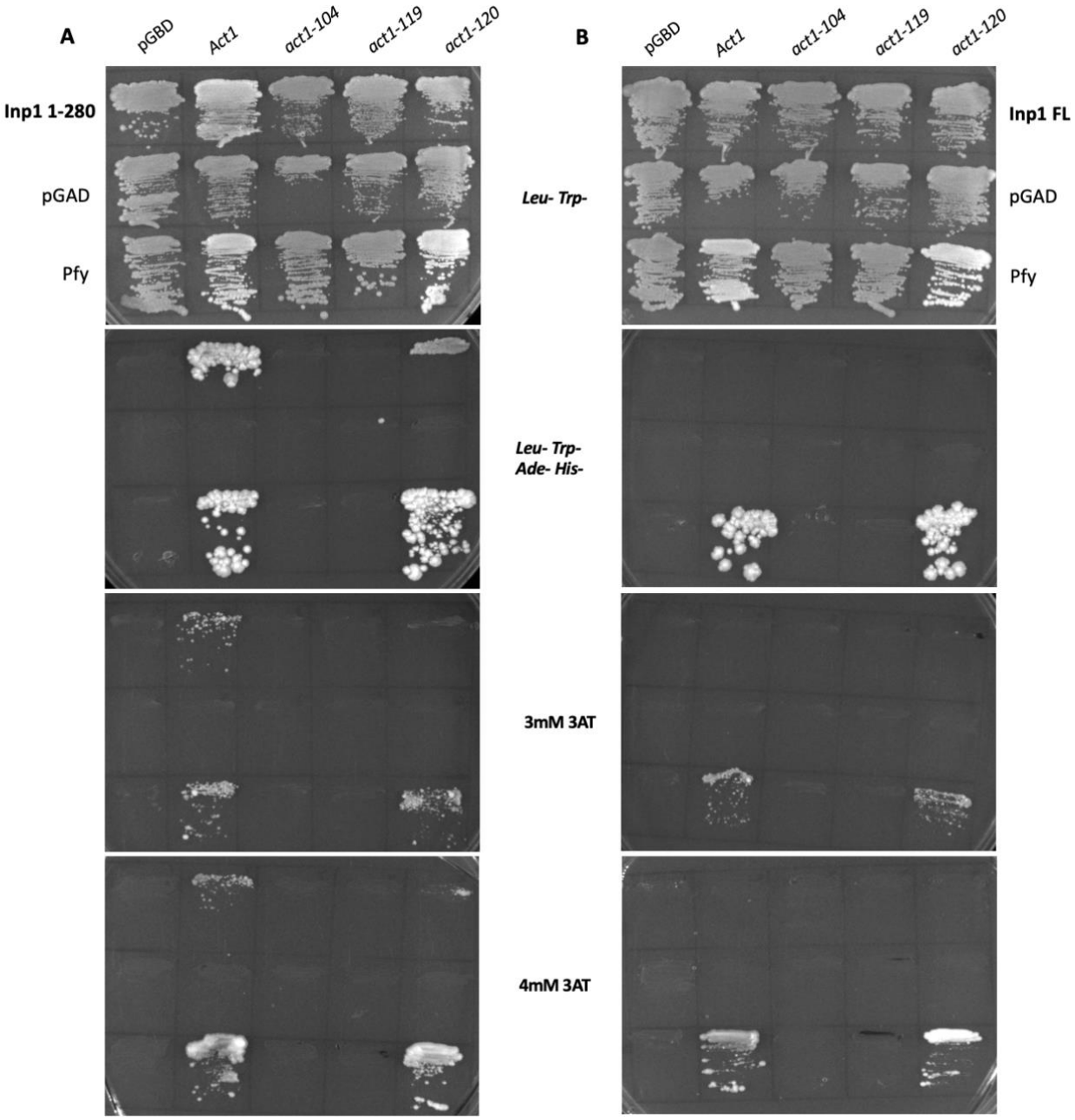

Figure 3. 14: Inp1 interacts with actin in yeast two-hybrid approach. Strains expressing 4 different actin alleles were examined for their ability to interact with A) Inp1 1-280 and B) Inp1 full length. All samples were mated on YPD plates then diploids were selected on Leu-Trp- plates before being restreaked on Leu-Trp-Ade-His- plates with/without 3mM and 4mM 3AT. Pfy protein was used as a positive control, while empty pGAD and pGBD plasmids were used as negative controls with all samples.

3.8 The middle domain of Inp1 interacts with Srv2

Since functions of the N and C terminus of Inp1 have been characterised and its middle domain function is not characterised yet, our goal was to characterise the role of the middle domain of Inp1 in *S. cerevisiae* in the hope of gaining insight into its contributions to its function. We first attempted to gain insights into the function of Inp1's middle domain using various bioinformatic approaches. We first analysed the protein structure predictions from AlphaFold to identify any structural features that might provide clues to the domain's function. We also searched for conserved domains and motifs in InterPro and Pfam databases, which could suggest potential roles or interactions for the middle domain.

To investigate the evolutionary conservation of the middle domain, we performed multiple sequence alignments using tools like Clustal Omega and T-Coffee, comparing Inp1 homologs from various species. This analysis aimed to identify conserved residues or regions that might be functionally important. We also utilized protein-protein interaction prediction tools, such as STRING and IntAct, to explore potential interactors or protein complexes involving Inp1's middle domain.

Additionally, we analysed the domain's physicochemical properties, such as hydrophobicity, isoelectric point, and disorder prediction, using tools like ProtParam and IUPred. These analyses could help determine if the middle domain has any particular structural or functional characteristics that set it apart from the rest of the protein.

Despite these extensive bioinformatic efforts, our analyses did not provide any significant information that could help determine the function of the middle domain. It has been thought that identifying proteins that can interact with Inp1's middle domain may deliver an initial understanding of the function of the middle domain. For this purpose, large-scale Y2H screens were performed (by Hybrigenics Services SAS) to identify more proteins that are able to interact with the middle domain of Inp1.

In this yeast two-hybrid approach, the middle domain of Inp1 (aa 73-280) was constructed as a Gal4-binding domain fusion in the pB66 vector. Almost 58 million interactions were tested. The results obtained gave 20 positive clones that were processed (listed in Figure 3.15). Proteins were divided into categories depending on the confidence of interaction. The category of moderate confidence in the interaction included several proteins: Zip1, Uga1, Myo3, Myo5, Msn3 and Jsn1. Only one protein was in the category of highest confidence, Srv2.

The Srv2 (cyclase associated protein CAP in mammals) is a highly conserved actin binding protein in eukaryotes. It contains several domains promoting actin turnover. Its C-terminus contains two actin binding regions, a WH2 and a ‘β-sheet’, which enable C-Srv2 to strongly interact with ADP-G-actin. It has also the ability to displace cofilin from ADP-actin monomers and catalyze nucleotide exchange by facilitating the exchange of ATP for ADP. Through these effects, actin monomers can be recycled by the C-terminal, and this is crucial in the quick turnover of the actin network *in vivo.* The N-terminal domain binds adenylate cyclase and promotes its activation by RAS (Mattila et al., 2004, Chaudhry et al., 2014, Chen et al., 2019). The Y2H results revealed that the middle domain of Inp1 (73-280) interacts with several

fragments of Srv2. These interacting fragments include amino acids 267-498, 270-492, 349-495, and 358-488. Notably, all these fragments encompass the WH2 domain (270-370), indicating its potential involvement in the interaction with Inp1's middle domain. The smallest fragment identified in our study is the C-terminal fragment spanning amino acids 358-488, which partially overlaps the WH2 domain and predominantly contains the beta-sheet region (370-526). This finding suggests that the C-terminal of Srv2 play a role in the interaction with Inp1's middle domain (Fig. 3.15).

A

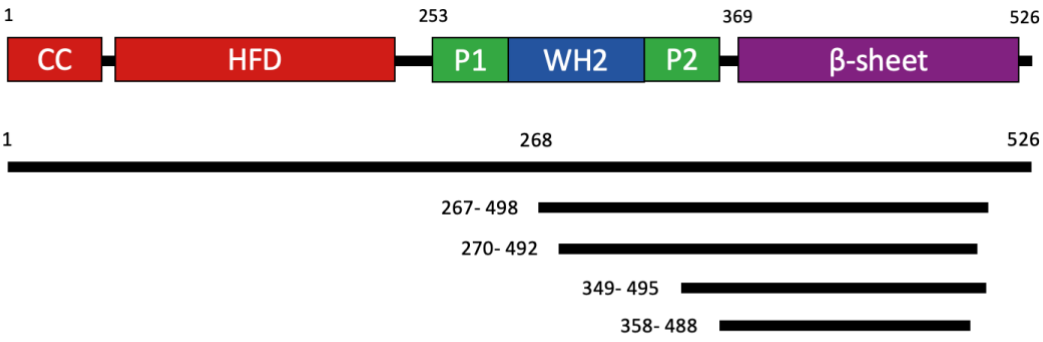

B

Clone Name	Type Seq	Gene Name (Best Match)	Chr	Protein Name	Start..Stop (nt)	Frame	Sense	PBS
pB66_A-17	5p/3p	YDR285W (zip1)	4, W	YDR285W (zip1)	474..1104	IF		D
pB66_A-21	5p/3p	YDR285W (zip1)	4, W	YDR285W (zip1)	474..1104	IF		D
pB66_A-18	5p/3p	YGL035C (mig1)	7, C	YGL035C (mig1)	108..741	IF		E
pB66_A-1	5p/3p	YGR019W (uga1)	7, W	YGR019W (uga1)	282..825	IF		D
pB66_A-6	5p/3p	YGR019W (uga1)	7, W	YGR019W (uga1)	282..825	IF		D
pB66_A-16	5p/3p	YJR091C (jsn1)	10, C	YJR091C (jsn1)	1008..1423	IF		D
pB66_A-13	5p/3p	YKL062W (msn4)	11, W	YKL062W (msn4)	1533..1861	IF		D
pB66_A-5	5p/3p	YKL129C (myo3)	11, C	YKL129C (myo3)	33..412	IF		D
pB66_A-8	5p/3p	YKL129C (myo3)	11, C	YKL129C (myo3)	33..412	IF		D
pB66_A-9	5p/3p	YKL129C (myo3)	11, C	YKL129C (myo3)	33..412	IF		D
pB66_A-7	5p/3p	YLR095C	12, W	YLR095C	967..460	??	N	N/A
pB66_A-10	5p/3p	YMR108W (ilv2)	13, C	YMR108W (ilv2)	2471..1789	??	N	N/A
pB66_A-11	5p/3p	YMR109W (myo5)	13, W	YMR109W (myo5)	222..402	IF		D
pB66_A-20	5p/3p	YNL138W (srv2)	14, W	YNL138W (srv2)	801..1492	IF		B
pB66_A-14	5p/3p	YNL138W (srv2)	14, W	YNL138W (srv2)	809..1475	OOF2		B
pB66_A-2	5p/3p	YNL138W (srv2)	14, W	YNL138W (srv2)	1044..1485	IF		B
pB66_A-4	5p/3p	YNL138W (srv2)	14, W	YNL138W (srv2)	1044..1485	IF		B
pB66_A-19	5p/3p	YNL138W (srv2)	14, W	YNL138W (srv2)	1044..1485	IF		B
pB66_A-3	5p/3p	YNL138W (srv2)	14, W	YNL138W (srv2)	1071..1465	IF		B
pB66_A-15	3p	YPL248C (gal4)	16, C	YPL248C (gal4)	..2643	??		N/A

Figure 3. 15: The yeast two-hybrid outcome. A) A line diagram displaying the truncations of Srv2, which were identified through a genome-wide Y2H screen with the peripheral membrane protein of Inp1 (73-280) as bait. B) List of proteins that interacted with the middle domain of Inp1 in different categories: High confidence in the interaction, B; Moderate confidence in the interaction, D; Interactions involving highly connected prey domains, warning of non-specific interaction, E; non-available, N/A. Srv2 fragments results are boxed in black.

To complement the Y2H outcome, the initial aim was to demonstrate Inp1 – Srv2 binding using an alternative approach.
MBP-Inp1 protein fragments 1-100 and 1-280 were expressed in *E. coli* BL21 DE3 and purified using Amylose beads (as described in Section 2.7.3). Srv2-ProtA protein was extracted from yeast as described in Section 2.7.5. Total lysates containing the Srv2-ProtA fusion were then incubated with Inp1 1-100 or Inp1 1-280 coated beads for 2h before being washing three times with F buffer. The samples were run on two gels using SDS-PAGE. One was analysed by western blot using anti-ProtA, and another gel was analysed by Coomassie blue staining.

The results show that Srv2 bound to MBP-Inp1 1-280 when it was present in Inp1 1-280 sample that was detected by anti-PAP. There was non-specific binding in both MBP which was used as negative control, and MBP-Inp1 1-100 samples. Quantification of protein bands reveals that there was a higher level of Srv2 in the sample incubated with MBP-Inp1 1-280 than in both the MBP and MBP-Inp1 1-100 samples. (Fig. 3.16).

To investigate the interaction between Srv2 and Inp1 *in vivo*, we performed a co-immunoprecipitation assay as detailed in Section 2.7.6. For this assay, we utilized three distinct yeast strains: (i) a strain co-expressing Srv2-GFP and Inp1-ProtA, to assess the potential interaction between these two proteins; (ii) a strain co-expressing Pnc1-GFP and Inp1-ProtA, which served as a control, as Pnc1 is known not to interact with Inp1; and (iii) a strain expressing Inp1-ProtA alone, which acted as a negative control to rule out non-specific binding. Samples were grown to log phase before being harvested followed by protein extraction. GFP proteins were pulled down using GFP-Trap beads (Chromo Tek) for 2h. Beads were washed three times before being analysed by SDS-PAGE and immunoblotting using anti-GFP and anti-ProtA antibodies.

The results demonstrated that Srv2 is able to bind Inp1. In total lysates (TL), Srv2-GFP and Pnc1-GFP were shown and Inp1 was not present in the anti-GFP blot. Inp1-ProtA appeared in all samples in the anti-ProtA blot. This confirms the inputs were correct. In the bound (B), Srv2-GFP and Pnc1-GFP were detected in the anti-GFP blot. Inp1-ProtA was shown in the Srv2-GFP sample anti-ProtA, and there was no Inp1 in the Pnc1-GFP sample. This demonstrates the interaction between Srv2 and Inp1 whilst Pnc1 showed no binding with Inp1 (Fig. 3.17).

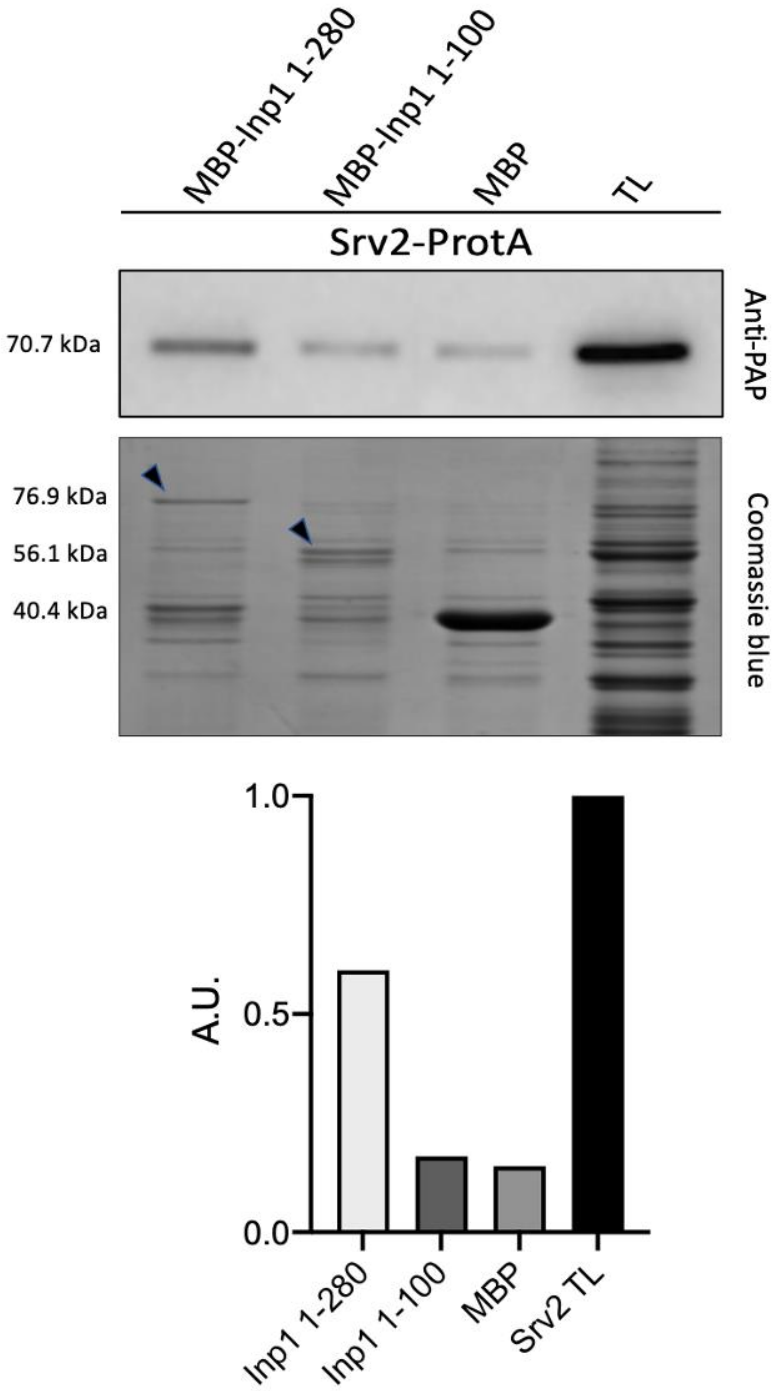

Figure 3. 16: *In vitro*, Srv2 binds the middle domain of Inp1 (1-280). MBP, MBP-Inp1 1-100 and MBP-Inp1 1-280 proteins were expressed in *E. coli* BL21 DE3 and purified using Amylose beads which were then added to Srv2-PrtoA total lysate. Samples were incubated for 2hr before being washed three times, followed by a separation using SDS-PAGE in two gels: one was followed by immunoblotting using anti-PAP, and another one was stained with Coomassie blue staining. TL: total lysate was used to show the input, while MBP and MBP-Inp1 1-100 were used as negative controls. The graph shows values of Srv2-ProtA in all samples. Bands were normalised against the input. Normalised the input was set to 1 A. U. where A. U. is arbitrary units.

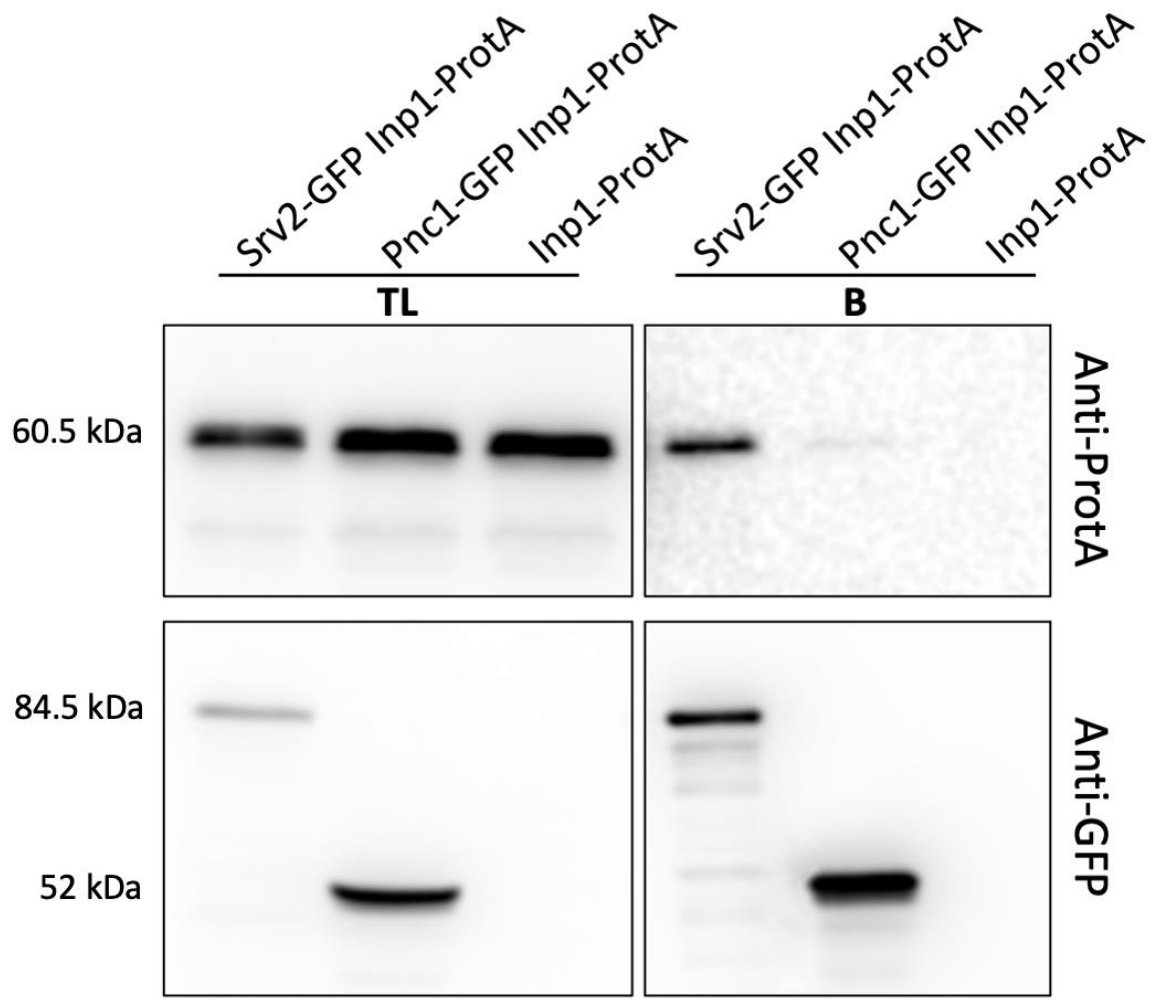

Figure 3. 17: *In vivo*, Srv2 interacts with Inp1. Co-immunoprecipitation (Co-IP) of Inp1 and Srv2 was performed. GFP-binding beads were utilised for pull-down GFP proteins. Pnc1-GFP and Inp1-ProtA were utilised as negative controls.

3.9 Discussion

An earlier study established Inp1 as the initial identified tether between the plasma membrane and peroxisome (PM-PER), showing that it fulfills the criteria for a contact site tether protein. Inp1, as a plasma membrane and peroxisome (PM-PER) tether, has been demonstrated to possess the structural and functional ability to interact with both plasma and peroxisomal membranes when situated in the proper subcellular location. Moreover, the introduction of synthetic PM-PER tethers can effectively restore retention in cells lacking Inp1. Additionally, Inp1 facilitates peroxisome retention through its C-terminal Pex3-binding domain and the N-terminal domain that connects to PI(4,5)P2, effectively forming a bridge between the peroxisome and plasma membranes (Hulmes et al., 2020). Similar findings to Inp1 function in *S. cerevisiae* have also been reported in *H. polymorpha*. The N-terminal domain of Inp1 was found to be crucial for plasma membrane association, while its C-terminal domain was necessary for peroxisome binding. The N-terminal domain of HpInp1 localises to the cell cortex, with a greater concentration of signal initially at the bud tip and later in the bud neck. It also has been shown that an intact actin cytoskeleton is required for Inp1 cortical localisation. When the actin cytoskeleton was disturbed by treating the cells with latrunculin-A, this resulted in the loss of cortical Inp1 patches, particularly around the bud' neck (Krikken et al., 2020).

In this chapter, we demonstrate a direct interaction between Inp1 and actin, in protein binding assays and using the yeast two hybrid approach. Further mapping of the interaction site reveals that, Inp1 1-100 is sufficient for the binding. The findings reveal a novel connection between actin and peroxisomes that is crucial for peroxisome organization. This relationship is distinct from the one mediated by Inp2 and Myo2, indicating that there are multiple mechanisms involved in the organization of peroxisomes and linking peroxisomes to the actin cytoskeleton. Understanding these various interactions will offer valuable insights into the overall process of peroxisome organization.

Other results generated revealed that the middle domain of Inp1 (aa 73-280) interacts with the highly conserved actin binding protein Srv2 through its C-terminus. The C-terminal region of Srv2 is also known to have a strong affinity for interacting with ADP-G-actin and recycling actin monomers, a crucial step in the rapid turnover of the actin network. Given the importance of Inp1 for peroxisome retention and the potential involvement of actin in this process, it is possible that Srv2 may also play a role in peroxisome dynamics, possibly through its effects on actin cytoskeleton organization (Fig. 3.18).

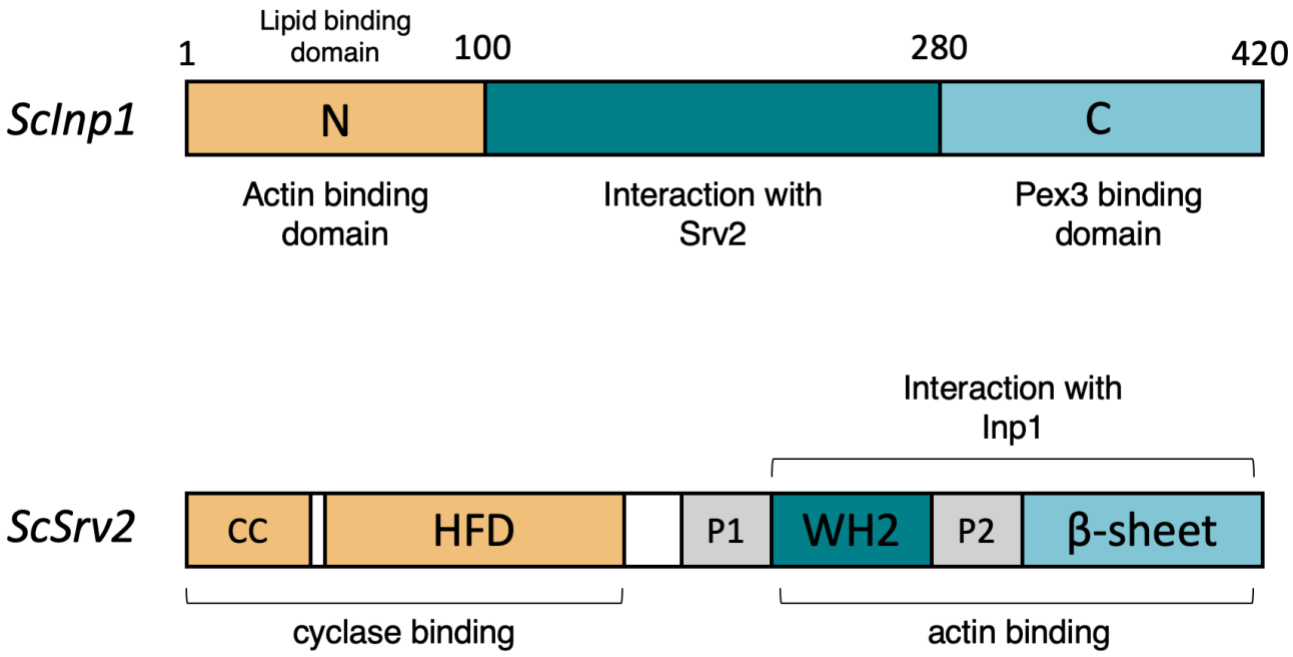

Figure 3. 18: Structural prediction and protein interactions of Inp1 with actin and Srv2: Identification of relevant binding regions. The schematic illustrates the interactions between Inp1, actin, and Srv2 proteins and the relevant binding regions identified in this chapter. Inp1 has three distinct domains: the N-terminus (1-100) is responsible for binding to actin and localizing to the plasma membrane; the middle domain exhibits interaction with Srv2 via its C-terminal; and the C-terminus (281-420) is essential for associating with peroxisomes through direct binding to the peroxisomal protein Pex3. Srv2 promotes actin turnover through two activities: C-Srv2, which contains two actin binding domains that interact with ADP-G-actin, displaces cofilin from ADP-actin monomers, and catalyses nucleotide exchange. This part of Srv2 has been shown to interact with the middle domain of Inp1. In contrast, N-Srv2 enhances cofilin-mediated severing and consists of an oligomerization domain and a helical folded domain.

In section 3.5, it was shown that disruption of the actin cytoskeleton caused abnormal peroxisome clustering at the bud neck. These findings underscore the importance of the actin cytoskeleton in regulating peroxisome distribution. Interestingly, peroxisome clustering in yeast have also been to shown to be induced by specific mutations in Inp1. The Rachubinski group studied the ER-peroxisome tether using a random mutagenesis approach on Inp1. One of these mutants was *inp1 T26M*, which changes the distribution of peroxisomes. This mutation was found to cause peroxisome clustering at the bud neck and to impair peroxisome transport to the bud (Knoblach & Rachubinski, 2018). Although the mutant *inp1 T26M* results in clustering peroxisomes, our results show that T26 is not involved in actin binding. One possibility is that T26 may have an effect on the lipid binding properties of the N-terminal domain, causing Inp1 to no longer be stably localised to the membrane. This could lead to an indirect loss of the interaction with actin. Interestingly, the N-terminal domain (1-99) of HpInp1 has been shown to accumulate at the cell cortex, with larger signal concentrations initially found at the bud tip and subsequently in the neck (Krikken et al., 2020). One possible explanation for these observations is that PI(4,5)P2 in budding yeast is not distributed uniformly around the entire plasma membrane but rather it is concentrated in certain regions where the cell is growing or dividing. Specifically, PI(4,5)P2 is enriched at the areas of polarized growth and the neck of the bud (Garrenton et al., 2010).
The observed phenotype of increased localization at the neck of buds has also been documented when expressing the PI(4,5)P2 binding PH domain "pleckstrin homology" of Num1 (Tang et al., 2009). The PH-domain of Num1 is a protein domain that specifically binds to PI(4,5)P2. The observation of the localization of this domain at the bud's neck further supports the proposition that the binding of PI(4,5)P2 by Inp1 plays a significant role in peroxisome clustering at the bud's neck.

Specific mutations in actin were also found to cause a phenotype in peroxisome organisation. The actin alleles mutants *act1-104* and *act1-116* affect the distribution of peroxisomes and they were found to be more clustered at the bud neck. This suggests a connection between peroxisome retention and actin. *Act1-104* [K315A, E316A] residues are likely located on the filament surface, and *act1-116* [D187A, K191A] residues are predicted to be on the protein face closest to the filament axis (Fig. 3.19).

Y2H results indicate that Inp1 (1-280) does not interact with mutant *act1-104*, indicating a potential Inp1-peroxisome binding site. It is possible that *act1-104* could indicate a residue that binds to Inp1, while *act1-116* may indirectly affect Inp1 binding through structural changes in the protein. For instance, the *act1-116* mutation could cause conformational changes in the actin filament that alter the accessibility of the Inp1 binding site or the overall stability of the actin-Inp1 complex.

The exact role of the *act1-116* mutant in peroxisome retention and its potential interaction with Inp1 is still unclear. However, further studies could explore the exact role of *act1-116* in peroxisome retention and its potential interaction with Inp1, examining the effects on Inp1 binding and understanding whether *act1-116* mutations influence Inp1 binding indirectly through structural changes, allosteric regulation, or another mechanism.

Previous studies have examined the sensitivity of mutated charged residue groups of *ACT1* to LatA and found them to be affected, suggesting that LatA binds to the ATP-binding pocket

where some of these residues are located. Additionally, it has been reported that when *act1-120* is mutagenized, it loses its ability to interact with fimbrin, possibly being part of the binding site (Holtzmanet al., 1994). These findings could be relevant to our hypothesis that *act1-104* might also be part of the binding site for Inp1 and Pfy. Specifically, the observations from the alanine scan collection of mutants indicate that mutations in certain actin residues can disrupt protein-protein interactions, possibly by altering binding sites. In our study, we found that Inp1 (1-280) did not interact with the mutant *act1-104*, which suggests that *act1-104* could represent a binding site for Inp1. Furthermore, it has been shown that *act1-104* does not interact with Las17, implying that this region may be involved in Las17 interaction (Urbanek et al., 2013). By considering these findings in the context of our results, we can better understand the potential role of *act1-104* in Inp1 binding.

Our hypothetical model presents a possible mechanism for Inp1-mediated peroxisome retention at the plasma membrane, incorporating our findings with *act1-104* and the potential influence of Lat-A.
In this model, Inp1 stabilizes its binding at the plasma membrane through multiple interactions. Its N-terminus binds to both F-actin and PIP2, which may provide sufficient tethering to retain peroxisomes in the mother cell. Under normal conditions, this dual interaction could prevent peroxisomes from being transported towards the mother-bud neck. However, when Lat-A is added or when actin binding is weakened, as observed in the *act1-104*-expressing mutant, peroxisomes can no longer be effectively retained in the mother cell and are instead transported closer to the mother-bud neck. Peroxisome transfer typically follows a directional path from the mother cell to the bud, with movement within the bud occurring from the tip to the neck. When actin cytoskeleton is disrupted, the peroxisomes exhibit a shift towards the bud neck. This altered movement aligns with the default direction of peroxisome transport, both in the mother cell and within the bud. The disruption of actin thus prompts a redirection of peroxisomes to the sites consistent with their natural movement. This change in distribution might be facilitated by the enrichment of PIP2 in the bud neck region, which could provide an additional anchoring site for Inp1, even in the absence of strong actin binding.

This chapter discussed the molecular mechanisms of Inp1 interactions, including the binding of its N-terminal domain with actin and the interaction of its middle domain with Srv2. The next chapter serves to investigate how Srv2 and its C-terminal contribute to peroxisome fission.

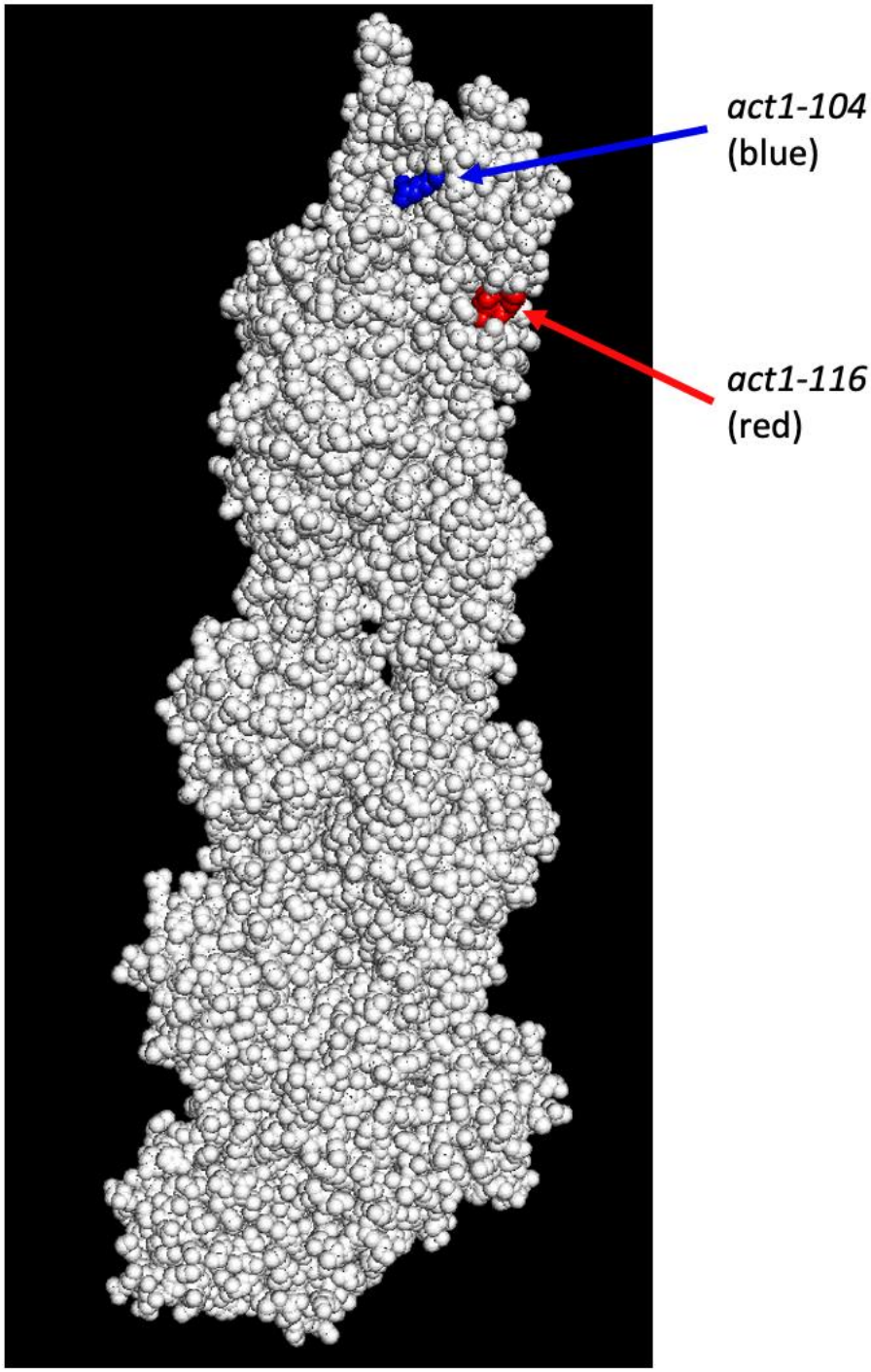

Figure 3. 19: The filament model of actin illustrates the mutated residues in blue for *act1-104* and in red for *act1-116*.

Chapter 4 – Srv2 regulates peroxisome fission

4.1 Introduction

Peroxisomes are required when cells are cultured using oleate (fatty acid) as the main carbon source, but they are not required when grown on glucose media (Kunau et al., 1995). Peroxisomes multiply through fission, also known as replicative multiplication, during glucose growth. However, on oleate media, they multiply by proliferation, and the membrane protein Pex11 is crucial to this process (Marshall et al., 1995; Erdmann & Blobel, 1995). In mammals, the fission of peroxisomes involves the coordinated action of Pex11 and the dynamin-related protein Drp/Dlp1. Dlp1 is also necessary for mitochondria fission (Pitts et al., 1999; Li & Gould, 2003). Furthermore, in *H. polymorpha*, peroxisome and mitochondrial fission are both mediated by a single Drp/Dnm1, and peroxisome fission is likewise reliant on Pex11 (Williams et al., 2015; Nagotu et al., 2008). However, the fission of peroxisomes in *S. cerevisiae* involves the participation of two Drp proteins, namely Dnm1 and Vps1 (Motley & Hettema, 2007). Dnm1 and Pex11 contribute to peroxisome proliferation in the presence of oleate (Marshall et al., 1995; Erdmann & Blobel, 1995; Kuravi et al., 2006). On the other hand, Vps1 plays a significant role in the replicative multiplication of peroxisome in the presence of glucose and proliferation is not stimulated (Hoepfner et al., 2001). While the overexpression of Dnm1 has been found to compensate the deficiency of Vps1 (Motley et al., 2008), Vps1 itself plays a crucial role in membrane transport between the late Golgi and endosomes, as well as being essential for endocytosis (Vater et al., 1992; Wilsbach & Payne, 1993; Smaczynska-de Rooij et al., 2010). Uncertainty exists about the recruitment of Vps1 to the various sites where it functions. However, Vps1 is known to localise to the endocytic site at a specific stage and is associated with the membrane invagination step during endocytosis (Smaczynska-de Rooij et al.,2015).

The group of peroxisomal membrane-associated proteins in *S. cerevisiae*, namely Pex11, Pex25, and Pex27, is collectively referred to as the Pex11 family. They have been connected to the regulation of peroxisome abundance through peroxisome fission. A deficiency of any of the Pex11 family proteins can lead to a reduction in the number of peroxisomes. Furthermore, the growth deficiency on oleate media is observed in cells lacking *pex11* or *pex25*, but not Pex27. (Tam et al., 2003; Rottensteiner et al., 2003). In cells, the maintenance of peroxisome quantity is achieved through a process of growth, followed by subsequent fission. There are four sequential processes involved in peroxisome multiplication: growth, elongation, constriction, and fission (Figure 4.1) (Schrader et al., 2012; Huber et al., 2012). Fis1 and Dlp1 are recruited through Pex11 to the site of peroxisomal membrane fission (Kobayashi et 43 al., 2007). Pex11 has been demonstrated to interact with Dlp1 in humans and Dnm1 in *H. polymorpha* both *in vitro* and *in vivo* (Kobayashi et al., 2007; Itoyama et al., 2013; Williams et al., 2015). However, there is no conclusive evidence that Pex11 and Dnm1 interact in *S. cerevisiae*.
The loss of *pex27* causes a significant reduction in the number of peroxisomes and an increase in peroxisome sizes. Peroxisomes in these cells have elongated shapes. Moreover, the loss of *pex25* results in one giant peroxisome or none. However, cells lacking *pex11* have a very small

reduction in peroxisome number. The elongated peroxisomes are not observed in *Δpex11* and *Δpex25* (Tower et al., 2011; Smith et al., 2002).

In the Hettema lab, it has been shown that peroxisome quantity and shape in *Δpex27* cells are very similar to *Δvps1* cells. Moreover, peroxisome quantity and shape in *Δdnm1Δpex27* cells resemble that of *Δdnm1Δvps1* cells, which usually have one elongated peroxisome. The same study demonstrated that Pex27 is crucial and required for Vps1 function in peroxisome fission. Moreover, there is an interaction between Pex27 and Vps1 (Ekal et al., 2023).

A recent study has identified an interaction between Srv2 and Dnm1 in mitochondria, leading to effortless mitochondrial function and a reduction in mitochondrial hyperfusion. This hyperfusion increases when their interaction is disrupted. In addition to its peroxisome function, Dnm1 is involved in the organization of mitochondria and is required for mitochondrial inheritance and fission (Chen et al., 2019).
Exploring the intricate mechanisms governing peroxisome fission is essential for comprehending cellular dynamics. Notably, Dnm1 and Vps1 have emerged as pivotal players in this process, contributing to the intricate orchestration of peroxisome division. Given that Srv2 has demonstrated interaction with Dnm1, a key regulator of both mitochondrial and peroxisomal fission, a pertinent question arises: Could Srv2 extend its influence to other factors influencing peroxisome fission, such as Vps1?
Our study aims to address this intriguing question by investigating whether Srv2 also engages in an interaction with Vps1. This exploration into potential novel interactions between Srv2 and Vps1 holds the promise of uncovering hitherto unknown links in the peroxisome fission pathway. Furthermore, the outcomes of this study could have broader implications, shedding light on the intricate network of protein-protein interactions that underlie peroxisome dynamics and division.
In addition to interpreting potential new interaction partners for Srv2, our study also seeks to delve into the broader role of Srv2 in peroxisome fission. By comprehensively understanding the contribution of Srv2, a multifunctional protein, to peroxisome dynamics, we hope to contribute to a more holistic understanding of the complex processes governing peroxisome biology. Ultimately, our investigation holds the potential to reveal novel insights into peroxisome fission, thereby advancing our understanding of cellular compartmentalization and organization.

This chapter further establishes the Srv2-Vps1 interaction through experimental validation. It also delves into the pivotal role of Srv2 in peroxisome fission, contributing valuable insights into the intricate mechanisms governing this essential cellular process.

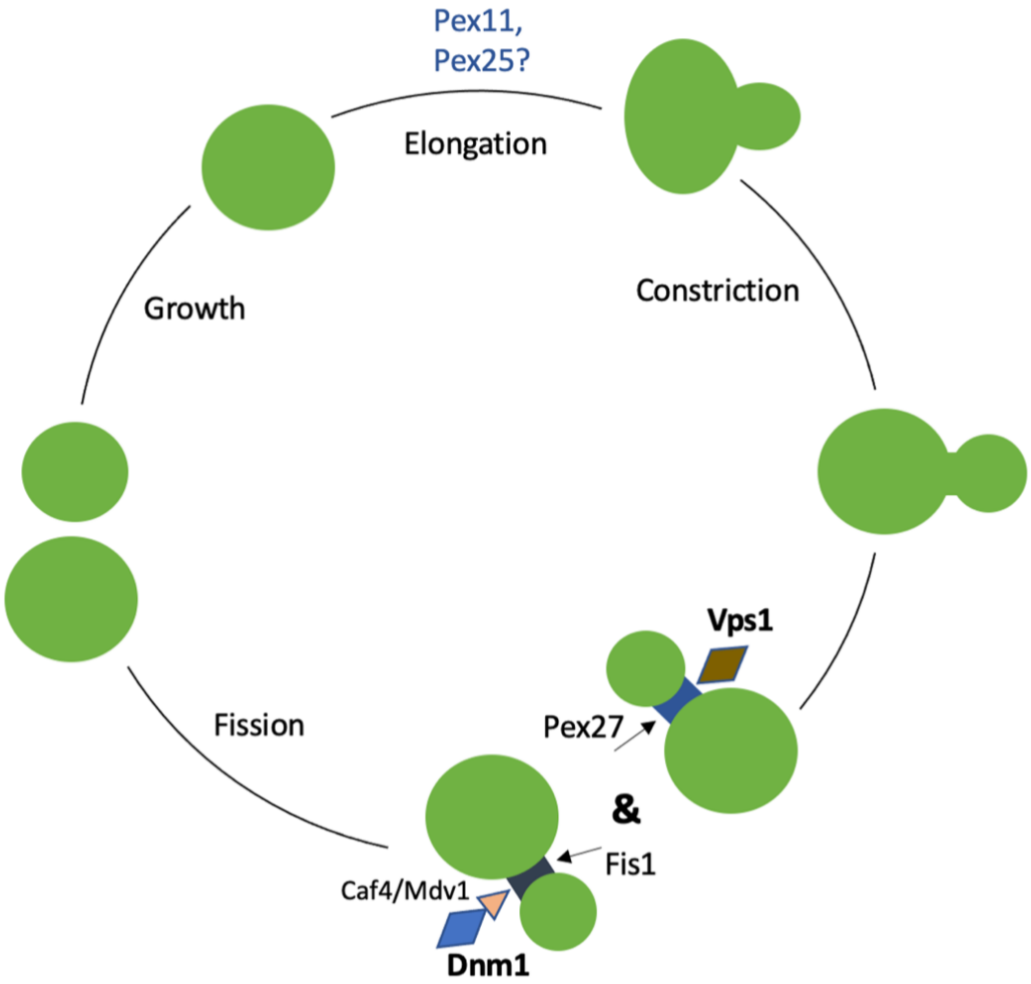

Figure 4. 1: Proposed peroxisome fission model in *S. cerevisiae*. The schematic diagram illustrates the proteins associated with Dnm1 and Vps1-dependent fission. Dnm1 recruitment necessitates the involvement of Fis1 and Mdv1 or Caf4. The precise role of Pex11 remains uncertain; however, it is speculated that it might aid in membrane remodeling and regulate the activity of Dnm1 GTPase. Pex25 may contribute to the early stage of fission and Pex27 contributes to Vps1 dependent fission. Diagram is not to scale.

4.2 Srv2 interacts with Vps1 *in vivo*

It has been indicated that Vps1 is responsible for regulating the number and size of peroxisomes, and that Dnm1 plays a role in the fission of peroxisomes and mitochondria. Additionally, a study by Chen et al. (2019) revealed an interaction between Dnm1 and Srv2, which affects the structure of the mitochondria network. The interaction between Srv2 and Dnm1 has been deemed critical for mitochondrial function. When this interaction is disrupted, it results in a hypoperfused mitochondrial network. Additionally, the deletion of Srv2 has been demonstrated to significantly impact mitochondrial shaping, resulting in an increased network of mitochondria (Chen et al., 2019).
To investigate the possibility of Srv2's involvement in peroxisome fission, we conducted *in vivo* co-immunoprecipitation assays to determine whether Srv2 interacts with Vps1.

In this assay, three different strains were used: WT cells expressing Vps1-GFP, WT cells expressing GFP-PTS1, the peroxisomal targeting signal 1 that is known not to binds Srv2, and WT cells without any tagged protein. GFP proteins were then pulled down using GFP-TRAP beads (Chromo Tek) before being separated on SDS-PAGE followed by western blot. Samples were detected using anti-GFP and anti-Srv2.

In figure 4.2 A, an anti-GFP blot was used to analyse the presence of Vps1 and PTS1 proteins in total lysate (TL) and bound lanes. The results show that Vps1 and PTS1 were detected in the TL lanes but not in the WT sample. However, in the bound lanes, Vps1 and PTS1 were more enriched, and the WT sample did not show any bands. In the anti-Srv2 blot, the results show that Srv2 was present in all samples in the TL lanes. However, in the bound lanes, Srv2 was only detected in the Vps1-GFP sample, indicating an interaction between Srv2 and Vps1. No additional bands were observed in the PTS1 and WT control samples in the anti-Srv2 blot.

Another Co-IP assay was performed in order to gain further evidence for Srv2–Vps1 interaction. Vps1-GFP was expressed in a C-terminally TAP-tagged Srv2 strain, and two controls were used: Vps1-GFP expressed in a WT strain and a TAP-tagged Srv2 strain. GFP proteins were pulled down using GFP-TRAP beads. Samples were then separated by SDS-PAGE followed by western blot. Proteins were detected using anti-GFP, anti-ProtA and anti-Vps1.

In the anti-GFP blot (Fig. 4.2 B), Vps1 appeared in the sample that co-expressed Srv2-TAP and Vps1-GFP, and in the sample expressing Vps1-GFP, no band was in the sample expressing Srv2-TAP in total lysate lanes (TL). In the bound lanes, Vps1-GFP was more enriched in the sample co-expressing Srv2-TAP and Vps1-GFP and the sample that expressed Vps1-GFP samples, and no band in the Srv2-TAP sample.
In the anti-PAP blot, Srv2 was detected in the sample that co-expressed Srv2-TAP and Vps1-GFP and in the sample expressing Srv2-TAP. No band in the Vps1-GFP sample in total lysate lanes (TL). In the bound lanes, only one band was detected which was in the sample that co-expressed Srv2-TAP and Vps1-GFP, and no more bands in both samples expressing Vps1-GFP or Srv2-TAP.

In the anti-Vps1 blot, the untagged Vps1 was detected in the sample co-expressing Srv2-TAP and Vps1-GFP, in the sample expressing Vps1-GFP and in the sample expressing Srv2-TAP (blue arrows). However, the tagged Vps1 was hardly seen in the sample expressing Vps1-GFP and in the sample co-expressing Srv2-TAP Vps1-GFP (red arrows), due to Vps1 antibodies having the ability to bind TAP tag protein. So, in total lysate lanes of the anti-Vps1 blot, anti-Vps1 detected the tagged and untagged Vps1, as well as Srv2-TAP-tagged in both samples of Srv2-TAP.

In the bound lanes, endogenous Vps1 also co-precipitated with Vps1-GFP, the tagged and untagged Vps1 (blue and red arrows) were clearly seen in the sample co-expressing Srv2-TAP Vps1-GFP and sample expressing Vps1-GFP. There was no interaction in the negative sample making these results more reliable. It is notable that Srv2-TAP (the middle bands) were detected by anti-Vps1. Taken together, these results strongly suggest that Srv2 interacts with Vps1.

Inp1 plays a crucial role in peroxisome inheritance and the data obtained in chapter 3 has shown that Srv2 interacts with Inp1. Vps1 regulates the size and number of peroxisomes, and the results in this section showed that Srv2 interacts with Vps1. Dnm1 is involved in the fission of mitochondria and peroxisome, and it has been shown that Srv2 interacts with Dnm1 (Chen et al., 2019). Taking all these together, it was intriguing to learn that Srv2 has a direct effect on peroxisomes.

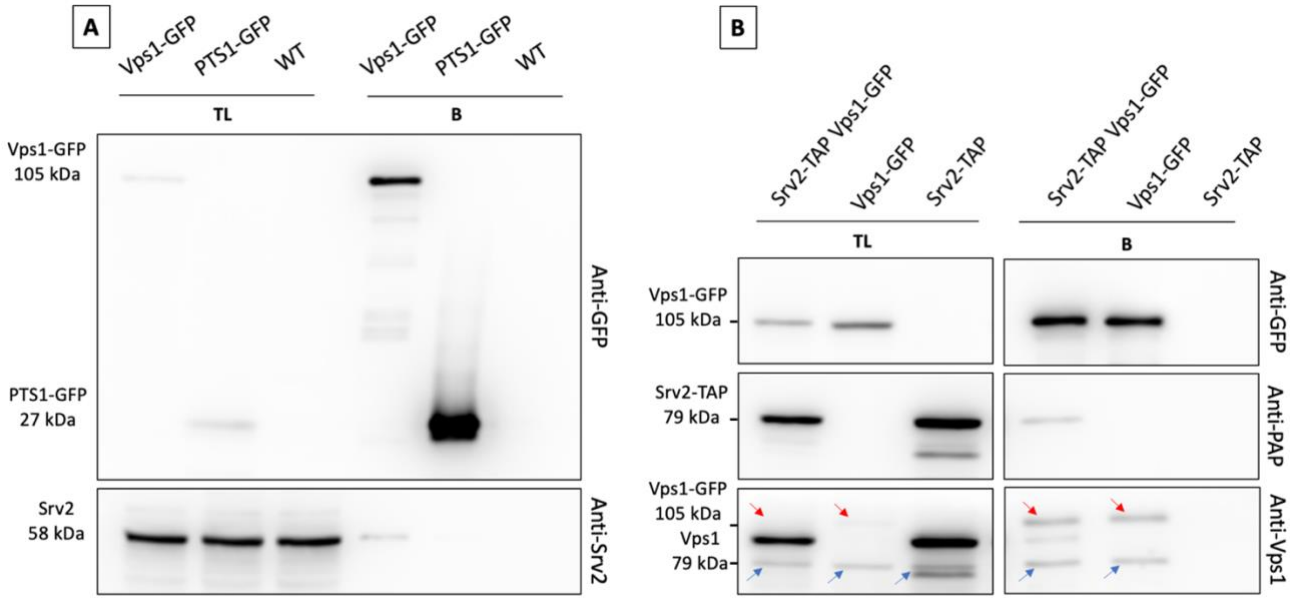

Figure 4. 2: Co-immunoprecipitation for the interaction between Srv2 and Vps1. Vps1-GFP was immunoprecipitated using GFP-TRAP beads and the IP samples were analysed by western blot using antibodies against GFP, TAP and Vps1. (A) Cells expressing Vps1-GFP, and the control GFP-PTS1 and WT with no tagged protein were used. GFP proteins were detected using anti-GFP (Upper box) and Srv2 was detected using anti-Srv2 (lower box). B) Cells expressing Srv2-TAP plus Vps1-GFP, Vps1-GFP and Srv2-TAP were used. GFP proteins were detected using anti-GFP (Upper box), Srv2-TAP was detected using anti-PAP (middle box) and endogenous Vps1 (blue arrows) and Vps1-GFP (red arrows) were detected using anti-Vps1 (lower box). The band shown between the blue and red arrows is Srv2-TAP, which was detected by anti-Vps1 (TL: total lysate:1, B: bound: 12.5).

4.3 Deletion of *SRV2* affects peroxisome number but not inheritance

The deletion of the *SRV2* gene results in many effects in yeast including an abnormal actin cytoskeleton, the reduced localization of proteins to the bud tip, abnormal lipid particle morphology, large cells sizes with elongated buds, a random budding pattern and slow cell growth (Gerst et al., 1991; Votjek et al., 1991; Jorgensen et al., 2002; Wu X & Jiang 2005; Bertling et al., 2007). The deletion of *SRV2* or CAP in *Drosophila*, *Dictyostelium*, and mammalian cells also leads to an accumulation of irregular structures of actin filament and abnormalities in actin-dependent cellular processes such as endocytosis and motility (Baum et al., 2000; Noegel et al., 2003; Bertling et al., 2004). In addition, Srv2/CAP overexpression in plants leads to defects in actin filament structures and issues in cell growth and division (Barrero et al., 2002). A recent study has shown that the deletion of *SRV2* in the budding yeast *S. cerevisiae* strongly affects the mitochondrial network where *Δsrv2* cells have elongated and hyperfused mitochondria. Moreover, Srv2 modulates both mitochondrial activity and

dynamics (Chen et al., 2019). In order to test the effect of Srv2 on peroxisomes, *SRV2* was deleted in WT cells (as described in Section 2.4.5).

It is known that the deletion of *SRV2* affects actin cables. Therefore, WT and *Δsrv2* cells were stained with the actin filaments dye rhodamine phalloidin (as described in section 2.8.6) in order to visualise actin and check the effect of *srv2* deletion.
As expected, the analysis results showed that the loss of *srv2* leads to the absence of extended F-actin cables, while cortical F-actin patches remain. In wild-type cells, actin cables are observed along the mother bud axis, as well as cortical actin patches (Fig. 4.3).

WT and *Δsrv2* cells expressing the peroxisomal marker mNG-PTS1 were grown to log phase before being imaged by fluorescent microscopy.
Analysis of these cells found that the number of peroxisomes in WT cells was as expected, about 7 peroxisomes per cell. However, the number of peroxisomes increased dramatically in *Δsrv2* cells, nearly double the number in WT cells.
Looking at peroxisome inheritance, it is observed that peroxisomes appear in almost all buds indicating that the inheritance of peroxisome is not affected by *srv2*, but indicating it might be part of peroxisome fission machinery (Fig. 4.4).
This exciting finding supported the hypothesis that Srv2 plays an important role in peroxisome fission.

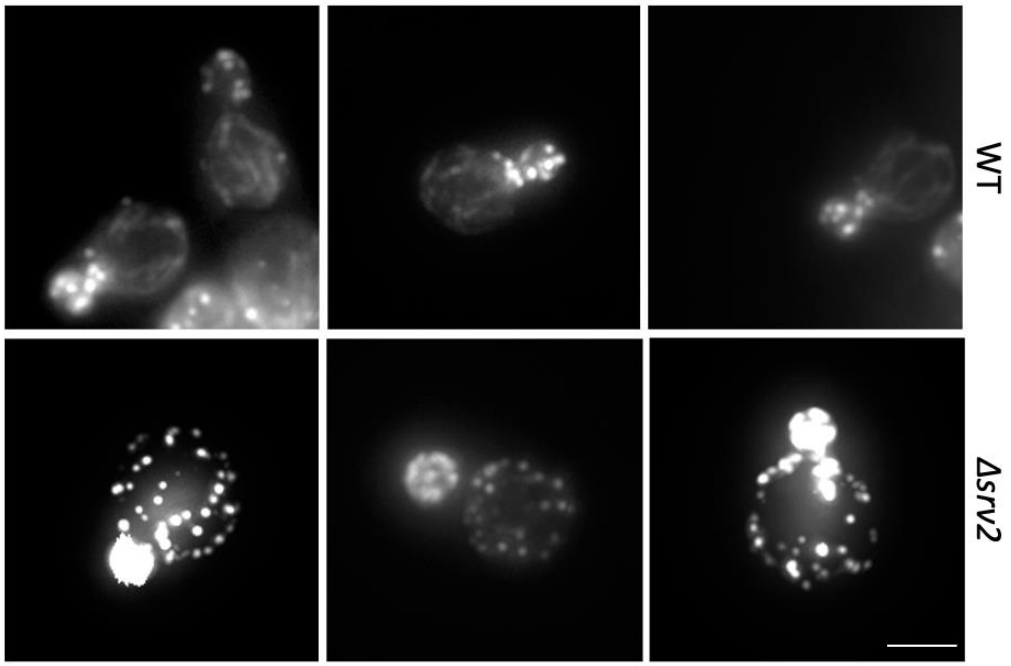

Figure 4. 3: Effect of *srv2* on actin filaments. WT (upper panel) and *Δsrv2* (lower panel) cells were stained with the rhodamine phalloidin stain in order to visualise actin cables. Bars, 5µm.

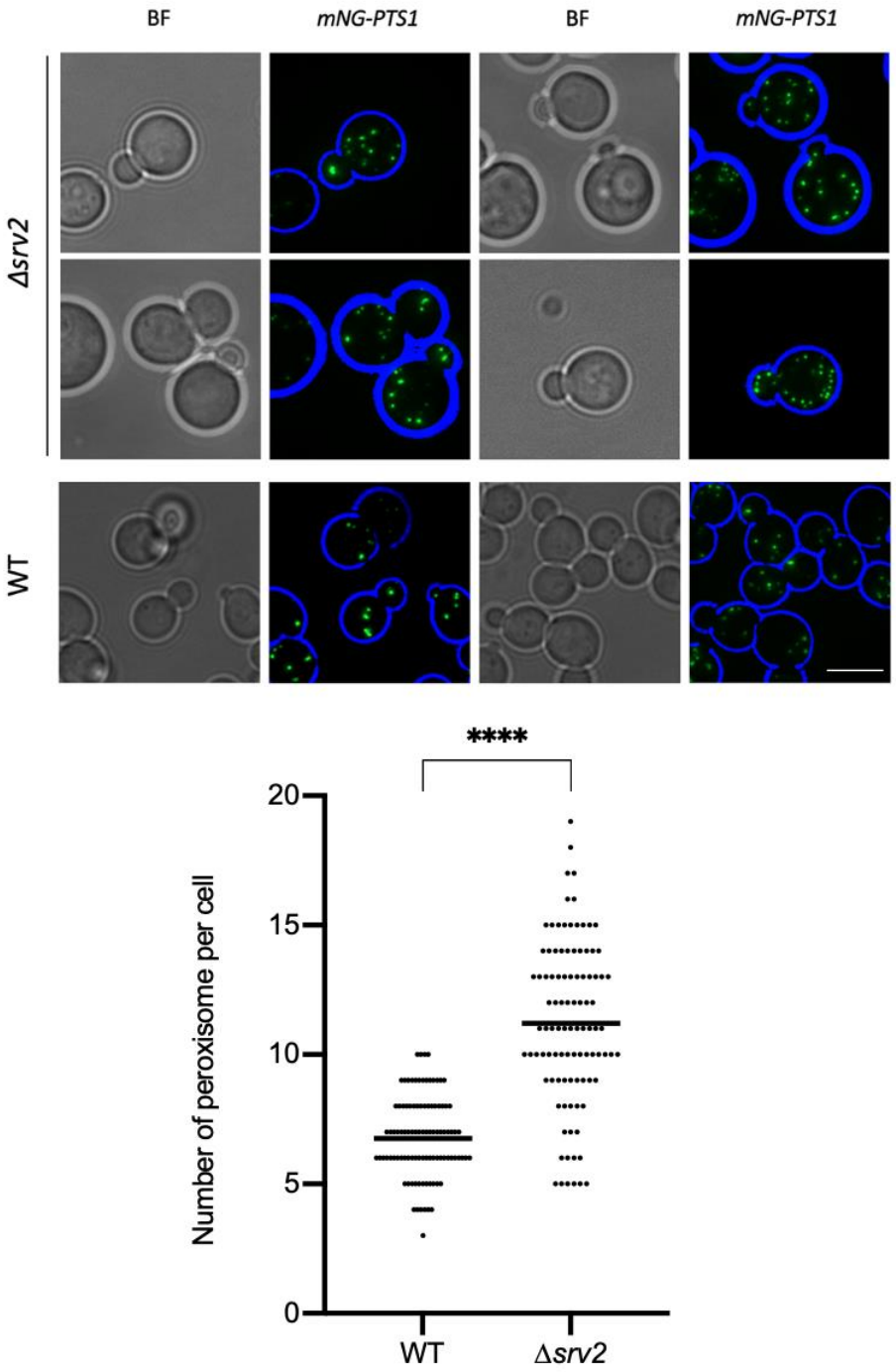

Figure 4. 4: Deletion of *SRV2* increases the number of peroxisomes. *Δsrv2* (upper panel) and WT (lower panel) cells were grown to log phase before being imaged in the presence of the peroxisomal marker mNG-PTS1. Bars, 5µm. The graph shows the quantitative analysis of peroxisome numbers per cell in both strains *Δsrv2* and WT. Peroxisomes were counted in 100 yeast cells from three independent experiments. Black bars represent means. Statistical significance was determined by unpaired student t test: ****P ≤ 0.0001.

4.4 Srv2 regulates peroxisome fission

To investigate the effect of Srv2 on peroxisome fission thoroughly, there are some mutant strains whose peroxisome number and size are known (Fig. 4.5). The mutant strains are *Δpex27, Δdnm1, Δdnm1Δpex27,* and *Δpex25*.
As discussed above, *Δpex27* and *Δvps1* have similar peroxisome phenotypes. The peroxisome number is small with elongated shapes (Ekal et al., 2023). Since the loss of *srv2* causes an increase in the number of peroxisomes, it was worth investigating its effect in *Δpex27* or *Δvps1*. The loss of *vps1* affects cells resulting in slow growth and then cells are more likely to be sick. Thus, we decided to start with *Δpex27* whose effect appears only on peroxisomes.

In order to investigate the *srv2* effect on *Δpex27, SRV2* was deleted in *Δpex27* strain. *Δpex27* and *Δsrv2Δpex27* cells were then grown to log phase before the cells were analysed by fluorescence microscopy.
In *Δpex27* cells, elongated peroxisomes were shown in small numbers, about 2-3 peroxisomes per cell. Interestingly, the results of the analysis of *Δsrv2Δpex27* cells show an increase in the number of peroxisomes while the elongated shape still appeared. Quantification analysis demonstrates that the average number of peroxisomes in *Δsrv2Δpex27* was nearly 7 peroxisomes per cell (Fig. 4.6).

The peroxisome fission occurs in two pathways which require two dynamin-related proteins, Dnm1 and Vps1 (Fig. 4.1). Fis1 and Mdv1/Caf4 are required for Dnm1 recruitment, while Vps1 and Pex27 function together and they require each other. Deleting *PEX27* means that one pathway is inhibited while another pathway still occurs by the Dnm1 group (Fig. 4.7). From these results, we can conclude that when one of the peroxisome fission pathways is blocked in the case of deleting *PEX27*, *srv2* still affects the number of peroxisomes which showed increasing in the number of peroxisomes in *Δsrv2Δpex27*. Thus, it was interesting to check the effect of deleting *SRV2* in *Δdnm1* strain and how similar it is to its effect in *Δsrv2Δpex27* cells.

There is no substantial effect on peroxisomes in *Δdnm1* cells where the number of peroxisomes is very similar to wild-type cells.
Continuing the investigation of the *srv2* effect, *SRV2* was deleted in *Δdnm1* strain. *Δdnm1* and *Δsrv2Δdnm1* cells were then grown to log phase and then were imaged using fluorescence microscopy.
In *Δdnm1* cells, normal peroxisome phenotype was shown in normal numbers, about 6-7 peroxisomes per cell. In *Δsrv2Δdnm1* cells, an increase in the number of peroxisomes was observed. Quantification analysis shows that the average number of peroxisomes in *Δsrv2Δdnm1* was nearly 9 peroxisomes per cell (Fig. 4.8).
By deleting *DNM1*, one fission pathway is blocked while fission can happen through the Vps1 group pathway (Fig. 4.7). These results indicate that deleting *SRV2* while one of the fission pathways is blocked, by deleting *PEX27* or *DNM1*, increases the number of peroxisomes, which leads to the idea that another pathway facilitates fission without any requirement for Srv2.

Therefore, we asked what would happen to peroxisomes if both pathways were blocked, in the double mutants *Δpex27Δdnm1*, in the case of deleting *SRV2*.

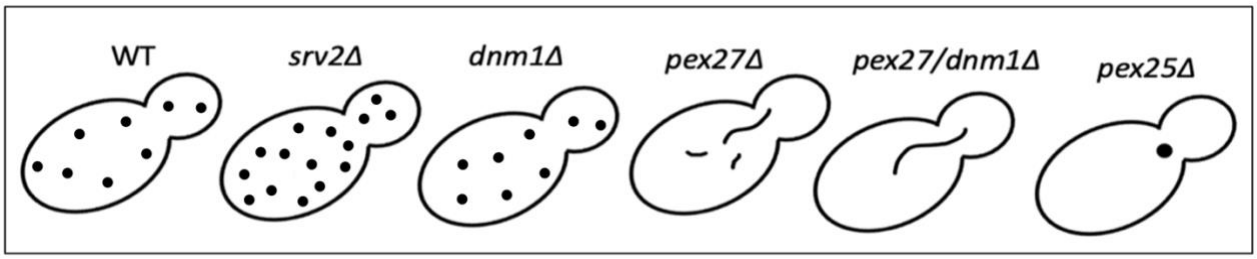

Figure 4. 5: Diagram illustrating the known peroxisome number and size in specific mutant backgrounds. WT: normal number of peroxisomes; *Δsrv2*: showed an increase in peroxisomes numbers; *Δdnm1*: normal number of peroxisomes; *Δpex27*: showed a decrease in peroxisomes numbers 2-3 elongated peroxisomes per cell; *Δpex27Δdnm1*: one elongated peroxisome per cell; *Δpex25*: one giant peroxisome per cell. Diagram is not to scale.

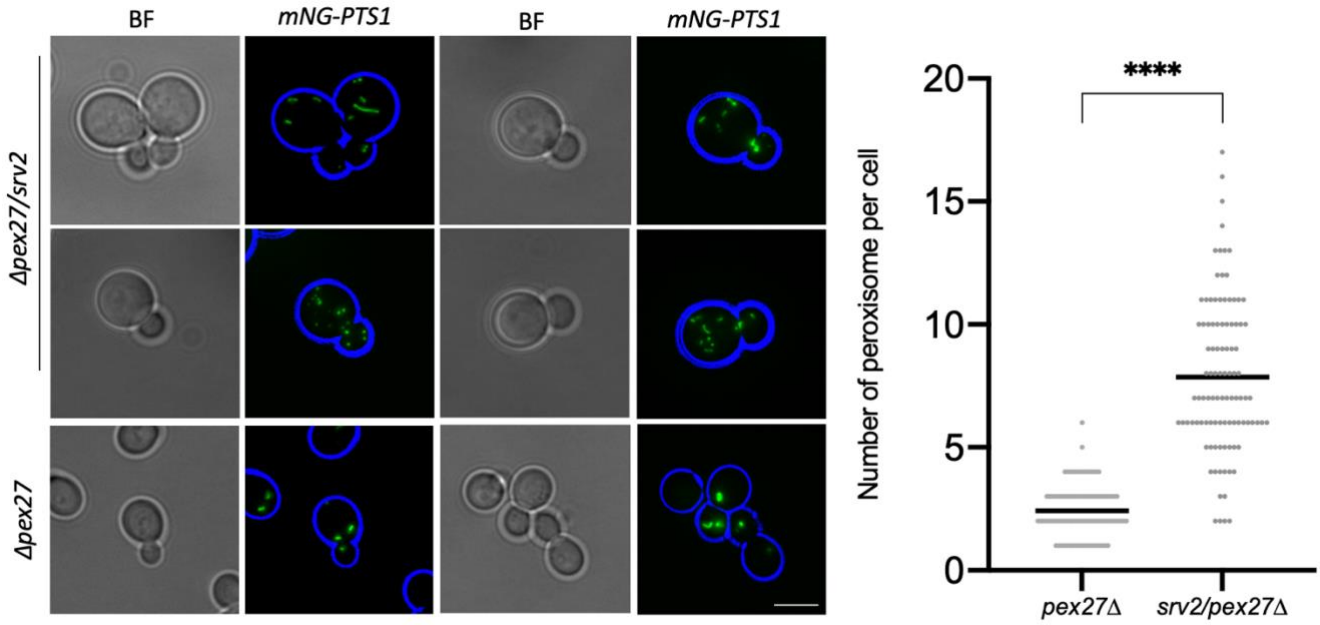

Figure 4. 6: The number of peroxisomes increases in *Δsrv2/pex27*. *Δsrv2Δex27* (upper panel) and *Δpex27* (lower panel) cells expressing the peroxisomal marker mNG-PTS1 were grown to log phase before being imaged. Bars, 5µm. The graph shows the quantitative analysis of peroxisome numbers per cell in both strains *Δpex27* and *Δsrv2Δpex27*. Peroxisomes were counted in 100 yeast cells from three independent experiments. Black bars represent means. Statistical significance was determined by unpaired student t test: ****P ≤ 0.0001.

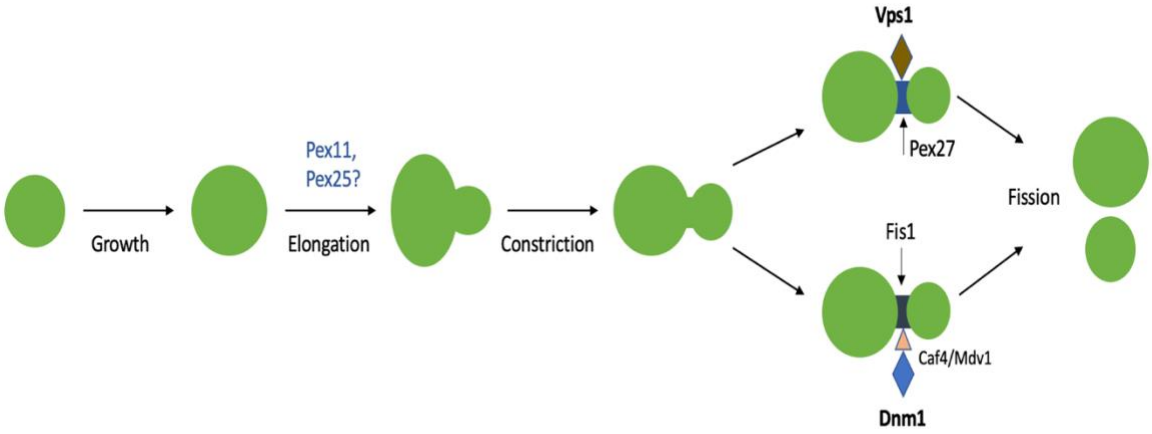

Figure 4. 7: Proposed model illustrating two pathways of peroxisome fission in *S. cerevisiae.* Fission occurs through two groups; Dnm1, which requires Fis1 and Mdv1/Caf4, and Vps1 group, which requires Pex27. Blocking one of these pathways will not completely block fission, as it can still be facilitated by another pathway.

In *Δpex27Δdnm1* cells, peroxisomes do not divide, and one frequently elongated peroxisome is observed in most cells. Upon cell division, these peroxisomes are maintained through division during cytokinesis. Hence, the next step was deleting *SRV2* in *Δpex27Δdnm1* strain that expressed the peroxisomal marker mNG-PTS1 and analysing peroxisomes in those cells. *Δpex27Δdnm1*, as a control, and *Δsrv2Δpex27Δdnm1* cells were grown to log phase and were imaged.
The results show that in *Δpex27Δdnm1* almost one elongated peroxisome per cell was found. Interestingly, peroxisome numbers in *Δsrv2Δpex27Δdnm1* cells remain the same as in *Δpex27Δdnm1* cells. In most cells, there was only one elongated peroxisome, as shown in the quantitative analysis (Fig. 4.9). We can conclude that in the case of blocking both peroxisome fission pathways by deleting *PEX27* and *DNM1*, the effect of losing *srv2* is not observed.

To confirm this finding, we then tested the effect of *srv2* deletion in *Δpex25* strain. Pex25 is necessary for peroxisome biogenesis and regulates peroxisome size and number. It has been proposed that Pex25 contributes to the early stages of peroxisome fission (Rottensteiner et al., 2003). In *Δpex25* cells, only one giant peroxisome can be found due to the inhibition of peroxisome fission.
We next asked whether the increase in peroxisome numbers is still present in *Δsrv2Δpex25*.

Consequently, *SRV2* was deleted in *Δpex25* cells, and log phase cells were imaged.
As expected, *Δpex25* cells showed only one giant peroxisome per cell supporting the idea that Pex25 play a crucial role in the early stages of peroxisome fission. However, the results also demonstrate that in *Δsrv2Δpex25* cells there was only one large peroxisome per cell (Fig. 4.10). These results lead us to hypothesize that the effect of deleting *SRV2* on peroxisomes is not significant when peroxisome fission pathways are inhibited, in *Δpex27Δdnm1* or in *Δpex25* cells.

In summary, In WT cells, peroxisome fission happens regularly and gives a normal number of peroxisomes, around 7 peroxisomes per cell. When cells lose *srv2,* peroxisome fission increases, resulting in a higher number of peroxisomes. In the case of blocking one of the fission pathways, by deleting *PEX27* or *DNM1*, *srv2* affects peroxisomes fission resulting in a larger number of peroxisomes. However, when peroxisome fission is blocked, by deleting *PEX27* and *DNM1* or *PEX25*, the effect of *srv2* deletion is not observed. All these data indicate that Srv2 works as a regulator of peroxisome fission.

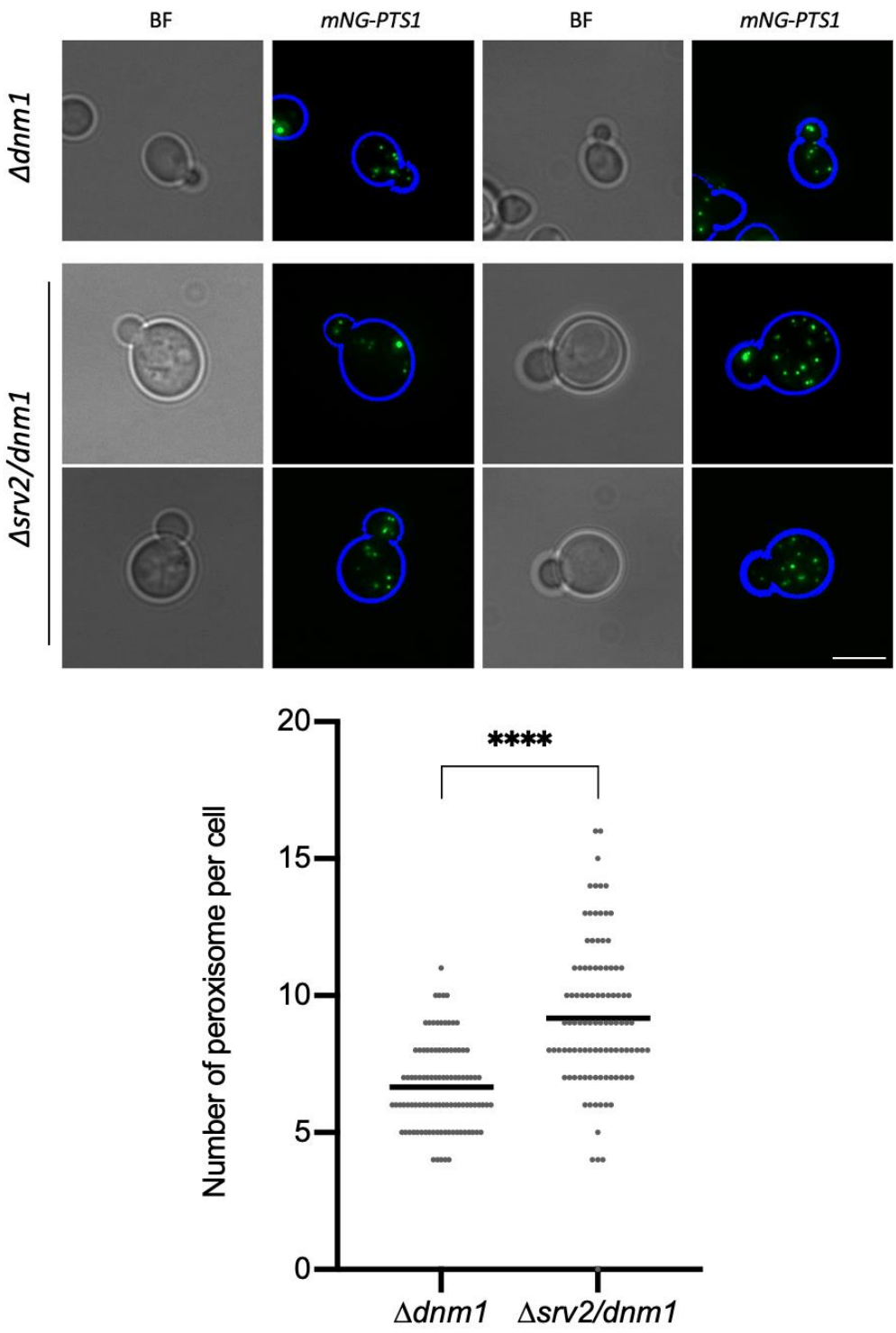

Figure 4. 8: The effect of *SRV2* on peroxisomes in *Δsrv2Δdnm1*. *Δdnm1* (upper panel) and *Δsrv2Δdnm1* (lower panel) cells expressing the peroxisomal marker mNG-PTS1 were grown to log phase before being imaged. Bars, 5µm. The graph illustrates the quantitative analysis of peroxisome numbers per cell in both strains *Δdnm1* and *Δsrv2Δdnm1*. Peroxisomes were counted in 100 yeast cells from three independent experiments. Black bars represent means. Statistical significance was determined by unpaired student t test: ****P ≤ 0.0001.

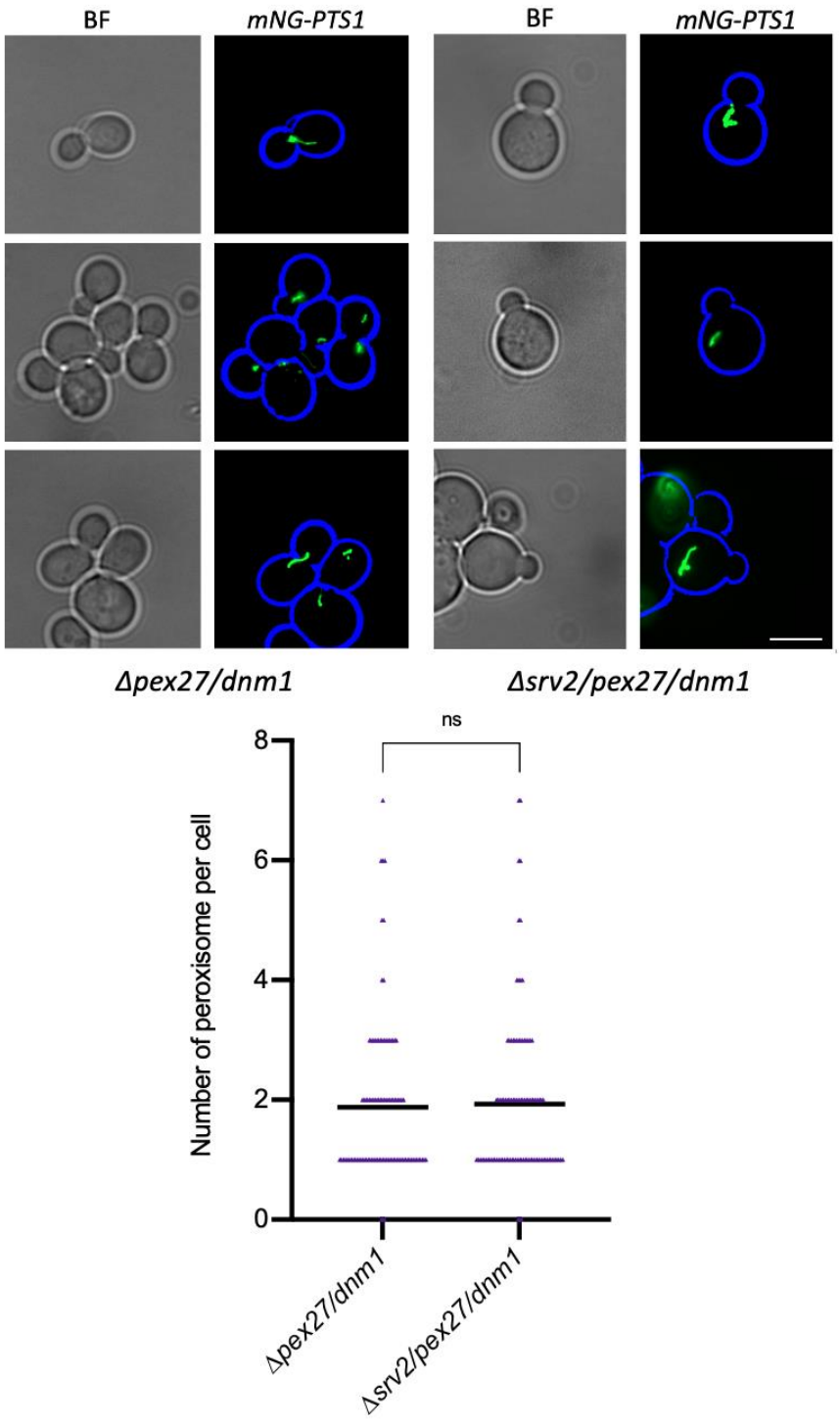

Figure 4. 9: *SRV2* has no effect on peroxisomes in *Δsrv2Δpex27Δdnm1*. *Δpex27Δdnm1* (left panel) and *Δsrv2Δpex27Δdnm1* (right panel) cells expressing the peroxisomal marker mNG-PTS1 were grown to log phase and peroxisomes were analysed. Bars, 5µm. The graph illustrates the quantitative analysis of peroxisome numbers per cell in both strains *Δpex27Δdnm1* and *Δsrv2Δpex27Δdnm1*. Peroxisomes were counted in 100 yeast cells from three independent experiments. Black bars represent means. Statistical significance was determined by unpaired student t test: ns: not significant.

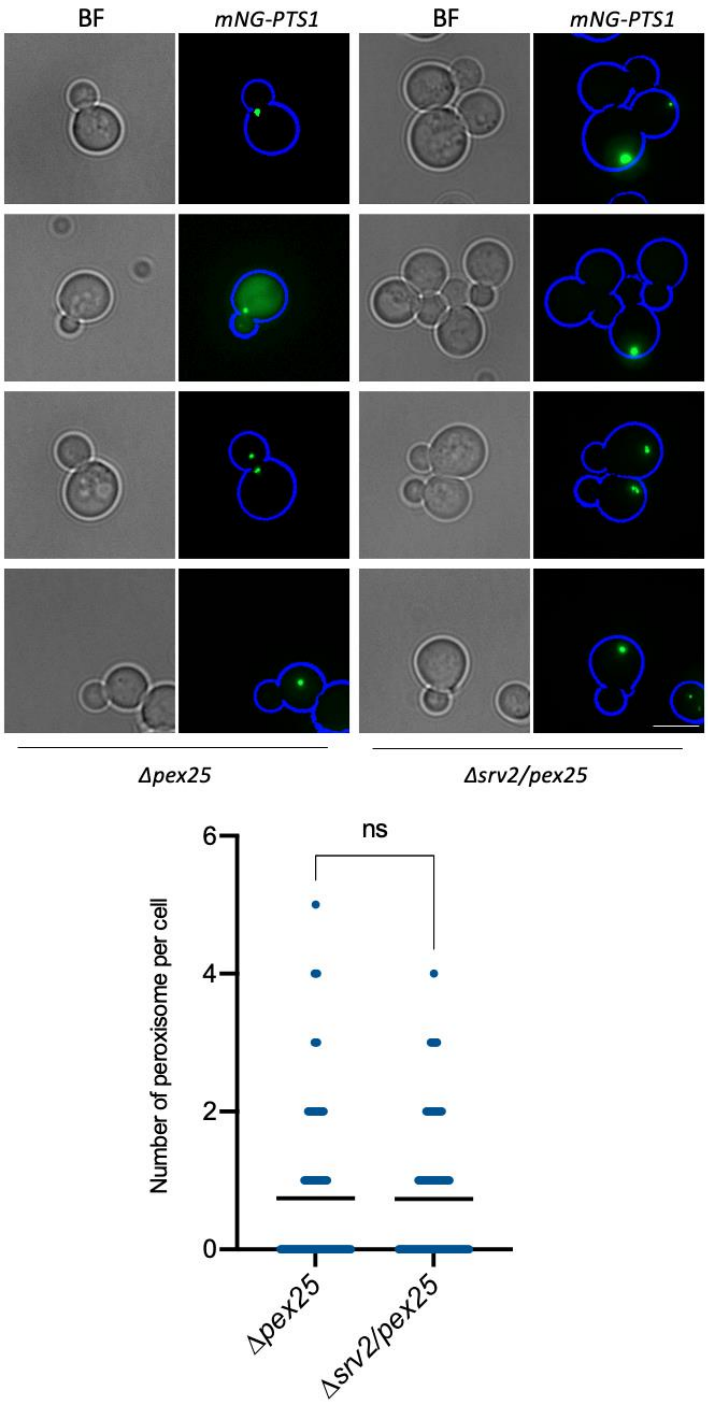

Figure 4. 10: The effect of *SRV2* on peroxisomes in *Δsrv2Δpex25*. *Δpex25* (left panel) and *Δsrv2Δpex25* (right panel) cells expressing the peroxisomal marker mNG-PTS1 were grown to log phase and peroxisomes were analysed. Bars, 5µm. The graph shows the quantitative analysis of peroxisome numbers per cell in both strains *Δpex25* and *Δsrv2Δpex25*. Peroxisomes were counted in 100 yeast cells from three independent experiments. Black bars represent means. Statistical significance was determined by unpaired student t test: ns: not significant.

4.5 The actin binding function of Srv2 is critical for peroxisome regulation

Srv2 protein contains a variety of motifs and domains. This include an N-terminal oligomerization domain, a dimeric helical folded domain (HFD), a Wasp homology 2 (WH2) domain, which is placed between two poly-proline (P1 and P2) motifs, and a dimeric folded domain known as the CARP domain, which is entirely composed of β-sheets, at the C-terminus (Fig. 4.11) (Ono, 2013). Srv2 plays a role in actin turnover by catalyzing nucleotide exchange and recycling actin monomers. The C-terminal domain of Srv2 binds to ADP-G-actin and competitively dispenses cofilin from ADP-actin monomers. Point mutations in this region can disrupt actin organization (Mattila et al., 2004; Balcer et al., 2003; Chaudhry et al., 2010). The N-terminal half of Srv2, however, promotes cofilin-mediated severing and consists of an oligomerization domain and a six-helix fold domain. The HFD alone produces anti-parallel dimers, while in the case of whole N-terminal hexamers, the HFDs are arranged in a star-like configuration composed of six symmetrical blades (Chaudhry et al., 2013; Quintero et al., 2009).

The two halves of Srv2/CAP have mostly been considered to play independent roles, although their linkage is proposed to enhance coordination of the two domains activities in particular contexts. This may help to explain why the linkage is conserved across distant animal, plant, and fungal species (Chaudhry et al., 2014). We next asked whether the N-terminal or the C-terminal domain is responsible for the effect of Srv2 on peroxisomes. In order to address this, we split *SRV2* into two halves, N-Srv2 and C-Srv2 domains (Fig. 4.11), and they were constructed into two separate plasmids.
We aimed first to check actin cables in the presence of these two halves of *SRV2*. Thus, *Δsrv2* cells were transformed with N-Srv2 or C-Srv2 constructs. WT, *Δsrv2*, *Δsrv2* expressing N-Srv2 and *Δsrv2* expressing C-Srv2 cells were then grown and stained by rhodamine phalloidin stain to visualize filamentous actin as described in Section 2.8.6.
As expected, WT cells showed polarized actin cables in almost all cells, while cortical actin patches were predominant in *Δsrv2* cells. Actin cables were also clearly observed in cells expressing the C-terminal domain. Cells expressing the N-Srv2 showed cortical actin patches and appeared to contain fewer actin cables than cables in cells expressing C-Srv2 (Fig. 4.11).

From the results presented, it can be concluded that the C-terminal fragment, but not the N-terminal fragment, of Srv2 contains the protein domain required for recycling actin monomers. Therefore, investigating the effect of C-Srv2 and N-Srv2 on peroxisomes will be the next goal.

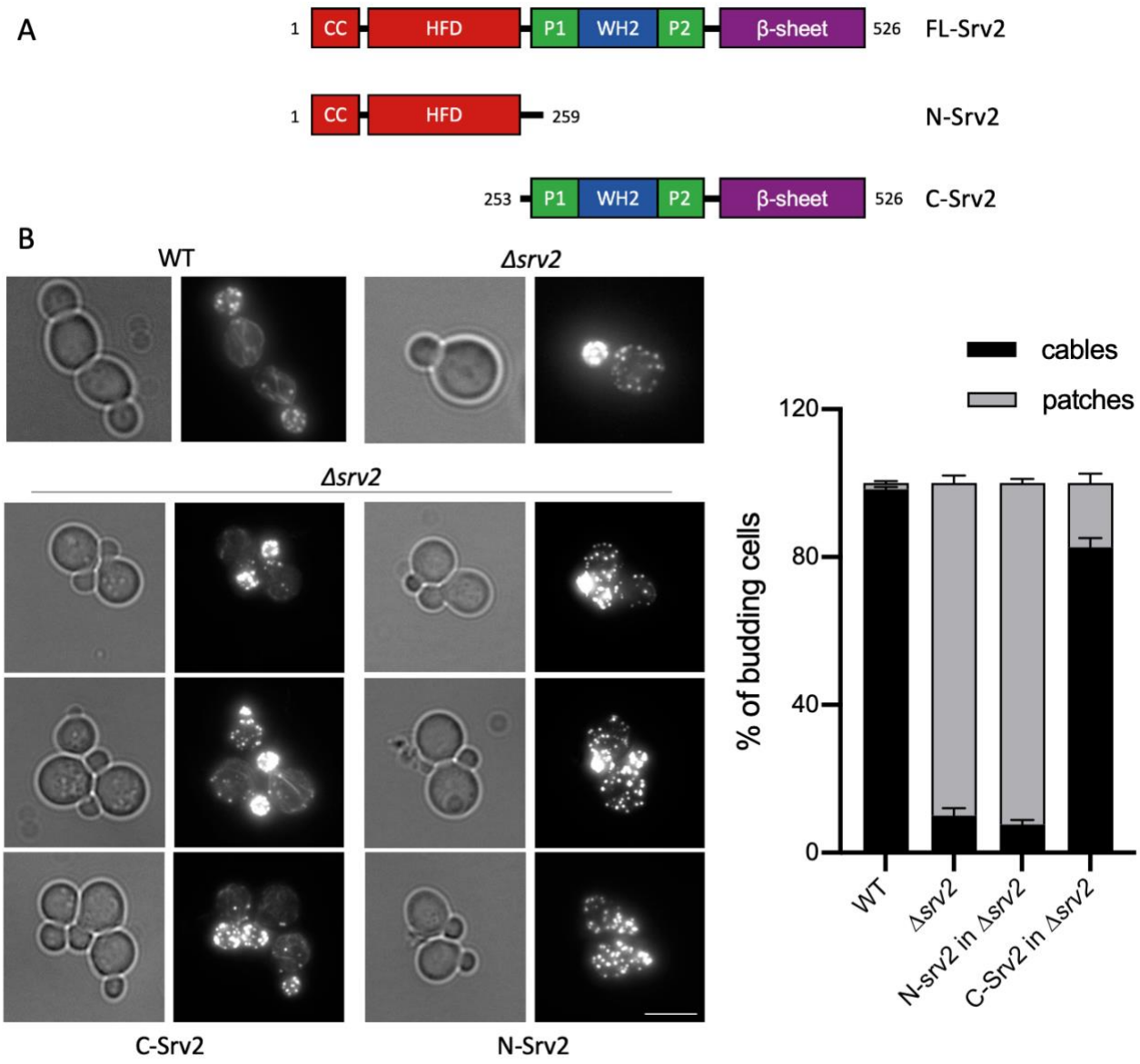

Figure 4. 11: Filaments actin in *Δsrv2* cells expressing Srv2 domains N-Srv2 and C-Srv2. A) Diagram illustrating the different domains within Srv2 and the constructs employed in these experiments. CC, Coiled-coils; HFD, helical folded domain; P, polyproline region; WH2, WASP-homology 2 domain. B) *Δsrv2* cells were transformed with N-Srv2 and C-Srv2 separately and grown to log phase. This was followed by staining with rhodamine phalloidin to visualize the actin. WT and *Δsrv2* cells were used as controls. Bar, 5µm. The graph shows a quantitative analysis of actin cables and batches in all cells. A minimum of 200 cells were counted from three separate experiments. Error bars represent SEM.

To explore the impact of N-Srv2 and C-Srv2 functions on peroxisomes, two strains were used, namely the *Δsrv2Δpex27* and *Δsrv2Δpex27Δdnm1* strains. The reason for choosing these particular strains is that the effect of *srv2* on peroxisomes is clear, and peroxisome number can be counted efficiently. In this experiment, *Δsrv2Δpex27* and *Δsrv2Δpex27Δdnm1* expressing the peroxisomal marker mNG-PTS1 were transformed with N-Srv2 and C-Srv2 constructs separately. *Δpex27* and *Δpex27Δdnm1* were used as controls. Log phase cells were then imaged.
Peroxisomes in *Δpex27* cells are elongated and their number is small. Peroxisomes were increased in *Δsrv2Δpex27* cells. *Δpex27* cells expressing N-Srv2 showed an increase in the number of peroxisomes and the elongated shape still appeared. In contrast, expression of C-terminal Srv2 showed the ability to restore the peroxisome number to that of *Δpex27* cells. The quantitative analysis showed a significant difference between peroxisome numbers in both strains compared with the controls, *Δpex27* and *Δsrv2Δpex27* strains (Fig. 4.12 A).

As shown in the section above, *Δpex27Δdnm1* and *Δsrv2Δpex27Δdnm1* cells showed only one elongated peroxisome per cell and that is due to the inhibition of fission pathways. In the case of expressing N-Srv2 or C-Srv2 in *Δsrv2Δpex27Δdnm1* cells, there were no significant differences between N-Srv2 and C-Srv2 in that the number remained the same as in *Δpex27Δdnm1*. Analysis of cells showed that cells had one peroxisome per cell in all strains including controls (Fig 4.12 B).

These results identified the effect of both domains of Srv2 on peroxisomes. The Srv2 C-terminal restores the peroxisome phenotype while the N-terminal does not, which lead us to conclude that the actin binding function of Srv2 is critical for peroxisome regulation.

Moreover, since neither domains of Srv2 shows any effect on peroxisome in *Δsrv2Δpex27Δdnm1* cells, this is another indication that Srv2 or its domains have no effect on peroxisomes when peroxisome fission pathways are inhibited.

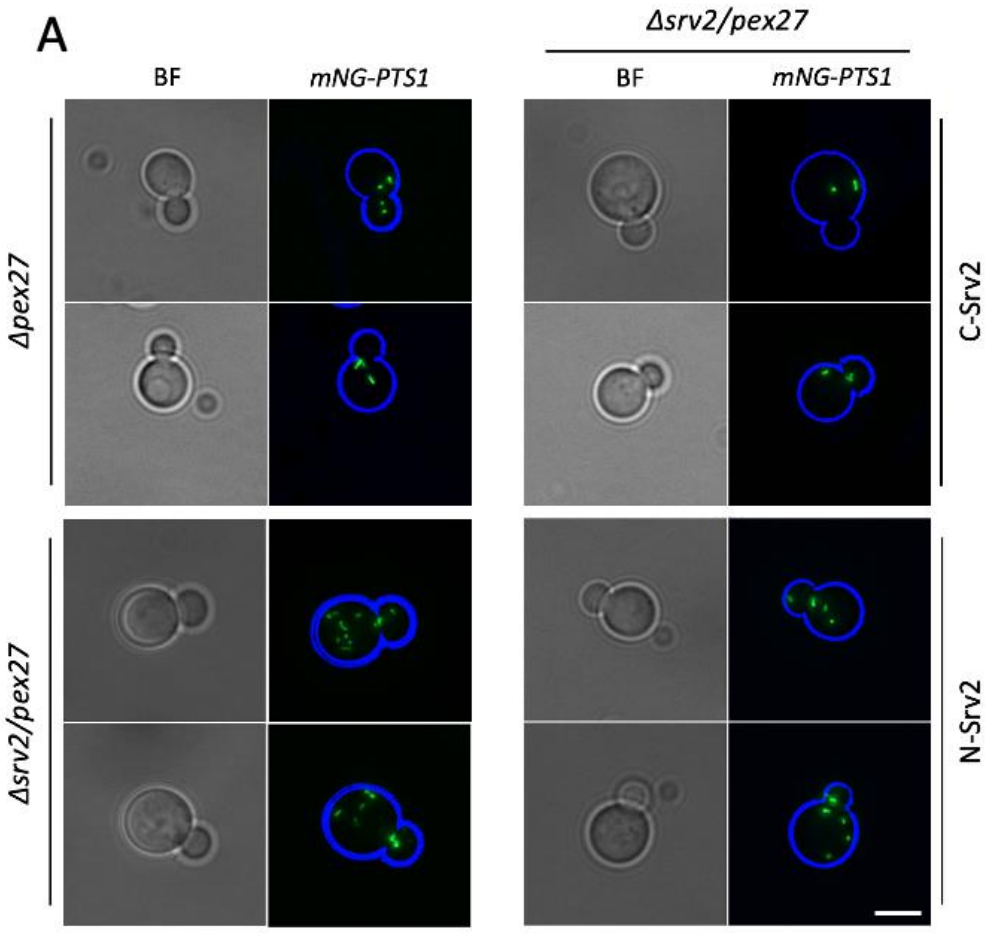
A
Δsrv2/pex27
BF
mNG-PTS1
BF
mNG-PTS1
Δpex27
C-Srv2
Δsrv2/pex27
N-Srv2

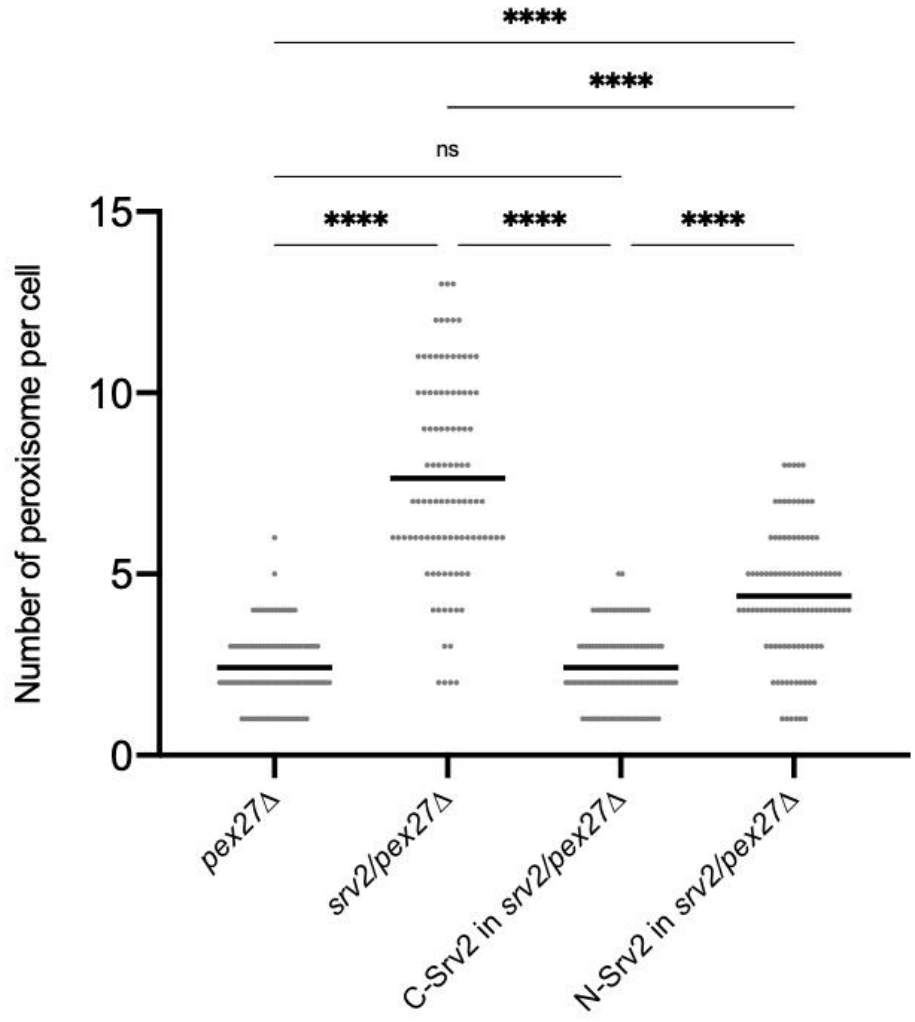
****
****
ns
****
****
****
Number of peroxisome per cell
15
10
5
0
pex27Δ
srv2/pex27Δ
C-Srv2 in srv2/pex27Δ
N-Srv2 in srv2/pex27Δ

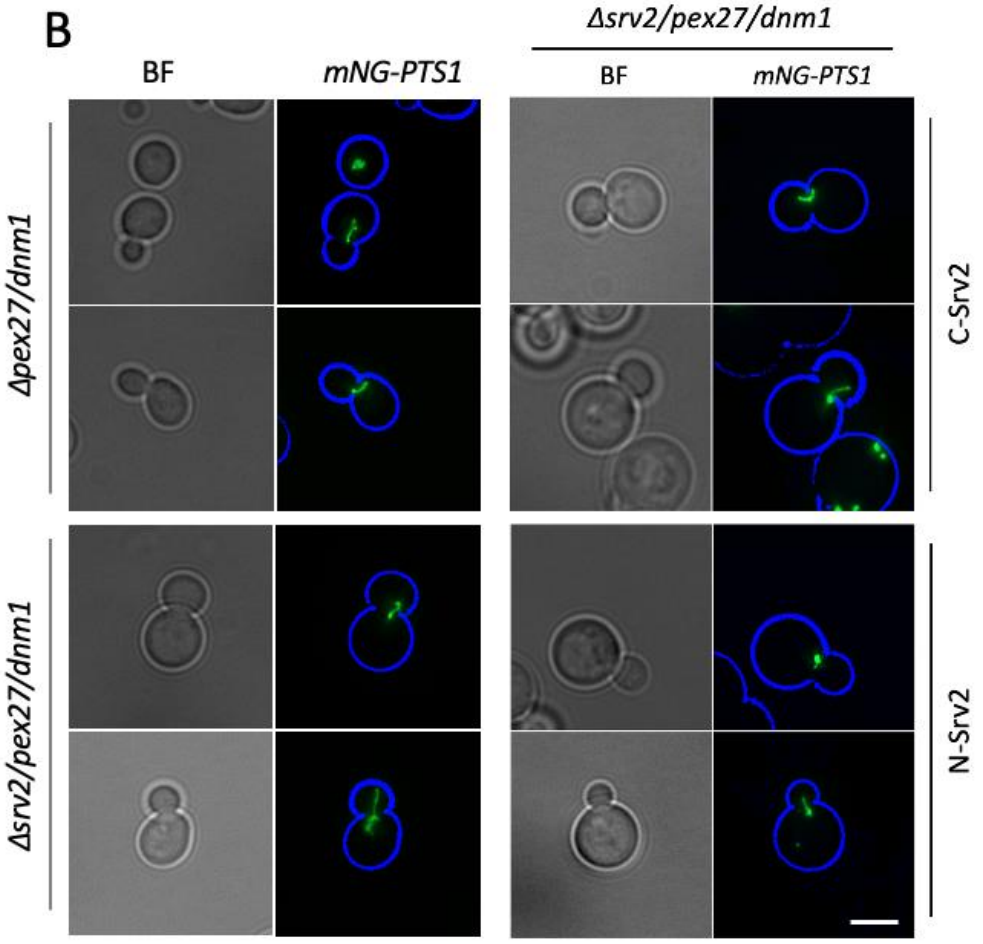
B
Δsrv2/pex27/dnm1
BF
mNG-PTS1
BF
mNG-PTS1
Δpex27/dnm1
Δsrv2/pex27/dnm1
C-Srv2
N-Srv2

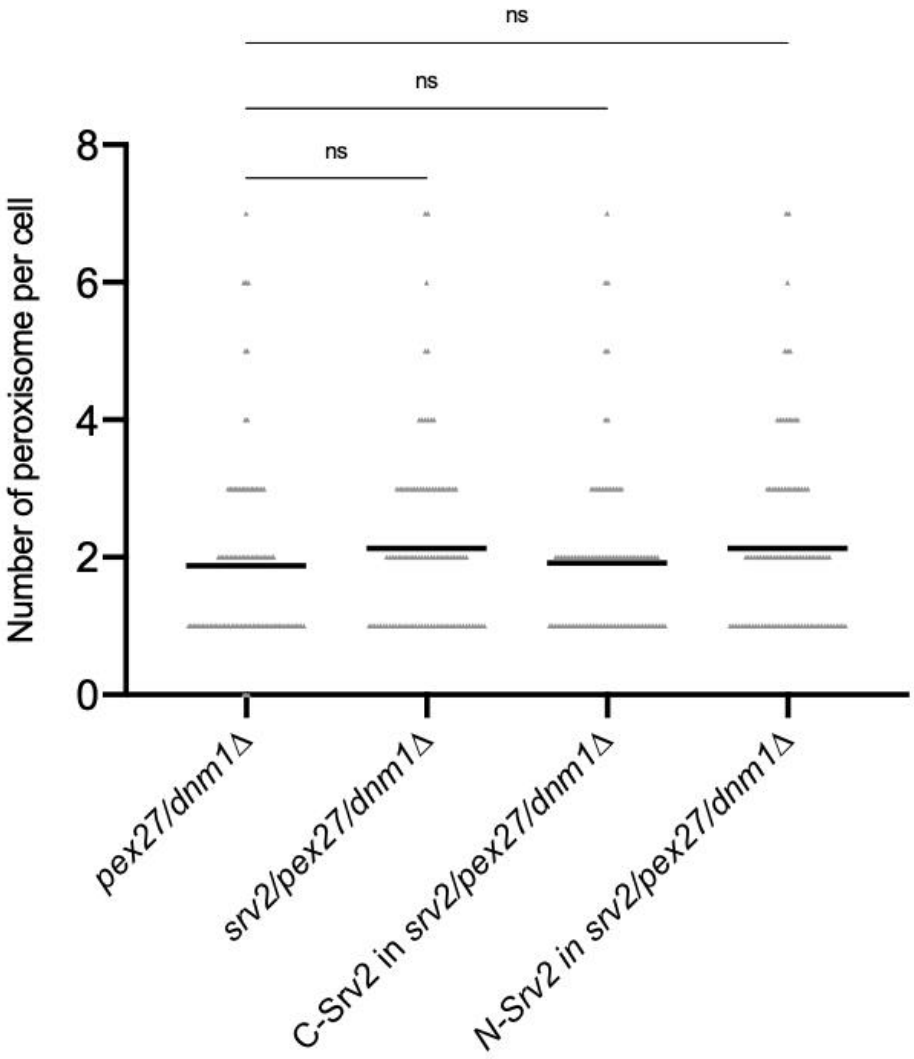
ns
ns
ns
Number of peroxisome per cell
8
6
4
2
0
pex27/dnm1Δ
srv2/pex27/dnm1Δ
C-Srv2 in srv2/pex27/dnm1Δ
N-Srv2 in srv2/pex27/dnm1Δ

Figure 4. 12: The Srv2 C-terminus is required for controlling peroxisome fission. A) N-Srv2 or C-Srv2 domains were expressed in *Δsrv2Δpex27* cells in the presence of the mNG-PTS1 marker. *Δpex27* and *Δsrv2Δpex27* were used as controls. Log phase cells were imaged. The graph illustrates the quantification of peroxisome number in each strain. B) *Δsrv2Δpex27Δdnm1* cells expressing the peroxisomal marker mNG-PTS1 were transformed with N-Srv2 and C-Srv2 separately. Log phase cells were imaged in the presence of control cells *Δpex27Δdnm1* and *Δsrv2Δpex27Δdnm1*. The graph represents the quantification of peroxisome number in each strain. Bars, 5µm. Three independent experiments were done, and peroxisomes were counted in 100 cells from each experiment. Black bars represent means. Statistical significance was determined by unpaired student t test: ****P ≤ 0.0001, ns: not significant.

Because the *SRV2* deletion also caused slower growth and an increase in cell size it was important to determine whether the increase in peroxisome is indirect due to these effects or whether it was specific and due to the importance of the actin binding function of Srv2.
The results from the section above demonstrate that although cells expressing N-Srv2 have an effect on peroxisomes, cells expressing either N-Srv2 or C-Srv2 have a similar cell size to one another. So, we can conclude that the increase in cell size is not responsible for the increase in peroxisome number. In addition, a yeast growth assay was performed in order to determine if the peroxisome phenotype is due to the slow growth of cells.
This assay compared five strains: WT, *Δsrv2* and *Δsrv2* carrying Srv2 full length, N-Srv2 and C-Srv2 separately.
The result showed that cells expressing N-Srv2 and C-Srv2 have very similar growth. The growth was near to that of WT and Srv2 full length, whereas the growth of *Δsrv2* cells was very slow (Fig. 4.13). This result leads us to conclude that the phenotype of *SRV2* deletion on peroxisomes is not due to the slow growth. Although N-Srv2 and C-srv2 cells have no difference in terms of growth, N-Srv2 still increases the number of peroxisomes while the C-terminus restores peroxisome numbers. We conclude that the increase in peroxisome is due to the importance of the actin binding function of Srv2.

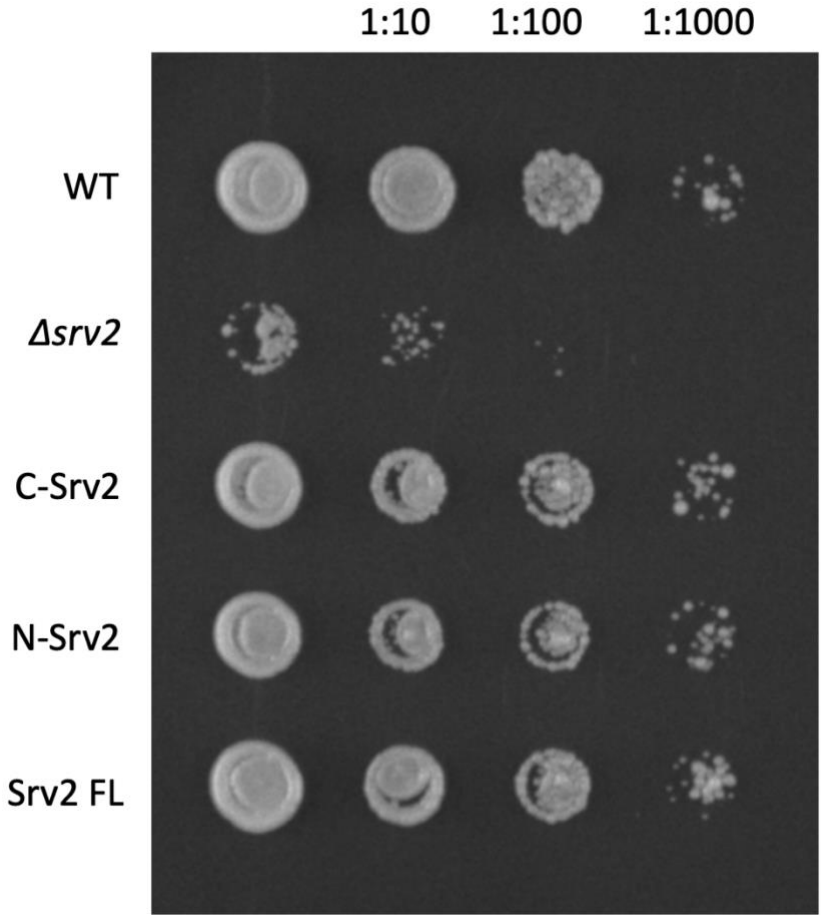

Figure 4. 13: Yeast growth assay of *Δsrv2* expressing N and C-terminus of Srv2. The indicated strains were subjected to serial dilutions and cultivated on a solid glucose medium without Leucine for a duration of 2 days at 30°C.

4.6 Srv2 works as a negative regulator of peroxisome fission

The studies above indicate that the absence of *srv2* leads to an increase in peroxisome number suggesting that Srv2 might negatively regulate peroxisome fission. We could then hypothesize that increased localization of Srv2 to peroxisomes might in turn lead to a reduction in peroxisome number. In order to examine the involvement of Srv2 in peroxisome fission, Srv2 was fused to Pex15, a peroxisomal membrane protein anchor with a cytosolic facing globular domain (Elgersma et al., 1997). This produced a fusion protein that exposed Srv2 to the cytosol and anchored it to the peroxisomal membrane by Pex15. The two proteins were separated by GFP (Fig. 4.13a). This fusion protein was under the control of the Srv2 promoter. A GFP-Pex15 under the control of the Srv2 promoter was used as a control. These fusion proteins were then co-expressed in strains with HcRed-SKL, the peroxisomal marker fused with Heteractis crispa red fluorescent protein.

Starting with WT cells, the results showed that the fusion protein Srv2-GFP-Pex15 causes a strong inhibition of peroxisome fission by stopping it from happening. Interestingly, cells expressing the Srv2-GFP-Pex15 fusion protein have one giant peroxisome compared with cells carrying GFP-Pex15 which have the normal number of peroxisomes.
For quantification purposes, cells were divided into 4 categories: normal peroxisomes, one giant peroxisome in the mother, one peroxisome in the bud and only GFP signals without any peroxisome signal. Cells expressing GFP-Pex15 have the usual peroxisome number and distribution, and almost all GFP signals were colocalized with peroxisomes. However, cells expressing Srv2-GFP-Pex15 fusion showed one big peroxisome per cell in most of the cells. Some cells showed peroxisome appearing in buds and some cells showed GFP signals without any labelled peroxisome. The nature of these GFP-labelled structures is still unclear but could be Srv2-GFP puncta cleaved from Pex15 or the Srv2-GFP-Pex15 released from peroxisomes and forming an aggregated structure (Fig. 4.14).
Similar results were found in the case of *Δsrv2* cells. In the control, in the form of *Δsrv2* cells expressing GFP-Pex15 under the control of an Srv2 promoter, the number of peroxisomes was high and similar to the *Δsrv2* peroxisome phenotype shown in Section 4.3. However, one peroxisome was found per cell in most the cells expressing the fusion protein Srv2-GFP-Pex15. Quantification analysis illustrates that most of cells expressing Srv2-GFP-Pex15 showed one peroxisome, and some showed peroxisome in buds. A small minority of cells showed GFP signals only with an absence of peroxisomes (Fig. 4.15).

This finding prompted us to analyse the actin filaments in the cells, to see whether or not they were affected.
WT and *Δsrv2* cells expressing GFP-Pex15 and Srv2-GFP-Pex15 fusion were stained using rhodamine phalloidin stain as described in Section 2.8.6. The results showed that actin filaments appeared normal in both WT cells that express GFP-Pex15 or Srv2-GFP-Pex15 fusion. In the case of *Δsrv2* cells, both cells expressing GFP-Pex15 or Srv2-GFP-Pex15 fusion showed actin patches more than cables compared with WT cells. However, it seems that cells expressing Srv2-GFP-Pex15 showed an increase in the number of actin cables when compared with cells lacking any *srv2* suggesting that the Srv2 on the peroxisome surface is able to partially rescue the defective phenotype of the *SRV2* deletion strain (Fig. 4.16). Due to this

finding, we can conclude that the fusion protein does not affect actin where actin cables and patches are similar to WT and *Δsrv2* cells respectively.

These interesting results lead us to hypothesise that Srv2 may work as a negative regulator in the process of peroxisome fission. This idea was investigated further by testing the fusion protein in mutant strains with clearly defined peroxisome phenotypes.

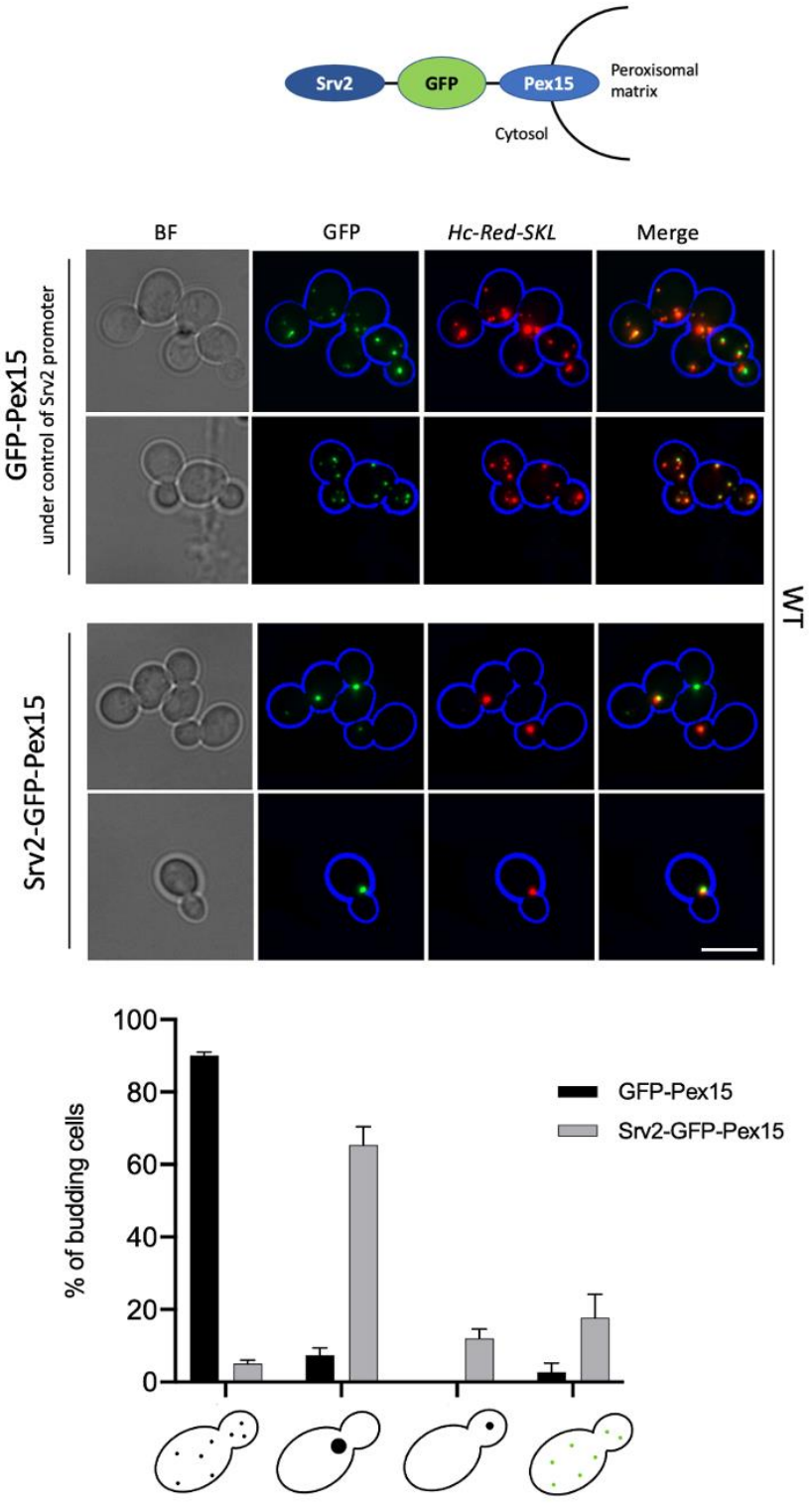

Figure 4. 14: Fusion protein Srv2-GFP-Pex15 expressing in WT cells. WT cells expressing Srv2-GFP-Pex15 or GFP-Pex15 in the presence of the peroxisomal marker HcRed-SKL were grown, and log phase cells were imaged. Bar, 5µm. The graph illustrates the quantitative analysis of peroxisome numbers per cell in both strains. Three independent experiments were done, and peroxisomes were counted in a minimum of 100 cells per strain from each experiment. Error bars represent SEM.

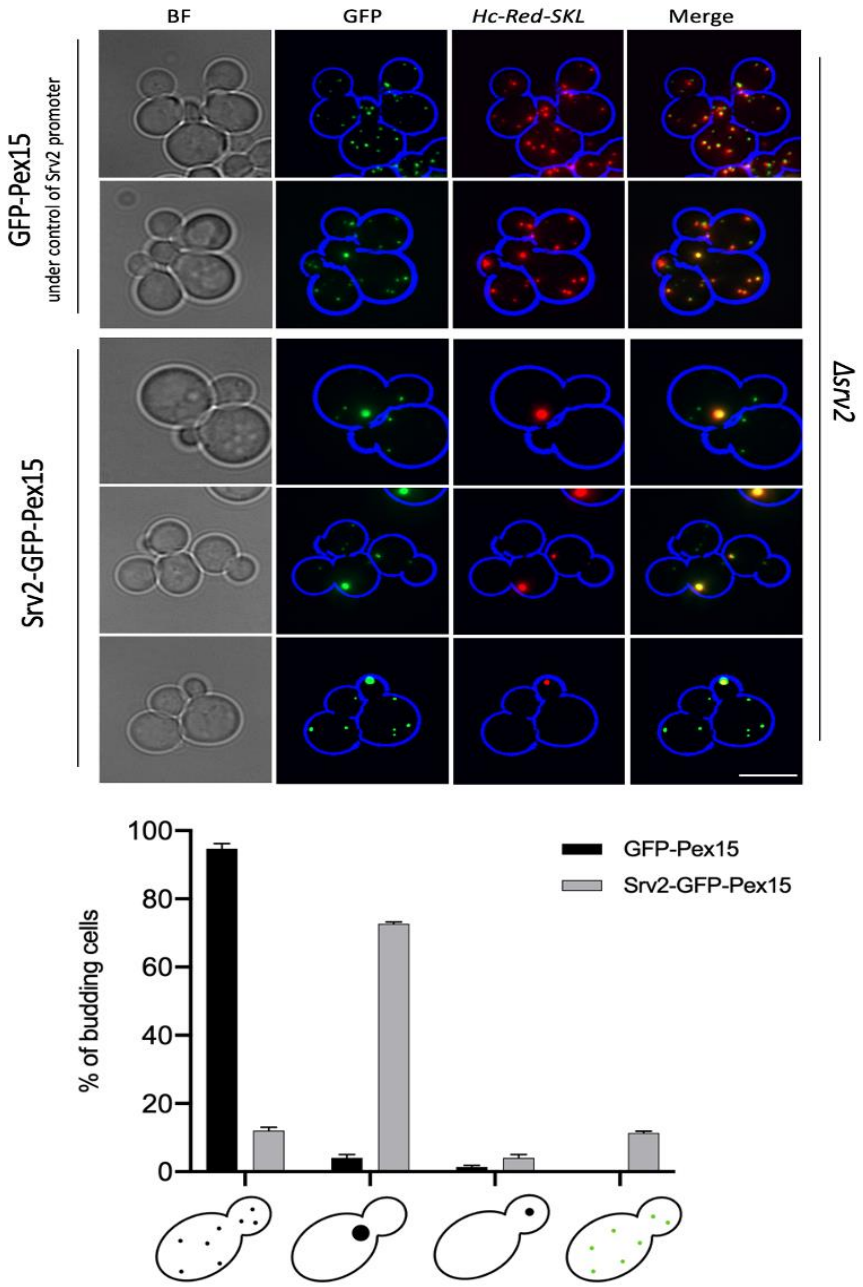

Figure 4. 16: Srv2-GFP-Pex15 fusion protein reduced the number of peroxisomes in *Δsrv2* cells. Log phase cells expressing either GFP-Pex15 or Srv2-GFP-Pex15 were imaged. Bar, 5µm. For quantification, peroxisomes were counted per cell, a minimum of 200 cells per strain, from three experiments. Error bars represent SEM.

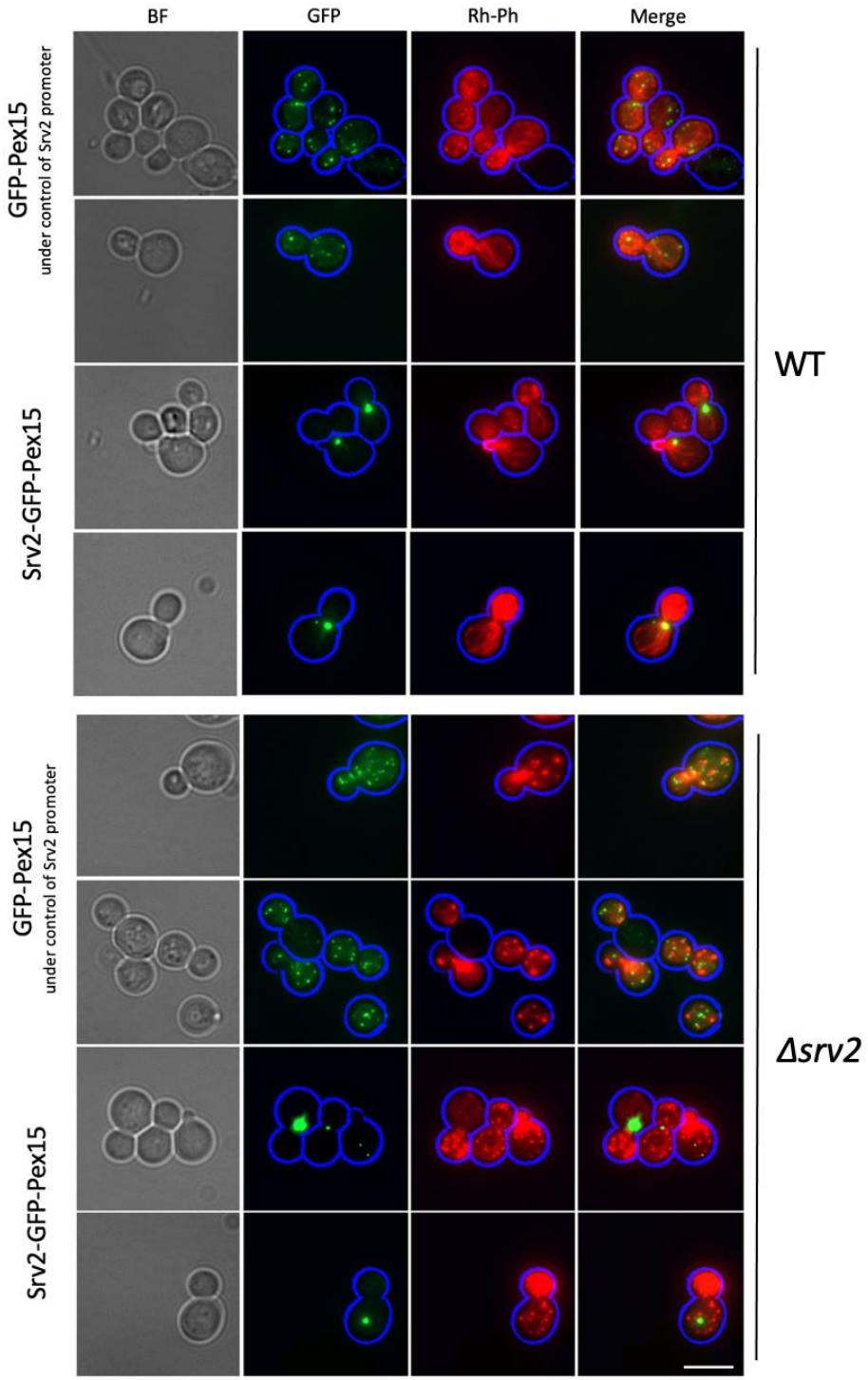

Figure 4. 15: Actin filaments in WT and *Δsrv2* cells expressing Srv2-GFP-Pex15 fusion protein. WT and *Δsrv2* cells expressing the fusion protein Srv2-GFP-Pex15 and GFP-Pex15 were stained using rhodamine phalloidin and analysed by fluorescent microscope. Bar, 5µm.

In order to do this, we transformed GFP-Pex15 or Srv2-GFP-Pex15 fusion into *Δpex27* cells expressing the peroxisomal marker HcRed-SKL. Cells were grown to log phase before being imaged. *Δpex27* cells usually have few, elongated peroxisomes. Similar results were found in the case of *Δpex27* cells expressing GFP-Pex15 where cells did not alter this phenotype and continued to have a small number of elongated peroxisomes. However, *Δpex27* cells that carry Srv2-GFP-Pex15 fusion showed one big peroxisome in the mother cells, while around 20% of the cells showed one peroxisome in the bud (Fig. 4.17).

The next strain tested was *Δsrv2Δpex27*. Fusion Srv2-GFP-Pex15 and GFP-Pex15 were transformed separately into *Δsrv2Δpex27* cells that expressed the HcRed-SKL marker. Peroxisomes were then counted in log phase cells. It has been shown previously in this chapter (Section 4.4) that *Δsrv2Δpex27* cells have a large number of peroxisomes. Here, cells expressing GFP-Pex15 showed a similar number of peroxisomes. On the other hand, there was a marked reduction in peroxisome numbers in cells expressing the fusion protein Srv2-GFP-Pex15. Most cells showed only one giant peroxisome per cell, and the elongated shape disappeared (Fig. 4.18).

The effect of Srv2-GFP-Pex15 fusion was tested in the *Δsrv2Δdnm1* strain. Cells expressing the HcRed-SKL marker were transformed with GFPpPex15 and Srv2-GFP-Pex15 separately and were grown to log phase and then imaged.
The fusion protein Srv2-GFP-Pex15 also showed an effect on peroxisomes in *Δsrv2Δdnm1* cells. The results demonstrate that the fusion protein leads to a reduction in peroxisome numbers. Cells carrying Srv2-GFP-Pex15 showed only one or two big peroxisomes per cell, while the number of peroxisomes was increased in the presence of GFP-Pex15 (Fig. 4.19).

Therefore, from all the above results it seems that Srv2 plays a vital role in regulation of peroxisome fission. Thus, we conclude that Srv2 works as a negative regulator of peroxisome fission.

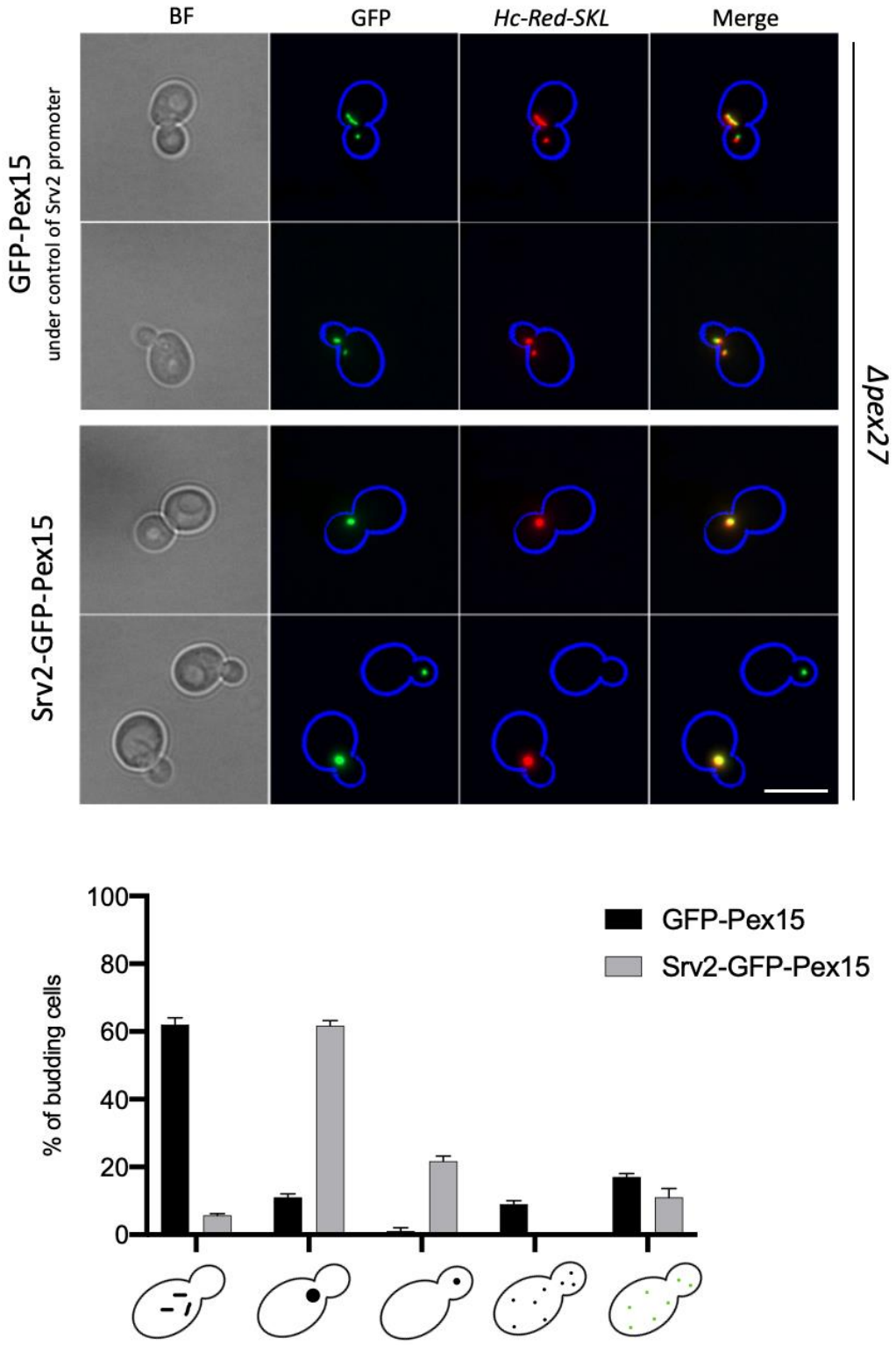

Figure 4. 17: The effect of the fusion protein Srv2-GFP-Pex15 on *Δpex27* cells. *Δpex27* cells expressing the HcRed-SKL marker were transformed with GFP-Pex15 or Srv2-GFP-Pex15 and then grown to log phase followed by imaging. Bar, 5µm. The graph shows the peroxisome number and shape in both strains. 3 different experiments were done, and peroxisomes were counted in more than 200 cells from each of these experiments. Error bars represent SEM.

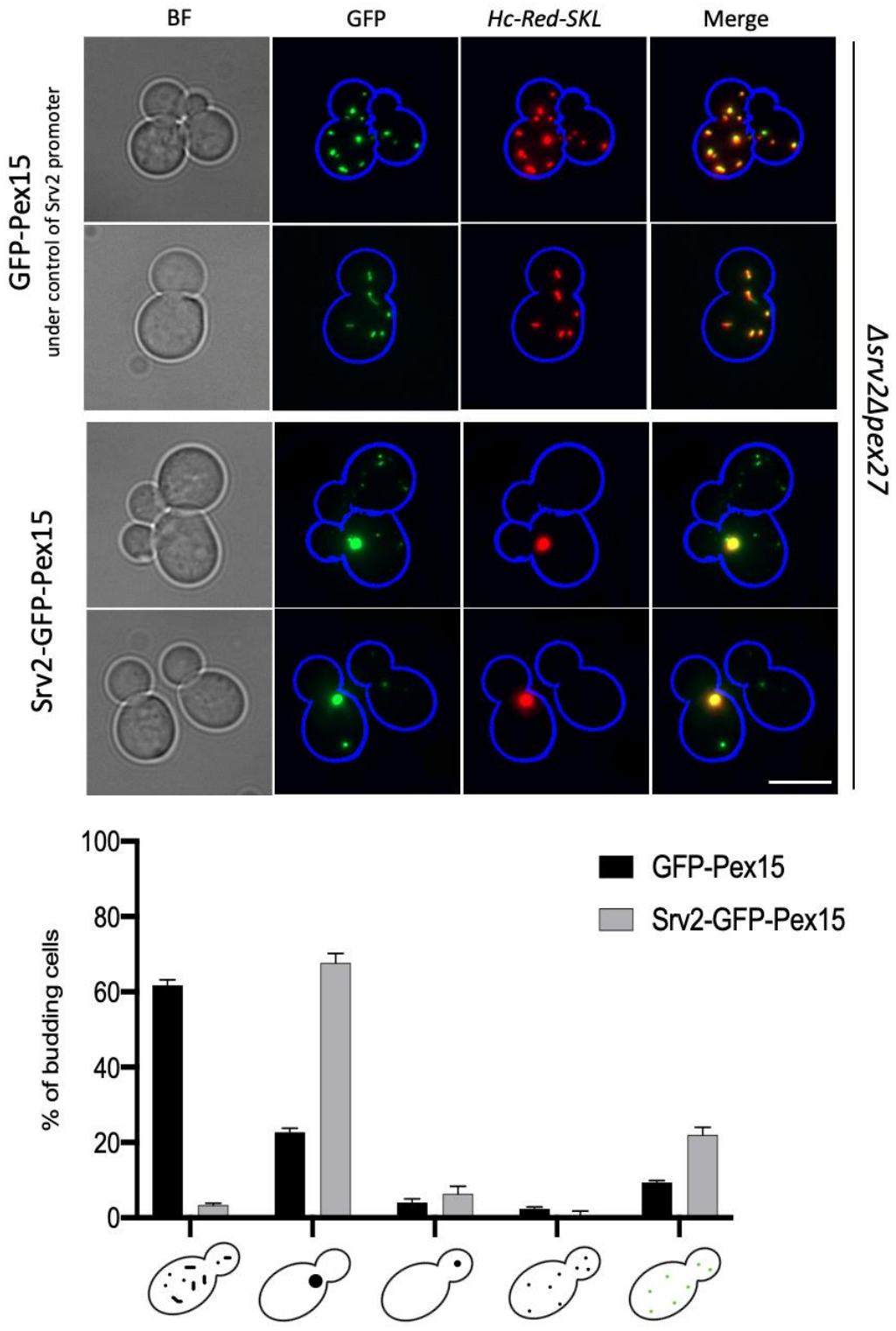

Figure 4. 18: The effect of Srv2-GFP-Pex15 fusion protein on peroxisomes in *Δsrv2Δpex27* cells. Cells expressing the HcRed-SKL marker were transformed with GFP-Pex15 or Srv2-GFP-Pex15 and then grown to log phase followed by imaging. Bar, 5µm. The graph showed the peroxisome number and shape in both strains. More than 200 cells were counted from 3 different experiments. Error bars represent SEM.

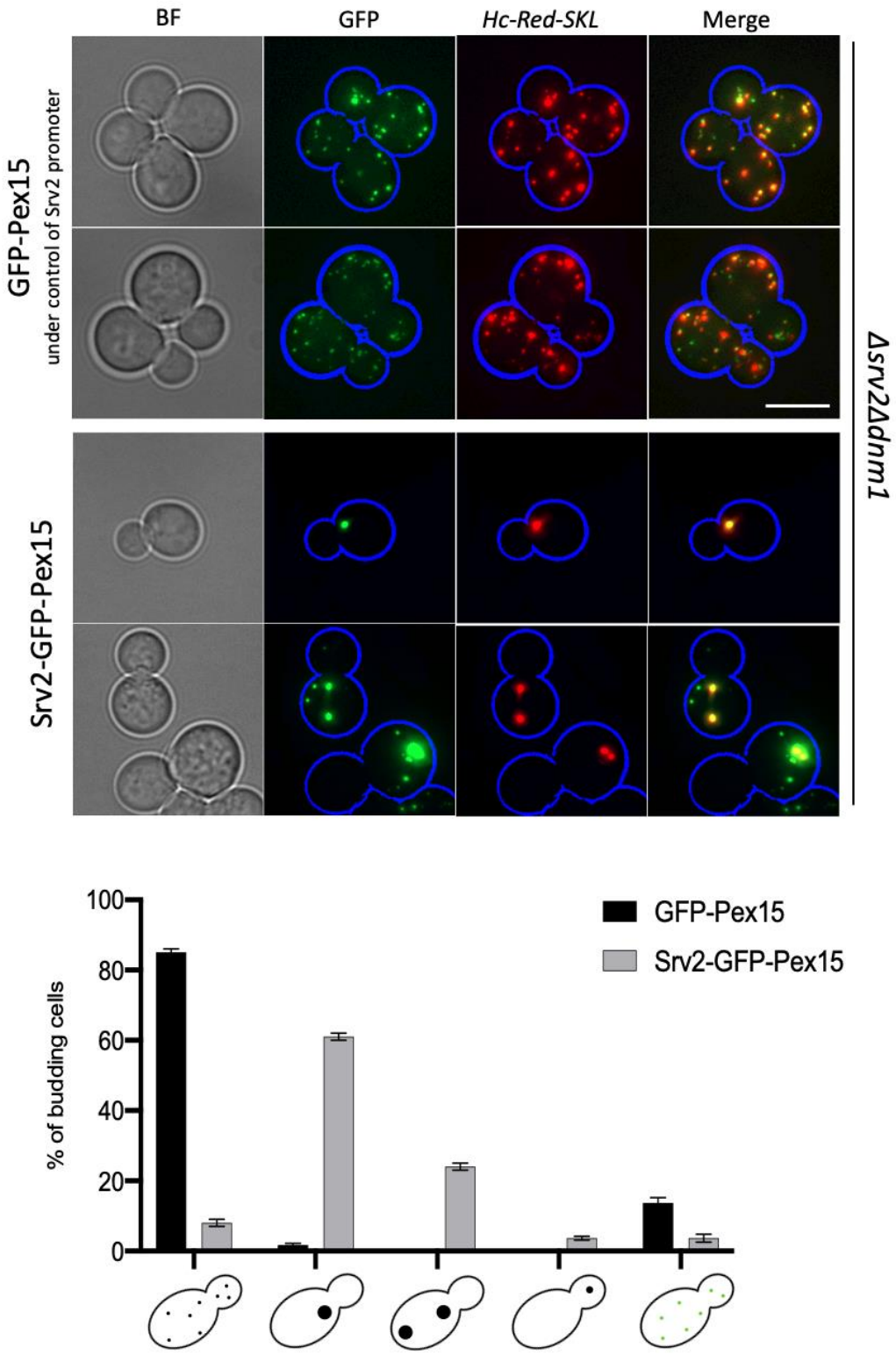

Figure 4. 19: *Δsrv2Δdnm1* cells expressing Srv2-GFP-Pex15 showed a reduction in peroxisome numbers. Cells expressing GFP-Pex15 or Srv2-GFP-Pex15 were imaged after growing to log phase. Bar, 5µm. The graph showed the peroxisome number in both strains. More than 200 cells were counted from 3 independent experiments. Error bars represent SEM.

4.7 Deletion of *SRV2* affects the mitochondrial morphology

Mitochondria are crucial organelles. The most important of their known functions is to provide cells with energy. Primarily, cells employ mitochondria for ATP production through the process of oxidative phosphorylation, where oxygen acts as the final receiver of electrons. Mitochondria are set apart from other organelles by their unique characteristics, which include a dual-layered membrane, a wavy cristae structure, and dynamic network interactions. The formation of the mitochondrial network is a continual process involving repeated anchoring, trafficking, fusion and fission. These operations not only shape the appearance of the mitochondrial network but also play a significant role in maintaining the balance and integrity of the mitochondria (Gomes et al., 2011; Blackstone and Chang, 2011; Chen et al., 2019).

In eukaryotes, substantial dynamin related GTPases are necessary in facilitating both the fusion and fission of membranes (Fig. 4.20). In yeast, Fzo1, Ugo1, and Mgm1 work together to promote the fusion of the outer and inner membranes of mitochondria (Wong et al., 2000; Hermann et al., 1998; Sesaki and Jensen, 2001). Cytosolic Dnm1 regulates fission of mitochondria by creating protein assemblies together with Fis1, Caf4, and/or Mdv1 (Legesse-Miller et al., 2003; Griffin et al., 2005; Chang and Blackstone, 2007). The endoplasmic reticulum mitochondria encounter structure (ERMES) also participates in the tightening process of mitochondria. It accomplishes this by encircling the mitochondria at active locations to aid in their division (Friedman et al., 2011).

Mitochondrial-actin cytoskeleton interactions are required for maintaining the typical form, movement, and distribution of mitochondria (Boldogh et al., 2006), and actin filaments also play a critical role in mitochondrial transport (Hermann et al., 1998; Fehrenbacher et al., 2004; Huckaba et al., 2004).

A recent study has demonstrated that Dnm1 interacts with Srv2. In addition, the loss of *srv2* has a strong effect on mitochondria which become irregular with a branched tubular shape (Chen et al., 2019).

Since *SRV2* deletion causes the peroxisomal number to increase, as shown previously in this chapter (Section 4.3), we sought to investigate the effect of *srv2* on mitochondria in all mutated strains that showed peroxisome phenotypes.

Mutated strains *Δsrv2, Δpex27, Δsrv2Δpex27, Δdnm1, Δsrv2Δdnm1, Δpex27Δdnm1* and *Δsrv2Δpex27Δdnm1* were transformed with the mitochondrial marker MDH1-mRuby and analysed by fluorescence microscopy.

It is known that the normal shape of mitochondria in WT cells is tubular. The analysis of these mutants found that the disruption of the *SRV2* gene affects the morphology of mitochondria. In *Δsrv2* cells, the wild type tubular mitochondrial morphology became fragmented. This indicates that the deletion of *SRV2* increased mitochondrial fission. This was compared with WT cells. This observation aligns with the findings of Chen et al. (2019), who also reported that deleting Srv2 leads to altered mitochondrial shape through increased fission.

The *PEX27* gene is known to not affect mitochondria, where its morphology appears to be tubular like WT. In my results, the majority of *PEX27* cells exhibit tubular mitochondria, while a very small portion show an irregular or fragmented mitochondrial shape. However, deleting *SRV2* in *Δpex27* cells caused the network to become tubular and to be branched which is similar to mitochondrial phenotype in *Δsrv2* cells.

The deletion of the *DNM1* gene affects the mitochondrial morphology. *Δdnm1* cells usually have collapsed mitochondria to one side of the cell (Otsuga et al., 1998). Interestingly, in

Δsrv2Δdnm1 the mitochondria network appeared to collapse near to the bud neck of cells appearing like a single giant mitochondrion. In addition, the mitochondrial network in *Δdnm1Δpex27* cells is collapsed on one side in the cell giving the same phenotype to *Δdnm1*. The deletion of *SRV2* in *Δpex27Δdnm1* cells affects the morphology where it appeared as giant mitochondria at the bud neck, similar to *Δsrv2Δdnm1* phenotype. Figure 4.21 illustrates all mitochondrial phenotypes found in all these strains.
For quantification, cells were divided into five mitochondrial morphology categories which were tubular (normal ones), fragmented, network like (collapsed at one side of the cell), giant mitochondria, and branched (large network) (Fig. 4.22). The more detailed analysis allows us to conclude that *srv2* influences the morphology of mitochondria, particularly by increasing mitochondrial fission. This is supported by the observed fragmented and branched tubular mitochondrial morphology in *Δsrv2* cells and *Δpex27Δdnm1* cells, respectively.

4.8 The actin binding function of Srv2 is critical for mitochondrial regulation

Deletion of *SRV2* has an effect on peroxisomes by increasing their numbers in cells lacking any *srv2*, and the C-terminus of Srv2 has the ability to rescue the peroxisome numbers (Section 4.5). In this section, we showed that the deletion of *SRV2* also affects mitochondrial morphology. Next, we aimed to investigate the effect of both N and C-terminus of Srv2 on the morphology of mitochondria.
Consequently, the Srv2 domain that is responsible for the effect on mitochondria was then the focus of our investigation.
Mutated strains expressing either the N-Srv2 or the C-Srv2 domains (Fig. 4.10) were analysed to check the morphology of mitochondria in the presence of the mitochondrial marker MDH1-mRuby.
The findings showed that C-terminal Srv2 can restore the mitochondrial phenotype in all cells lacking *srv2*. WT cells have tubular mitochondria and *Δsrv2* cells have fragmented mitochondria. *Δsrv2* cells expressing the C-Srv2 domain showed tubular mitochondria while cells expressing the N-Srv2 domain showed fragmented mitochondria. *Δsrv2Δpex27* cells showed large tubular and branched mitochondria. However, *Δsrv2Δpex27* carrying C-Srv2 showed normal tubular mitochondria and cells carrying N-Srv2 still showed branched mitochondria. *Δdnm1* cells have unique mitochondrial morphology which usually collapsed at one side of the cell. In the case of *Δsrv2Δdnm1*, most of the cells showed collapsed mitochondria close to the bud neck. C-Srv2 expressed in *Δsrv2Δdnm1* cells showed Δdnm1 phenotype, and N-Srv2 cells showed *Δsrv2Δdnm1* phenotype. The same phenotypes were found in *Δsrv2Δpex27Δdnm1* cells expressing N-Srv2 or C-Srv2 (Fig. 4.23).
These data further demonstrate that the role of Srv2 in actin assembly is vitally important for the dynamic procedures of mitochondria.

The data obtained and described in the above sections demonstrate that *srv2* influences both peroxisomes and mitochondria, and it is important for peroxisome fission and in facilitating mitochondrial morphology. Additionally, the data demonstrate the importance of the actin binding function of Srv2 for peroxisome and mitochondria regulation.

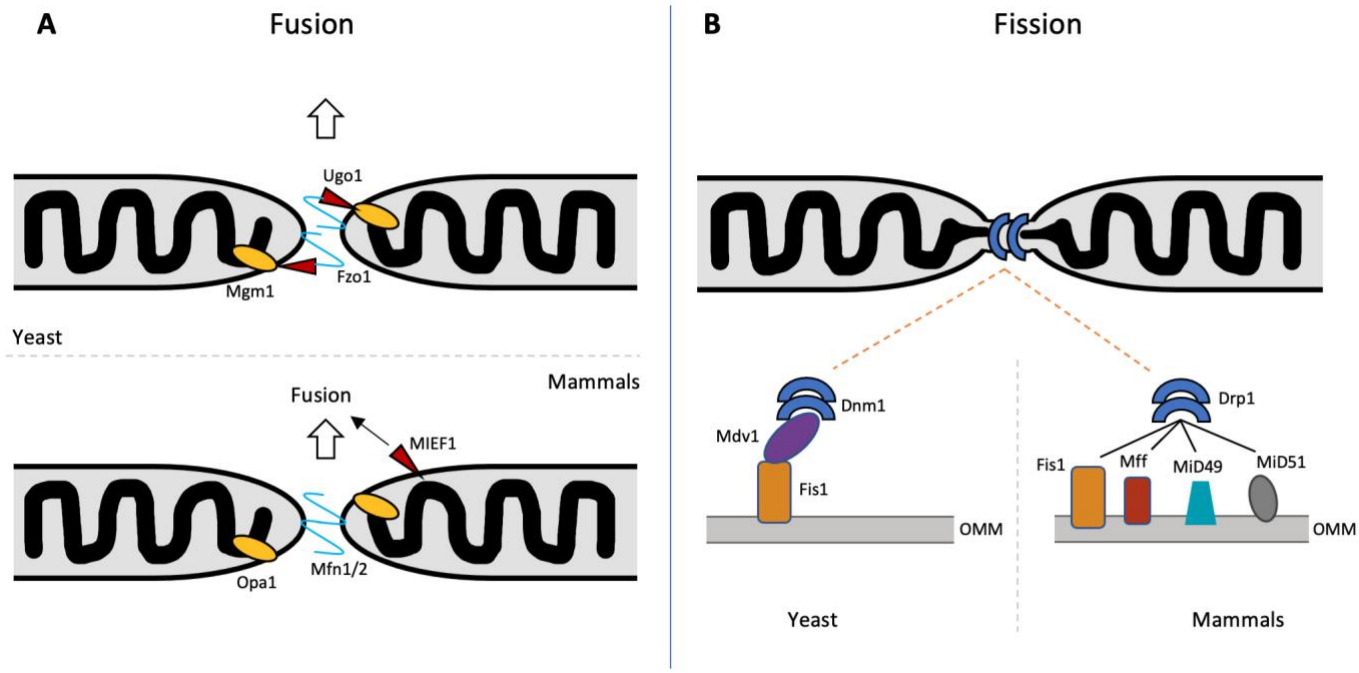

Figure 4. 20: Machinery for mitochondrial fusion and fission in mammals and yeasts. A) Proteins involved in the fusion process of mitochondria in yeast and mammals. In yeast, Fzo1 complexes are critical to facilitate mitochondrial outer membrane fusion. Mgm1p is required to promote inner membrane fusion. Ugo1p is thought to be involved in the coordination of outer and inner membrane fusion processes. In mammals, Mfn1 and Mfn2 collaborate to regulate the anchoring and fusing of the outer membranes of mitochondria. OPA1 is required for fusion of the inner membrane. MIEF1 is believed to facilitate mitochondrial fusion without the need for Mfn2. B) A model for the fission of mitochondria in mammals and yeasts. In yeast, Dnm1p mediates mitochondrial fission. Fis1p is situated on the outer mitochondrial membrane (OMM), with Mdv1 functioning as a connector for the assembly of the multi-part fission machinery. In mammalian organisms, Drp1 takes on the task of membrane fission. When a non-degradable guanosine-5'-triphosphate (GTP) substitute (-Methyleneguanosine-5’-triphosphate, or GMPPCP) is added, Drp1 naturally generates oligomers, which mimic the contractile heart of the fission apparatus. Numerous receptor proteins such as Mff , Fis1, MiD51, and MiD49 have been discovered. Diagram is not to scale.

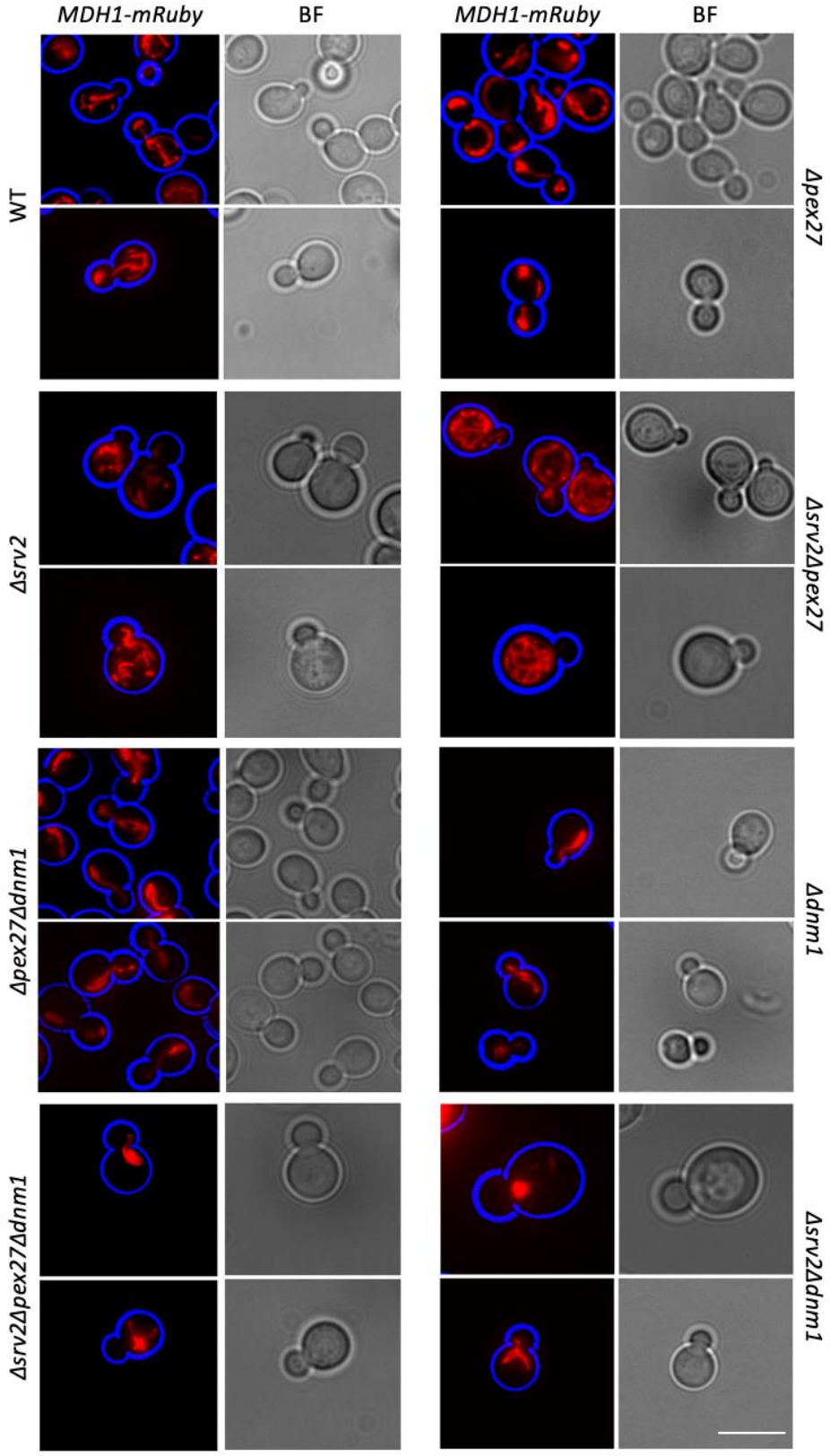

Figure 4. 21: Mitochondrial morphology in wild-type and some mutant strains. The effect of *SRV2* deletion on mitochondrial morphology. Strains were visualized using the fluorescent mitochondrial marker MDH1-mRuby. Bar, 5µm.

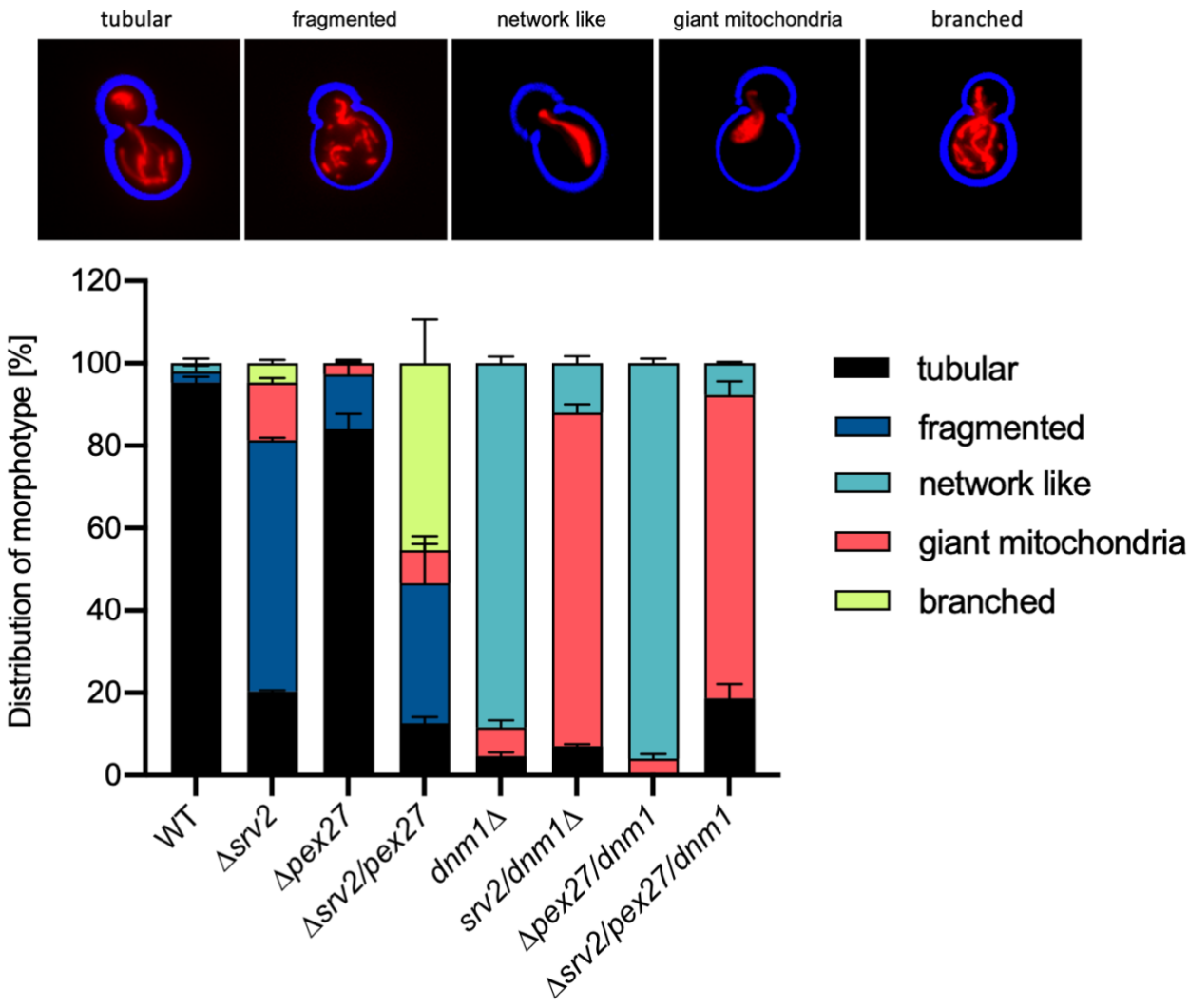

Figure 4. 22: Quantification of the mitochondrial morphology observed upon deletion of *SRV2* in some mutated strains as indicated. The morphology of mitochondria is classified into five major categories. Mitochondrial morphology was analysed in a minimum of 200 cells in each strain from 3 independent experiments. Error bars represent SEM.

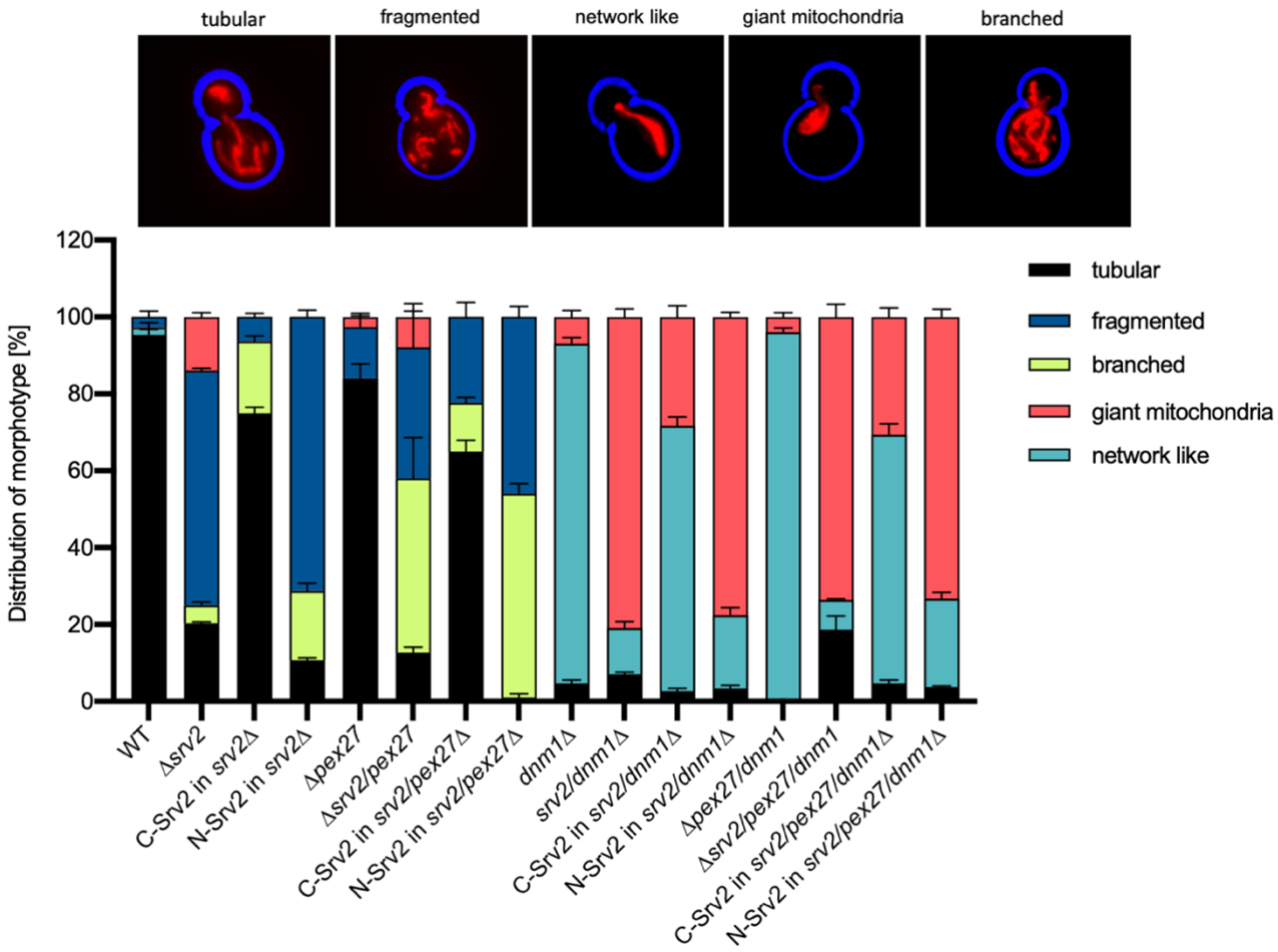

Figure 4. 23: The effect of N and C terminals of Srv2 on mitochondrial morphology. The graph represents the quantitative analysis of the morphology of mitochondria in cells lacking any *SRV2*, expressing C-Srv2 or N-Srv2 domains. Three independent experiments were performed, and mitochondria were analysed in 300 cells from each strain. Error bars represent SEM.

4.9 Discussion

In *S. cerevisiae*, two dynamin-related proteins (Drps), Vps1 and Dnm1, participate in peroxisome fission (Motley and Hettema, 2007). Besides its role in peroxisomes, Dnm1 also plays a part in organizing mitochondria, being essential for mitochondrial inheritance and fission. A recent study identified a link between Srv2 and Dnm1 in relation to mitochondrial fission (Chen et al., 2019). This study demonstrated that Srv2 functions as a pro fission factor, influencing the shape and respiration of yeast mitochondria by controlling the assembly of actin.
Given that both Vps1 and Dnm1 are implicated in peroxisome fission and that Srv2 has been demonstrated to interact with Dnm1, it was of interest to explore the possibility of Srv2 interacting with Vps1 and whether Srv2 has any functional role in the Vps1-mediated pathway in the case of peroxisome fission. In this chapter, we have demonstrated the Srv2–Vps1 interaction *in vivo*. The binding has been shown by co-immunoprecipitation using anti-Srv2 and anti-PAP making these results reliable. This result suggested to us the likelihood of a role of Srv2 in peroxisome fission since deletion of *SRV2* has been shown to affect mitochondrial morphology by increasing its network (Chen et al., 2019). Given the known roles of Srv2 and Vps1 in the regulation of actin and peroxisome biogenesis (Balcer et al., 2003; Motley and Hettema, 2007), their interaction could potentially facilitate the coordination of these processes. For instance, Srv2 may help regulate Vps1 function in peroxisome fission by modulating the actin cytoskeleton at the site of the peroxisome, or *vice versa*. The interaction between these proteins may also affect other cellular processes involving both actin dynamics and peroxisome transport.

Our results shown here confirm that deletion of *SRV2* dramatically affects peroxisomes. As shown in section 4.3, *Δsrv2* cells had a high number of peroxisomes compared with wild-type cells suggesting a possible role in the peroxisome fission machinery. However, it is remarkable that peroxisomes appear in almost all buds indicating that the inheritance of peroxisome is not affected by *srv2* deletion. In section 4.4, Srv2 was shown to be a regulator of peroxisome fission and this was confirmed by deleting *srv2* in some mutant strains (*Δpex27, Δdnm1, Δdnm1Δpex27,* and *Δpex25)* whose peroxisome number and size are known (Fig. 4.5).
A recent study showed that *Δpex27* and *Δvps1* cells have similar peroxisome phenotypes where the peroxisome number is small with elongated shapes. This study also revealed that Pex27 is essential for the function of Vps1 in peroxisome fission and that there is an interaction between Pex27 and Vps1. Similarly, the peroxisome number and morphology in *Δdnm1Δpex27* cells are comparable to those in *Δdnm1Δvps1* cells, which typically have one elongated peroxisome (Ekal et al., 2023). The loss of *vps1* affects cells resulting in slow growth and then cells are more likely to be sick. Thus in the study here, we decided to work with *pex27*Δ rather than *vps1*Δ.
The results showed that deleting *SRV2* affects peroxisomes in *Δsrv2Δpex27* and *Δsrv2Δdnm1* cells. However, there was no effect observed on peroxisomes in *Δsrv2Δpex27Δdnm1* and *Δsrv2Δpex25* cells. It is known that peroxisome fission is mediated by two pathways: Dnm1 which requires Fis1 and Caf4 or Mdv1, and another pathway involves Vps1 and Pex27. In the case of peroxisome fission in both *Δdnm1Δpex27* or *Δdnm1Δvps1* strains, only one peroxisome is present. In addition, Pex25 play an important role in early stages of peroxisome fission, and deletion of *PEX25* results in one giant peroxisome. The results obtained indicate that deleting *SRV2* while one of the fission pathways is blocked, by deleting *PEX27* or *DNM1*,

leads to an increase in the number of peroxisomes, which suggests that another pathway facilitates fission without any regulation by Srv2. However, the effect of *SRV2* deletion is not evident when fission pathways are inhibited, *Δpex27Δdnm1* and *Δpex25*. The data obtained strongly suggest that Srv2 plays a crucial role in regulating the process of peroxisome fission (Fig 4. 24).

Since *srv2* affects peroxisomes, we aimed to test the Srv2 domains and investigate which domain is responsible for the function. The C-terminal region of Srv2 binds strongly to ADP-G-actin and also facilitates nucleotide exchange and the displacement of cofilin from ADP-actin monomers, promoting ATP for ADP exchange. As a result, C-Srv2 plays a vital role in actin monomers recycling, which is a crucial step for quick actin network turnover *in vivo*. (Mattila et al., 2004; Balcer et al., 2003). The N-terminal domain of Srv2 promotes cofilin-mediated severing (Chaudhry et al., 2013). It has been shown that the C-terminal of Srv2 which functions in actin dynamics is critical for mitochondrial morphology (Chen et al., 2019). We showed similar results in section 4.5 where the data indicate that the actin binding function of Srv2 is critical for peroxisome regulation. The C-terminal of Srv2 restores the peroxisome phenotype in *Δsrv2* and *Δsrv2Δpex27* cells, while peroxisomes are still affected in the presence of the N-terminal of Srv2. Additionally, actin cables were more prominent in *Δsrv2* cells expressing C-Srv2, while they were less clear in the presence of the N-terminal.

SRV2 deletion is known to cause slower growth and an increase in cell size. To determine whether the increase in peroxisome is a result of the effects of slower growth and larger cell size caused by *SRV2* deletion, or due to the role of Srv2's actin binding function, experiments were conducted. The findings in section 4.5 indicate that while cells expressing N-Srv2 have an impact on peroxisomes, cells expressing either N-Srv2 or C-Srv2 exhibit similar cell sizes. Therefore, the increase in cell size cannot be attributed to an increase in peroxisomes. In addition, a yeast growth assay was conducted to rule out slow cell growth as a contributing factor to the peroxisome phenotype. The results show that cells expressing N-Srv2 and C-Srv2 have similar growth rates to that of the wild type and full-length Srv2, while the growth of *Δsrv2* cells is considerably slower (Fig. 4.13). This finding suggests that the slow growth of cells does not contribute to the peroxisome phenotype. Although there is no difference in growth between N-Srv2 and C-Srv2 cells, the former still increases the number of peroxisomes, while the latter restores peroxisome numbers. Therefore, we can conclude that the increase in peroxisomes is attributable to the actin binding function of Srv2.

An interesting finding showed that Srv2 functions as a negative regulator of peroxisome fission. Srv2 was fused to the tail-anchored peroxisomal membrane protein Pex15. This produced a fusion protein where Srv2 is present in the cytosol and is fastened to the peroxisomal membrane via Pex15. This fusion protein was under the control of the Srv2 promoter. Cells expressing Srv2-GFP-Pex15 fusion showed one giant peroxisome per cell suggesting that peroxisome fission is blocked. This fusion protein was tested in WT, *Δsrv2, Δpex27, Δsrv2Δpex27* and *Δsrv2Δdnm1* strains and all of them showed the same results.
Taken together the data reveal that Srv2 is a negative regulator of peroxisome fission (Fig 4. 25). It may bind to peroxisomes through its interaction with actin filaments, and it has been shown to be important for the recruitment of the fission machinery to the organelle which we could occur through Inp1.

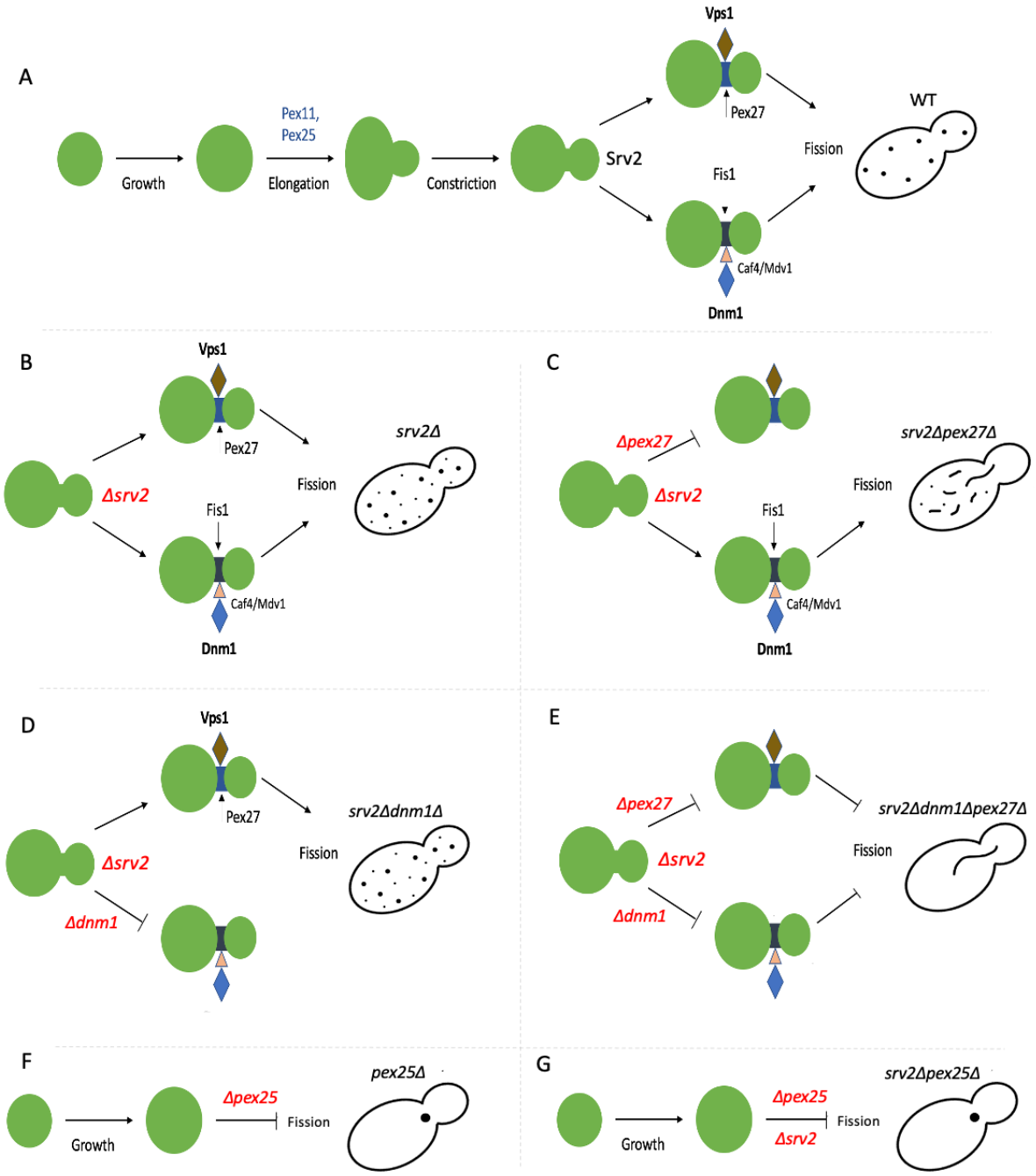

Figure 4. 24: Srv2 regulates the process of peroxisome fission. A) In WT cells, peroxisome fission occurs through two distinct pathways: Vps1, which requires Pex27, and Dnm1, which requires Fis1, both resulting in a normal number of peroxisomes. B) In *Δsrv2* cells, the number of peroxisomes increases, indicating that fission pathways are not properly regulated. C) In *Δsrv2Δpex27* cells, peroxisomes are still affected, suggesting that the Dnm1 pathway is causing fission without regulation. D) In *Δsrv2Δdnm1* cells, peroxisome numbers increase, suggesting that fission occurs through the Pex27 pathway in the absence of the regulator Srv2. E) When both fission pathways are blocked *(Δpex27Δdnm1*), there is no effect on peroxisomes, even in the absence of Srv2. F) and G) Deleting *PEX25* blocks fission, resulting in one peroxisome per cell, and the same effect is observed in *Δsrv2Δpex25* cells.

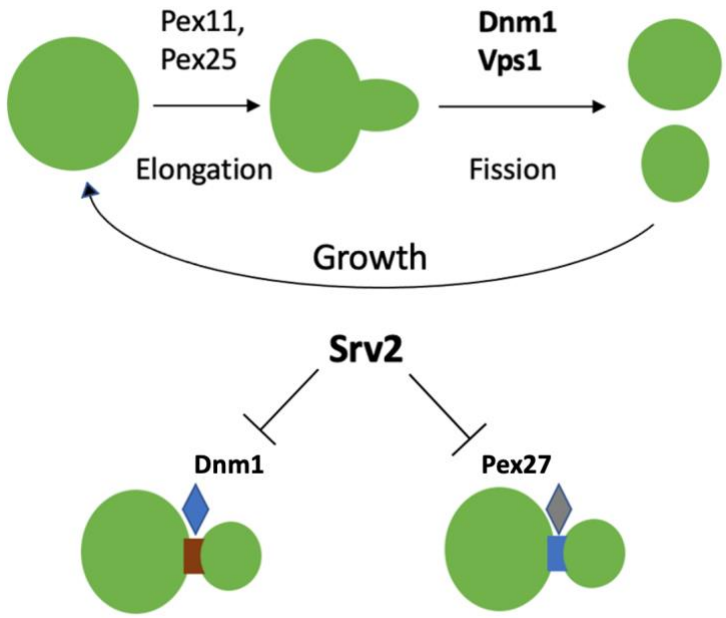

Figure 4. 25: Srv2 is a negative regulator of peroxisome fission. Srv2 is instrumental in regulating peroxisome fission, specifically in pathways involving Dnm1 and Pex27. This protein plays a crucial role in recruiting the fission machinery to peroxisomes, ensuring proper organelle function

Chapter 5 – Discussion

The primary goal of this study was to investigate the molecular details of Inp1 and its contribution to peroxisome dynamics. Our findings have revealed new insights into links between Inp1 and the actin cytoskeleton (chapter 3) and between Srv2 and peroxisomal fission (chapter 4). This chapter aims to bring these findings together and to explore how Srv2 functions as a central component in a mechanism linking peroxisomal organisation with peroxisome fission.
Our findings have led to a new proposed model for peroxisome fission during asymmetric cell division, in which Srv2 plays a key role. Chapters 3 and 4 discuss the specific experimental data that supports these findings. Finally, in this chapter, we discuss the broader implications of our discovery that Srv2 acts to link Inp1, the actin cytoskeleton and peroxisome fission through Srv2 regulation.

In this study, we found that the processes of peroxisome tethering and fission are closely linked, primarily because both involve elements of the actin cytoskeleton. The actin cytoskeleton plays a crucial role in maintaining cellular architecture and mediating various cellular processes, including organelle positioning and division. The interdependence between tethering and fission processes in peroxisomes, as evidenced by the involvement of actin cytoskeleton proteins, provides a significant contribution to our understanding of peroxisome dynamics. Our study has revealed that Inp1 interacts with the actin cytoskeleton, effectively facilitating peroxisome positioning within the cell and playing a pivotal role in tethering. Concurrently, we have identified Srv2, an actin-associated protein, as a crucial participant in peroxisomal fission. The Srv2-peroxisome interaction is indispensable for regulating peroxisome fission during asymmetric cell division. By uncovering the role of the actin cytoskeleton in both tethering and fission processes, our findings illuminate the complex interplay of these events, offering a valuable advancement in our comprehension of peroxisome dynamics within cells (Fig. 5.1).

The identification of these molecular links between tethering, fission, and the actin cytoskeleton not only provides a deeper understanding of the underlying mechanisms governing peroxisome dynamics but also highlights the intricate coordination between cellular structures and organelle behavior. This discovery contributes to our growing knowledge of cellular processes and may pave the way for future research into the regulation and manipulation of organelle dynamics in various biological contexts.

When comparing the inheritance, tethering, and fission mechanisms of peroxisomes in yeast with those of other organelles, we can observe some interesting analogies and differences. For instance, in yeast cells, both mitochondria and vacuoles rely on the cytoskeleton for proper positioning and division. In the case of yeast mitochondria, the actin cytoskeleton plays a crucial role in their positioning, movement, and fission. Proteins such as Num1, Mdm36, and the dynamin-related protein Dnm1 are involved in these processes (Hammermeister et al., 2010). A recent paper demonstrated that Srv2, a protein we found to be involved in peroxisome fission, also acts as a pro-fission factor that adjusts the shape and respiration of yeast mitochondria by overseeing the assembly of actin (Chen et al., 2019). This

finding suggests the possibility of a shared mechanism involving the actin cytoskeleton and Srv2 in the regulation of both peroxisome and mitochondrial dynamics.

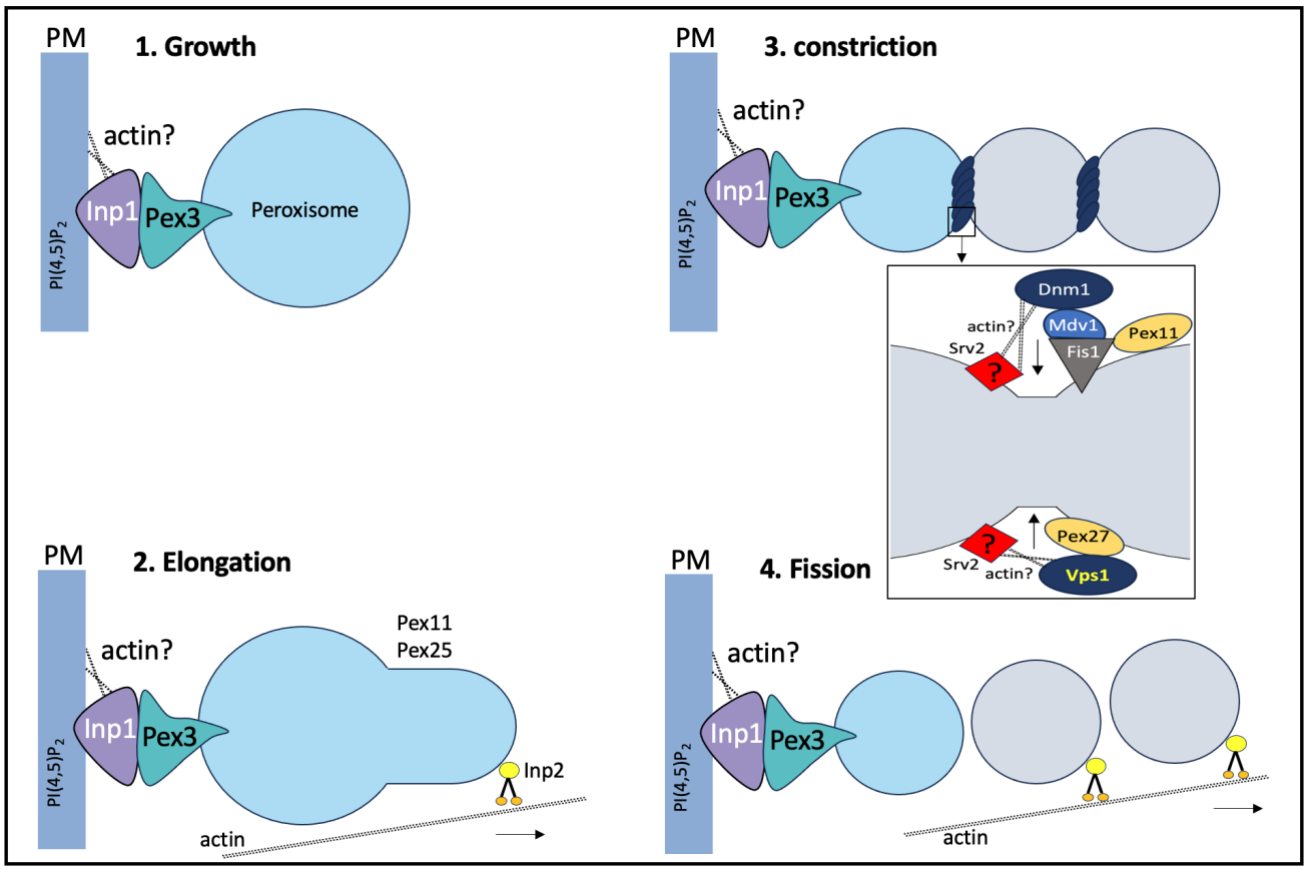

Figure 5. 1: Proposed roles of Inp1, actin, and Srv2 in peroxisome tethering and fission. Inp1 plays a pivotal role in peroxisome tethering by directly binding to Pex3 and the plasma membrane (PM). It further engages with actin, potentially contributing to peroxisome-PM tethering. Srv2 regulates peroxisome fission by interacting with actin filaments. When associated with the peroxisomal membrane, Srv2 could inhibit fission by impeding the recruitment or activity of fission machinery proteins. Srv2's interactions with Dnm1, responsible for peroxisome and mitochondrial fission, and Vps1, which modulates peroxisome fission by regulating their size and quantity, underscore its central role in fission regulation. The significance of Srv2's interactions with Dnm1 and Vps1 suggests its involvement in modulating protein activities, oligomerization, or membrane recruitment, thereby finely controlling the fission process. Additionally, Srv2 might act as a scaffold, orchestrating the assembly and disassembly of multiple fission machinery components, thus ensuring precise coordination.

In mammalian cells, mitochondrial division also relies on the cytoskeleton, particularly actin and myosin. The process involves the recruitment of endoplasmic reticulum (ER), formation of actin cables between the mitochondria and ER, and constriction of the inner mitochondrial membrane (IMM) before dynamin-related protein-1 (Drp1) recruitment. Notably, phosphatidylinositol 4-Phosphate (PI4P) binding proteins, such as GOLPH3 and Rab11, are integral to this process. GOLPH3 (Vps74 in yeast), induces membrane curvature to promote vesicle scission from the trans Golgi network (TGN). It alternates between Golgi and mitochondrial membranes and has an impact on mitochondrial mass by controlling lipid production. Furthermore, GOLPH3 may interact with non-muscular Myosin II, which is implicated in mitochondrial division, hinting at a complex regulatory network (Nakashima-Kamimura et al., 2005; Taft et al., 2013; Burke et al., 2014; Landry et al., 2014; Wood et al., 2009; Rahajeng et al., 2019; Yang and Svitkina 2019). Rab11, another PI4P-binding protein, is involved in the last stage of membrane scission through the vesicle release process, and has been discovered at mitochondrial fission locations, where it rearranges the actin cytoskeleton and controls the trafficking of Drp1. The involvement of PI4P binding proteins in mitochondrial membrane remodeling and scission further highlights the complexity of mitochondrial dynamics in mammalian cells (Tábara et al., 2021). Additionally, a study in 2020 has shown that the mammalian homolog of Srv2 (CAP) acts as a pro-fission protein in mitochondrial dynamics, specifically in the context of septic cardiomyopathy. The research demonstrates that CAP promotes mitochondrial fission via the Mst1-Drp1 axis, thereby contributing to cardiomyocyte death and myocardial depression (Shang et al., 2020).

Our findings on peroxisomes in yeast, specifically the roles of Inp1 and Srv2 in tethering and fission, can be contextualized within the broader landscape of organelle dynamics across both yeast and mammalian cells. The reliance on the actin cytoskeleton and the involvement of Srv2 in the fission processes of both peroxisomes and mitochondria in yeast, where they share mechanisms such as the involvement of Dnm1, highlights the crucial role of Srv2. Additionally, the similarities in actin-dependent mitochondrial division in mammals, which also share fission mechanisms such as the involvement of Drp1 and Mff with peroxisome fission, further indicate the potential role of CAP (Srv2 in yeast) in fission process of peroxisomes. Our findings in yeast could potentially inform studies on the regulation of peroxisome dynamics in mammalian cells.

An important aspect of understanding the molecular mechanisms underlying peroxisome tethering and fission is to examine the binding regions of the proteins involved, such as Inp1, Srv2, and Vps1. By analysing these regions, we can gain insights into whether the interactions between these proteins and the actin cytoskeleton occur simultaneously or if there is competition for binding sites. For example, in addition to its interaction with Pex3 via its C-terminal, Inp1 contains the N-terminal region that interacts with the plasma membrane and the actin cytoskeleton, while the middle domain is responsible for its interaction with Srv2. This suggests that Inp1 can simultaneously engage with both Srv2 and the actin cytoskeleton, facilitating tethering and proper organelle positioning. Interestingly, a previous study suggested a potential interaction between Inp1 and Vps1, which could imply that Inp1 might also be involved in peroxisome fission (Fagarasanu et al., 2005). Further investigation is needed to validate this proposed interaction and its functional implications.
Likewise, Srv2 may possess distinct binding regions for interacting with the actin cytoskeleton, Inp1, and Vps1. These interactions allow Srv2 to play a central role in coordinating peroxisome

fission. However, it is also possible that certain binding regions overlap or are in close proximity, which could lead to competition between different binding partners. This competition might serve as a regulatory mechanism to fine-tune the balance between peroxisome tethering and fission, ensuring proper organelle dynamics.

As Inp1, Srv2, and Vps1 all have numerous interacting partners (Fig. 5.1), understanding their roles in peroxisome dynamics necessitates further investigation into the structural details of these proteins and their interactions. Determining whether these interactions occur simultaneously or through competitive binding is crucial for elucidating the complexity of peroxisome behavior regulation within cells. Future studies focusing on these aspects will significantly contribute to our understanding of the intricate orchestration of peroxisome dynamics and the interplay of various proteins involved in these processes.

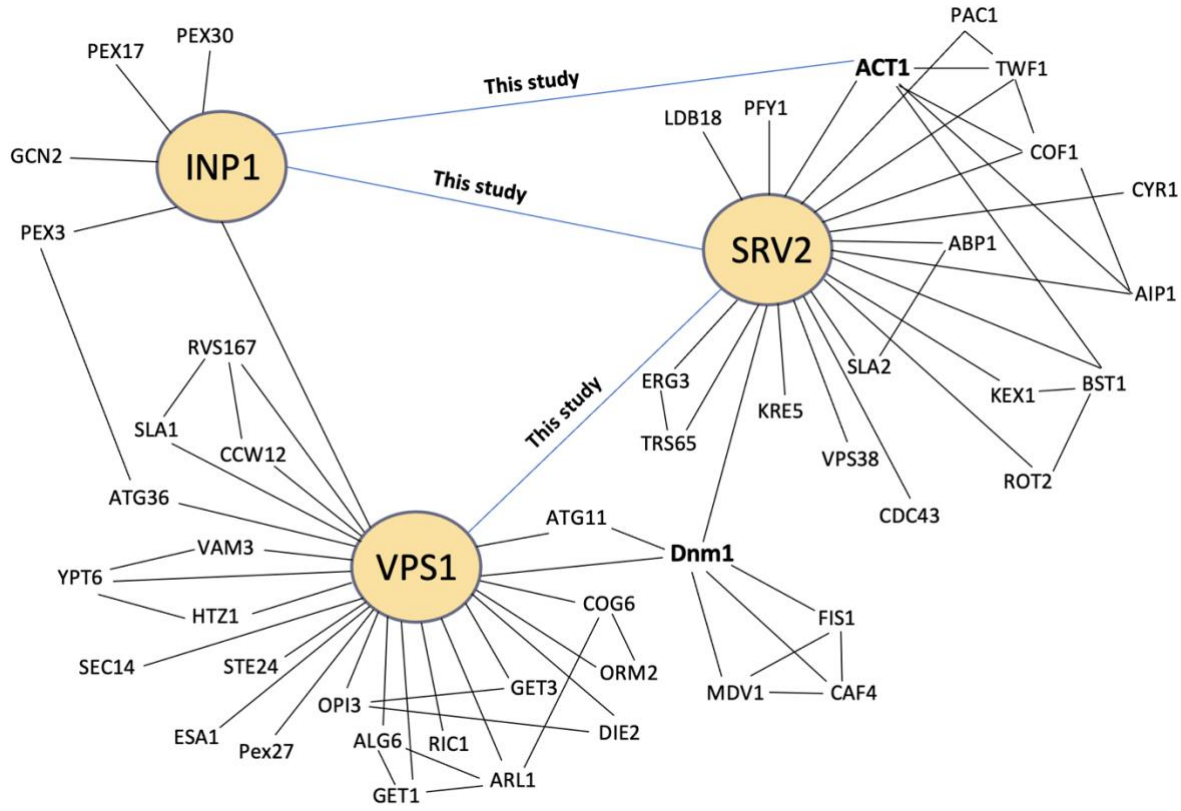

Figure 5. 2: Complex interactions among Inp1, Srv2, and Vps1 proteins in *S. cerevisiae*. This diagram illustrates the elaborate network of genetic and physical interactions among Inp1, Srv2, and Vps1 proteins in *S. cerevisiae*, emphasizing their potential roles in peroxisome fission. Inp1 binds to both Act1 and Srv2, while Srv2 interacts with Act1, Vps1, and Dnm1. Dnm1 is suggested to interact with Vps1, which in turn is reported to bind Inp1. This comprehensive representation highlights the intricate relationships between these proteins, suggesting a coordinated function in the regulation of peroxisome retention and fission processes (from Saccharomyces Genome Database).

The potential for post-translational modifications (PTMs) to regulate interactions among proteins involved in peroxisomal dynamics can also be considered. PTMs, including phosphorylation, ubiquitination, acetylation, and farnesylation, are capable of modulating

protein activity, localization, and interactions with other proteins, playing crucial roles in a variety of cellular processes. Recent phosphoproteomic studies in *S. cerevisiae* have identified several phosphorylation sites, such as S77, S112, S115, and S273, within the middle domain of Inp1 (Holt et al., 2009; MacGilvray et al., 2020; Lanz et al., 2021). These phosphorylation events could potentially modulate Inp1-Srv2 interactions and their involvement in peroxisome tethering and fission processes. For example, phosphorylation at specific sites in Inp1's middle domain may alter its affinity for Srv2, thereby affecting the tethering and fission processes. Similarly, numerous phosphorylated residues (S292, T295, S342, S343, S346, S347, S350, S352, S362, T388, S454, S463, S471, and S519) and a monoacetylated residue (K516) have been identified in Srv2. These residues are located in the region of Srv2 that was found to interact with Inp1 in the Hybrigenics screen (Albuquerque et al., 2008; Henriksen et al., 2012;Lanz et al., 2021; Lao et al., 2018; MacGilvray et al., 2020; Swaney et al., 2013; Zhou et al., 2021). Further investigation is required to determine the roles of these post-translational modifications (PTMs) in modulating the interaction between Srv2's C-terminal and Inp1, as well as their impact on peroxisome dynamics and the interaction with Vps1.

A study on the yeast Ras protein and adenylyl cyclase interaction revealed that farnesylation of Ras led to a 5- to 10-fold increase in Ras-dependent activation of adenylyl cyclase activity, with the stimulatory effect attributed to the association of adenylyl cyclase with CAP. This association is suggested to be responsible for the observed impact of Ras posttranslational modification on its activity (Shima et al., 1997). This example demonstrates how PTMs can modulate protein-protein interactions in yeast and raises the question of whether similar mechanisms might be at play in the regulation of peroxisome fission processes involving Inp1 and Srv2.

Regarding peroxisome and mitochondrial fission mechanisms, it is known that the dynamin-related protein Drp1 in mammals and its yeast homolog Dnm1 are regulated by phosphorylation. In particular, phosphorylation of Drp1 at Ser616 and dephosphorylation at Ser637 promote its activation and translocation to the mitochondria, thus enhancing mitochondrial fission (Chang and Blackstone, 2010). Although the specific phosphorylation sites and their regulatory roles in Dnm1 remain less characterized than those of Drp1, phosphorylation of Dnm1 is also known to modulate its activity and ability to oligomerize, ultimately affecting the fission process of these organelles (Jahani-Asl and Slack 2007).

Further experimental studies and investigations into potential PTMs, such as phosphorylation events, and their effects on proteins involved in peroxisomal and mitochondrial fission, including Inp1-Srv2 and Srv2-Vps1 interactions, are needed to provide valuable insights into the regulatory mechanisms governing these processes. Identifying these PTMs and their functional consequences would enhance our understanding of how cells fine-tune organelle dynamics in response to various cellular cues and environmental conditions. Some potential experimental approaches include performing site-directed mutagenesis to mimic or prevent phosphorylation at the identified sites in Inp1 and Srv2, conducting *in vitro* binding assays to test direct interactions between wild-type or mutated Inp1 and Srv2, investigating the effects of kinase inhibition or overexpression on Inp1-Srv2 and Srv2-Vps1 interactions and peroxisome dynamics, and employing live-cell imaging techniques to visualize peroxisome distribution, motility, and morphology in yeast cells expressing wild-type or mutated genes. Consequently, integrating this knowledge with our current findings may contribute to a more

comprehensive understanding of the roles and regulations of Inp1, Srv2, and other proteins involved in peroxisome dynamics.

Based on our results and the current understanding of peroxisomal inheritance in yeast, we can compare and contrast these findings with what is known about peroxisomal inheritance in mammalian cells. The roles of Inp1 and Srv2 (CAP in mammals) in peroxisomal tethering and fission, as well as the involvement of the actin cytoskeleton in yeast, can be used as a starting point for this comparison.

In mammalian cells, peroxisomal inheritance is less well understood, but there are some similarities and differences worth mentioning. For example, the involvement of the cytoskeleton in peroxisomal dynamics is conserved in mammalian cells, although microtubules primarily facilitate peroxisome movement and inheritance, rather than actin filaments as in yeast. Additionally, the mammalian peroxisome biogenesis factor PEX11 plays a role in peroxisome fission, similar to the role of Vps1 in yeast.

The roles of Inp1 in yeast may not have direct homologs in mammalian cells, and other proteins or molecular mechanisms might be involved in regulating peroxisomal inheritance in these organisms. Nevertheless, given its known function in actin dynamics, the role of Srv2 (CAP in mammals) in peroxisomal tethering and fission could be conserved between yeast and mammalian cells. While the specific proteins and molecular mechanisms involved in peroxisomal inheritance might differ across species, certain elements hint at conserved aspects. Examining peroxisomal tethering during asymmetric cell divisions, such as in the context of stem cells, could provide valuable insights into potential conserved processes. Specifically, it might elucidate whether there are more shared mechanisms between yeast and mammalian cells than currently understood.
Research conducted on mouse skin stem cells revealed that peroxisomes are typically inherited symmetrically during cell division, with both daughter cells receiving a similar number of these organelles (Asare et al., 2017). This symmetrical inheritance of peroxisomes was identified as a critical factor in regulating the differentiation of stem cells into different cell types. disturbances in peroxisome inheritance symmetry, achieved through the knockdown of the PEX11b gene (which is vital for peroxisome biogenesis), led to an increased tendency for stem cells to differentiate into non-stem cell types. This highlighted the importance of balanced peroxisome inheritance in maintaining the stem cell population. Moreover, peroxisomes were found to be essential for proper spindle alignment, with improper peroxisome inheritance leading to potential cell division defects (Asare et al., 2017). These findings underscore the importance of peroxisomes in stem cell division, and hint at potential similarities in peroxisomal inheritance mechanisms across different cell types. Further studies, particularly those that explore peroxisomal inheritance during asymmetric stem cell division, may lead to a deeper understanding of peroxisomal inheritance in mammalian cells and discern how it parallels and diverges from yeast models.

5.1 Future directions to investigate the roles of Srv2 and Inp1 in peroxisome fission regulation

In Chapter 3, we found that the C-terminal of Srv2 interacts with the middle domain of Inp1, which plays a critical role in peroxisome retention. In Chapter 4, we demonstrated that C-terminal of Srv2 is essential for restoring normal peroxisome numbers. Taken together, these findings indicate a potential role for Inp1 in the function of Srv2 as a negative regulator of peroxisome fission. In addition to the Inp1-Srv2 interaction, we also found an interaction between Srv2 and Vps1, a key protein in peroxisome fission. These findings suggest a potential network of interactions among these proteins, implicating them in the process of peroxisome fission. Given these interactions, it is possible that Inp1 also plays a role in peroxisome fission.

The intriguing finding that Srv2 acts as a negative regulator of peroxisome fission, as demonstrated by the Srv2-GFP-Pex15 fusion p[rotein experiment, highlights the importance of Srv2 in the regulation of peroxisome fission through its interaction with actin filaments. When anchored to the peroxisomal membrane, Srv2 may inhibit peroxisome fission by preventing the recruitment or activity of fission machinery proteins. As previously mentioned, Srv2 interacts with Dnm1, which is involved in regulating both peroxisome and mitochondrial fission, and with Vps1, which plays a role in peroxisome fission by regulating the size and number of peroxisomes. The crucial role of Srv2 in peroxisome fission regulation suggests that its interactions with Dnm1 and Vps1 have functional significance. Srv2 may modulate the activities, oligomerization, or recruitment of these proteins to the peroxisomal membrane by binding to them, ultimately controlling the fission process. Srv2 could also serve as a scaffold that brings together multiple components of the fission machinery, coordinating their assembly and disassembly. As a result, several hypotheses have yet to be fully explored and warrant further investigation.

5.1.1 Could the regulation of peroxisome fission by Srv2 be mediated by Inp1?

The interaction between the C-terminal of Srv2 and the middle domain of Inp1, along with the essential role of the C-terminal of Srv2 in restoring peroxisome phenotype, suggests a potential role for Inp1 in the function of Srv2 as a negative regulator of peroxisome fission. To further investigate this possibility, future research could utilize computational tools to predict the interaction between the middle domain of Inp1 and the C-terminal of Srv2. Following this, mutagenesis could be performed in the middle domain of Inp1 to disrupt the Srv2-Inp1 interaction, and then the impact on peroxisome fission can be investigated. Additionally, the effects of specific point mutations in the C-terminal domain of Srv2, known to disrupt its function, such as *srv2-98* in the WH2 domain and *srv2-108* and *srv2-109* in the β-sheet domain can be tested. Assessing the effects of these mutations on the Inp1-Srv2 interaction and peroxisome fission regulation will contribute to a better understanding of Inp1's role in peroxisome fission regulation.

5.1.2 Could Inp1 have a role in peroxisome fission?

Given that Srv2 is known to interact with the fission proteins Dnm1 and Vps1, as well as Inp1, and considering previous findings from the Rachubinski group which showed that Inp1 interacts with Pex30, Pex25, and Vps1 — key regulators of peroxisome biogenesis

(Fagarasanu et al., 2005) — we hypothesize that Inp1 might play a role in peroxisome fission, potentially through interactions with Vps1 or Pex25.
To investigate this hypothesis, future experiments could employ protein-protein interaction studies both *in vitro* and *in vivo*. *In vitro* studies could include pull-down assays, while *in vivo* investigations could utilize techniques such as co-immunoprecipitation or yeast two-hybrid assays, to explore potential interactions between Inp1 and peroxisome fission proteins like Vps1 and Pex25.
Should these assays demonstrate an interaction between Inp1 and Vps1, we could further investigate the functional implications of this interaction.

5.1.3 Could Srv2 interact with other peroxisome fission proteins such as Pex11, Pex25, or Pex27?

Considering the known roles of Pex11, Pex25, and Pex27 in peroxisome dynamics, and the evidence suggesting interactions of Srv2 with Dnm1 and Vps1 – proteins involved in peroxisome fission, it is plausible that Srv2 might also interact with other peroxisome fission proteins to modulate peroxisome fission and proliferation.
The Rachubinski group's report demonstrating that Inp1 interacts with Pex30, Pex25, and Vps1 (Fagarasanu et al., 2005), in conjunction with findings showing Srv2's interaction with Dnm1 (Chen et al., 2019) and Vps1 (this study), strengthens the hypothesis that Srv2 might interact with other proteins involved in peroxisome fission such as Pex11, Pex25, or Pex27. We propose that Srv2 may modulate the activities or recruitment of these proteins to the peroxisomal membrane through direct interaction, thereby controlling the fission process. It could also function as a scaffold, coordinating the assembly and disassembly of multiple components of the fission machinery.
The mechanisms underlying these potential interactions, such as whether they involve direct binding or are mediated through other proteins like Inp1, and the specific domains involved, are all subjects for future investigation. Ultimately, understanding the functional consequences of Srv2's interactions with peroxisome fission proteins may further elucidate Srv2's roles in peroxisome fission and its potential as a negative regulator.
Future studies could employ yeast two-hybrid assays or co-immunoprecipitation experiments to identify direct interactions between Srv2 and these proteins. Such interactions could be tested both in the presence and absence of Inp1 to investigate whether Inp1 mediates these interactions.

In conclusion, the work described in this thesis offers valuable contributions to the field by revealing new insights into the molecular mechanisms underlying peroxisome tethering and fission in yeast, with a focus on the roles of Inp1 and Srv2. The results suggest evolutionary conservation between peroxisome dynamics in yeast and mitochondrial fission mechanisms in both yeast and mammals and possibly indicates a universal strategy for regulating organelle behavior across species. This knowledge is particularly relevant for understanding fundamental cell biology principles and has potential implications for human health, as defects in peroxisome function are linked to several diseases.

Chapter 6 – Gene editing and tool development in *D. hansenii*

6.1 Introduction

Microorganisms are used in biotechnology to create new materials. One reason for the growing interest in exploiting microbial metabolic processes in biotechnological chemical synthesis is the limited supply of mineral oils (Mattanovich et al., 2014) and their environmental impact. Bacteria are one group of microorganisms while yeasts and other fungi are another type of microbes employed in biotechnology. For certain biotechnological processes, yeasts are preferable over bacteria because they have lower dietary needs and the capacity to acquire the post-translational modifications required for creating physiologically active proteins (Vieira Gomes et al., 2018), including the generation of metabolites and recombinant proteins (Mattanovich et al., 2014). They are also particularly appropriate to produce certain compounds, including ethanol, due to their metabolic capabilities and the ease with which they can be grown and manipulated in the laboratory (Sánchez et al., 2006; Mabee et al., 2010). The yeast *S. cerevisiae* has received the greatest attention in the food and beverage industries. Because of *S. cerevisiae's* exceptional molecular genetic and physiological characterisation, the yeast may be utilised to manufacture heterologous proteins such as the hepatitis B surface antigen and insulin over many years (Mattanovich et al., 2014). Additionally, *S. cerevisiae* has been employed for hundreds of years to produce alcohol and, subsequently, to leaven bread (Zhang et al., 2015). Because *S. cerevisiae* is not always the chosen host to utilise in biotechnology, corporations have begun to explore other yeasts that are more stress tolerant and are highly promising for biotechnology. Various yeasts have been discovered to be more effective in the manufacture of various recombinant proteins whereas other are thought to be more suitable to produce lipid derived metabolites (Mattanovich et al., 2014) including the stress-resistant, halotolerant yeast *Debaryomyces hansenii*.

Debaryomyces hansenii is a non-pathogenic yeast that is osmotolerant and an extremophile. This particular yeast, a member of the ascomycetes family, undergoes vegetative reproduction through the formation of multilateral budding (Mishra and Baranwal, 2009). It can be encountered in saline environments such as oceans and in food products that have been salted (Prista et al., 2005). *D. hansenii* possesses the capability to flourish in environments with high salt concentrations, such as 4 M sodium chloride (NaCl), whereas *S. cerevisiae* is unable to thrive in environments with NaCl concentrations exceeding 1.7 M (Aggarwal and Mondal, 2009). It can be found in a variety of foods, including cheese, sausages, soy sauce, and brines where it contributes to development of flavours. *D. hansenii* is subjected to stress conditions other than high salt concentration, such as high and low temperatures, low pH, and the presence of preservatives, highlighting its ability to withstand diverse challenging circumstances (Almagro et al., 2000). *D. hansenii's* osmo-tolerance is an important feature for its application in biotechnology because microbials contamination can be kept at bay using high osmotic media through addition of salt or other osmotics (Johnson, 2011).

According to Gientka et al. (2017), *D. hansenii,* being an oleaginous yeast, has the remarkable capacity to accumulate neutral lipids, accounting for more than 20% of its biomass. The capacity to accumulate huge volumes of lipids opens up the economic possibility of biodiesel generation and the synthesis of lipids or lipid derivatives.
D. hansenii produces compounds that inhibit other yeasts, which holds potential for managing yeast infections (Johnson, 2011). It tolerates high nitrite levels, utilizing it as a nitrogen source (Vigliotta et al., 2007), and withstands the potent biocide chlorine dioxide (ClO2) (Ramirez-Orozco et al., 2001). This versatile yeast has a variety of biotechnological applications, such as xylitol, ethanol, and bioflavour production, protein synthesis, and involvement in meat and dairy fermentation processes. Its capacity to generate valuable compounds and enhance the flavor and quality of various food products makes it significant in both food and industrial biotechnology (Gírio et al.2000; Güneşer et al., 2015; Durá et al., 2004; Padilla et al, 2014).

In some circumstances, *D. hansenii* is a preferred host for biotechnology, and unlike *S. cerevisiae*, it generally interprets CTGs codons, which are commonly associated with leucine, as serine (Jeffries and Cregg 2010). Moreover, due to limited research conducted on *D. hansenii*, there is a scarcity of molecular tools available for studying this yeast. The Genolevures consortium has sequenced and annotated the whole genome of *D. hansenii*, which is currently available at https://www.ncbi.nlm.nih.gov/genome/ (Dujon et al., 2004; Aggarwal and Mondal, 2009).

Despite the fact that most *D. hansenii* isolates are assumed to be haploid, further research has revealed variations in genome size and genome duplication. The genomic analysis revealed that diploid heterozygous strains exhibited a considerable decrease in heterozygozity (Petersen and Jespersen, 2004; Jacques et al., 2015). Following translocation, a multitude of alleles with different sizes can be generated, and certain strains of *D. hansenii* can be diploid or even aneuploid (Petersen and Jespersen, 2004). Many additional yeast species have documented chromosome number variations (Petersen and Jespersen 2004; Jacques et al., 2009; Jacques et al., 2010).

Previously, an economic and rapid gene disruption strategy was developed for genome alterations in *S. cerevisiae* and *S. pombe*. This method uses a selectable marker flanked by short regions of identity to the site of genome modification that would induce integration of the selectable cassette into that precise site in the genome through homologous recombination (HR). These constructs can easily be synthesised by PCR amplification of the marker cassette with primers containing 50 bp extensions identical to the sequence around the target site (see fig. 2.1) (Baudin et al., 1993; Kaur et al., 1996). Although recently, *D. hansenii* is more intensely being studied for its biotechnological potential, there have been few studies on genetically manipulating this yeast and the tools available are restricted. A small number of studies discuss the use of HR in *D. hansenii* genome modification (Minhas et al., 2009; Yaguchi al., 2017; Navarrete et al., 2022). In homologous recombination, two DNA sequences are exchanged at a region of aligned DNA sequence homology (Kuzminov, 2011). The method used for HR is based on a plasmid by designing a marker with two flanked regions of the targeted gene. Because of the poor HR effectiveness in *D. hansenii*, it is challenging to disrupt genes (Prista et al., 2016); for this reason, 1 kb flanks upstream and downstream of the open reading frame (ORF) are still being used for gene disruption in *D. hansenii*.

Working with non-conventional yeasts can present numerous challenges. Besides the difficulty in gene disruption or modification requiring 1 kb flanking regions, approximately half of the *D. hansenii* genes tested in our lab possess multiple copies in the standard strains used (unpublished data). Consequently, deleting these genes necessitates additional efforts to create a second knockout construct.
This work initiated the task of developing alternative tools that allow fast mutant generation. The revolution caused by the introduction of the CRISPR-Cas9 technique in biological research in the lab made me excited about trying it on *D. hansenii*. Unfortunately, at that time no such system was available for *D. hansenii*, but it has been developed for related yeasts that belong to the CTG clade (Lombardi et al., 2019). The principle of the CRISPR-Cas system - an immune response system found in prokaryotes- is that it utilises non-coding RNAs to guide the enzyme Cas9 to cause DNA cleavage in a specific site. Subsequently, this system has been harnessed to build a simple editing tool for the eukaryotic genome incorporating such aspects as knockout or knockin. To perform gene disruption, a single-guide RNA (sgRNA) is generated to guide the Cas9 to a specific location of the genome in order to cut it (Figure 6.1).

The main aim of the research described in this chapter is to generate new tools to efficiently modify the *D. hansenii* genome. Initially it describes the attempts to develop a CRISPR-Cas9 system but in parallel we tested a homologous recombination (HR) gene disruption strategy using short HR flanks, and these results are also described.

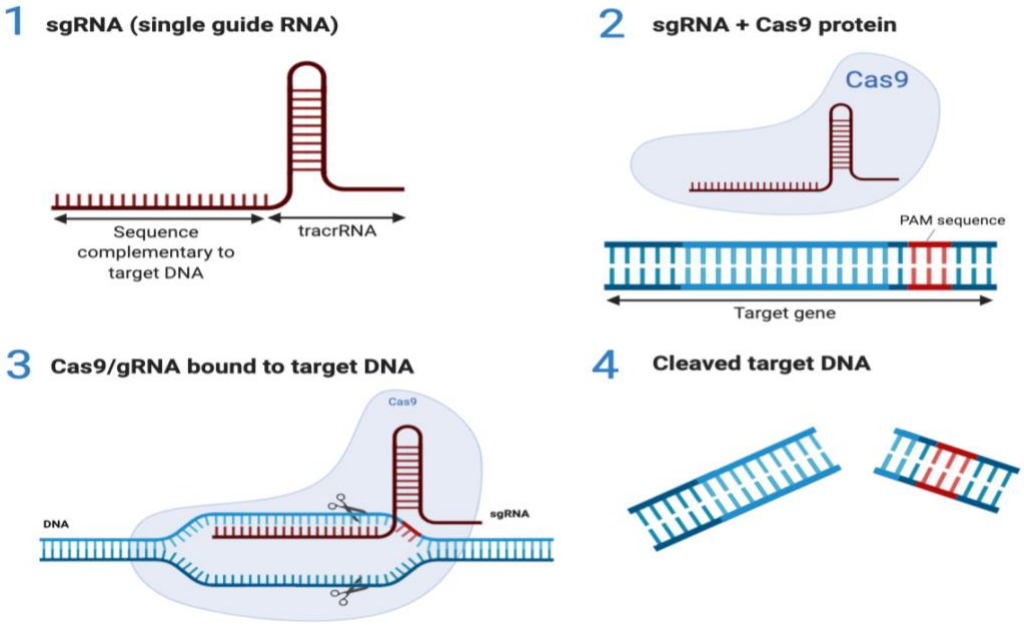

Figure 6. 1: Creating gene disruption by CRISPR/Cas9. 1) the sgRNA consists of two parts: a 20 bp sequence specific to the DNA target, fused to the tracrRNA. 2) the sgRNA interacts and binds with the Cas9 protein, which has DNA endonuclease activity. 3) when Cas9 finds the PAM (Protospacer Adjacent Motif) sequence, it unwinds the bases upstream of the PAM and pairs them with the complementary region on the gRNA. 4) the CRISPR-Cas9 complex induces a double-stranded cleavage of the targeted DNA. (Adapted from Doudna and Charpentier 2014).

6.2 Results

6.2.1 CRISPR-Cas9 system

As gene editing techniques were limited in *D. hansenii*, we explored the potential of adapting CRISPR-based tools from related yeasts. Through extensive literature review, we identified a CTG-adapted plasmid that had been effectively used for gene editing in multiple yeast species (Lombardi et al., 2019). It was decided to introduce this system and adapt it to use in *D. hansenii.*

To examine the CRISPR-Cas9 system *in D. hansenii*, it is useful to start targeting some genes whose disruptions are easily detected. Therefore, the *ADE2* and *GUT2* genes have been chosen for the knockout experiments. The disruption of the *ADE2* gene can be easily detected by observing the accumulation of a red pigment in the colonies, which results from the accumulation of a precursor in the adenine biosynthesis pathway (Rébora et al., 2001). This visible phenotype allows for a straightforward screening of successful *ADE2* gene knockouts (Fig. 6.2). On the other hand, the disruption of the *GUT2* gene, which is involved in glycerol metabolism, can be detected by monitoring the inability of the mutant strains to grow on glycerol-containing media. Strains with a disrupted *GUT2* gene will be unable to utilize glycerol as a carbon source, providing a clear and simple readout for successful gene knockout experiments (Sprague and Cronan 1977) (Fig. 6.3).

The pCT-tRNA plasmid expresses CAS9 under the *M. guilliermondii* TEF1 promoter and carries the SAT1 selectable marker gene (nourseothricin resistance) regulated by the *C. dubliniensis TEF1* promoter and *MgPGK1* terminator. The sgRNA expression cassette is controlled by the *A. gossypii TEF1* promoter and *ScCYC1t* terminator. The mature sgRNA is released by endogenous yeast RNase Z cleavage after the $tRNA^{Ala}$ and self-splicing before the hepatitis delta virus (HDV) ribozyme. The function of the HDV ribozyme in this system is to cleave the RNA transcript precisely at the 3' end of the gRNA sequence, ensuring the proper formation and functionality of the gRNA. This cleavage is essential for the gRNA to guide the Cas9 nuclease to the target DNA sequence effectively. This design aimed to improve sgRNA maturation using endogenous RNase P and Z for posttranscriptional cleavage and create a more versatile platform for swapping gRNA sequences without the constraints of the HH ribozyme's unique 5' sequence. The plasmids enable ligation of 23-bp annealed oligonucleotides into a cloning cassette with two nonpalindromic SapI sites at the tRNA-gRNA junction. This allows easy gRNA introduction by designing two 20-base oligonucleotides with overhangs compatible with SapI sites for cloning and expression. Sap1 has unique properties. It recognizes the specific palindromic sequence 5'-GCTCTTC-3' and cleaves the DNA to generate 5' overhangs (sticky ends). The uniqueness of this recognition site can minimize the chances of unwanted cleavage in the gRNA sequence or vector. The oligonucleotides have CAA overhangs, creating sticky ends for ligation into the SapI-digested vector (Fig. 6.4 A).
The design of the guide RNAs (gRNAs) was done with the help of the CRISPRdirect website (http://crispr.dbcls.jp/) – *D. hansenii* ASM644v2 (Feb 2015) genome. This website gives an appropriate selection of target sites for CRISPR-Cas9 and a diminished potential number of off-target sites and more features. (Fig. 6.4 A). Then guide targets (20 bp) were generated with overhanging ends that were compatible with two SapI sites that can be fitted with the pCT-tRNA plasmid (Fig. 6.4 B & C).

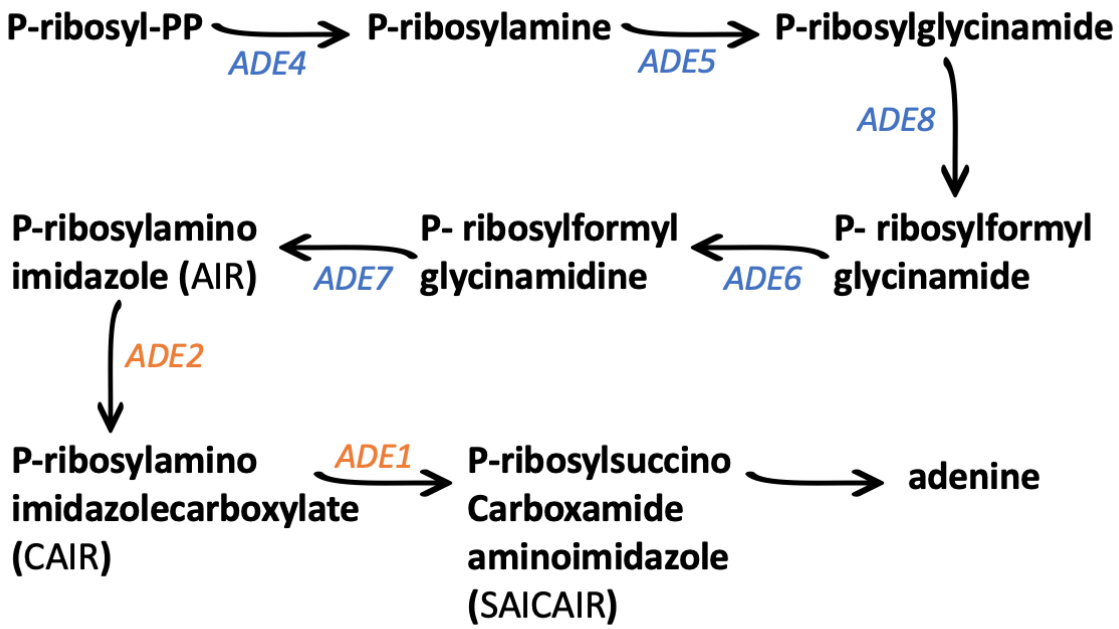

Figure 6. 2: The adenine biosynthesis pathway. *ADE1* and *ADE2* mutations, which usually block an earlier step in adenine biosynthesis, cause the intermediate AIR to accumulate. This is converted to form the red pigment. Adapted from (Rébora et al., 2001).

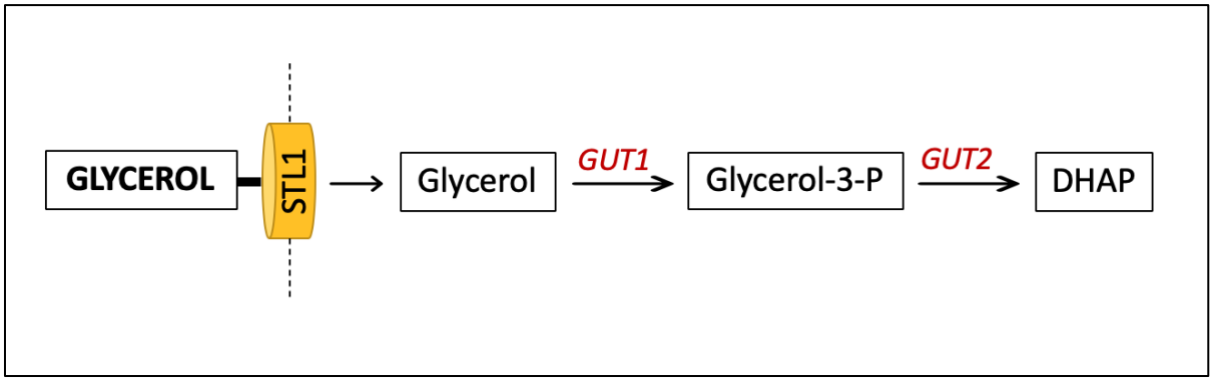

Figure 6. 3: The pathway of the utilization of glycerol as a carbon source. The pathway starts with the import of glycerol into the cell, which is mediated by the symporter *STL1*. Once inside the cell, glycerol is converted into glycerol-3-phosphate by the cytoplasmic enzyme glycerol kinase (*GUT1*). Glycerol-3-phosphate then enters the mitochondria, where it is further metabolized by the mitochondrial glycerol-3-phosphate dehydrogenase (*GUT2*), which is a flavin adenine dinucleotide (FAD)-dependent enzyme. *GUT2* converts glycerol-3-phosphate to dihydroxyacetone phosphate (DHAP), which can then leave the mitochondria and enter the cytoplasm, where it can join the glycolytic or gluconeogenic pathways as a source of energy and carbon for the cell (Adapted from Turcotte et al., 2009).

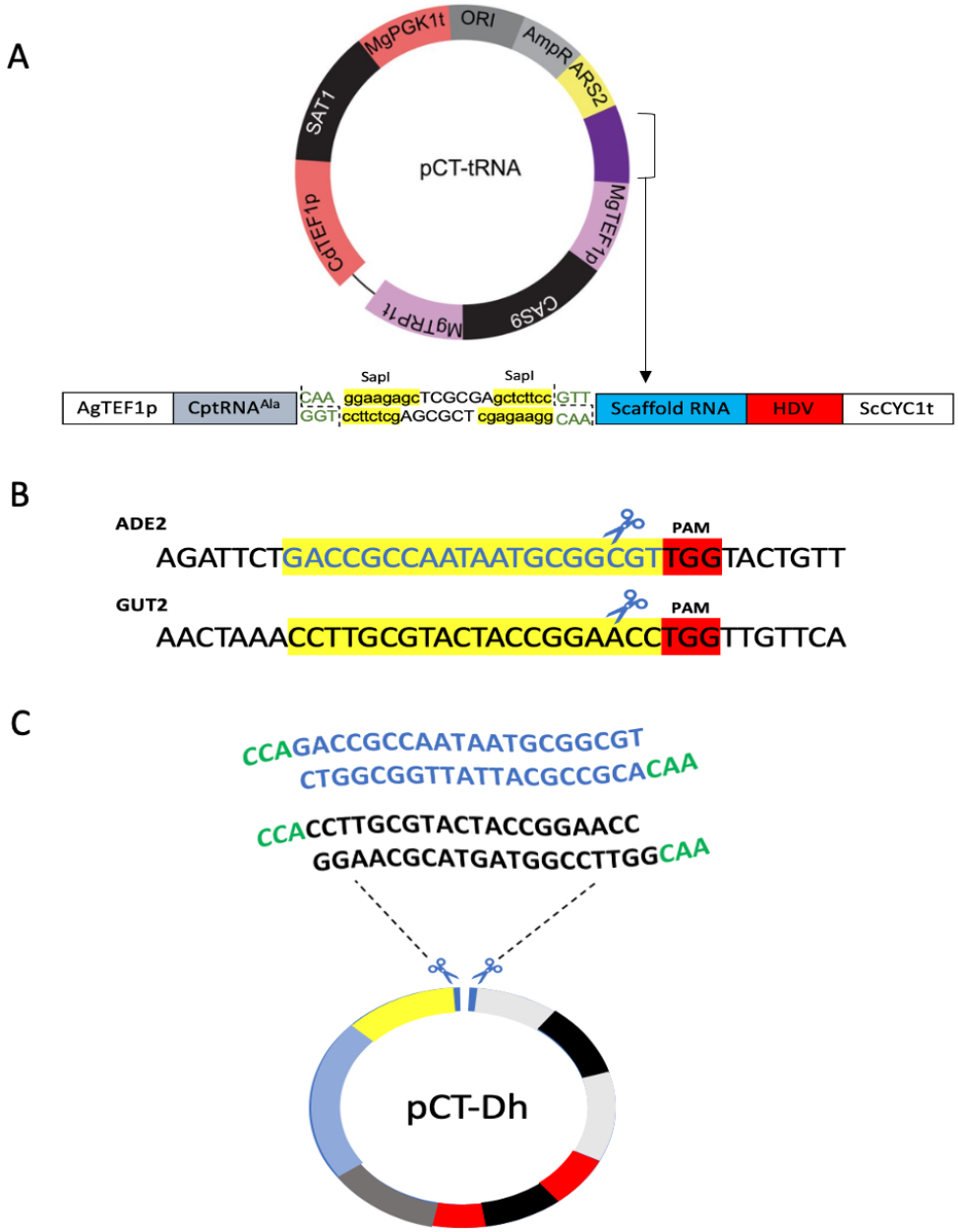

Figure 6. 4: Designing gRNAs for Targeted Disruption of *ADE2* and *GUT2* Genes. A) The pCP-tRNA plasmid system enables gene editing in *D. hansenii*. This plasmid includes the SAT1 gene (conferring nourseothricin resistance), the autonomously replicating sequence 7 (ARS7) from *C. parapsilosis*, and the CAS9 gene under the control of the *M. guilliermondii* TEF1 promoter. The plasmid map highlights the cassette responsible for sgRNA expression in purple, and a more detailed representation is provided in the accompanying scheme. The cassette consists of the *Ashbya gossypii* TEF1 promoter, followed by the $tRNA^{Ala}$ sequence, two SapI restriction sites, the scaffold RNA, the HDV ribozyme, and finally the ScCYC1t terminator. B) The gRNAs, highlighted in yellow, targeting genes *ADE2* and *GUT2*, as suggested by the CRISPRdirect website, and followed by the PAM sequence (highlighted in red). Scissors in blue represent the Cas9 cut. C) The DNA oligos and

their complementary sequences were designed (blue: *ADE2*; black: *GUT2*) with Sap1 overhanging ends (in green) that matched the plasmid.

This follows what Lombardi and her group (2019) have proven about the experimental success of this plasmid and its CRISPR system for gene editing on *C. tropicalis*, which is very similar to *D. hansenii*. In addition, Lombardi et al. (2017) proved that this system works in other Candida species such as *C. parapsilosis, C. metapsilosis, C. orthopsilosis* and *C. metapsilosis*.

After successfully transforming the pCT-tRNA plasmids carrying gRNAs targeting *ADE2* and *GUT2* genes, along with control plasmids without any gRNAs, in *D. hansenii* NCYC102 cells, the cells were assessed for gene disruption. However, it is worth noting that the efficiency of the CRISPR system was observed to be low, with very few colonies growing compared to wild-type cells expressing a plasmid without any gRNA. In the control transformations with no gRNA, there were more than 40 colonies per transformation, suggesting that the presence of gRNA had a negative impact on yeast viability. The transformation was attempted multiple times using different amounts of DNA plasmid (0.3, 0.6, 1, 1.5 and 2 µg), targeting both *ADE2* and *GUT2* genes in the *D. hansenii* NCYC102 strain. Despite these efforts, the number of colonies consistently remained low (3-5 colonies per transformation) when gRNA was present, suggesting that the reduced colony count may be indicative of a negative impact on yeast viability due to the CRISPR system (Fig. 6.5).

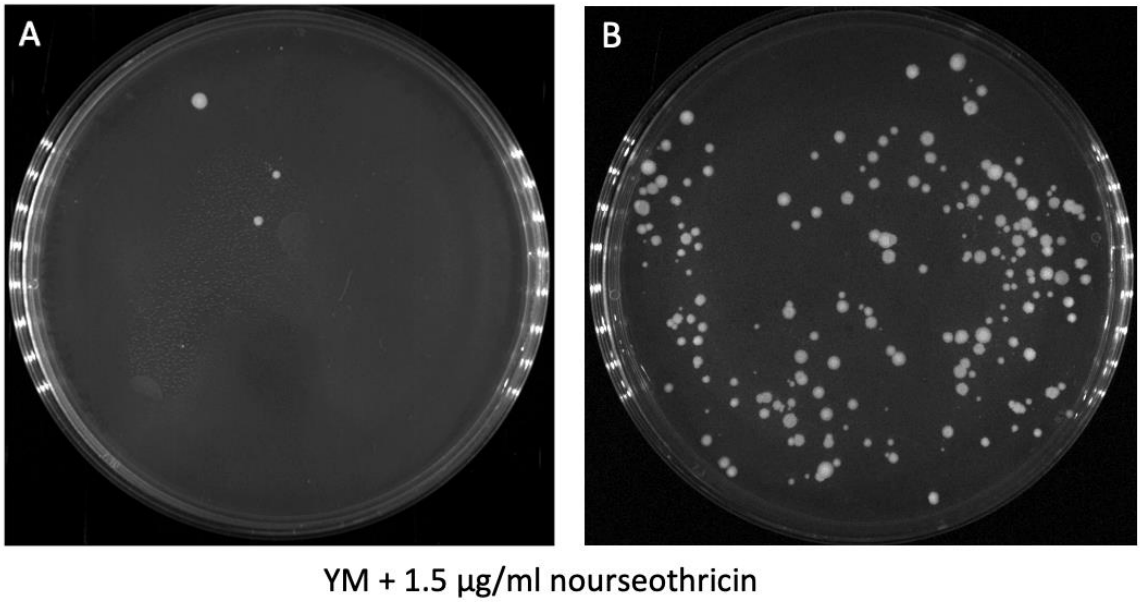

Figure 6. 5: Low efficiency of the CRISPR/Cas9 system in *D. hansenii*. A) CRISPR/Cas9 plasmid containing a gRNA targeting *ADE2* results in a low number of colonies compared to the control B) which shows high transformation efficiency when using an empty CRISPR plasmid without any gRNA. Both plates contain YM-nourseothricin (1.5 µg/ml).

However, cells transformed with the *ADE2*-targeting plasmid were effectively edited, with approximately 80% exhibiting a pink hue on YM media and demonstrating an inability to grow in YM media without adenine. This is because *ADE2* encodes an enzyme involved in the biosynthesis of adenine, and disruption of this gene blocks an earlier step in the pathway. As a result, adenine auxotrophs accumulate a reddish intermediate in the adenine biosynthetic pathway, leading to a build-up of these intermediate metabolites that give the cells a distinctive pink/red colour on YM media (Rébora et al., 2001). In the absence of exogenous adenine, which cannot be synthesized due to the gene disruption, the cells are unable to grow, highlighting the essential role of *ADE2* in adenine biosynthesis (Fig. 6.6 A).

On the other hand, cells expressing *GUT2*-targeting plasmid could not grow on YM2-glycerol media in contrast to WT strains that have grown. Yeast cells can utilize glycerol as a sole carbon source, with glycerol being imported by the symporter sugar transporter-like protein (*STL1*). Once inside the cell, the cytoplasmic enzyme glycerol kinase (encoded by *GUT1*) phosphorylates glycerol to form glycerol-3 phosphate, which then enters the mitochondria. Within the mitochondria, the mitochondrial glycerol-3-phosphate dehydrogenase (encoded by *GUT2*) oxidizes glycerol-3-phosphate to dihydroxyacetone phosphate (DHAP), which can then be metabolized further by the cell (Fig. 6.4). Defects in *GUT2* can prevent yeast cells from utilizing glycerol and impair their ability capable of thriving in growth media that solely rely on glycerol as the carbon source (Sprague and Cronan 1977) (Fig. 6.6 B).

In addition to the low efficiency of the CRISPR system in the NCYC102 strain, it is notable that targeting the *ADE2* gene by CRISPR/Cas9 resulted in the region around the Cas9 cut being unable to be amplified using primers 500bp upstream and downstream of the cut site. This amplification was performed to check and sequence the CRISPR/Cas9-induced mutations in the target gene. However, this region was easily amplified in WT cells. Although the upstream and downstream regions were able to be amplified separately, the difficulty in amplifying the region around the Cas9 cut suggests that chromosomal translocation occurred as a result of Cas9 cleavage (Fig. 6.7). This chromosomal translocation could potentially explain the low number of transformants observed. From these results, we can conclude that while the CRISPR/Cas9 system can work in *D. hansenii*, it may not be the most appropriate tool due to these issues. However, two years later, two papers reported successful use of the CRISPR/Cas9 system in this yeast (Spasskaya et al., 2021; Strucko et al., 2021).

As a result of these findings, we aimed to find an alternative, efficient, and economical way to edit the *D. hansenii* genome.

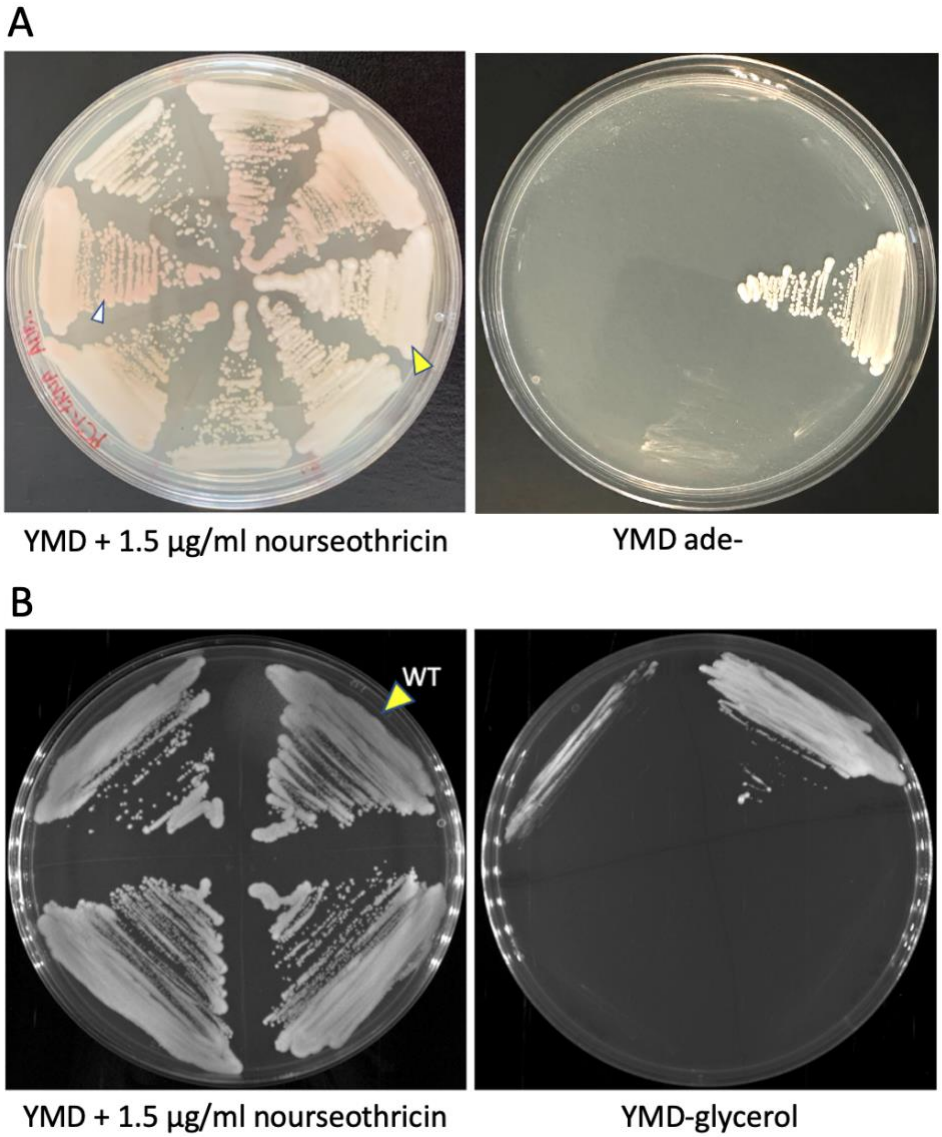

Figure 6. 6: Editing of *ADE2* and *GUT2* genes using CRISPR/Cas9 in *D. hansenii*. A) Cells transformed with plasmids targeting *ADE2* exhibit a pink hue (white arrow as an example) due to adenine auxotroph, in contrast to the white colour of WT cells (yellow arrow). Pink colonies were streaked for better visualization, as the colour was light and difficult to distinguish. Transformant cells were unable to grow in the minimal adenine-deficient (ade-) medium, unlike the control (WT) cells. B) Transformed cells with plasmids targeting *GUT2* were grown on YM-nourseothricin (1.5 µg/ml). Then, cells were streaked onto YM2-Glycerol plates. *GUT2* transformed cells were unable to grow in YM2-Glycerol compared to WT which was able to grow in the same media (arrowed in yellow).

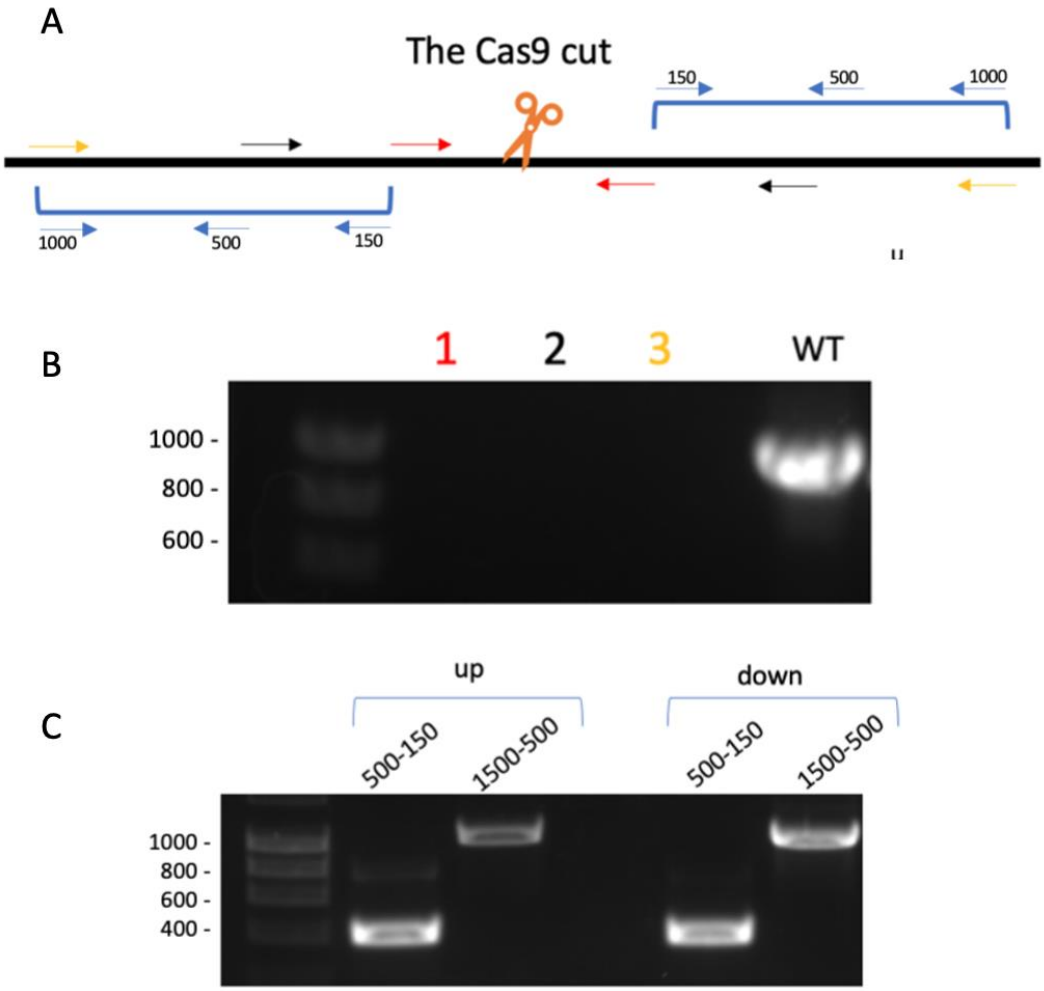

Figure 6. 7: Issues of the CRISPR/Cas9 system in *D. hansenii* targeting *ADE2* gene. A) Diagram illustrates the Cas9 cut and upstream and downstream primers used to sequence region around the cut. Numbers represent distance from cut site. B) The region around the Cas9 cut could not be amplified in the mutant strains, as opposed to the successful amplification observed in the wild-type control (same primers used in sample 2). C) Upstream and downstream regions of the Cas9 cut were amplified separately (blue brackets in the diagram shown in B).

6.2.2 Gene disruption by HR with short flanks

Targeted gene replacement, employed to create knock-out or knock-in mutants, is an effective strategy for studying gene function and regulation. This technique is also fundamental for generating genetically engineered strains for biotechnological applications. To date, only a limited number of studies have reported the development of research tools for *D. hansenii*, including gene disruption via homologous recombination using extensive flanking regions, random integration plasmids, and CRISPR-Cas9 mediated gene targeting (Minhas et al., 2009, 2012; Biswas et al., 2013; Chawla et al., 2017; Defosse et al., 2018; Strucko et al., 2021; Spasskaya et al., 2021). Homologous recombination in *D. hansenii* has been reported to be inefficient (Minhas et al., 2009; 2012; Strucko et al., 2021; Spasskaya et al., 2021), and targeted gene replacement typically requires 1 kb long-length homologous flanking fragments (Minhas et al., 2009; Yaguchi al., 2017; Navarrete et al., 2022). This method relies on multiple plasmid construction steps to generate gene targeting constructs and utilizes auxotrophic markers. Furthermore, some recent CRISPR-Cas9 approaches still require auxotrophic markers for transformant selection (e.g., Spasskaya et al., 2021), limiting these techniques to a single strain.

The PCR-mediated gene disruption method, developed for gene targeting in *S. cerevisiae*, is one of the simplest methods of genomic modification (Baudin et al., 1993). This technique involves amplifying a selectable marker using PCR, extending the cassette with 35-50 bp flanking regions identical to the target site in the genome on either side. Upon transformation, these short flanking regions guide the selectable marker to the precise genomic site through homologous recombination. This methodology has facilitated the systematic analysis of each gene and protein in *S. cerevisiae* and led to the development of gene targeting techniques in *Schizosaccharomyces pombe* and *Kluyveromyces lactis* (Kaur et al., 1997; Kooistra et al., 2004).

In the initial studies conducted in *S. cerevisiae*, auxotrophic markers were used for the purpose of gene targeting. However, this approach had a limitation, as these markers share sequences with the host genome, which could guide to gene conversions that restore the auxotrophic phenotype, making the selection process less reliable. To overcome this issue and improve the targeting efficiency, researchers began to use heterologous selectable markers, which are derived from other organisms and do not share sequences with the host genome. This new approach significantly enhanced the reliability and efficiency of gene targeting in *S. cerevisiae*, as evidenced by studies conducted by Wach et al. (1994) and Bahler et al. (1998).

Our lab aimed to enhance the efficiency of homologous recombination (HR) mediated genome editing in wild-type isolates of *D. hansenii* by developing a fully heterologous marker, which reduces the background of gene conversions caused by auxotrophic mutations. Our group created novel selectable marker cassettes composed exclusively of heterologous DNA sequences that confer Hygromycin B or G418 resistance to *D. hansenii* transformants. Following the development of the heterologous marker conferring Hygromycin B or G418 resistance to *D. hansenii* transformants, we then aimed to optimize the process by reducing the length of the HR flanks. Our motivation for reducing the homology arm length was to

explore the possibility of achieving efficient HR-mediated gene disruption in *D. hansenii* using shorter homology arms, as has been demonstrated in other yeast species such as *S. cerevisiae* and *S. pombe.* Previous studies have shown that short homology arms of 30-50 bp and 80-100 bp, respectively, were sufficient for efficient gene disruption in these yeast species (Hegemann et al., 2014; Baudin et al., 1993; Kaur, Ingavale and Bachhawat, 1996). We tested different homology arm lengths, ranging from 750 bp down to 100 bp, including very short homology arms of 75 bp, 65 bp, and 50 bp, to determine the optimal homology arm length for efficient HR-mediated gene disruption in *D. hansenii*. To contribute to this work, I focused on targeting the *ADE2* gene using short-length flanks (75 bp, 65 bp, and 50 bp) and assessed their efficiency.

The knockout cassette with Hygromycin marker was accomplished through PCR using specific forward and reverse primers that contain 50 bp, 65 bp and 75 bp identical to the upstream and downstream of *ADE2* gene. PCR fragments were then transformed into yeast as described in section 2.4.4.

The protocol suggested that the appropriate concentration of DNA needed in each transformation is 2 µg. However, this did not result in many transformants. Thus, several transformations were done with various DNA concentrations to calculate the best concentration for use in the transformation process. The results indicate that 0.5 µg DNA (in a maximum volume of 2 µl) provides the highest number of colonies. Consequently, this concentration was used in most of the experiments (Fig 6. 8).

0.5 µg of PCR fragments flanked with 50bp were transformed into 3 different strains of *D. hansenii* – NCYC 102, NCYC 3363 and NCYC 3981, and grown for 3 days on YM Deb plates containing hygromycin. Transformed colonies were streaked onto the minimal adenine-deficient (ade-) plates to assess gene disruption efficiency. The results show that 28 out of 31 NCYC 3363 colonies and 19 out of 20 NCYC 3981 colonies were knocked out, as evidenced by their inability to grow on ade- plates (Fig. 6.9 A). However, all colonies from the *D. hansenii* NCYC 102 strain were able to grow on ade- plates.

0.6 µg of PCR fragments with 65bp were transferred into all three strains as explained above, resulting in 10 of the 11 colonies of the NCYC 3363 strain being knocked out, 11 of the 11 colonies from the NCYC 3981 strain were knocked out, and all colonies from NCYC 102 strain continued to grow on the ade- plate.

0.6 µg of PCR fragments with 75bp were transferred into the three strains and the results show that 16 of the 17 NCYC 3363 colonies were knocked out, 9 out of 9 NCYC 3981 colonies were knocked out, and all colonies from NCYC 102 strain continued to grow on the ade- plate. All these results are listed in Table 6.1.

Through PCR analysis, we were able to confirm the accurate integration of the hygromycin resistance (HygR) cassette into the *ADE2* locus. This validation was performed on a selection of adenine auxotrophs derived from each strain background investigated in our study (Fig. 6.9 C). The successful integration of the HygR cassette within the *ADE2* gene is crucial for generating adenine auxotrophs, and our results demonstrate the effectiveness of our gene knockout approach across different strain backgrounds.

These results demonstrate that gene deletion by HR with short flanks is highly efficient in *D. hansenii*, achieving efficiency rates of up to 95%. We conclude that gene disruption by HR serves as a valuable tool for enabling rapid and efficient DNA integration. Cassettes with flanking sequences of 50 bp can be readily generated through one-step PCR amplification using adapted primers. With these PCR-based methods and reagents, genetic modification of *D. hansenii* isolates has become more economical and accessible. This will facilitate in-depth study of this yeast and its development for biotechnological applications.

Table 6. 1 – The results of *ADE2* gene knockout.

***D. hansenii* strains**	**75 bp**	**KO**	**65 bp**	**KO**	**50 bp**	**KO**
NCYC 102	100-150	0	100-120	0	100-150	0
NCYC 3363	17	16	11	10	31	28
NCYC 3981	9	9	11	11	20	19

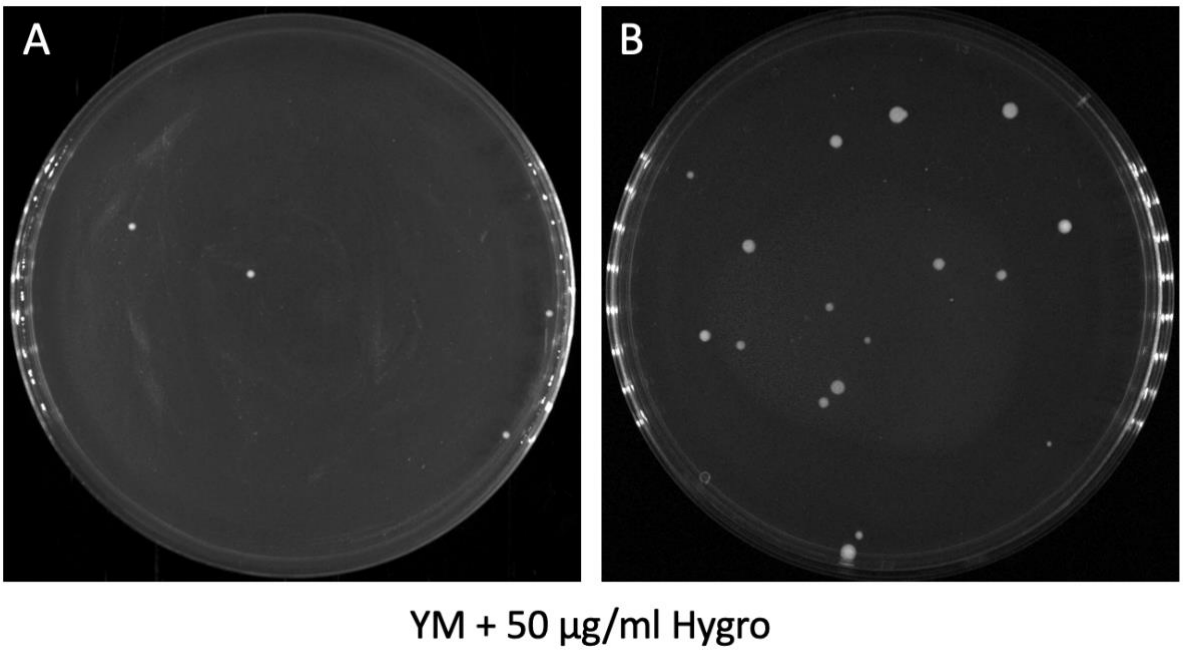

Figure 6. 8: Comparison of the effectiveness of transformation in *D. hansenii* with various DNA concentrations. A) 2 µg of DNA shows low efficiency, while B) 0.5 µg of DNA improves transformation efficiency.

A

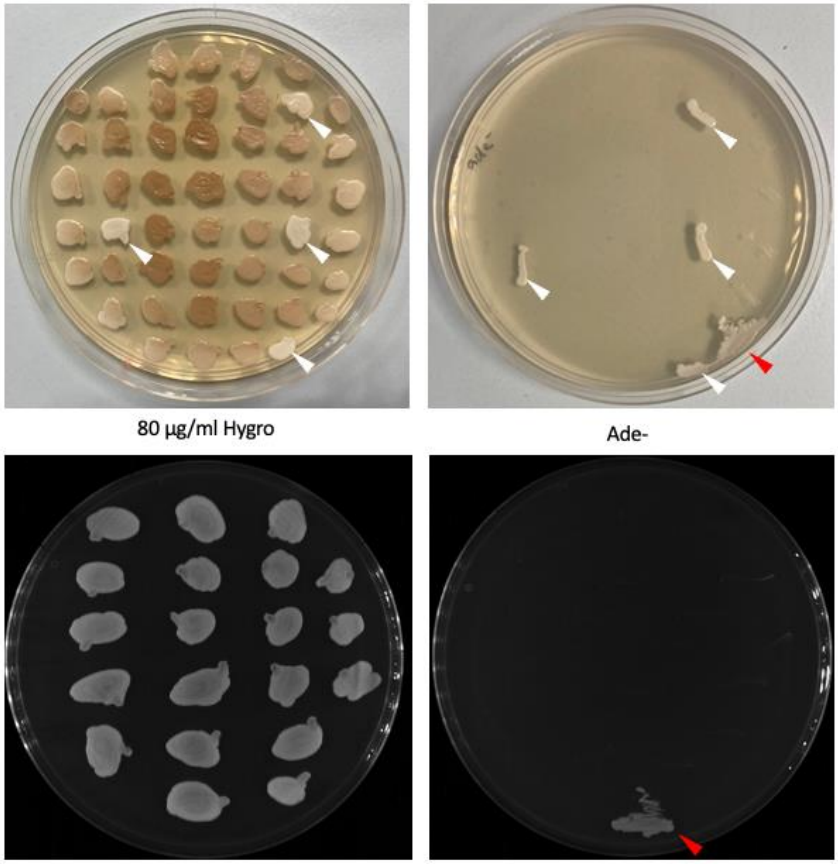
80 µg/ml Hygro
Ade-

B

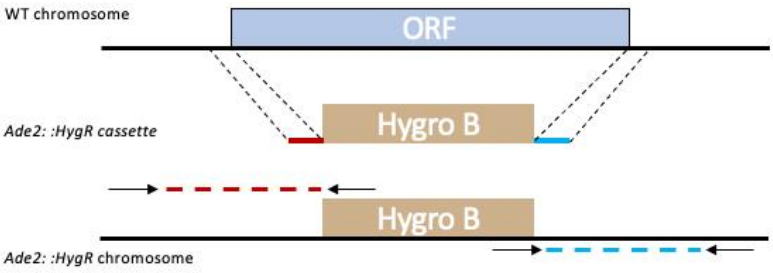
WT chromosome
ORF
Ade2: :HygR cassette
Hygro B
Hygro B
Ade2: :HygR chromosome

C

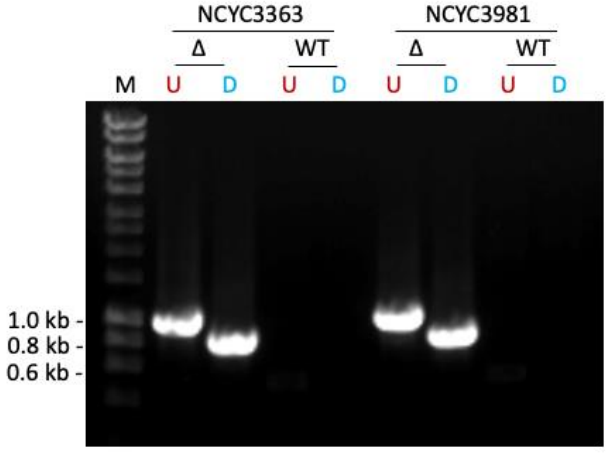
NCYC3363
NCYC3981
Δ
WT
Δ
WT
M
U
D
U
D
U
D
U
D
1.0 kb -
0.8 kb -
0.6 kb -

Figure 6. 9: Deletion of the *ADE2* gene by homologous recombination using short flanking regions. A) Cells expressing the hygromycin resistance marker were able to grow on YM media containing 80 µg/ml hygromycin, and the accumulation of red pigment confirms the disruption of the *ADE2* gene. White cells on hygromycin medium are adenine prototrophs (white arrows). These cells were unable to grow on the minimal adenine-deficient (ade-) medium, unlike the WT (red arrow), which could not grow on hygromycin plates. B) Schematic representation of the open reading frame and hygromycin marker cassette used for *ADE2* deletion. Red and blue lines represent the 50 bp flanking sequences located immediately upstream and downstream of the *ADE2* ORF. C) Agarose gel electrophoresis analysis of PCR products from wild type cells (WT) and *ADE2* knockout cells (Δ) in the strains NCYC3363 and NCYC3891. Successful *ADE2* knockout was identified by amplifying the hygromycin B cassette in the resistant transformants from the respective strains (M: marker; U: upstream; D: downstream).

6.3 Discussion

Industrial biotechnology is a rapidly growing industry, entailing developing of production of compounds by micro-organisms. Examples include bioethanol, biochemicals based on fatty acids such as biosurfactants and biofuels. There is a need to move from petrochemically-generated production using restricted sources, to the production of such molecules using genetically engineered microorganisms that can grow on sustainable feedstocks. This is a very significant change, as it offers unlimited and environmentally-sustainable production (Lynd et al., 2005; Runguphan and Keasling, 2014). Therefore, the production of such high-yield chemicals involves searching for suitable hosts that can withstand the stresses of the biotechnological cycle.

Although *D. hansenii* is a haploid yeast, the existing literature and experiments in the lab indicate that this yeast might be partially diploid, suggesting that certain genes have two or more copies. For example, in *D. hansenii* NCYC102 strain has more than one copy of the *ARG1* gene while in other strains which are *D. hansenii* NCYC3363 and *D. hansenii* NCYC3981 there is only one copy of this gene (unpublished data). The reason for this is unclear, but it has been suggested that either the return to haploidy after self-mating may be relatively slow, or that regions of the genome are readily duplicated. Additionally, this diploidy might be unstable and be a remnant of a previous sexual event as it is reported by Jacques et al. (2009) that *D. hansenii* might contain two different alleles for a gene or genomic region coming from different parents. There are three distinct populations of *D. hansenii*, including one which is also referred to as *C. famata* var. *famata*, as well as the presence of haploid and heterozygous diploid strains arising from crosses of *D. hansenii* strains. The existence of such claims makes the use of the CRISPR-Cas9 system, which is a powerful tool for editing genomes, an efficient option for studying *D. hansenii*.

At the time, *D. hansenii* did not have a developed CRISPR system, although such systems had been established for related yeasts in the CTG clade (Lombardi et al., 2019). We aimed to assess the efficiency of this system in *D. hansenii* by targeting the *ADE2* and *GUT2* genes. Our data demonstrated that these genes (*ADE2* and *GUT2*) were disrupted by the CRISPR/Cas9 system. However, the efficiency was quite low, as evidenced by the limited number of colonies obtained. Our findings, which revealed chromosomal translocation when the region surrounding the Cas9 cut could not be amplified, in contrast to WT cells that were easily amplified, strongly suggest the reason for the low efficiency of the CRISPR system. This result implies that the system might be detrimental to the cells, potentially due to the promoters used for Cas9 expression, which may lead to high expression levels. Moreover, the stability and replication of plasmids in *D. hansenii* remain uncertain due to the use of the ARS sequence, and it is unclear whether they integrate or are merely diluted out over time. Subsequently, two studies (Spasskaya et al., 2021; Strucko et al., 2021) successfully implemented the CRISPR/Cas9 system in *D. hansenii*, employing distinct strategies.

Spasskaya et al. (2021) utilized a Cas9 gene optimized for expression in *C. elegans*, where the non-optimal CTG codon is replaced by alternative leucine codons. Cas9 expression was driven by the GDP1 promoter from *D. hansenii*. Recognizing that the sgRNA expression level is critical

for CRISPR/Cas system activity in yeasts, the researchers tested several predicted *D. hansenii* RNA polymerase III promoters and found that pSCR1 provided the highest sgRNA expression level.

In the second study, Strucko et al. (2021) developed CRISPR systems containing ARS sequences that played a crucial role in enhancing system efficiency. Notably, they also developed a CRISPR/Cas9 system based on a dominant marker (*NAT*^{CUG}), which facilitates gene editing in prototrophic strains of *D. hansenii* without the limitations associated with auxotrophic markers. One system featured a fusion of two ARS sequences—*CfARS16* from *Candida famata* and *panARS* from *Kluyveromyces lactis*—while the second, m-ARS, contained a centromere and three ARS sequences: a fusion of CEN6/ARSH4 from *S. cerevisiae, CfARS16* from *Candida famata* and *panARS* from *Kluyveromyces lactis*. Both systems employed sgRNA flanked by native tRNA^{Gly} sequences, which demonstrated improved targeting efficiency compared to the system I used, where sgRNA was flanked by tRNA^{Ala}.

These studies highlight the importance of optimizing various aspects of the CRISPR/Cas9 system, such as Cas9 expression, sgRNA expression, and ARS sequences, to enhance its efficiency and applicability in *D. hansenii*.

Since the CRISPR/Cas9 system was not the appropriate tool at the time, we sought to find an efficient tool which easily allows gene disruption. After the successful development of the heterologous marker conferring Hygromycin B or G418 resistance to *D. hansenii* transformants by our lab, our aim was to improve the frequency of HR by reducing the HR flanks, which were 1 kb flanks. To investigate the relationship between HR frequency and flanking fragment length, disruption cassettes were constructed with 750, 500, 250,100, 75, 65, and 50 bp homologous flanking DNA of multiple genes. My contribution to this large-scale investigation was on the *ADE2* gene using very short flanks of 75, 65, and 50 bp. Hygromycin cassettes were amplified by PCR and transformed into three *D. hansenii* strains: NCYC102, NCYC3363 and NCYC3981. A significant finding is that targeting the *ADE2* gene in NCYC102 and attempting to insert the hygroB cassette resulted in all transformants being able to grow on ade- plates. This suggests that this strain may possess multiple copies of the gene in question, similar to the *ARG1* gene, which our lab has found to have more than one copy in this strain (unpublished data). However, it is important to note that we did not test the integration of the hygroB cassette in these cells. The observed growth on ade- plates could be due to the lack of hygroB integration or the presence of multiple *ADE2* gene copies in the strain. Further investigations, such as integration testing using PCR, are necessary to confirm the integration of the hygroB cassette, better understand the underlying mechanisms behind the observed growth on ade- plates, and determine whether this strain indeed has multiple copies of the *ADE2* gene.
Disruption of the *ADE2* gene in NCYC3363 and NCYC3981 is highly efficient with HR short flanks. Around 95% of cells showed a gene disruption by accumulating red pigment and not growing on YM media lacking any adenine.

The unique advantage of *S. cerevisiae* has long been its ability to achieve a remarkably high percentage (up to 100% in certain cases) of homologous recombination (HR) when transforming DNA with 50 bp flanking regions. This same outcome was subsequently observed in *S. pombe* (Kaur et al., 1996) and *K. lactis* strain (Kooistra et al. 2004). Here, we

show that successful gene replacement can be accomplished with a success rate of 95% using flanking regions as short as 50 base pairs. Despite previous studies indicating that gene targeting through homologous recombination necessitates long regions of homology to target sites and generally occurs at a low efficiency, our experiments demonstrated otherwise. In our attempts to delete the *ADE2* gene in NCYC3363 and NCYC3981, only 4 out of 51 transformants were mistargeted. Similarly, in the case of the *ARG1* gene in the same strains, our lab member Sondon found that only 1 out of 22 transformants was mistargeted. These findings suggest that homologous recombination can be more efficient than previously thought. One possible explanation for the discrepancy between our findings and previous studies could be the use of auxotrophic markers in earlier research. Given that these markers share identical DNA sequences with the host genome, gene conversions might restore auxotrophy, leading to reduced targeting efficiency, as has been previously observed in *S. cerevisiae* (Wach et al., 1994).
Short homology arms can definitely induce gene targeting, as demonstrated by the exceptional efficacy of targeted gene disruption in our study, which prompted us to look into this possibility. However, we observed a decrease in the number of transformants. By optimizing the electroporation protocol, we have discovered that using 500 ng PCR product consistently yields between 15-50 transformants per electroporation. Our findings are consistent with Spasskaya et al. (2021) study, where they found that double-strand breaks (DSBs) induced by the CRISPR-Cas9 system can be repaired by homologous recombination using 90 bp oligonucleotides in *D. hansenii*. This further highlights that short homologous flanks are adequate for gene repair by homologous recombination in this yeast.

This efficient tool enables rapid and precise DNA replacement at specific loci. By generating cassettes with short flanking sequences through one-step PCR amplification using appropriate primers, we have demonstrated for the first time that a 50 bp flank approach works effectively in *D. hansenii*, providing a fast and successful strategy for HR cloning. This breakthrough is likely to inspire more researchers to work with *D. hansenii*, saving time and resources while expanding the molecular tools available for yeast modification. The innovative PCR-mediated technique can now be applied for gene tagging, overexpression, and other applications, laying a solid foundation for future biotechnological work with *D. hansenii*. Moreover, the utilization of PCR-based genome modifications with heterologous selectable markers allows for the systematic analysis of not only the laboratory strain DH9 but also wild isolates of *D. hansenii*. This further broadens the scope of research and potential applications in this yeast species.

References

Adams, I.R., and Kilmartin, J.V. (2000). Spindle pole body duplication: a model for centrosome duplication? Trends Cell Biol 10, 329-335.

Agranoff, B. W., Bradley, R. M., and Brady, R. O., (1958). The enzymatic synthesis of inositol phosphatide. The Journal of Biological Chemistry, 233(5), 1077–1083.

Aggarwal, M. and Mondal, A. K. (2009). Debaryomyces hansenii: An osmotolerant and halotolerant yeast', in Yeast Biotechnology: Diversity and Applications. Dordrecht: Springer Netherlands, pp. 65–84.

Albuquerque, C.P., Smolka, M.B., Payne, S.H., Bafna, V., Eng, J. and Zhou, H., (2008). A multidimensional chromatography technology for in-depth phosphoproteome analysis. Molecular & Cellular Proteomics, 7(7), pp.1389-1396.

Amberg, D.C., Basart, E. and Botstein, D., (1995). Defining protein interactions with yeast actin in vivo. Nature structural biology, 2(1), pp.28-35.

Arai, S., Noda, Y., Kainuma, S., Wada, I., and Yoda, K. (2008). Ypt11 functions in bud-directed transport of the Golgi by linking Myo2 to the coatomer subunit Ret2. Curr Biol 18, 987-991.

Audhya, A., and Emr, S. D. (2002). Stt4 PI 4-kinase localizes to the plasma membrane and functions in the Pkc1-mediated MAP kinase cascade. Developmental Cell, 2(5), 593– 605.

Asare, A., Levorse, J. and Fuchs, E., (2017). Coupling organelle inheritance with mitosis to balance growth and differentiation. Science, 355(6324), p.eaah4701.

Baker, A., Hogg, T.L. and Warriner, S.L., (2016). Peroxisome protein import: a complex journey. Biochemical Society Transactions, 44(3), pp.783-789.

Balcer, H.I., Goodman, A.L., Rodal, A.A., Smith, E., Kugler, J., Heuser, J.E. and Goode, B.L., (2003). Coordinated regulation of actin filament turnover by a high-molecular-weight Srv2/CAP complex, cofilin, profilin, and Aip1. Current Biology, 13(24), pp.2159-2169.

Balla, T., Szentpetery, Z., and Kim, Y. J. (2009). Phosphoinositide signaling: new tools and insights. Physiology, Vol. 24, 231–244.

Barrero, R.A., Umeda, M., Yamamura, S. and Uchimiya, H., (2002). Arabidopsis CAP regulates the actin cytoskeleton necessary for plant cell elongation and division. The Plant Cell, 14(1), pp.149-163.

Baudin, A. et al. (1993). A simple and efficient method for direct gene deletion in Saccharomyces cerevisiae. Nucleic Acids Research, 21(14), pp.

Baudhuin, P., Beaufay, H., and De Duve, C. (1965). Combined biochemical and morphological study of particulate fractions from rat liver: Analysis of Preparations Enriched in Lysosomes or in Particles Containing Urate Oxidase, D-Amino Acid Oxidase, and Catalase. The Journal of Cell Biology, 26(1), 219–243.

Baum, B., Li, W. and Perrimon, N., (2000). A cyclase-associated protein regulates actin and cell polarity during Drosophila oogenesis and in yeast. Current Biology, 10(16), pp.964-973.

Beach, D.L., Thibodeaux, J., Maddox, P., Yeh, E., and Bloom, K. (2000). The role of the proteins Kar9 and Myo2 in orienting the mitotic spindle of budding yeast. Curr Biol 10, 1497-1506.

Bernhard, W., and Rouiller, C. (1956). Close topographical relationship between mitochondria and ergastoplasm of liver cells in a definite phase of cellular activity. The Journal of Biophysical and Biochemical Cytology, 2(4, Suppl), 73–78.

Bertling, E., Hotulainen, P., Mattila, P.K., Matilainen, T., Salminen, M. and Lappalainen, P., (2004). Cyclase-associated protein 1 (CAP1) promotes cofilin-induced actin dynamics in mammalian nonmuscle cells. Molecular Biology of The Cell, 15(5), pp.2324-2334.

Bertling, E., Quintero-Monzon, O., Mattila, P.K., Goode, B.L. and Lappalainen, P., (2007). Mechanism and biological role of profilin-Srv2/CAP interaction. Journal of Cell Science, 120(7), pp.1225-1234.

Besprozvannaya, M., Dickson, E., Li, H., Ginburg, K. S., Bers, D. M., Auwerx, J., and Nunnari, J. (2018). GRAM domain proteins specialize functionally distinct ER-PM contact sites in human cells. ELife, 7.

Bharti, P., Schliebs, W., Schievelbusch, T., Neuhaus, A., David, C., Kock, K., Herrmann, C., Meyer, H.E., Wiese, S., Warscheid, B. and Theiss, C., (2011). PEX14 is required for microtubule-based peroxisome motility in human cells. Journal of Cell Science, 124(10), pp.1759-1768.

Binns, D., Januszewski, T., Chen, Y., Hill, J., Markin, V. S., Zhao, Y., … Goodman, J. M. (2006). An intimate collaboration between peroxisomes and lipid bodies. Journal of Cell Biology, 173(5), 719–731.

Birschmann, I., Stroobants, A. K., van den Berg, M., Schäfer, A., Rosenkranz, K., Kunau, W.- H., and Tabak, H. F. (2003). Pex15p of Saccharomyces cerevisiae provides a molecular basis for recruitment of the AAA peroxin Pex6p to peroxisomal membranes. Molecular Biology of The Cell, 14(6), 2226–2236.

Blackstone, C. and Chang, C.R., (2011). Mitochondria unite to survive. Nature Cell Biology, 13(5), pp.521-522.

Blakeslee, A., (1904), August. Sexual reproduction in the Mucorineae. In Proceedings of the American Academy of Arts and Sciences. *40(4), 205-319*.

Breuer, U., and Harms, H., (2006). Debaryomyces hansenii-an extremophilic yeast with biotechnological potential. Yeast. *23, 415-437*.

Bobola, N., Jansen, R.P., Shin, T.H., and Nasmyth, K. (1996). Asymmetric accumulation of Ash1p in postanaphase nuclei depends on a myosin and restricts yeast mating-type switching to mother cells. Cell 84, 699-709.

Bohl, F., Kruse, C., Frank, A., Ferring, D., and Jansen, R.P. (2000). She2p, a novel RNA-binding protein tethers ASH1 mRNA to the Myo4p myosin motor via She3p. EMBO J 19, 5514-5524.

Boekhout, T. and Robert, V. eds., (2003). Yeasts in food. Elsevier.

Brooks, A.A., (2008). Ethanol production potential of local yeast strains isolated from ripe banana peels. African Journal of Biotechnology, 7(20).

Boldogh, I.R. and Pon, L.A., (2006). Interactions of mitochondria with the actin cytoskeleton. Biochimica et Biophysica Acta (BBA)-Molecular Cell Research, 1763(5-6), pp.450-462.

Boldogh, I.R., Yang, H.C., Nowakowski, W.D., Karmon, S.L., Hays, L.G., Yates, J.R., 3rd, and Pon, L.A. (2001). Arp2/3 complex and actin dynamics are required for actin-based mitochondrial motility in yeast. Proc Natl Acad Sci U S A 98, 3162-3167.

Braverman, N. E., D'Agostino, M. D., and MacLean, G. E. (2013). Peroxisome biogenesis disorders: Biological, clinical and pathophysiological perspectives. Developmental Disabilities Research Reviews, 17(3), 187–196.

Brown, F. R., McAdams, A. J., Cummins, J. W., Konkol, R., Singh, I., Moser, A. B., and Moser, H. W. (1982). Cerebro-hepato-renal (Zellweger) syndrome and neonatal adrenoleukodystrophy: similarities in phenotype and accumulation of very long chain fatty acids. The Johns Hopkins Medical Journal, 151(6), 344–351.

Brückner, A., Polge, C., Lentze, N., Auerbach, D. and Schlattner, U., (2009). Yeast two-hybrid, a powerful tool for systems biology. International Journal of Molecular Sciences, 10(6), pp.2763-2788.

Burnett, S. F., Farré, J. C., Nazarko, T. Y., and Subramani, S. (2015). Peroxisomal Pex3 activates selective autophagy of peroxisomes via interaction with the pexophagy receptor Atg30. Journal of Biological Chemistry, 290(13), 8623–8631.

Cali, B.M., Doyle, T.C., Botstein, D. and Fink, G.R., (1998). Multiple functions for actin during filamentous growth of Saccharomyces cerevisiae. Molecular Biology of the Cell, 9(7), pp.1873-1889.

Campellone, K.G. and Welch, M.D., (2010). A nucleator arms race: cellular control of actin assembly. Nature Reviews Molecular Cell Biology, 11(4), pp.237-251.

Carmichael, R.E. and Schrader, M., (2022). Determinants of peroxisome membrane dynamics. Frontiers in Physiology, 13, p.834411.

Caydasi, A.K., and Pereira, G. (2012). SPOC alert--when chromosomes get the wrong direction. Exp Cell Res 318, 1421-1427.

Caydasi, A.K., Ibrahim, B., and Pereira, G. (2010). Monitoring spindle orientation: Spindle position checkpoint in charge. Cell Div 5, 28.

Chang, C.R. and Blackstone, C., (2007). Drp1 phosphorylation and mitochondrial regulation. EMBO reports, 8(12), pp.1088-1089.

Chang, C.R. and Blackstone, C., (2010). Dynamic regulation of mitochondrial fission through modification of the dynamin-related protein Drp1. Annals of the new York Academy of Sciences, 1201(1), pp.34-39.

Chang, J., Mast, F. D., Fagarasanu, A., Rachubinski, D. A., Eitzen, G. A., Dacks, J. B., and Rachubinski, R. A. (2009). Pex3 peroxisome biogenesis proteins function in peroxisome inheritance as class V myosin receptors. Journal of Cell Biology, 187(2), 233-246.

Chaudhry, F., Breitsprecher, D., Little, K., Sharov, G., Sokolova, O. and Goode, B.L., (2013). Srv2/cyclase-associated protein forms hexameric shurikens that directly catalyze actin filament severing by cofilin. Molecular Biology of The Cell, 24(1), pp.31-41.

Chaudhry, F., Jansen, S., Little, K., Suarez, C., Boujemaa-Paterski, R., Blanchoin, L. and Goode, B.L., (2014). Autonomous and in trans functions for the two halves of Srv2/CAP in promoting actin turnover. Cytoskeleton, 71(6), pp.351-360.

Chaudhry, F., Little, K., Talarico, L., Quintero-Monzon, O. and Goode, B.L., (2010). A central role for the WH2 domain of Srv2/CAP in recharging actin monomers to drive actin turnover in vitro and in vivo. Cytoskeleton, 67(2), pp.120-133.

Chen, C., Li, J., Qin, X. and Wang, W., (2020). Peroxisomal membrane contact sites in mammalian cells. Frontiers in Cell and Developmental Biology, 8, p.512.

Chen, Y.C., Cheng, T.H., Lin, W.L., Chen, C.L., Yang, W.Y., Blackstone, C. and Chang, C.R., (2019). Srv2 is a pro-fission factor that modulates yeast mitochondrial morphology and respiration by regulating actin assembly. Iscience, 11, pp.305-317.

Chernyakov, I., Santiago-Tirado, F., and Bretscher, A. (2013). Active segregation of yeast mitochondria by Myo2 is essential and mediated by Mmr1 and Ypt11. Curr Biol 23, 1818-1824.

Coffey, A. G., Daly, C. and Fitzgerald, G. (1994). The impact of biotechnology on the dairy industry. Biotechnology Advances, 12(4), pp. 625–633.

Copeland, D. E., and Dalton, A. J. (1959). An association between mitochondria and the endoplasmic reticulum in cells of the pseudobranch gland of a teleost. The Journal of Biophysical and Biochemical Cytology, 5(3), 393–396.

Costello, J. L., Castro, I. G., Hacker, C., Schrader, T. A., Metz, J., Zeuschner, D., … Schrader, M. (2017). ACBD5 and VAPB mediate membrane associations between peroxisomes and the ER. Journal of Cell Biology, 216(2), 331–342.

Costello, J. L., Castro, I. G., Schrader, T. A., Islinger, M., and Schrader, M. (2017). Peroxisomal ACBD4 interacts with VAPB and promotes ER-peroxisome associations. Cell Cycle, Vol. 16, 1039–1045.

Covill-Cooke, C., Toncheva, V.S. and Kittler, J.T., (2020). Regulation of peroxisomal trafficking and distribution. Cellular and Molecular Life Sciences, 78(5), pp.1929-1941.

Csordás, G., Várnai, P., Golenár, T., Roy, S., Purkins, G., Schneider, T. G., … Hajnóczky, G. (2010). Imaging Interorganelle Contacts and Local Calcium Dynamics at the ER-Mitochondrial Interface. Molecular Cell, 39(1), 121–132.

David, C., Koch, J., Oeljeklaus, S., Laernsack, A., Melchior, S., Wiese, S., … Brocard, C. (2013). A combined approach of quantitative interaction proteomics and live-cell imaging reveals a regulatory role for endoplasmic reticulum (ER) Reticulon Homology Proteins in peroxisome biogenesis. Molecular and Cellular Proteomics, 12(9), 2408–2425.

Danner, H. and Braun, R. (1999). Biotechnology for the production of commodity chemicals from biomass. Chemical Society Reviews. Royal Society of Chemistry, 28(6), pp. 395–405.

De Duve, C., and Baudhuin, P. (1966). Peroxisomes (microbodies and related particles). Physiol Rev, 46(2), 323–357.

Dickson, E. J., and Hille, B. (2019). Understanding phosphoinositides: Rare, dynamic, and essential membrane phospholipids. Biochemical Journal, Vol. 476, 1–23.

Distel, B., Erdmann, R., Gould, S. J., Blobel, G., Crane, D. I., Cregg, J. M., … Veenhuis, M. (1996). A unified nomenclature for peroxisome biogenesis factors. The Journal of Cell Biology, 135(1), 1–3.

Dietrich, D., Seiler, F., Essmann, F. and Dodt, G., (2013). Identification of the kinesin KifC3 as a new player for positioning of peroxisomes and other organelles in mammalian cells. Biochimica et Biophysica Acta (BBA)-Molecular Cell Research, 1833(12), pp.3013-3024.

Dodatko, T., Fedorov, A.A., Grynberg, M., Patskovsky, Y., Rozwarski, D.A., Jaroszewski, L., Aronoff-Spencer, E., Kondraskina, E., Irving, T., Godzik, A. and Almo, S.C., (2004). Crystal

structure of the actin binding domain of the cyclase-associated protein. Biochemistry, 43(33), pp.10628-10641.

Dominguez, R. and Holmes, K.C., (2011). Actin structure and function. Annual Review of Biophysics, 40, pp.169-186.

Domínguez, J. M. et al. (1999). Xylitol production from wood hydrolyzates by entrapped Debaryomyces hansenii and Candida guilliermondii cells. Applied Biochemistry and Biotechnology - Part A Enzyme Engineering and Biotechnology.

Doolittle, L.K., Rosen, M.K. and Padrick, S.B., (2013). Measurement and analysis of in vitro actin polymerization. Adhesion Protein Protocols, pp.273-293.

Dodt, G., Warren, D., Becker, E., Rehling, P. and Gould, S.J., (2001). Domain mapping of human PEX5 reveals functional and structural similarities to Saccharomyces cerevisiae Pex18p and Pex21p. Journal of Biological Chemistry, 276(45), pp.41769-41781.

Drees, B.L., Sundin, B., Brazeau, E., Caviston, J.P., Chen, G.C., Guo, W., Kozminski, K.G., Lau, M.W., Moskow, J.J., Tong, A. and Schenkman, L.R., (2001). A protein interaction map for cell polarity development. The Journal of Cell Biology, 154(3), pp.549-576.

Drubin, D.G., Miller, K.G. and Botstein, D., (1988). Yeast actin-binding proteins: evidence for a role in morphogenesis. The Journal of Cell Biology, 107(6), pp.2551-2561.

Dujon, B. et al. (2004). Genome evolution in yeasts. Nature. Nature Publishing Group, 430(6995), pp. 35–44.

Durá, M. A., Flores, M. and Toldrá, F. (2004). Effect of Debaryomyces spp. on the proteolysis of dry-fermented sausages. Meat Science. Elsevier, 68(2), pp. 319–328.

Dyer, J. M., McNew, J. A., and Goodman, J. M. (1996). The sorting sequence of the peroxisomal integral membrane protein PMP47 is contained within a short hydrophilic loop. Journal of Cell Biology, 133(2), 269–280.

Ebberink, M.S., Mooyer, P.A., Koster, J., Dekker, C.J., Eyskens, F.J., Dionisi-Vici, C., Clayton, P.T., Barth, P.G., Wanders, R.J. and Waterham, H.R., (2009). Genotype-phenotype correlation in PEX5-deficient peroxisome biogenesis defective cell lines. Human mutation, 30(1), pp.93-98.

Eisenberg-Bord, M., Shai, N., Schuldiner, M., and Bohnert, M. (2016). A Tether Is a Tether Isa Tether: Tethering at Membrane Contact Sites. Developmental Cell, Vol. 39, 395 409.

Eitzen, G., Wang, L., Thorngren, N. and Wickner, W., (2002). Remodeling of organelle-bound actin is required for yeast vacuole fusion. The Journal of Cell Biology, 158(4), pp.669-679.

Ekal, L., Alqahtani, A.M. and Hettema, E.H., (2023). The dynamin-related protein Vps1 and the peroxisomal membrane protein Pex27 function together during peroxisome fission. Journal of Cell Science, pp.jcs-246348.

El Magraoui, F., Bäumer, B. E., Platta, H. W., Baumann, J. S., Girzalsky, W., and Erdmann, R. (2012). The RING-type ubiquitin ligases Pex2p, Pex10p and Pex12p form a heteromeric complex that displays enhanced activity in an ubiquitin conjugating enzyme selective manner. FEBS Journal, 279(11), 2060–2070.

Elgersma, Y., Kwast, L., van den Berg, M., Snyder, W. B., Distel, B., Subramani, S., and Tabak,H. F. (1997). Overexpression of Pex15p, a phosphorylated peroxisomal integral membrane protein required for peroxisome assembly in S.cerevisiae, causes proliferation of the endoplasmic reticulum membrane. The EMBO Journal, 16(24), 7326–7341.

Elgersma, Y., van den Berg, M., Tabak, H. F., and Distel, B. (1993). An efficient positive selection procedure for the isolation of peroxisomal import and peroxisome assembly mutants of Saccharomyces cerevisiae. Genetics, 135(3), 731–740.

Erdmann, R., and Blobel, G. (1995). Giant peroxisomes in oleic acid-induced Saccharomyces cerevisiae lacking the peroxisomal membrane protein Pmp27p. The Journal of Cell Biology, 128, 509-523.

Erdmann, R., and Schliebs, W. (2005). Peroxisomal matrix protein import: The transient pore model. Nature Reviews Molecular Cell Biology, Vol. 6, 738–742.

Erdmann, R., Veenhuis, M., Mertens, D., and Kunau, W. H. (1989). Isolation of peroxisomedeficient mutants of Saccharomyces cerevisiae. Proceedings of the National Academy of Sciences, 86(14), 5419–5423.

Eshel, D., Urrestarazu, L.A., Vissers, S., Jauniaux, J.C., van Vliet-Reedijk, J.C., Planta, R.J., and Gibbons, I.R. (1993). Cytoplasmic dynein is required for normal nuclear segregation in yeast. Proc Natl Acad Sci U S A 90, 11172-11176.

Esnay, N., Dyer, J.M., Mullen, R.T. and Chapman, K.D., (2020). Lipid droplet–peroxisome connections in plants. Contact, 3, p.2515256420908765.

Estrada, P., Kim, J., Coleman, J., Walker, L., Dunn, B., Takizawa, P., Novick, P., and Ferro-Novick, S. (2003). Myo4p and She3p are required for cortical ER inheritance in Saccharomyces cerevisiae. The Journal of Cell Biology 163, 1255-1266.

Fabre, E., Muller, H., Therizols, P., Lafontaine, I., Dujon, B. and Fairhead, C., (2005). Comparative genomics in hemiascomycete yeasts: evolution of sex, silencing, and subtelomeres. Molecular biology and evolution, *22(4), 856-873*.

Fagarasanu, A., Fagarasanu, M., Eitzen, G.A., Aitchison, J.D., and Rachubinski, R.A. (2006). The peroxisomal membrane protein Inp2p is the peroxisome-specific receptor for the myosin V motor Myo2p of Saccharomyces cerevisiae. Dev Cell 10, 587-600.

Fagarasanu, M., Fagarasanu, A., Tam, Y.Y., Aitchison, J.D., and Rachubinski, R.A. (2005). Inp1p is a peroxisomal membrane protein required for peroxisome inheritance in Saccharomyces cerevisiae. The Journal of Cell Biology 169, 765-775.

Fan, J., Li, X., Issop, L., Culty, M., and Papadopoulos, V. (2016). ACBD2/ECI2-mediated peroxisome-mitochondria interactions in leydig cell steroid biosynthesis. Molecular Endocrinology, 30(7), 763–782.

Fang, Y., Morrell, J. C., Jones, J. M., and Gould, S. J. (2004). PEX3 functions as a PEX19 docking factor in the import of class I peroxisomal membrane proteins. The Journal of Cell Biology, 164(6), 863–875.

Farré, J.C., Carolino, K., Stasyk, V., Stasyk, O.G., Hodzic, Z., Agrawal, G., Till, A., Proietto, M., Cregg, J., Sibirny, A.A. and Subramani, S., (2017). A new yeast peroxin, Pex36, a functional homolog of mammalian PEX16, functions in the ER-to-peroxisome traffic of peroxisomal membrane proteins. Journal of Molecular Biology, 429(23), pp.3743-3762.

Farré, J.C., Mahalingam, S.S., Proietto, M. and Subramani, S., (2019). Peroxisome biogenesis, membrane contact sites, and quality control. EMBO reports, 20(1), p.e46864.

Fatichenti, F., Bergere, J., Deiana, P. and Farris, G., (1983). Antagonistic activity of Debaryomyces hansenii towards Clostridium tyrobutyricum and Cl. butyricum. Journal of Dairy Research. 50(4), 449-457.

Fehrenbacher, K.L., Yang, H.C., Gay, A.C., Huckaba, T.M. and Pon, L.A., (2004). Live cell imaging of mitochondrial movement along actin cables in budding yeast. Current Biology, 14(22), pp.1996-2004.

Feliciano, D., Tolsma, T.O., Farrell, K.B., Aradi, A. and Di Pietro, S.M., (2015). A second Las17 monomeric actin-binding motif functions in Arp2/3-dependent actin polymerization during endocytosis. Traffic, 16(4), pp.379-397.

Fidaleo, M. (2010). Peroxisomes and peroxisomal disorders: the main facts. Experimental and Toxicologic Pathology: Official Journal of the Gesellschaft Für Toxikologische Pathologie, 62(6), 615–625.

Flores, M. et al. (2017). Screening of Debaryomyces hansenii Strains for Flavor Production under a Reduced Concentration of Nitrifying Preservatives Used in Meat Products. Journal of Agricultural and Food Chemistry, 65(19), pp. 3900–3909.

Friedman, J.R., Lackner, L.L., West, M., DiBenedetto, J.R., Nunnari, J. and Voeltz, G.K., (2011). ER tubules mark sites of mitochondrial division. Science, 334(6054), pp.358-362.

Gandre-Babbe, S., and van der Bliek, A. M. (2008). The novel tail-anchored membrane protein Mff controls mitochondrial and peroxisomal fission in mammalian cells. Molecular Biology of the Cell, 19(6), 2402–2412.

Garrenton, L. S., Stefan, C. J., McMurray, M. A., Emr, S. D., and Thorner, J. (2010). Pheromone-induced anisotropy in yeast plasma membrane phosphatidylinositol- 4,5-bisphosphate distribution is required for MAPK signaling. Proceedings of the National Academy of Sciences of the United States of America, 107(26), 11805–11810.

Gerst, J.E., Ferguson, K.E.N.N.E.T.H., Vojtek, A.N.N.E., Wigler, M.I.C.H.A.E.L. and Field, J., (1991). CAP is a bifunctional component of the Saccharomyces cerevisiae adenylyl cyclase complex. Molecular and cellular biology, 11(3), pp.1248-1257.

Gientka, I. et al. (2017). dentification and Characterization of Oleaginous Yeast Isolated from Kefir and Its Ability to Accumulate Intracellular Fats in Deproteinated Potato Wastewater with Different Carbon Sources. BioMed Research International. 17;2017.

Gírio, F. M. et al. (2000). Polyols production during single and mixed substrate fermentations in Debaryomyces hansenii. Bioresource Technology. Elsevier, 71(3), pp. 245–251.

Gomes, L.C., Benedetto, G.D. and Scorrano, L., (2011). During autophagy mitochondria elongate, are spared from degradation and sustain cell viability. Nature Cell Biology, 13(5), pp.589-598.

Gotte, K., Girzalsky, W., Linkert, M., Baumgart, E., Kammerer, S., Kunau, W. H., and Erdmann, R. (1998). Pex19p, a farnesylated protein essential for peroxisome biogenesis. Molecular and Cellular Biology, 18(1), 616–628.

Gould, S J, Keller, G. A., Hosken, N., Wilkinson, J., and Subramani, S. (1989). A conserved tripeptide sorts proteins to peroxisomes. The Journal of Cell Biology, 108(5), 1657-1664.

Gould, Stephen J., McCollum, D., Spong, A. P., Heyman, J. A., and Subramani, S. (1992). Development of the yeast Pichia pastoris as a model organism for a genetic and molecular analysis of peroxisome assembly. Yeast, 8(8), 613–628.

Gouveia, A. M., Reguenga, C., Oliveira, M. E., Sa-Miranda, C., and Azevedo, J. E. (2000). Characterization of peroxisomal Pex5p from rat liver. Pex5p in the Pex5p-Pex14p membrane complex is a transmembrane protein. The Journal of Biological Chemistry, 275(42), 32444–32451.

Güneşer, O. et al. (2015). Bioflavour production from tomato and pepper pomaces by Kluyveromyces marxianus and Debaryomyces hansenii. Bioprocess and Biosystems Engineering. Springer Berlin Heidelberg, 38(6), pp. 1143–1155.

Gray, E. G. (1963). Electron microscopy of presynaptic organelles of the spinal cord. Journal of Anatomy, 97(Pt 1), 101–106.

Griffin, E.E., Graumann, J. and Chan, D.C., (2005). The WD40 protein Caf4p is a component of the mitochondrial fission machinery and recruits Dnm1p to mitochondria. The Journal of Cell Biology, 170(2), pp.237-248.

Hammermeister, M., Schödel, K. and Westermann, B., (2010). Mdm36 is a mitochondrial fission-promoting protein in Saccharomyces cerevisiae. Molecular biology of the cell, 21(14), pp.2443-2452.

Hariri, H., Speer, N., Bowerman, J., Rogers, S., Fu, G., Reetz, E., … Henne, W. M. (2019). Mdm1 maintains endoplasmic reticulum homeostasis by spatially regulating lipid droplet biogenesis. Journal of Cell Biology, 218(4), 1319–1334.

Henriksen, P., Wagner, S.A., Weinert, B.T., Sharma, S., Bačinskaja, G., Rehman, M., Juffer, A.H., Walther, T.C., Lisby, M. and Choudhary, C., (2012). Proteome-wide analysis of lysine acetylation suggests its broad regulatory scope in Saccharomyces cerevisiae. Molecular and Cellular Proteomics, 11(11), pp.1510-1522.

Hermann, G.J., Thatcher, J.W., Mills, J.P., Hales, K.G., Fuller, M.T., Nunnari, J. and Shaw, J.M., (1998). Mitochondrial fusion in yeast requires the transmembrane GTPase Fzo1p. The Journal of Cell Biology, 143(2), pp.359-373.

Hettema, E. H., Erdmann, R., van der Klei, I. J., and Veenhuis, M. (2014). Evolving models for peroxisome biogenesis. Current Opinions in Cell Biology, 29(100), 25-30.

Hettema, E. H., Girzalsky, W., van Den Berg, M., Erdmann, R., and Distel, B. (2000). Saccharomyces cerevisiae pex3p and pex19p are required for proper localization and stability of peroxisomal membrane proteins. The EMBO Journal, 19(2), 223–233.

Hirve, N., Rajanikanth, V., Hogan, P. G., and Gudlur, A. (2018). Coiled-Coil Formation Conveys a STIM1 Signal from ER Lumen to Cytoplasm. Cell Reports, 22(1), 72–83.

Hoepfner, D., Schildknegt, D., Braakman, I., Philippsen, P., and Tabak, H. F. (2005). Contribution of the endoplasmic reticulum to peroxisome formation. Cell, 122(1), 85–95.

Hoepfner, D., Van Den Berg, M., Philippsen, P., Tabak, H.F. and Hettema, E.H., (2001). A role for Vps1p, actin, and the Myo2p motor in peroxisome abundance and inheritance in Saccharomyces cerevisiae. The Journal of Cell Biology, 155(6), pp.979-990.

Höhfeld, J., Veenhuis, M., and Kunau, W. H. (1991). PAS3, a Saccharomyces cerevisiae gene encoding a peroxisomal integral membrane protein essential for peroxisome biogenesis. The Journal of Cell Biology, 114(6), 1167–1178.

Holt, L.J., Tuch, B.B., Villén, J., Johnson, A.D., Gygi, S.P. and Morgan, D.O., (2009). Global analysis of Cdk1 substrate phosphorylation sites provides insights into evolution. Science, 325(5948), pp.1682-1686.

Holtzman, D.A., Wertman, K.F. and Drubin, D.G., (1994). Mapping actin surfaces required for functional interactions in vivo. The Journal of Cell Biology, 126(2), pp.423-432.

Honsho, M, Tamura, S., Shimozawa, N., Suzuki, Y., Kondo, N., and Fujiki, Y. (1998). Mutation in PEX16 is causal in the peroxisome-deficient Zellweger syndrome of complementation group D. American Journal of Human Genetics, 63(6), 1622–1630.

Honsho, Masanori, and Fujiki, Y. (2001). Topogenesis of peroxisomal membrane protein requires a short, positively charged intervening-loop sequence and flanking hydrophobic segments: Study using human membrane protein PMP34. Journal of Biological Chemistry, 276(12), 9375–9382.

Hua, R., Cheng, D., Coyaud, É., Freeman, S., Di Pietro, E., Wang, Y., … Kim, P. K. (2017). VAPs and ACBD5 tether peroxisomes to the ER for peroxisome maintenance and lipid homeostasis. Journal of Cell Biology, 216(2), 367–377.

Huber, A., Koch, J., Kragler, F., Brocard, C., and Hartig, A. (2012). A subtle interplay between three Pex11 proteins shapes de novo formation and fission of peroxisomes. Traffic, 13, 157-167.

Huckaba, T.M., Gay, A.C., Pantalena, L.F., Yang, H.C. and Pon, L.A., (2004). Live cell imaging of the assembly, disassembly, and actin cable–dependent movement of endosomes and actin patches in the budding yeast, Saccharomyces cerevisiae. The Journal of Cell Biology, 167(3), pp.519-530.

Hulmes, G.E., Hutchinson, J.D., Dahan, N., Nuttall, J.M., Allwood, E.G., Ayscough, K.R. and Hettema, E.H., (2020). The Pex3–Inp1 complex tethers yeast peroxisomes to the plasma membrane. Journal of Cell Biology, 219(10).

Hutchins, M.U., Veenhuis, M., and Klionsky, D.J. (1999). Peroxisome degradation in Saccharomyces cerevisiae is dependent on machinery of macroautophagy and the Cvt pathway. J Cell Sci 112 (Pt 22), 4079-4087.

Hwang, E., Kusch, J., Barral, Y., and Huffaker, T.C. (2003). Spindle orientation in Saccharomyces cerevisiae depends on the transport of microtubule ends along polarized actin cables. Journal of Cell Biology. 161, 483-488.

Itoh, T., Toh, E.A., and Matsui, Y. (2004). Mmr1p is a mitochondrial factor for Myo2p-dependent inheritance of mitochondria in the budding yeast. EMBO J 23, 2520-2530.

Itoh, T., Watabe, A., Toh, E.A., and Matsui, Y. (2002). Complex formation with Ypt11p, a rab-type small GTPase, is essential to facilitate the function of Myo2p, a class V myosin, in mitochondrial distribution in Saccharomyces cerevisiae. Molocular Cell Biology 22, 7744-7757.

Itoyama, A., Michiyuki, S., Honsho, M., Yamamoto, T., Moser, A., Yoshida, Y., and Fujiki, Y. (2013). Mff functions with Pex11pbeta and DLP1 in peroxisomal fission. Biol Open 2, 998-1006.

Jacques, N., Zenouche, A., Gunde-Cimerman, N. and Casaregola, S., (2015). Increased diversity in the genus Debaryomyces from Arctic glacier samples. Antonie Van Leeuwenhoek, *107*, pp.487-501.

Jacques, N., Sacerdot, C., Derkaoui, M., Dujon, B., Ozier-Kalogeropoulos, O. and Casaregola, S., (2010). Population polymorphism of nuclear mitochondrial DNA insertions reveals widespread diploidy associated with loss of heterozygosity in Debaryomyces hansenii. Eukaryotic Cell, 9(3), pp.449-459.

Jacques, N., Mallet, S. and Casaregola, S., (2009). Delimitation of the species of the Debaryomyces hansenii complex by intron sequence analysis. International Journal of Systematic and Evolutionary Microbiology, 59(5), pp.1242-1251.

Jahani-Asl, A. and Slack, R.S., (2007). The phosphorylation state of Drp1 determines cell fate. EMBO reports, 8(10), pp.912-913.

Jeffries, T. W. and Cregg, J. M. (2010) 'Protein Expression in Nonconventional Yeasts', Genetics, Strain Improvement and Recombinant Proteins, (64), pp. 302–311.

Jin, Y., and Weisman, L.S. (2015). The vacuole/lysosome is required for cell-cycle progression. Elife 4.

Jin, Y., Sultana, A., Gandhi, P., Franklin, E., Hamamoto, S., Khan, A.R., Munson, M., Schekman, R., and Weisman, L.S. (2011). Myosin V transports secretory vesicles via a Rab GTPase cascade and interaction with the exocyst complex. Dev Cell 21, 1156-1170.

Johnston, G.C., Prendergast, J.A., and Singer, R.A. (1991). The Saccharomyces cerevisiae MYO2 gene encodes an essential myosin for vectorial transport of vesicles. Journal of Cell Biology. 113, 539-551.

Jones, J. M., Morrell, J. C., and Gould, S. J. (2004). PEX19 is a predominantly cytosolic chaperone and import receptor for class 1 peroxisomal membrane proteins. Journal of Cell Biology, 164(1), 57–67.

Johnson, E. A. and Echavarri-Erasun, C. (2011). Debaryomyces - an overview, in Kurtzman, C. P., W, F. J., and Teun, B. (eds) The Yeasts. fifth, pp. 21–44.

Jorgensen, P., Nishikawa, J.L., Breitkreutz, B.J. and Tyers, M., (2002). Systematic identification of pathways that couple cell growth and division in yeast. Science, 297(5580), pp.395-400.

Joshi, A. S., Huang, X., Choudhary, V., Levine, T. P., Hu, J., and Prinz, W. A. (2016). A family of membrane-shaping proteins at ER subdomains regulates pre-peroxisomal vesicle biogenesis. Journal of Cell Biology, 215(4), 515–529.

Joshi, S., Agrawal, G., and Subramani, S. (2012). Phosphorylation-dependent Pex11p and Fis1p interaction regulates peroxisome division. Molecular Biology of The Cell, 23(7), 1307–1315.

Kakimoto, Y., Tashiro, S., Kojima, R., Morozumi, Y., Endo, T., and Tamura, Y. (2018). Visualizing multiple inter-organelle contact sites using the organelle-Targeted split-GFP system. Scientific Reports, 8(1), 1–13.

Kaur, R., Ingavale, S. S. and Bachhawat, A. K. (1996). PCR-Mediated Direct Gene Disruption in Schizosaccharomyces Pombe. Nucleic Acids Research, 25(5), pp. 1080–1081.

Keller, G.-A., Gould, S., Delucat, M., and Subramani, S. (1987). Firefly luciferase is targeted to peroxisomes in mammalian cells. Cell Biology, 84, 3264–3268.

Kiel, J. A. K. W., Veenhuis, M., and van der Klei, I. J. (2006). PEX genes in fungal genomes: common, rare or redundant. Traffic (Copenhagen, Denmark), 7(10), 1291–1303.

Kim, P. K., Mullen, R. T., Schumann, U., and Lippincott-Schwartz, J. (2006). The origin and maintenance of mammalian peroxisomes involves a de novo PEX16-dependent pathway from the ER. Journal of Cell Biology, 173(4), 521–532.

Kim, Y. J., Guzman-Hernandez, M. L., and Balla, T. (2011). A highly dynamic ER-derived phosphatidylinositol-synthesizing organelle supplies phosphoinositides to cellular membranes. Developmental Cell, 21(5), 813–824.

Klionsky, D.J. (1997). Protein transport from the cytoplasm into the vacuole. J Membr Biol 157, 105-115.

Klouwer, F. C. C., Berendse, K., Ferdinandusse, S., Wanders, R. J. A., Engelen, M., and Poll-The, B. T. (2015). Zellweger spectrum disorders: clinical overview and management approach. Orphanet Journal of Rare Diseases, 10(1), 151.

Knoblach, B., and Rachubinski, R. A. (2019). Determinants of the assembly, integrity andmaintenance of the endoplasmic reticulum-peroxisome tether. Traffic, 20(3), 213–225.
Knoblach, B., Sun, X., Coquelle, N., Fagarasanu, A., Poirier, R. L., and Rachubinski, R. A. (2013). An ER-peroxisome tether exerts peroxisome population control in yeast. EMBO Journal, 32(18), 2439–2453.

Kobayashi, S., Tanaka, A., and Fujiki, Y. (2007). Fis1, DLP1, and Pex11p coordinately regulate peroxisome morphogenesis. Exp Cell Res, 313, 1675-1686.

Koch, J., Pranjic, K., Huber, A., Ellinger, A., Hartig, A., Kragler, F., and Brocard, C. (2010). PEX11 family members are membrane elongation factors that coordinate peroxisome proliferation and maintenance. Journal of Cell Science, 123(19), 3389–3400.

Kohno, H., Tanaka, K., Mino, A., Umikawa, M., Imamura, H., Fujiwara, T., … Takai, Y. (1996). Bni1p implicated in cytoskeletal control is a putative target of Rho1p small GTP binding protein in Saccharomyces cerevisiae. The EMBO Journal, 15(22), 6060–6068.

Kooistra, R., Hooykaas, P.J. and Steensma, H.Y., (2004). Efficient gene targeting in Kluyveromyces lactis. Yeast, 21(9), pp.781-792.

Kragt, A., Voorn-Brouwer, T., Van Den Berg, M., and Distel, B. (2005). Endoplasmic reticulum-directed Pex3p routes to peroxisomes and restores peroxisome formation in a Saccharomyces cerevisiae pex3Δ strain. Journal of Biological Chemistry, 280(40), 34350–34357.

Krikken, A. M., Huala, W., de Boer, R., Devos, D. P., Levine, T. P., and van der Klei, I. J. (2020). Peroxisome retention involves Inp1-dependent peroxisome-plasma membrane contact sites in yeast. Journal of Cell Biology. 219(10).

Kors, S., Hacker, C., Bolton, C., Maier, R., Reimann, L., Kitchener, E.J., Warscheid, B., Costello, J.L. and Schrader, M., (2022). Regulating peroxisome–ER contacts via the ACBD5-VAPB tether by FFAT motif phosphorylation and GSK3β. Journal of Cell Biology, 221(3).

Ksiazek, D., Brandstetter, H., Israel, L., Bourenkov, G.P., Katchalova, G., Janssen, K.P., Bartunik, H.D., Noegel, A.A., Schleicher, M. and Holak, T.A., (2003). Structure of the N-terminal domain of the adenylyl cyclase-associated protein (CAP) from Dictyostelium discoideum. Structure, 11(9), pp.1171-1178.

Kunau, W.H., Dommes, V., and Schulz, H. (1995). beta-oxidation of fatty acids in mitochondria, peroxisomes, and bacteria: a century of continued progress. Prog Lipid Res 34, 267-342.

Kuravi, K., Nagotu, S., Krikken, A.M., Sjollema, K., Deckers, M., Erdmann, R., Veenhuis, M., and van der Klei, I.J. (2006). Dynamin-related proteins Vps1p and Dnm1p control peroxisome abundance in Saccharomyces cerevisiae. J Cell Sci, 119, 3994-4001.

Kuzminov, A. (2011). Homologous Recombination-Experimental Systems, Analysis and Significance.

Lackner, L. L., Ping, H., Graef, M., Murley, A., and Nunnari, J. (2013). Endoplasmic reticulum associated mitochondria-cortex tether functions in the distribution and inheritance of mitochondria. Proceedings of the National Academy of Sciences of the United States of America, 110(6), E458-67.

Lam, S. K., Yoda, N., and Schekman, R. (2011). A vesicle carrier that mediates peroxisome protein traffic from the endoplasmic reticulum. Proceedings of the National Academy of Sciences of the United States of America, Vol. 108, E51–E52.

Lanz, M.C., Yugandhar, K., Gupta, S., Sanford, E.J., Faça, V.M., Vega, S., Joiner, A.M., Fromme, J.C., Yu, H. and Smolka, M.B., (2021). In-depth and 3-dimensional exploration of the budding yeast phosphoproteome. EMBO reports, 22(2), p.e51121.

Lao, J.P., Ulrich, K.M., Johnson, J.R., Newton, B.W., Vashisht, A.A., Wohlschlegel, J.A., Krogan, N.J. and Toczyski, D.P., (2018). The yeast DNA damage checkpoint kinase Rad53 targets the exoribonuclease, Xrn1. G3: Genes, Genomes, Genetics, 8(12), pp.3931-3944.

Lazarow, P. B., and Fujiki1, Y. (1985). Biogenesis of peroxisomes. Annual Reviews of Cell Biology, 1, 489-530.

Leathers, T. D. and Gupta, S. C. (1997). Xylitol and riboflavin accumulation in xylose-grown cultures of Pichia guilliermondii. Applied Microbiology and Biotechnology, 47(1), pp. 58–61.

Legesse-Miller, A., Massol, R.H. and Kirchhausen, T., (2003). Constriction and Dnm1p recruitment are distinct processes in mitochondrial fission. *Molecular biology of the cell*, 14(5), pp.1953-1963.

Legesse-Miller, A., Zhang, S., Santiago-Tirado, F.H., Van Pelt, C.K., and Bretscher, A. (2006). Regulated phosphorylation of budding yeast's essential myosin V heavy chain, Myo2p. Mol Biol Cell 17, 1812-1821.

Lewis, S. C., Uchiyama, L. F., and Nunnari, J. (2016). ER-mitochondria contacts couple mtDNA synthesis with Mitochondrial division in human cells. Science, 353(6296).

Li, X. and Gould, S.J., (2003). The dynamin-like GTPase DLP1 is essential for peroxisome division and is recruited to peroxisomes in part by PEX11. Journal of Biological Chemistry, 278(19), pp.17012-17020.

Li, X. and Gould, S.J., (2002). PEX11 promotes peroxisome division independently of peroxisome metabolism. The Journal of Cell Biology, 156(4), pp.643-651.

Li, Y.Y., Yeh, E., Hays, T., and Bloom, K. (1993). Disruption of mitotic spindle orientation in a yeast dynein mutant. Proc Natl Acad Sci U S A 90, 10096-10100.

Lipatova, Z., Tokarev, A.A., Jin, Y., Mulholland, J., Weisman, L.S., and Segev, N. (2008). Direct interaction between a myosin V motor and the Rab GTPases Ypt31/32 is required for polarized secretion. Mol Biol Cell 19, 4177-4187.

Liu, H., Tan, X., Veenhuis, M., McCollum, D., and Cregg, J. M. (1992). An efficient screen for peroxisome-deficient mutants of Pichia pastoris. Journal of Bacteriology, 174(15), 4943–4951.

Loewen, C.J., Roy, A. and Levine, T.P., (2003). A conserved ER targeting motif in three families of lipid binding proteins and in Opi1p binds VAP. The EMBO journal, 22(9), pp.2025-2035.

Lombardi, L., Turner, S.A., Zhao, F. and Butler, G., (2017). Gene editing in clinical isolates of Candida parapsilosis using CRISPR/Cas9. Scientific Reports, 7(1), pp.1-11.

Lombardi, L., Oliveira-Pacheco, J. and Butler, G., (2019). Plasmid-based CRISPR-Cas9 gene editing in multiple Candida species. MSphere, 4(2), pp.e00125-19.

Long, R.M., Gu, W., Lorimer, E., Singer, R.H., and Chartrand, P. (2000). She2p is a novel RNA-binding protein that recruits the Myo4p-She3p complex to ASH1 mRNA. EMBO J 19, 6592-6601.

López-Linares, J. C. et al. (2018). Xylitol production by Debaryomyces hansenii and Candida guilliermondii from rapeseed straw hemicellulosic hydrolysate. Bioresource Technology. Elsevier, 247(July 2017), pp. 736–743.

Lynd, L., van Zyl, W., McBride, J., and Laser, M., (2005). Consolidated bioprocessing of cellulosic biomass: an update. Current Opinion in Biotechnology. *16, 577-83*.

Mabee, W. E., & Saddler, J. N. (2010). Bioethanol from lignocellulosics: Status and perspectives in Canada. Biofuels, Bioproducts and Biorefining, 4(2), 125-136.

MacGilvray, M.E., Shishkova, E., Place, M., Wagner, E.R., Coon, J.J. and Gasch, A.P., (2020). Phosphoproteome response to dithiothreitol reveals unique versus shared features of Saccharomyces cerevisiae stress responses. Journal of Proteome Research, 19(8), pp.3405-3417.

Marshall, P.A., Krimkevich, Y.I., Lark, R.H., Dyer, J.M., Veenhuis, M., and Goodman, J.M. (1995). Pmp27 promotes peroxisomal proliferation. Journal of Cell Biology. 129, 345-355.

Mast, F. D., Herricks, T., Strehler, K. M., Miller, L. R., Saleem, R. A., Rachubinski, R. A., and Aitchison, J. D. (2018). ESC RT-III is required for scissioning new peroxisomes from the endoplasmic reticulum. Journal of Cell Biology, 217(6), 2087–2102.

Mast, F. D., Jamakhandi, A., Saleem, R. A., Dilworth, D. J., Rogers, R. S., Rachubinski, R. A., and Aitchison, J. D. (2016). Peroxins Pex30 and Pex29 dynamically associate with reticulons to regulate peroxisome biogenesis from the endoplasmic reticulum. Journal of Biological Chemistry, 291(30), 15408–15427.

Mattanovich, D., Sauer, M. and Gasser, B. (2014) 'Yeast biotechnology: teaching the old dog new tricks', Microbial Cell Factories. BioMed Central, 13(1), p. 34.

Matsumoto, N., Tamura, S., and Fujiki, Y. (2003). The pathogenic peroxin Pex26p recruits the Pex1p–Pex6p AAA ATPase complexes to peroxisomes. Nature Cell Biology, 5(5), 454–460.

Matsuzono, Y., Kinoshita, N., Tamura, S., Shimozawa, N., Hamasaki, M., Ghaedi, K., … Fujiki, Y. (1999). Human PEX19: cDNA cloning by functional complementation, mutation analysis in a patient with zellweger syndrome, and potential role in peroxisomal membrane assembly. Proceedings of the National Academy of Sciences of the United States of America, 96(5), 2116–2121.

Matsuzono, Y., Matsuzaki, T., and Fujiki, Y. (2006). Functional domain mapping of peroxin Pex19p: Interaction with Pex3p is essentail for function and translocation. Journal of Cell Science, 119(17), 3539–3550.

Mattila, P.K., Quintero-Monzon, O., Kugler, J., Moseley, J.B., Almo, S.C., Lappalainen, P. and Goode, B.L., (2004). A high-affinity interaction with ADP-actin monomers underlies the mechanism and in vivo function of Srv2/cyclase-associated protein. Molecular Biology of The Cell, 15(11), pp.5158-5171.

Mavoungou, C., Israel, L., Rehm, T., Ksiazek, D., Krajewski, M., Popowicz, G., Noegel, A.A., Schleicher, M. and Holak, T.A., (2004). NMR structural characterization of the N-terminal domain of the adenylyl cyclase-associated protein (CAP) from Dictyostelium discoideum. Journal of Biomolecular NMR, 29, pp.73-84.

Mayerhofer, P. U., Bañó-Polo, M., Mingarro, I., and Johnson, A. E. (2016). Human Peroxin PEX3 Is Co-translationally Integrated into the ER and Exits the ER in Budding Vesicles. Traffic, 17(2), 117–130.

Meinecke, M., Bartsch, P., and Wagner, R. (2016). Peroxisomal protein import pores. Biochimica et Biophysica Acta - Molecular Cell Research, 1863(5), 821–827.

Meinecke, M., Cizmowski, C., Schliebs, W., Krüger, V., Beck, S., Wagner, R., and Erdmann, R. (2010). The peroxisomal importomer constitutes a large and highly dynamic pore. Nature Cell Biology, 12(3), 273–277.

Miller, R.K., and Rose, M.D. (1998). Kar9p is a novel cortical protein required for cytoplasmic microtubule orientation in yeast. Journal of Cell Biology. 140, 377-390.

Miller, R.K., Cheng, S.C., and Rose, M.D. (2000). Bim1p/Yeb1p mediates the Kar9p-dependent cortical attachment of cytoplasmic microtubules. Mol Biol Cell. 11, 2949-2959.

Minhas, A., Biswas, D. and Mondal, A. K. (2009). Development of host and vector for high-efficiency transformation and gene disruption in Debaryomyces hansenii. FEMS Yeast Research. Oxford University Press, 9(1), pp. 95–102.

Miranda, I., Silva, R., and Santos, M., (2006). Evolution of the genetic code in yeasts. Yeast. *23, 203-13*.

Mishra, S. and Baranwal, R. (2009). Yeast biotechnology: Diversity and applications, Yeast Biotechnology: Diversity and Applications.

Morand, O., Allen, L., Zoeller, R., and Raetz, C. (1990). A rapid selection for animal cell mutants with defective peroxisomes. *Biochimica et Biophysica Acta (BBA)* – General Subjects, 1034(2), 132–141.

Motley, A. M., Galvin, P. C., Ekal, L., Nuttall, J. M., and Hettema, E. H. (2015). Reevaluation of the role of Pex1 and dynamin-related proteins in peroxisome membrane biogenesis. The Journal of Cell Biology, 211(5), 1041–1056.

Motley, A.M., and Hettema, E.H. (2007). Yeast peroxisomes multiply by growth and division. Journal of Cell Biology. 178, 399-410.

Motley, A.M., Ward, G.P., and Hettema, E.H. (2008). Dnm1p-dependent peroxisome fission requires Caf4p, Mdv1p and Fis1p. J Cell Sci, 121, 1633-1640.

Munck, J.M., Motley, A.M., Nuttall, J.M., and Hettema, E.H. (2009). A dual function for Pex3p in peroxisome formation and inheritance. Journal of Cell Biology. 187, 463-471.

Muntau, A. C., Mayerhofer, P. U., Paton, B. C., Kammerer, S., and Roscher, A. A. (2000). Defective peroxisome membrane synthesis due to mutations in human PEX3 causes Zellweger syndrome, complementation group G. American Journal of Human Genetics, 67(4), 967–975.

Muntau, A. C., Roscher, A. A., Kunau, W. H., and Dodt, G. (2003). The interaction between human PEX3 and PEX19 characterized by fluorescence resonance energy transfer (FRET) analysis. European Journal of Cell Biology, 82(7), 333–342.

Murley, A., Sarsam, R. D., Toulmay, A., Yamada, J., Prinz, W. A., and Nunnari, J. (2015). Ltc1 is an ER-localized sterol transporter and a component of ER-mitochondria and ER-vacuole contacts. Journal of Cell Biology, 209(4), 539–548.

Musacchio, A., and Salmon, E.D. (2007). The spindle-assembly checkpoint in space and time. Nat Rev Mol Cell Biol 8, 379-393.

Nagotu, S., Saraya, R., Otzen, M., Veenhuis, M., and van der Klei, I.J. (2008). Peroxisome proliferation in Hansenula polymorpha requires Dnm1p which mediates fission but not de novo formation. Biochim Biophys Acta, 1783, 760-769.

Navarrete, C. et al. (2022). DebaryOmics: an integrative –omics study to understand the halophilic behaviour of Debaryomyces hansenii. Microbial Biotechnology, 15(4), pp. 1133–1151.

Norkrans, B., (1966). Studies on Marine Occurring Yeasts: Growth Related to pH, NaCl Concentration and Temperature. Archiv. Mikrobiol. *54, 374-392*.

Nunnari, J., and Walter, P. (1996). Regulation of organelle biogenesis. Cell 84, 389-394.

Opaliński, Ł., Bartoszewska, M., Fekken, S., Liu, H., De Boer, R., Van Der Klei, I., Veenhuis, M. and Kiel, J.A., (2012). De novo peroxisome biogenesis in Penicillium chrysogenum is not dependent on the Pex11 family members or Pex16. PloS one, 7(4), p.e35490.

Opaliński, Ł., Kiel, J.A., Williams, C., Veenhuis, M. and Van Der Klei, I.J., (2011a). Membrane curvature during peroxisome fission requires Pex11. The EMBO Journal, 30(1), pp.5-16.

Opaliński, Ł., Veenhuis, M. and Van der Klei, I.J., (2011b). Peroxisomes: membrane events accompanying peroxisome proliferation. The International Journal of Biochemistry and Cell Biology, 43(6), pp.847-851.

Osman, C., Voelker, D. R., and Langer, T. (2011). Making heads or tails of phospholipids in mitochondria. Journal of Cell Biology, Vol. 192, 7–16.

Otsuga, D., Keegan, B.R., Brisch, E., Thatcher, J.W., Hermann, G.J., Bleazard, W. and Shaw, J.M., (1998). The dynamin-related GTPase, Dnm1p, controls mitochondrial morphology in yeast. The Journal of cell biology, 143(2), pp.333-349.

Otzen, M., Rucktaschel, R., Thoms, S., Emmrich, K., Krikken, A.M., Erdmann, R., and van der Klei, I.J. (2012). Pex19p contributes to peroxisome inheritance in the association of peroxisomes to Myo2p. Traffic 13, 947-959.

Padilla, B., Manzanares, P. and Belloch, C. (2014). Yeast species and genetic heterogeneity within Debaryomyces hansenii along the ripening process of traditional ewes' and goats' cheeses. Food Microbiology. Elsevier Ltd, 38, pp. 160–166.

Palmer, S.E., Smaczynska-de Rooij, I.I., Marklew, C.J., Allwood, E.G., Mishra, R., Johnson, S., Goldberg, M.W. and Ayscough, K.R., (2015). A dynamin-actin interaction is required for vesicle scission during endocytosis in yeast. Current Biology, 25(7), pp.868-878.

Palmer, S.E., Smaczynska-de Rooij, I.I., Marklew, C.J., Allwood, E.G., Mishra, R., Goldberg, M.W. and Ayscough, K.R., (2015). A Charge Swap mutation E461K in the yeast dynamin Vps1 reduces endocytic invagination. Communicative and Integrative Biology, 8(4), p.e1051274.

Peng, Y., and Weisman, L.S. (2008). The cyclin-dependent kinase Cdk1 directly regulates vacuole inheritance. Dev Cell 15, 478-485.

Pernice, W.M., Vevea, J.D., and Pon, L.A. (2016). A role for Mfb1p in region-specific anchorage of high-functioning mitochondria and lifespan in Saccharomyces cerevisiae. Nat Commun 7, 10595. Peroxisome development in yeast is associated with the

formation of Pex3-dependent peroxisome-vacuole contact sites. Biochimica et Biophysica Acta - Molecular Cell Research, 1866(3), 349–359.

Petriv, O. I., Tang, L., Titorenko, V. I., and Rachubinski, R. A. (2004). A New Definition for the Consensus Sequence of the Peroxisome Targeting Signal Type 2. Journal of Molecular Biology, 341(1), 119–134.

Petersen, K. M. and Jespersen, L. (2004). Genetic diversity of the species Debaryomyces hansenii and the use of chromosome polymorphism for typing of strains isolated from surface-ripened cheeses. Journal of Applied Microbiology, 97, pp. 205–213.

Ping, H. A., Kraft, L. M., Chen, W. T., Nilles, A. E., and Lackner, L. L. (2016). Num1 anchors mitochondria to the plasma membrane via two domains with different lipid binding specificities. Journal of Cell Biology, 213(5), 513–524.

Pitts, K.R., Yoon, Y., Krueger, E.W., and McNiven, M.A. (1999). The dynamin-like protein DLP1 is essential for normal distribution and morphology of the endoplasmic reticulum and mitochondria in mammalian cells. Mol Biol Cell, 10, 4403-4417.

Platta, H. W., and Erdmann, R. (2007). The peroxisomal protein import machinery. FEBS Letters, Vol. 581, 2811–2819.

Platta, H. W., El Magraoui, F., Bäumer, B. E., Schlee, D., Girzalsky, W., and Erdmann, R. (2009). Pex2 and pex12 function as protein-ubiquitin ligases in peroxisomal protein import. Molecular and Cellular Biology, 29(20), 5505–5516.

Poirier, Y., Antonenkov, V. D., Glumoff, T., and Hiltunen, J. K. (2006). Peroxisomal β-oxidation—A metabolic pathway with multiple functions. Biochimica et Biophysica Acta (BBA) - Molecular Cell Research, 1763(12), 1413–1426.

Poll-The, B. T., Saudubray, J. M., Ogier, H. A., Odièvre, M., Scotto, J. M., Monnens, L., … Schutgens, R. B. (1987). Infantile Refsum disease: an inherited peroxisomal disorder. Comparison with Zellweger syndrome and neonatal adrenoleukodystrophy. European Journal of Pediatrics, 146(5), 477–483.

Prinz, W. A. (2014). Bridging the gap: Membrane contact sites in signaling, metabolism, and organelle dynamics. Journal of Cell Biology, Vol. 205, 759–769.

Prinz, W. A., Toulmay, A., and Balla, T. (2020). The functional universe of membrane contactsites. Nature Reviews Molecular Cell Biology, Vol. 21, 7–24.

Prista, C. et al. (2005). Mechanisms underlying the halotolerant way of Debaryomyces hansenii', FEMS Yeast Research. Oxford University Press, pp. 693–701.

Prista, C. et al. (2016). The halotolerant Debaryomyces hansenii, the Cinderella of non-conventional yeasts. Yeast. John Wiley and Sons, Ltd, 33(10), pp. 523–533.

Pruyne, D., Evangelista, M., Yang, C., Bi, E., Zigmond, S., Bretscher, A., and Boone, C. (2002). Role of formins in actin assembly: Nucleation and barbed-end association. Science, 297(5581), 612–615.

Quintero-Monzon, O., Jonasson, E.M., Bertling, E., Talarico, L., Chaudhry, F., Sihvo, M., Lappalainen, P. and Goode, B.L., (2009). Reconstitution and dissection of the 600-kDa Srv2/CAP complex. Journal of Biological Chemistry, 284(16), pp.10923-10934.

Quintero-Monzon, O., Rodal, A.A., Strokopytov, B., Almo, S.C. and Goode, B.L., (2005). Structural and functional dissection of the Abp1 ADFH actin-binding domain reveals versatile in vivo adapter functions. Molecular Biology of The Cell, 16(7), pp.3128-3139.

Ramírez-Orozco, M., Hernández-Saavedra, N. Y. and Ochoa, J. L. (2001). Debaryomyces hansenii growth in nonsterile seawater ClO2 - Peptone-containing medium. Canadian Journal of Microbiology, 47(7), pp. 676–679.

Ramos, J. et al. (2017). Debaryomyces hansenii strains from Valle de los pedroches Iberian dry meat products: Isolation, identification, characterization, and selection for starter cultures. Journal of Microbiology and Biotechnology, 27(9), pp. 1576–1585.

Rao, V., Srinivas, K., Sujini, G. and Kumar, G., (2014). Protein-protein interaction detection: methods and analysis. International journal of proteomics, 1–12.

Ratledge, C., (2002). Regulation of lipid accumulation in oleaginous micro-organisms. Biochemical Society Transactions. 30, 1047-1050.

Rhodin, J., (1954). Correlation of ultrastructural organization and function in normal and experimentally changed proximal convoluted tubule cells of the mouse kidney. Thesis Kalolinska Instutet.

Rizzuto, R., Brini, M., Murgia, M., and Pozzan, T. (1993). Microdomains with high Ca2+ close to IP3-sensitive channels that are sensed by neighboring mitochondria. Science, 262(5134), 744–747.

Rooij, I.I.S.D., Allwood, E.G., Aghamohammadzadeh, S., Hettema, E.H., Goldberg, M.W. and Ayscough, K.R., (2010). A role for the dynamin-like protein Vps1 during endocytosis in yeast. Journal of Cell Science, 123(20), pp.3496-3506.

Rottensteiner, H., Stein, K., Sonnenhol, E. and Erdmann, R., (2003). Conserved function of pex11p and the novel pex25p and pex27p in peroxisome biogenesis. Molecular Biology of the Cell, 14(10), pp.4316-4328.

Rottensteiner, H., Stein, K., Sonnenhol, E., and Erdmann, R. (2003). Conserved function of pex11p and the novel pex25p and pex27p in peroxisome biogenesis. Mol Biol Cell, 14, 4316-4328.

Runguphan, W., and Keasling, J., (2014). Metabolic engineering of Saccharomyces cerevisiae for production of fatty acid-derived biofuels and chemicals. Metab. Eng. 21, 103-13.

Saarikangas, J., Zhao, H., and Lappalainen, P. (2010). Regulation of the actin cytoskeletonplasma membrane interplay by phosphoinositides. Physiological Reviews, Vol. 90, 259–289.

Sacksteder, K. A., Jones, J. M., South, S. T., Li, X., Liu, Y., and Gould, S. J. (2000). PEX19 binds multiple peroxisomal membrane proteins, is predominantly cytoplasmic, and is required for peroxisome membrane synthesis. Journal of Cell Biology, 148(5), 931–944.

Santos, M., Imanaka, T., Shio, H., Small, G., and Lazarow, P. (1988). Peroxisomal membrane ghosts in Zellweger syndrome--aberrant organelle assembly. Science, 239(4847), 1536–1538.

Sánchez, N. S. et al. (2006). Glycolytic sequence and respiration of Debaryomyces hansenii as compared to Saccharomyces cerevisiae', Yeast. John Wiley and Sons, Ltd, 23(5), pp. 361–374.

Saraya, R., Cepinska, M.N., Kiel, J.A., Veenhuis, M., and van der Klei, I.J. (2010). A conserved function for Inp2 in peroxisome inheritance. Biochim Biophys Acta 1803, 617-622.

Satyanarayana, T. and Kunze, G. eds., (2009). Yeast biotechnology: diversity and applications (Vol. 78). (Dordrecht: Springer).

Schmidt, F., Treiber, N., Zocher, G., Bjelic, S., Steinmetz, M. O., Kalbacher, H., … Dodt, G. (2010). Insights into peroxisome function from the structure of PEX3 in complex with a soluble fragment of PEX19. Journal of Biological Chemistry, 285(33), 25410–25417.

Schrader, M., Godinho, L.F., Costello, J.L. and Islinger, M., (2015). The different facets of organelle interplay—an overview of organelle interactions. Frontiers in Cell and Developmental Biology, 3, p.56.

Schrader, M., Bonekamp, N.A., and Islinger, M. (2012). Fission and proliferation of peroxisomes. Biochim Biophys Acta, 1822, 1343-1357.

Schrader, M. and Fahimi, H.D., (2006). Growth and division of peroxisomes. International Review of Cytology, 255, pp.237-290.

Schuldiner, M., Metz, J., Schmid, V., Denic, V., Rakwalska, M., Schmitt, H. D., … Weissman, J. S. (2008). The GET Complex Mediates Insertion of Tail-Anchored Proteins into the ER Membrane. Cell, 134(4), 634–645.

Sellers, J.R., and Veigel, C. (2006). Walking with myosin V. Curr Opin Cell Biol 18, 68 73.

Seiler, H. and Busse, M. (1990). The yeasts of cheese brines. International Journal of Food Microbiology, 11(3–4), pp. 289–303.

Sesaki, H. and Jensen, R.E., (2001). UGO1 encodes an outer membrane protein required for mitochondrial fusion. The Journal of cell biology, 152(6), pp.1123-1134.

Shai, N., Yifrach, E., van Roermund, C. W. T., Cohen, N., Bibi, C., IJlst, L., … Zalckvar, E. (2018). Systematic mapping of contact sites reveals tethers and a function for the peroxisome-mitochondria contact. Nature Communications, 9(1), 1761.

Shang, X., Zhang, Y., Xu, J., Li, M., Wang, X. and Yu, R., (2020). SRV2 promotes mitochondrial fission and Mst1-Drp1 signaling in LPS-induced septic cardiomyopathy. Aging (Albany NY), 12(2), p.1417.

Shibata, H., Kashiwayama, Y., Imanaka, T., and Kato, H. (2004). Domain architecture and activity of human Pex19p, a chaperone-like protein for intracellular trafficking of peroxisomal membrane proteins. Journal of Biological Chemistry, 279(37), 38486–38494.

Shima, F., Yamawaki-Kataoka, Y., Yanagihara, C., Tamada, M., Okada, T., Kariya, K.I. and Kataoka, T., (1997). Effect of association with adenylyl cyclase-associated protein on the interaction of yeast adenylyl cyclase with Ras protein. Molecular and Cellular Biology, 17(3), pp.1057-1064.

Shimozawa, N., Suzuki, Y., Zhang, Z., Imamura, A., Ghaedi, K., Fujiki, Y., and Kondo, N. (2000). Identification of PEX3 as the gene mutated in a Zellweger syndrome patient lacking peroxisomal remnant structures. Human Molecular Genetics, 9(13), 1995–1999.

Simon, V.R., Karmon, S.L., and Pon, L.A. (1997). Mitochondrial inheritance: cell cycle and actin cable dependence of polarized mitochondrial movements in Saccharomyces cerevisiae. Cell Motil Cytoskeleton 37, 199-210.

Smaczynska-de, R., II, Allwood, E.G., Aghamohammadzadeh, S., Hettema, E.H., Goldberg, M.W., and Ayscough, K.R. (2010). A role for the dynamin-like protein Vps1 during endocytosis in yeast. J Cell Sci, 123, 3496-3506.

Smith, J. J. and Aitchison, J. D. (2013). Peroxisomes take shape. Nature Reviews Molecular Cell Biology, 14(12), 803-817.

Smith, J.J., Marelli, M., Christmas, R.H., Vizeacoumar, F.J., Dilworth, D.J., Ideker, T., Galitski, T., Dimitrov, K., Rachubinski, R.A., and Aitchison, J.D. (2002). Transcriptome profiling to identify genes involved in peroxisome assembly and function. J Cell Biol, 158, 259-271.

Sørensen, B. B. (1997). Lipolysis of pork fat by the meat starter culture Debaryomyces hansenii at various environmental conditions. International Journal of Food Microbiology. Elsevier, 34(2), pp. 187–193.

South, S. T., and Gould, S. J. (1999). Peroxisome synthesis in the absence of preexisting peroxisomes. Journal of Cell Biology, 144(2), 255–266.

Spasskaya, D.S., Kotlov, M.I., Lekanov, D.S., Tutyaeva, V.V., Snezhkina, A.V., Kudryavtseva, A.V., Karpov, V.L. and Karpov, D.S., (2021). CRISPR/Cas9-mediated genome engineering reveals the contribution of the 26S proteasome to the extremophilic nature of the yeast Debaryomyces hansenii. ACS Synthetic Biology, 10(2), pp.297-308.

Sprague, G.F. and Cronan, J.E., (1977). Isolation and characterization of Saccharomyces cerevisiae mutants defective in glycerol catabolism. Journal of Bacteriology, 129(3), pp.1335-1342.

Srivastava, J. and Barber, D., (2008). Actin co-sedimentation assay; for the analysis of protein binding to F-actin. Fournal of Visualized Experiments, (13), p.e690.

Strucko, T., Andersen, N.L., Mahler, M.R., Martínez, J.L. and Mortensen, U.H., (2021). A CRISPR/Cas9 method facilitates efficient oligo-mediated gene editing in Debaryomyces hansenii. Synthetic Biology, 6(1), p.ysab031.

Swaney, D.L., Beltrao, P., Starita, L., Guo, A., Rush, J., Fields, S., Krogan, N.J. and Villén, J., (2013). Global analysis of phosphorylation and ubiquitylation cross-talk in protein degradation. Nature Methods, 10(7), pp.676-682.

Swayne, T. C., Zhou, C., Boldogh, I. R., Charalel, J. K., McFaline-Figueroa, J. R., Thoms, S., Pon, L. A. (2011). Role for cER and Mmr1p in anchorage of mitochondria at sites of polarized surface growth in budding yeast. Current Biology, 21(23), 1994–1999.

Swinkels, B. W., Gould, S. J., and Subramani, S. (1992). Targeting efficiencies of various permutations of the consensus C-terminal tripeptide peroxisomal targeting signal. FEBS Letters, 305(2), 133–136.

Tábara, L.C., Morris, J.L. and Prudent, J., (2021). The complex dance of organelles during mitochondrial division. Trends in Cell Biology, 31(4), pp.241-253.

Takizawa, P.A., and Vale, R.D. (2000). The myosin motor, Myo4p, binds Ash1 mRNA via the adapter protein, She3p. Proc Natl Acad Sci U S A 97, 5273-5278.

Takita Y, Takahara M, Nogami S, Anraku, Ohya Y., (1997). Applications of the long and accurate polymerase chain reaction method in yeast molecular biology: direct sequencing of the amplified DNA and its introduction into yeast. Yeast 13:763–768

Tam, Y. Y. C., Fagarasanu, A., Fagarasanu, M., and Rachubinski, R. A. (2005). Pex3p initiates the formation of a preperoxisomal compartment from a subdomain of the endoplasmic reticulum in Saccharomyces cerevisiae. Journal of Biological Chemistry, 280(41), 34933–34939.

Tam, Y.Y., Torres-Guzman, J.C., Vizeacoumar, F.J., Smith, J.J., Marelli, M., Aitchison, J.D., and Rachubinski, R.A. (2003). Pex11-related proteins in peroxisome dynamics: a role for the novel peroxin Pex27p in controlling peroxisome size and number in Saccharomyces cerevisiae. Mol Biol Cell 14, 4089-4102.

Tanaka, C., Tan, L. J., Mochida, K., Kirisako, H., Koizumi, M., Asai, E., … Nakatogawa, H. (2014). Hrr25 triggers selective autophagy-related pathways by phosphorylating receptor proteins. Journal of Cell Biology, 207(1), 91–105.

Tang, F., Kauffman, E.J., Novak, J.L., Nau, J.J., Catlett, N.L., and Weisman, L.S. (2003). Regulated degradation of a class V myosin receptor directs movement of the yeast vacuole. Nature 422, 87-92.

Tang, X., Punch, J. J., and Lee, W.-L. (2009). A CAAX motif can compensate for the PH domain of Num1 for cortical dynein attachment. Cell Cycle (Georgetown, Tex.), 8(19), 3182–3190.

Thoms, S., Harms, I., Kalies, K. U., and Gärtner, J. (2012). Peroxisome Formation Requires the Endoplasmic Reticulum Channel Protein Sec61. Traffic, 13(4), 599–609.

Titorenko, V. I., Smith, J. J., Szilard, R. K., and Rachubinski, R. A. (1998). Pex20p of the Yeast Yarrowia lipolytica Is Required for the Oligomerization of Thiolase in the Cytosol and for Its Targeting to the Peroxisome. The Journal of Cell Biology, 142(2), 403–420.

Tower, R.J., Fagarasanu, A., Aitchison, J.D., and Rachubinski, R.A. (2011). The peroxin Pex34p functions with the Pex11 family of peroxisomal divisional proteins to regulate the peroxisome population in yeast. Mol Biol Cell*,* 22, 1727-1738.

Tsukamoto, T., Yokota, S., and Fujiki, Y. (1990). Isolation and characterization of Chinese hamster ovary cell mutants defective in assembly of peroxisomes. The Journal of Cell Biology, 110(3), 651–660.

Urbanek, A.N., Smith, A.P., Allwood, E.G., Booth, W.I. and Ayscough, K.R., (2013). A novel actin-binding motif in Las17/WASP nucleates actin filaments independently of Arp2/3. Current Biology, 23(3), pp.196-203.

Urquhart, A. J., Kennedy, D., Gould, S. J., and Crane, D. I. (2000). Interaction of Pex5p, the type 1 peroxisome targeting signal receptor, with the peroxisomal membrane proteins Pex14p and Pex13p. Journal of Biological Chemistry, 275(6), 4127–4136.

Ušaj, M. M., Brložnik, M., Kaferle, P., Žitnik, M., … Petrovič, U. (2015). Genome-Wide Localization Study of Yeast Pex11 Identifies Peroxisome-Mitochondria Interactions through the ERMES Complex. Journal of Molecular Biology, 427(11), 2072-2087.

Valm, A. M., Cohen, S., Legant, W. R., Melunis, J., Hershberg, U., Wait, E., … Lippincott-Schwartz, J. (2017). Applying systems-level spectral imaging and analysis to reveal theorganelle interactome. Nature, Vol. 546, 162–167.

Van Den Tempel, T. and Jakobsen, M., (2000). The technological characteristics of Debaryomyces hansenii and Yarrowia lipolytica and their potential as starter cultures for production of Danablu. International Dairy Journal. Elsevier, 10(4), pp. 263–270.

Van Der Zand, A., Braakman, I., and Tabak, H. F. (2010). Peroxisomal membrane proteins insert into the endoplasmic reticulum. Molecular Biology of the Cell, 21(12), 2057–2065.

Van Der Zand, A., Gent, J., Braakman, I., and Tabak, H. F. (2012). Biochemically distinct vesicles from the endoplasmic reticulum fuse to form peroxisomes. Cell, 149(2), 397–409.

Vater, C.A., Raymond, C.K., Ekena, K., Howald-Stevenson, I., and Stevens, T.H. (1992). The VPS1 protein, a homolog of dynamin required for vacuolar protein sorting in Saccharomyces cerevisiae, is a GTPase with two functionally separable domains. J Cell Biol, 119, 773-786.

Veenhuis, M., Mateblowski, M., Kunau, W. H., and Harder, W. (1987). Proliferation of microbodies in *Saccharomyces cerevisiae*. Yeast, 3(2), 77–84.

Vida, T.A. and Emr, S.D., (1995). A new vital stain for visualizing vacuolar membrane dynamics and endocytosis in yeast. The Journal of Cell Biology, 128(5), pp.779-792.

Vigliotta, G. et al. (2007). Nitrite metabolism in Debaryomyces hansenii TOB-Y7, a yeast strain involved in tobacco fermentation. Applied Microbiology and Biotechnology. Springer-Verlag, 75(3), pp. 633–645.

Vojtek, A., Haarer, B., Field, J., Gerst, J., Pollard, T.D., Brown, S. and Wigler, M., (1991). Evidence for a functional link between profilin and CAP in the yeast S. cerevisiae. Cell, 66(3), pp.497-505.

Walch-Solimena, C., and Novick, P. (1999). The yeast phosphatidylinositol-4-OH kinase Pik1 regulates secretion at the Golgi. Nature Cell Biology, 1(8), 523–525.

Wanders, R. J. A., and Waterham, H. R. (2006). Peroxisomal disorders: the single peroxisomal enzyme deficiencies. Biochimica et Biophysica Acta, 1763(12), 1707–1720.

Wanders, R.J.A. (2018). Peroxisomal disorders: Improved laboratory diagnosis, new defects and the complicated route to treatment. Mol Cell Probes 40, 60-69.

Wang, Sihui, Idrissi, F. Z., Hermansson, M., Grippa, A., Ejsing, C. S., and Carvalho, P. (2018). Seipin and the membrane-shaping protein Pex30 cooperate in organelle budding from the endoplasmic reticulum. Nature Communications, 9(1).

Wang, Songyu, Tukachinsky, H., Romano, F. B., and Rapoport, T. A. (2016). Cooperation of the ER-shaping proteins atlastin, lunapark, and reticulons to generate a tubular membrane network. ELife.

Wang, Y.X., Catlett, N.L., and Weisman, L.S. (1998). Vac8p, a vacuolar protein with armadillo repeats, functions in both vacuole inheritance and protein targeting from the cytoplasm to vacuole. J Cell Biol 140, 1063-1074.

Warren, G., and Wickner, W. (1996). Organelle inheritance. Cell 84, 395-400.

Waterham, H. R., Ferdinandusse, S., and Wanders, R. J. A. (2016). Human disorders of peroxisome metabolism and biogenesis. Biochimie et Biophysica Acta, 1863(5), 922- 933.

Wertman, K.F., Drubin, D.G. and Botstein, D., (1992). Systematic mutational analysis of the yeast ACT1 gene. Genetics, 132(2), pp.337-350.

West, M., Zurek, N., Hoenger, A., and Voeltz, G. K. (2011). A 3D analysis of yeast ER structure reveals how ER domains are organized by membrane curvature. Journal of Cell Biology, 193(2), 333–346.

Williams, C., Opalinski, L., Landgraf, C., Costello, J., Schrader, M., Krikken, A.M., Knoops, K., Kram, A.M., Volkmer, R., and van der Klei, I.J. (2015). The membrane remodeling protein 116 Pex11p activates the GTPase Dnm1p during peroxisomal fission. Proc Natl Acad Sci USA, 112, 6377-6382.

Williams, C., van den Berg, M., Geers, E., and Distel, B. (2008). Pex10p functions as an E3 ligase for the Ubc4p-dependent ubiquitination of Pex5p. Biochemical and Biophysical Research Communications, 374(4), 620–624.

Wilsbach, K., and Payne, G.S. (1993). Vps1p, a member of the dynamin GTPase family, is necessary for Golgi membrane protein retention in Saccharomyces cerevisiae. *EMBO J*, 12, 3049-3059.

Winder, S.J. and Ayscough, K.R., (2005). Actin-binding proteins. *Journal of cell science*, 118(4), pp.651-654.

Wong, E.D., Wagner, J.A., Gorsich, S.W., McCaffery, J.M., Shaw, J.M. and Nunnari, J., (2000). The dynamin-related GTPase, Mgm1p, is an intermembrane space protein required for maintenance of fusion competent mitochondria. The Journal of cell biology, 151(2), pp.341-352.

Wu, F., de Boer, R., Krikken, A., Akşit, A., Bordin, N., Devos, D., and van der Klei, I. (2020). Pex24 and Pex32 are required to tether peroxisomes to the ER for organelle biogenesis, positioning and segregation. Journal of Cell Science, jcs.246983.

Wu, H., de Boer, R., Krikken, A.M., Akşit, A., Yuan, W. and van der Klei, I.J., (2019). Peroxisome development in yeast is associated with the formation of Pex3-dependent peroxisome-vacuole contact sites. Biochimica et Biophysica Acta (BBA)-Molecular Cell Research, 1866(3), pp.349-359.

Wu, X. and Jiang, Y.W., (2005). Genetic/genomic evidence for a key role of polarized endocytosis in filamentous differentiation of S. cerevisiae. Yeast, 22(14), pp.1143-1153.

Yagita, Y., Shinohara, K., Abe, Y., Nakagawa, K., Al-Owain, M., Alkuraya, F. S., and Fujiki, Y. (2017). Deficiency of a Retinal Dystrophy Protein, Acyl-CoA Binding Domain-containing 5 (ACBD5), Impairs Peroxisomal β-Oxidation of Very-long-chain Fatty Acids. Journal of Biological Chemistry, 292(2), 691–705.

Yaguchi, A., Rives, D. and Blenner, M., (2017). New kids on the block: emerging oleaginous yeast of biotechnological importance. AIMS Microbiology, 3(2), pp. 227–247.

Yamamoto, A., Nagai, K., Yamasaki, M., and Matsuhashi, M. (1990). Solubilization of aster-forming proteins from yeast: possible constituents of spindle pole body and reconstitution of asters in vitro. Cell Struct Funct 15, 221-228.

Yau, R.G., Wong, S., and Weisman, L.S. (2017). Spatial regulation of organelle release from myosin V transport by p21-activated kinases. J Cell Biol 216, 1557-1566.

Yu, J. W., Mendrola, J. M., Audhya, A., Singh, S., Keleti, D., DeWald, D. B., … Lemmon, M. A. (2004). Genome-wide analysis of membrane targeting by S. cerevisiae pleckstrin homology domains. Molecular Cell, 13(5), 677–688.

Yusof, A.M., Hu, N.J., Wlodawer, A. and Hofmann, A., (2005). Structural evidence for variable oligomerization of the N-terminal domain of cyclase-associated protein (CAP). *Proteins: Structure,* Function, and Bioinformatics, 58(2), pp.255-262.

Zhang, K. et al. (2015). Genomic reconstruction to improve bioethanol and ergosterol production of industrial yeast Saccharomyces cerevisiae', Journal of Industrial Microbiology and Biotechnology, 42(2), pp. 207–218.

Zhou, X., Li, W., Liu, Y. and Amon, A., (2021). Cross-compartment signal propagation in the mitotic exit network. Elife, 10, p.e63645.